Ph.D. Program in Civil, Chemical and Environmental Engineering

Curriculum in Structural and Geotechnical Engineering, Mechanics and Materials

Department of Civil, Chemical and Environmental Engineering

Polytechnic School, University of Genoa, Italy.

General Method of Wind-Induced Fatigue Analysis of Slender Structures

Michela Damele, MSc.

GENERAL METHOD OF WIND-INDUCED FATIGUE ANALYSIS OF SLENDER STRUCTURES

BY

MICHELA DAMELE, MSC.

Dissertation discussed in partial fulfillment of
the requirements for the Degree of

DOCTOR OF PHILOSOPHY

Civil, Chemical and Environmental Engineering
curriculum in Structural and Geotechnical Engineering, Mechanics and Materials,
Department of Civil, Chemical and Environmental Engineering, University of Genoa, Italy

November, 2020

Advisor(s):
Prof. Maria Pia Repetto – Department of Civil, Chemical and Environmental Engineering, Polytechnic School, University of Genoa, Italy

External Reviewers:
Prof. Francesco Ricciardelli – Department of Engineering, University of Campania "Luigi Vanvitelli", Italy
Prof. Frank Kemper – Institute of Steel Construction, RWTH Aachen University, Germany

Examination Committee:
Prof. Luca Bruno – Department of Structural Engineering and Geotechnical Studies, Polytechnic University of Turin, Italy
Prof. Dario Peduto – Department of Civil Engineering, University of Salerno, Italy
Prof. Sergio Lagomarsino –Department of Civil, Chemical and Environmental Engineering, Polytechnic School, University of Genoa, Italy

Ph.D. program in Civil, Chemical and Environmental Engineering

Curriculum in Structural and Geotechnical Engineering, Mechanics and Materials

Cycle XXXII

ABSTRACT

Wind-induced fatigue is a critical issue in design of many slender structures, but suitable engineering and standards procedures are still fragmentary. On the basis of the closed form solution proposed by Repetto and Solari (2012), this PhD Thesis develops a complete and general procedure for determining the wind-induced fatigue damage of slender structures, suitable for engineering calculations and code provisions.

A new generalization of the closed form solution is proposed, covering a wide range of resistance fatigue curve types, suitable for different materials and different cyclic loading conditions. The final formulation results in complete accordance with Eurocode format for wind induced Ultimate Limit State analysis.

The set of required input parameters is discussed, taking into account simultaneous alongwind and crosswind structural responses due to turbulence. Simple expressions coherent with standard format are defined for both alongwind and crosswind fatigue analysis.

The significance of different contributions to crosswind-induced fatigue is examined. Although engineering procedures estimate separately crosswind maximum response to gust buffeting and to critical vortex shedding conditions, there's no guarantee such assumption would provide reliable fatigue predictions. Therefore, the possibility of separating the effects of the vortex shedding in fatigue analysis is investigated, as well as the role of parameters uncertainties in response and in fatigue evaluations, suggesting new formulations of the cycle number due to VIV.

Finally, some case studies are discussed validating the proposed model.

INDEX

CHAPTER 1 - INTRODUCTION 1

CHAPTER 2 - WIND-INDUCED FATIGUE ON SLENDER STRUCTURES . 5

2.1. Introduction 5

2.2. General framework of fatigue analysis 7

2.2.1. Fatigue phenomenon and analysis 7

2.2.2. Different approaches and fatigue resistance 11

2.2.3. Cycles counting methods 17

2.3. Basis of alongwind-induced fatigue methods 26

2.3.1. Wind field, loading and induced response model 28

2.3.2. Alongwind induced-fatigue analyses in frequency domain 38

2.3.3. Hypothesis and analytical assumptions 48

CHAPTER 3 - FATIGUE RESISTANCE CURVES GENERALIZATION 55

3.1. Introduction 55

3.2. Closed-form solution of mean damage 57

3.2.1. Zero level solution of damage 59

3.2.2. Bi-modal factor 61

3.2.3. Mean stress factor 64

3.2.4. Generalized fatigue curve factor 66

3.3. From the closed-form solution to the final formulation 72

CHAPTER 4 – ALONGWIND AND CROSSWIND GUST – INDUCED FATIGUE 77

4.1. Introduction 77

4.2. Turbulence-induced fatigue analytical model 78

4.2.1. Simplified and detailed calculations 84

4.3. Input parameters definition 88

4.3.1. Resistance and structural input parameters 88

4.3.2. Climatological input parameters 89

4.3.3. Response input parameters 91

4.3.4. Alongwind response input parameters 92

4.3.5. Crosswind response input parameters 98

CHAPTER 5 – CROSSWIND RESPONSE IN FATIGUE ANALYSIS 103

5.1. Introduction 103

5.2. Vortex shedding-induced vibrations 105

5.2.1. The vortex-shedding on slender structures 106

5.2.2. The spectral model 111

5.2.3. "Forced vibration" and "lock-in" regimes 114
5.2.4. Code design procedure: response and fatigue calculation 118

5.3. Crosswind turbulence and VIV-induced fatigue 123
5.3.1. Case study: Chimney 1 125
5.3.2. Case study: Chimney 2a 135
5.3.3. Case study: Chimney 2b 146
5.3.4. Case study: Chimney 3 156
5.3.5. Case study: Pole 166
5.3.6. Summary and comparison of results 170

5.4. Review of the VIV-induced fatigue standard method 174
5.4.1. Weibull model of the parent population of the mean wind velocity 174
5.4.2. Band of wind velocities with vortex-induced vibrations 197
5.4.3. VIV response uncertainties propagation 203
5.4.4. Comparison between standard method and the proposed formulation 210

CHAPTER 6 – EXAMPLES OF FATIGUE CALCULATIONS FOR BUFFETING 216

6.1. Introduction 216

6.2. Antenna supporting pole 217

6.3. Urban light pole 223
6.3.1. Numerical analysis 224
6.3.2. Analytical analysis 226

6.4. Anemometric pole 229

6.5. Traffic signal support structure 233
6.5.1. Analytical analysis with equivalent ideal stresses 234
6.5.2. Analytical analysis with shear stresses 239

6.6. Aluminium pole 241

6.7. Antenna mast 243

CHAPTER 7 – CONCLUSIONS 247

APPENDIX A 250

REFERENCES 255

SYMBOLS 264

CHAPTER 1 - INTRODUCTION

Slender, light, flexible and low damped structures are commonly built nowadays, and these kinds of structures are highly sensitive to wind-induced actions and vibrations.

The presence of a structure in a wind field distorts the flow, producing complex aerodynamic phenomena that may be expressed as drag and lift forces, in alongwind and crosswind directions respectively, and a torsional moment around the structural axis. These actions are characterized by a mean part, mainly associated with the mean wind velocity, and by a nil mean fluctuating part, depending on two distinct excitation mechanisms: the oncoming turbulence and the vortex shedding. The atmospheric turbulence produces structural oscillations whose amplitudes increases on increasing of the mean wind velocity; the vortex induced vibrations constitute a complex physical phenomenon which is the essential element of the crosswind structural response when the shedding frequency is resonant with a structural natural mode.

Since wind-induced actions may produce large vibrations at moderate and frequent wind velocities, slender structures may undergo a great number of stress cycles that lead to damage accumulation and may determine the structural failure without exceeding design wind velocities and ultimate strenghts. Different structural typologies, such as urban light poles, guyed masts, chimneys, suspended and cable-stayed bridges, wind turbines and many others, are really sensitive to fatigue phenomenon; this remark is confirmed by several damages and collapses observed in many parts of the world (Robertson et al., 2001; Peil and Behrens, 2002; Caracoglia and Jones, 2006; Pritchard, 1984).

Wind-induced fatigue failures can be categorized into distinct types: low-cycle fatigue, in which the stresses can exceed the yield point of material, and high-cycle fatigue, in which the material behaviour is elastic, resulting from dynamic response to wind loading during structural life. Failures of the first type have occurred, for instance, in light gauge steel roofing in hurricanes and tropical cyclones in the United States and Australia. These failures can be prevented by relatively simple and cheap solutions, such as larger washers. High-cycle turbulence-induced fatigue failures are characterized by slow accumulation of damage and they may take several years to occur. The stresses are often, but not exclusively, generated by alongwind turbulence (Holmes and Rofail, 2008). High-cycle fatigue failures resulting from crosswind response due to vortex shedding can occur in a very short period after completion of a structure such as chimney, if the critical wind speed for vortex-induced vibrations is a moderate, frequently-occurring wind speed value. The design solution for this type of fatigue failure is to reduce the peak stress range below the ‘endurance limit’, or ‘fatigue limit’ so that theoretically no fatigue damage should occur. Vortex-

induced vibrations can be mitigated by several methods: increasing mass, increasing damping (including auxiliary damping), or by aerodynamic means such as helical strakes or fins.

The importance of the wind-induced fatigue was first emphasised during the early stages of the research activities in wind engineering, in the 60's (Davenport, 1966). Notwithstanding this, there is a quite lack of contributions until the last 80's. Later on, interest in wind-induced fatigue has increased, and several papers dealing with this matter have been published since the 90's, dealing with partial aspects of the problem. Three main lines of approach have been taken.

The first makes recourse to traditional cycle counting procedures in a time domain. This approach is burdensome since it needs long time-histories related to all the loading conditions being considered, and the numerical application of the Rainflow counting method in order to build a cycle histogram; however, it still represents the main procedure adopted in some applications (van Staalduinen, 1993; Peil and Nolle, 1994).

The second approach applies frequency domain criteria in the probabilistic environment of random dynamics. Some procedures have been proposed for alongwind-induced fatigue, assuming the stress power spectral density as narrow-band (Mikitarenko and Perelmuter, 1998; Petrov, 1998). Deoliya and Datta (2002) analysed an antenna mast under alongwind forces and determined the mean total damage using six different assumptions for the stress range probability distribution. This showed a wide scatter in results, indicating that the narrow-band assumption always provides the maximum damage estimation.

The third line of research introduces simplified methods addressed to standards. Patel and Freathy (1984) and Wyatt (1984, 2004) adopted a time-domain approach and semi-empirical formulae to consider the combined effects of the quasi-static and resonant parts of the wind-induced response, assuming that the fatigue curve is a straight line on a log-log scale. Holmes (2002) analysed the alongwind-induced fatigue and derived two closed form solutions that represent, respectively, an upper and a lower bound of the mean total damage: the first was obtained representing the stress process as a narrow band; the second was related to the lower bound of the damage correction factor due to Wirshing and Light (1980). This method is simple to apply (Robertson et al., 2004), it allows one to consider directionality effects very easily (Holmes and Rofail, 2008), it requires the knowledge of a few basic parameters and a set of simplified assumptions; however, it leads to results that, depending on the spectral properties of the stress processes and on the choice of the stress parameters and the fatigue *S-N* curve, may be largely approximated. Kemper and Feldmann (2011) proposed an approach based on a closed-form solution applicable for random wide-banded responses and for arbitrary *S-N* curves; it adopts a frequency based cycle counting method from Dirlik (1985) in order to obtain a cycle histogram and it takes into account the Weibull distribution for the parent population of mean wind velocity. Recently, Kemper (2019) proposed developments of the method, based on so-called damage equivalence factors.

At the beginning of the new millennium, research contributions were organized to be included in international and national standards, codes and recommendations, without reaching an effective generalization of the procedures proposed. As a result, at present, literature on the wind-induced fatigue is prolific but quite disjointed and incomplete. Some design codes furnish approximate estimating methods for the crosswind-induced fatigue due to vortex induced vibrations. European international code provides a simple formulation for determining the alongwind-induced fatigue phenomenon, which is not suitable in every possible case (Eurocode 1, 2005; CNR, 2008).

Due to the importance of developing studies on the wind-induced fatigue analysis, in order to improve the basic conceptual and theoretical knowledge in the field and to derive reliable criteria for engineering purposes, a wide research project was carried out by Repetto and Solari between 2001 and 2012. A refined closed-form solution of the alongwind-induced fatigue of steel slender structures has been obtained, from which a simplified procedure suitable for engineering evaluation and code provisions has been derived (Repetto and Solari, 2009, 2012; CNR review, 2018).

This thesis tries to give a decisive contribution to this important achievement, generalizing the method for a broader range of cases and situations. The proposed method, in the absence of deeper analyses, can be applied to slender structures or structural elements of different materials subjected to the joint effect of static and variable loads induced by the wind and other permanent loads acting on the structure. The simultaneous effect of other variable loads, such as mobile loads, traffic and waves, is not taken into account. The procedure allows to evaluate the wind induced fatigue life of structures due to the longitudinal and lateral turbulence actions. Conservatively, the proposed method considers the wind blowing from the most unfavourable direction for the structural response (non-directional analysis). The vortex shedding-induced fatigue is analysed and discussed separately, providing many considerations and suggestions about the current standard method (Eurocode 1, 2005).

The aim of the thesis is pursued organizing the work in two significant steps. The first step revises the fatigue analysis approaches for structures, focusing attention on fatigue resistance curves provided by codes and recommendations and on the analytical formulation derived by Repetto and Solari in 2012, identifying its hypotheses and limitations. Reviewing the whole analytical demonstration, a new generalized simplified formulation suitable for engineering procedures format has been obtained, valid for different materials and for different stress conditions. The second step, carried out in parallel with the previous one, starts from the general framework of the wind-induced response analysis of slender structures, arriving to a generalized strategy to evaluate both alongwind and crosswind induced fatigue on slender structures, considering both turbulence and vortex shedding effects. All the input parameters are discussed and their equations are defined according to standards format. A final focus is intended to investigate the propagation of uncertainties in vortex shedding induced fatigue assessment by means of some case studies.

The first step of the study is developed in Chapters 2 and 3. Chapter 2 introduced the state of the art about wind-induced fatigue on slender structures, firstly describing the fatigue phenomenon, different approaches to determine fatigue resistance according to international recommendations, cycles counting methods proposed in scientific literature. Then it focuses on the alongwind-induced response and fatigue fundamentals, in particular on hypotheses and assumptions at the basis of Repetto and Solari model. Chapter 3 derived the closed-form solution introducing the first original contribution of the thesis to the original method: it generalizes the whole formulation by taking into account different possible fatigue resistance curve trends. In particular, the novelty is the Generalized fatigue curve factor. All formula are simplified in accordance with standard format.

The second step of the research project is developed in Chapters 4 and 5. Chapter 4 reports the general alongwind and crosswind turbulence-induced fatigue method and two levels of calculation are defined for some particular cases. The analytical model requires the definition of many input parameters, each of them is described in this Chapter in simple format. On the other hand, Chapter 5 focuses on vortex shedding-induced vibrations effect on fatigue damage. It firstly describes the phenomenon and the most commonly adopted mathematical models. As concerns code design procedures to estimate vortex induced vibrations (VIV) response and fatigue, different case studies are analysed. The possibility to study separately gust buffeting and VIV effects in fatigue analysis, as well as in ultimate response analysis, is discussed. Then, the VIV-induced fatigue standard method is studied in detail and some suggestions are proposed. VIV response uncertainties propagation role is considered.

Chapter 6 includes some examples for each of the problems dealt with, in order to illustrate the reliability of the proposed solutions compared with the inspections or with the numerical solutions and to point out the most noteworthy engineering considerations from both a qualitative and a quantitative viewpoint.

The conclusions are summarised in Chapter 7, illustrating the main results and some possible future perspectives for further developing research activities on this important topic.

Appendix A reports some mathematical derivations not included in the main text.

CHAPTER 2 - WIND-INDUCED FATIGUE ON SLENDER STRUCTURES

2.1. INTRODUCTION

Fatigue of materials is a critical phenomenon of damage which can lead to structural failure under cyclic actions of amplitude lower than design loads, without appreciable plastic deformations. Thus, fatigue may determine weak structural failure without exceeding ultimate strength. This phenomenon is one of the most critical failure modes to be considered in mechanical and structural engineering. More than 80% of all observed service failures in mechanical and structural systems are due to fatigue. Moreover, fatigue failures are often catastrophic, coming without warning.

Although the fatigue phenomenon has been largely studied in history from sixties of the 19th century on, this matter is still affected by many uncertainties: laboratory data do not cover all possible loading cases and are characterized by an enormous statistical scatter; environmental processes that produce fatigue loading are affected by many uncertainties; cycles counting and cumulative fatigue damage procedures are often based on many simplified assumptions; the geometry of the components and the presence of defects and discontinuities complicate the prediction of initiation and propagation of fatigue cracks; the effects of temperature and corrosion on fatigue strength are not yet well known. Facing with these issues, some methods have been developed to model and analyse the fatigue phenomenon from an engineering point of view.

Fatigue damage of structural and non-structural components depends, in general, on the number of stress cycles, the stress ranges of cycles and the mechanical properties of the material.

Fatigue predictions can follow several approaches, differing in the level of stress and strain analysis used (IIW Recommendations, 2016; Fricke, 2014). The general criterion is that the level of stress and strain analysis in the design phase must match that used in the determination of fatigue strength data. Factors that are ignored in the stress analysis, are left to the fatigue strength criteria, which are generally determined empirically, on the base of laboratory data on material specimens or structural component. Considering the conventional nominal stress approach, the fatigue strength of a structural component is obtained by *S-N* experimental curves provided by codes. Fatigue international standards and recommendations give information on structural fatigue resistance for steel and aluminum components (Eurocode 3, 2005; Eurocode 9, 1998; IIW Recommendations, 2016; Aluminum Design Manual, 2015). Fatigue resistance of other materials used in civil engineer is a very critical issue.

Then, cycles counting represents the fundamental step in the fatigue damage evaluation to provide a quantitative definition of the actual loading condition on the structure. Definition of reliable “cycle

counting methods" is one of the main issues of research works in fatigue field. These methods are necessary to identify the number of cycles that stresses the structures and to obtain a "cycle histogram" from the stress time-history at the detail.

Thus, once the fatigue approach is determined, the fatigue strength criteria are defined and a reliable cycles counting method is applied, a fatigue analysis can be carried out. The total cumulative damage is expressed by means of a suitable cumulative damage law. Among all the proposed procedures, the linear accumulation law is still adopted in many standards. The critical total damage value, corresponding to failure, is conventionally defined as equal to one (Miner, 1945). The fatigue life is defined as the time in which total damage reaches the unit.

Slender structures exposed to wind may experience large vibrations and repeated stress cycles, so that they can be strongly affected by fatigue. In these situations, damage often appears in the welded or bolded joints. Several collapses due to wind loading are related to fatigue (Holmes, 2002; Repetto and Solari 2010). This phenomenon may occur at moderate and frequent wind velocities and can be related to the dynamic response of structure to turbulence actions or to the vortex shedding phenomenon. Typical kinds of structures sensitive to wind induced fatigue are, for instance, urban light poles, masts, towers and traffic signal structures, that are strongly affected by dynamic response due to turbulence action; chimneys or cylindrical part of structures, that suffer for vortex shedding induced-vibrations; other complex structures such as wind turbines, bridges and cranes, which can be damaged by the non-linear combination of wind and other variable loading fatigue.

This Chapter gives a general overview on the fatigue analysis procedures, particularly within the wind loading field. In Section 2.2 the attention is focused on different approaches and cycles counting methods descriptions, whereas Section 2.3 deals with fatigue induced by wind loading, explaining the basis of the mathematical models concerning the phenomenon, focusing on alongwind-induced fatigue of steel slender structures.

In particular, Section 2.2 describes the general framework of fatigue analysis according to three paragraphs. Paragraph 2.2.1 introduces the fatigue phenomenon with its physical characteristics and the basics of commonly used approaches in engineering sectors. Therefore, in Paragraph 2.2.2, some stress-resistance fatigue approaches are briefly illustrated; *S-N* fatigue resistance curves for different structural details are introduced and their characteristics are shown, according to current standards and codes. Then Paragraph 2.2.3 deals with cycles counting methods; definitions for a deterministic time-history and for a random loading process are presented, discussing different approaches in time-domain or in frequency-domain.

Section 2.3 presents the basis of alongwind-induced fatigue methods proposed in literature, which have tried to address the shortcomings identified in the codes and standards methods. In particular, Repetto and

Solari (2012) proposed a procedure for determining alongwind-induced fatigue in closed form, thanks to the introduction of a hierarchy of hypotheses. First, the main concepts concerning wind field, wind loading and wind-induced response are introduced in Paragraph 2.3.1. Secondly, a suitable bi-modal counting method to obtain the cycle histogram in closed form, knowing the alongwind structural response on varying wind velocity, is defined in Paragraph 2.3.2 (Repetto and Solari, 2006). Finally, simplifying hypotheses adopted in order to obtain a closed form solution of the problem are introduced in Paragraph 2.3.3 (Repetto and Solari, 2009, 2012).

2.2. GENERAL FRAMEWORK OF FATIGUE ANALYSIS

Fatigue is a complex, local and progressive phenomenon of damage accumulation that takes place in structural components subjected to time-varying external loading, giving rise to a deterioration of the material strength that can lead to structural failure without appreciable plastic deformations. At present, phenomenological and analytical models are available for assessing the fatigue damage and the fatigue life of structures.

2.2.1. Fatigue phenomenon and analysis

The qualitative description of the phenomenon takes a lead from the observations of the cracked surface of specimens since the 60's (Peterson, 1960; Cazaud, 1969; Barsom, 1971). When a specimen is subjected to a fluctuating stress, many changes take place at the atomic level: a migration of dislocations and a localised plastic deformation. Multiple micro-cracks are created, growing slowly and independently in a shear mode: this is called *crack initiation phase*. The initiation of the crack involves a small area of the surface; the presence of superficial defects of the material can lead to initiate and propagate the phenomenon. The micro-cracks interact with each other, until they link creating a dominant crack. This crack begins to grow rapidly into the cross-section, during the *crack propagation phase*. The failure occurs when the residual cross-section area does not resist to the external action any further.

The crack look is due to these three phases: the initiation period (cyclic slip, crack nucleation and micro-crack growth), the macro-crack growth period and the final failure. The first phase imply decohesion in the material, visible as a fracture, in which striations can be detected. They indicate that crack extension occurred in a cycle-by-cycle sequence. Striations also show that the crack front is not simply a single straight line, but it is indeed a curved line and the crack tip is rounded. Basic aspects of the fatigue crack initiation process are: the significance of the free material surface, the irreversibility of cyclic slip, and environmental effects on micro-crack initiation. It is worth notice that fatigue crack initiation is a surface phenomenon. As soon as cracks are growing into the material away from the free surface, only the ends of the crack front can be observed at that free surface. If the cross-section can be observed after the propagation phase, the fatigue fractures look rather flat as viewed by the unaided eye,

but under the microscope the crack growth path could be rather irregular, going up and down in some random way depending on the type of material. As a result, fatigue on a microscale can be significantly different for different materials (Schijve, 2003).

Many different external conditions may affect the fatigue physical phenomenon. For instance, the corrosion due to environmental characteristics has a great effect on the fatigue behaviour of metals, reducing drastically the fatigue resistance of specimens (Brown, 1977).

In order to obtain fatigue data, it is necessary to run tests on the macroscopic behaviour of the material or structural component of interest, up to now.

Starting from the experiences of Wohler (1860-70), the fatigue strength of a specimen is obtained by counting the number N of the cycles with constant amplitude Δ that produces fatigue failure. The number N of the cycles leading to failure increases on decreasing the stress amplitude Δ of the cycles (Fig. 2.1).

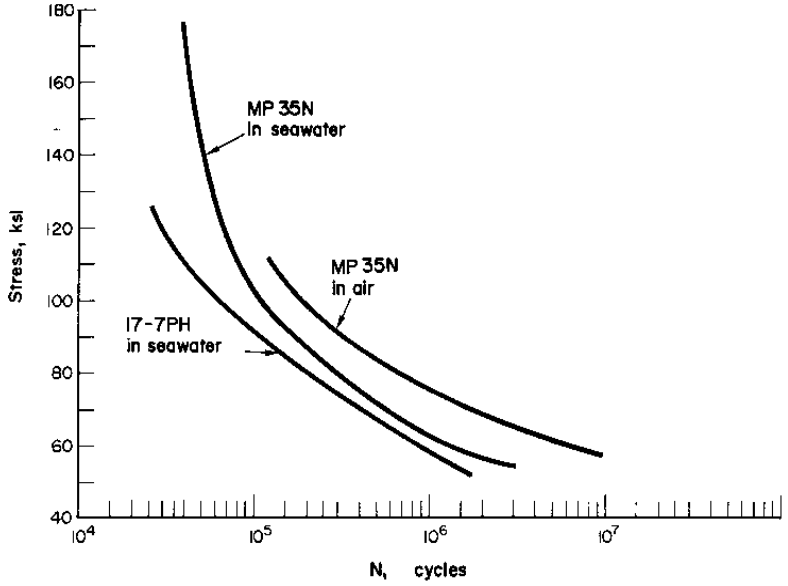

Figure 2.1: Original Wohler diagrams.

The effect of the non-null mean value of the cyclic stress has been analysed by many authors. Goodman (1930) proposed a diagram in which, fixed the number of cycles, the amplitude of the cycles leading to failure is given as a function of the mean stress. Fig. 2.2 shows the simplified form of a family of Goodman diagrams corresponding to different number of cycles; the mean value of the loading is reported in abscissa, the mean and maximum values of the constant amplitude cycles can be read on the ordinate. The equivalent amplitude Δ_e is the amplitude of the nil mean cycles equivalent, in terms of damage, to the amplitude Δ associated with a mean stress $\bar{s}$. It is expressed by:

$$\Delta_e = \frac{\Delta s_u}{s_u - \bar{s}} \tag{2.1}$$

where s_u is the ultimate strength.

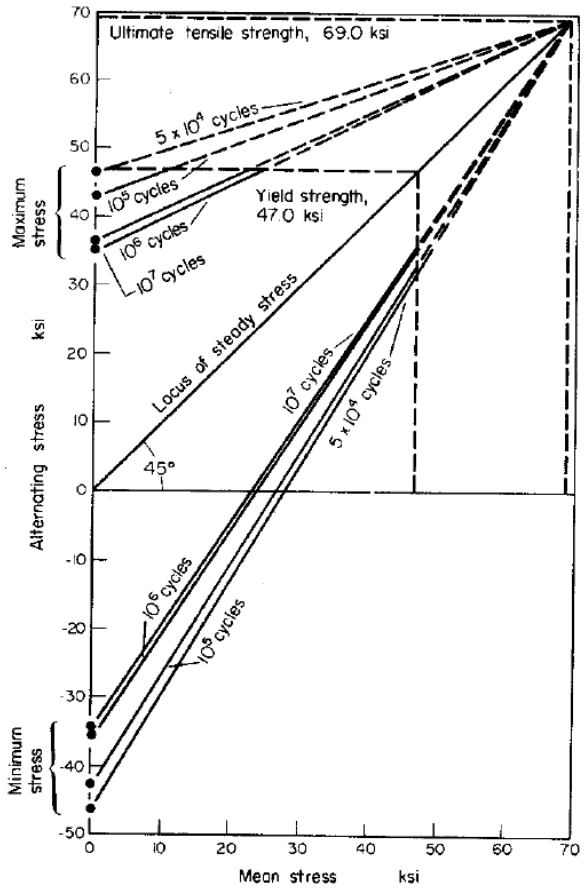

Figure 2.2: Modified Goodman diagrams.

The general frame of fatigue analysis is described below.

In fatigue analysis, loading actions and fatigue resistance should be related by means of appropriate assessment procedures. Actions, resistance and assessment procedure must be consistent with each other, so the level of structural response analysis in the design phase matches that used in the determination of fatigue strength data. Factors ignored in the stress analysis should be considered empirically in fatigue strength criteria.

The conventional fatigue analysis starts from the knowledge of appropriate fatigue strength curves showing the number of cycles at constant amplitude leading to failure. Fatigue curves are obtained from fatigue tests, in which material specimens or structural components are undertaken to a zero mean constant amplitude sinusoidal loading history, and the number of cycles until failure is counted. Note that, in general, the input of fatigue analysis can be represented by a stress or strain time history. When a large number of samples are tested with a range of constant loading amplitudes, the results are said to define the fatigue curve of the material. For many materials or structural components, the curve is well

approximated by a straight line in bi-logarithmic scale. However, a wide variety of empirical forms of fatigue curves are employed. Models used in mechanical and structural practice define the fatigue curves, referred to as *S-N* curves, as broken line in which the *k*-th segment is given by:

$$N\Delta^{m_k} = a_k \qquad \left(\Delta^{(k-1)} \le \Delta \le \Delta^{(k)}\right) \tag{2.2}$$

where a_k and m_k are constants depending on the material or structural component, N is the number of cycles that causes the failure, Δ is the stress cycles amplitude (Fig. 2.3).

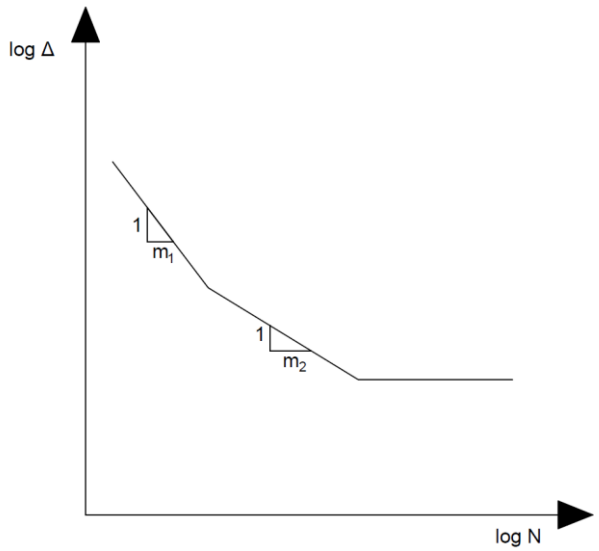

Figure 2.3: *S-N* curves in log-log scales expressed as broken lines.

Fatigue tests of some materials show an endurance limit Δ_L, i.e. a value of cycles amplitude below which N tends to infinite and fatigue failure does not occur. This limit, namely *cut-off limit*, gives rise to a horizontal segment in the broken line in Eq. (2.2). The presence of a non-null mean stress can be taken into account using Goodman relationship, substituting the equivalent amplitude given in Eq. (2.1) into Eq. (2.2).

The *S-N* approach works for high cycle fatigue, in which the elastic behaviour of materials is assumed until failure. A strain-life model may be used to analyse the high-strain low-cycle fatigue range, in which the loading amplitude is near the elastic strength of material and the plastic behaviour becomes essential (Ballio and Castiglioni, 1994; Ballio et al. 1997).

The fatigue analysis under nil mean constant amplitude stress histories is completely defined by the appropriate fatigue curve. The fatigue analysis under variable amplitude stress histories becomes more difficult. Fatigue damage increases in a cumulative manner. The fatigue failure occurs when the total accumulated damage reaches a critical value. The cumulative damage rate depends both on the amplitude of the cycles and on their sequence, as well as many other aspects.

In 1945 the Palmgren-Miner linear accumulation rule was proposed (Miner 1945), based on the assumption of constant work absorption per cycle, according to which one cycle of amplitude Δ produces a fraction of damage equal to:

$$d(\Delta) = \frac{1}{N(\Delta)} \tag{2.3}$$

$N(\Delta)$ being the failure number of cycles with Δ constant amplitude. Assuming that the fractional damages due to different stress cycles amplitude Δ_j (j = 1,2…) can be linearly added, the total cumulative damage is expressed by:

$$D = \sum_j d_j \tag{2.4}$$

where d_j is the fraction of damage induced by the j-th block of cycles of amplitude Δ_j:

$$d_j = \frac{n_j}{N_j} \tag{2.5}$$

Experimental results performed by Miner (1945) showed that failure could occur at different values of the total damage: if the loading sequence presented decreasing cycles amplitudes, failure occurred at D<1; if the loading sequence presented increasing cycles amplitudes, failure occurred at D>1. As the Palmgren-Miner rule disregards the loading sequence, the critical total damage value, corresponding to failure, is conventionally defined as equal to one; the fatigue life is defined as the time in which D reaches the unit. The linear Miner accumulation law remains the most commonly adopted so far.

2.2.2. Different approaches and fatigue resistance

The fatigue life prediction of structural components requires appropriate stress analyses, adapted to the method of the fatigue analysis. Three basic approaches to fatigue life prediction are here introduced: the nominal stress approach, the structural geometric (or hot spot) stress approach and the local notch stress or strain approach. They differ in the level of stress and strain analysis, both for the design calculations and for the determination of fatigue properties from the test specimens. It is determinant that the level of stress analysis adopted corresponds to the fatigue assessment procedure applied. The correspondence between the fatigue actions and the fatigue resistance curves for the three basic approaches is:

- Nominal stress – *S-N* curves of classified structural details;
- Geometric (hot spot) stress – *S-N* curves in terms of geometric stress;
- Effective notch stress – Universal *S-N* curve

It is worth notice that the stress range is defined as the difference between the maximum and the minimum value of the stress cycles:

$$\Delta = \sigma_{max} - \sigma_{min} \tag{2.6}$$

The nominal stress is defined as the global stress calculated in the cross-section under consideration, assuming a linear elastic behaviour of the material and disregarding the local stress raising effects of the welded joint, but including the stress raising effects of the macro-geometric shape of the component in the vicinity of the joint. The fatigue resistance *S-N* curves of classified structural details are based on nominal stress, disregarding the stress concentrations due to the welded joint. Therefore, the measured nominal stress must exclude the stress or strain concentration due to the corresponding discontinuity in the structural component.

The geometric stress approach is recommended for welded joints characterized by a structural geometry not comparable with any classified structural detail. The structural or geometric stress σ_{hs} at the hot spot includes all stress raising effects of a structural detail excluding that due to the local weld profile itself. So, the non-linear peak stress σ_{nl} caused by the local notch, i.e. the weld toe, is excluded from the structural stress (Fig.2.4 a). The structural stress is dependent on the global dimensional and loading parameters of the component in the vicinity of the joint. It is determined on the surface at the hot spot of the component which is to be assessed. The structural hot-spot stress can be determined using reference points by extrapolation to the weld toe under consideration from stresses at reference points (Fig. 2.4 b).

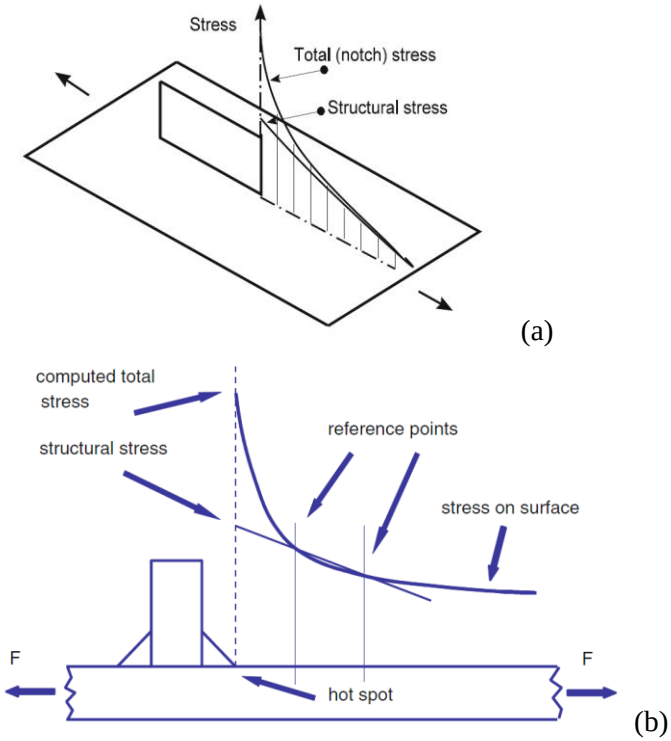

Figure 2.4: Notch stress and structural hot-spot stress (a); definition of structural hot-spot stress (b) (Figures © IIW, 2016).

Methods and formulae to calculate the hot-spot stress are provided by some international recommendation (e.g. IIW, 2016), using measurements or adopting the Finite Element Analysis (FEA) to evaluate the stress values in the reference points. The FEM mesh needs particular attention, especially near the critical points (Niemi E, Fricke W, Maddox SJ, 2006). An important advantage of the geometric stress approach is the possibility of predicting the fatigue life of many types of joint configurations using a single reference *S-N* curve, which differs for weld types, material, thicknesses or environmental effects. An alternative way is to evaluate fatigue resistance using a reference detail; the procedure allows to correct the *S-N* curve obtained with the nominal stress approach corresponding to a detail category selected as close as possible to the geometric and loading parameters of the structural details under analysis.

Effective notch stress is the total stress at the root of a notch, obtained assuming linear-elastic material behaviour. To take account of the variation of the weld shape parameters, as well as of the non-linear material behaviour at the notch root, the actual weld contour is replaced by an effective one. For fatigue assessment, the effective notch stress is compared with a single fatigue resistance curve, although it is necessary to check that the fatigue resistance curve for parent metal is not exceeded in the direct vicinity of the weld. More details for practical application can be found in reference (Fricke W, 2008).

Obviously, due to the simplicity of the stress analysis required, the fatigue assessment adopted in many structural codes is based on the nominal stress range. However, the classification of structural details and welded joints used by this approach can not be actually completed, even if it can be improved ever more.

The fatigue *S-N* curve of each structural detail is based on representative experimental investigations on small size or full-scale specimens. The fatigue resistance data are usually obtained from constant amplitude tests by measuring the number of cycles until failure, corresponding to any value of nominal stress range. The nominal stress range is measured in structural points remote from all discontinuities, where all structural and local notch effect are negligible. Conventionally, the complete rupture in small size specimens and the observation of a through wall crack in large components are usually considered, respectively, as failure criteria.

As previously mentioned (Paragraph 2.2.1), the *S-N* curves are of the form:

$$N = \frac{a}{\Delta^m} \tag{2.7}$$

where N is the number of cycles that causes the failure; a is a constant value; Δ is the nominal normal or shear stress range; m is the slope of the curve in the bi-logarithmic scale, which may adopt different values over the range of possible fatigue lives, from the low endurance to the high cycle regime.

All fatigue resistance data are given as characteristic values, which are assumed to represent a survival probability of at least 95%, calculated from the mean value on the basis of two-sided 75% tolerance limits

of the mean, unless otherwise stated. Other existing definitions as e.g. a survival probability of 95% on the basis of 95% one-sided limit of the mean or mean minus two standard deviations corresponding to a survival probability of 97.7% are practically equal for engineering applications.

The nominal stress range should be within the limits of the elastic properties of the material. The range of the design values of the stress range shall not exceed $1.5 \cdot f_y$ for nominal normal stresses or $1.5 \cdot f_y/\sqrt{3}$ for nominal shear stresses.

The fatigue resistance of a welded joint is also limited by the fatigue resistance of the parent material.

The fatigue curves are based on representative experimental investigations and thus include the effects of:

- structural hot spot stress concentrations due to the detail shown;
- local stress concentrations due to the weld geometry;
- weld imperfections consistent with normal fabrication standards;
- direction of loading;
- high residual stresses;
- metallurgical conditions;
- welding process (fusion welding, unless otherwise stated);
- inspection procedure, if specified;
- post weld treatment, if specified.

Furthermore, within the limits imposed by static strength considerations, the fatigue curves of welded joints are independent of the tensile strength of the material.

Each fatigue strength *S-N* curve is identified by a particular shape in the bi-logarithmic diagram and by the fatigue class Δ_C = the characteristic fatigue strength of the detail in MPa at N_C = 2 million cycles, which is constant and different for every classified structural detail of a material. The first characterization depends on the material and the stress field nature in the analysed cross-section (normal or shear stresses). The second characterization depends on the particular structural detail configuration.

As regard the *S-N* fatigue curve shapes, the scatter obtained by experimental tests is usually approximated by broken straight lines in bi-logarithmic scale (see Section 2.2.1). Fatigue international standards and recommendations give information on structural fatigue resistance for steel and aluminum components; in Europe in particular, steel material is concerned in Eurocode 3 (2005) and in IIW Recommendation (2016); aluminium material in Eurocode 9 (1998) and in IIW Recommendation (2016). Other materials are analysed in many research works and specific recommendations. Some examples are “Specification for Aluminum Structures: Aluminum Design Manual 2015” which are American recommendations concerning aluminium details fatigue resistance (Aluminum Association, 2015) and research works which provide *S-N* fatigue experimental curves of particular details of different materials,

such as aluminium (Atzori et al., 2009; Daneshkhah and Menzemer, 2017) or composite materials (Sharba et al., 2016).

Usually, linear curves in the bi-logarithmic diagram are provided for some particular materials such as some types of glasses, composites and concretes. Fatigue resistance of composite materials is a very critical issue, due to the variety of parameters and governing mechanisms. Main parameters influencing fatigue resistance are basic constituent, fiber properties, matrix properties, ply orientation and fiber fraction (Bathias, 2011). Bilinear curves may be distinct in two kinds, one is characterized by a cut-off limit and the other by two different slopes. Examples related to the bilinear type are *S-N* curves for shear stresses in steel elements and for aluminium ones. Finally, trilinear curves (e.g. *S-N* curves for normal stresses in steel elements) have two different slopes and a cut-off limit, but they are about to be adapted to bilinear shape (IIW, 2016).

The most common case concerns the fatigue curves for nominal normal stress amplitudes corresponding to steel structural details. The code (Eurocode 3, 2005) provides trilinear curves in bi-logarithmic scale (Fig. 2.5) represented in analytical form as:

$$\begin{aligned} N &\to \infty && \text{for} && \Delta \le \Delta_L \\ N &= a_2 / \Delta^{\,5} && \text{for} && \Delta_L < \Delta < \Delta_D \\ N &= a_1 / \Delta^{\,3} && \text{for} && \Delta \ge \Delta_D \end{aligned} \tag{2.8}$$

where a_1 and a_2 are constant parameters for the respective broken lines; Δ_L and Δ_D are two amplitude values corresponding to the cut-off limit at N_L = 10^8 and to the knee of the curve at N_D = 5 x 10^6, respectively.

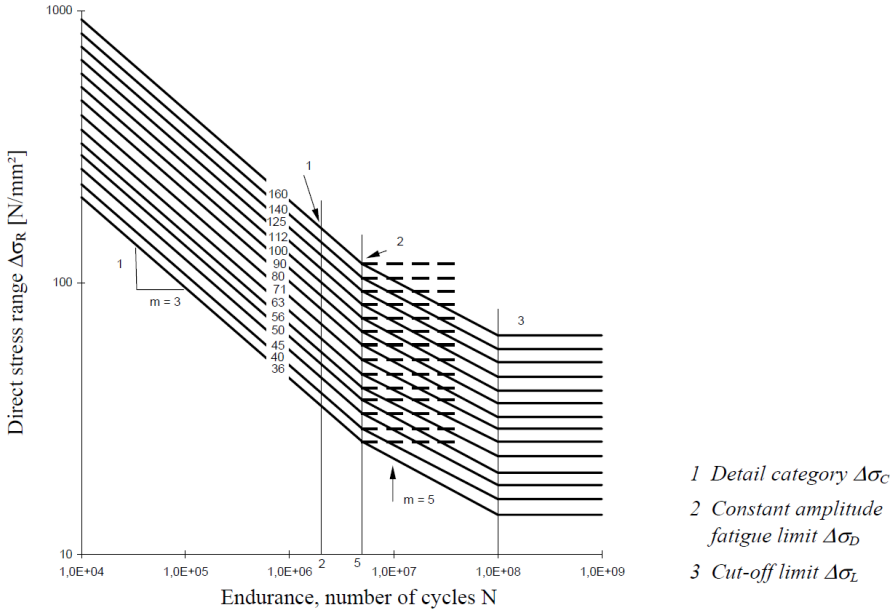

Figure 2.5: Standard set of *S-N* curves for normal stresses in steel elements (Figure © Eurocode 3, 2005).

Codes also provide bilinear fatigue curves for shear stresses corresponding to steel structural details (Eurocode 3, 2005). Trilinear tending to bilinear curves are provided for aluminium structural elements (Eurocode 9, 1998).

The more recent IIW Recommendation (2016) tries to give an effective and consistent set of *S-N* fatigue curves for these two materials, both for direct and for tangential stresses, with only one approximated shape: the bilinear shape, with or without the cut-off limit, with different slope values for different cases. These new bilinear curves give the same results in terms of fatigue analysis than the ones provided by Eurocodes. Therefore, the same basic case of normal stresses in steel details is represented by the curves in Figure 2.6 and by the equation:

$$\begin{aligned} N &\to \infty \quad \text{for} \quad \Delta \le \Delta_L \\ N &= a/\Delta^{\,3} \quad \text{for} \quad \Delta \ge \Delta_L \end{aligned} \tag{2.9}$$

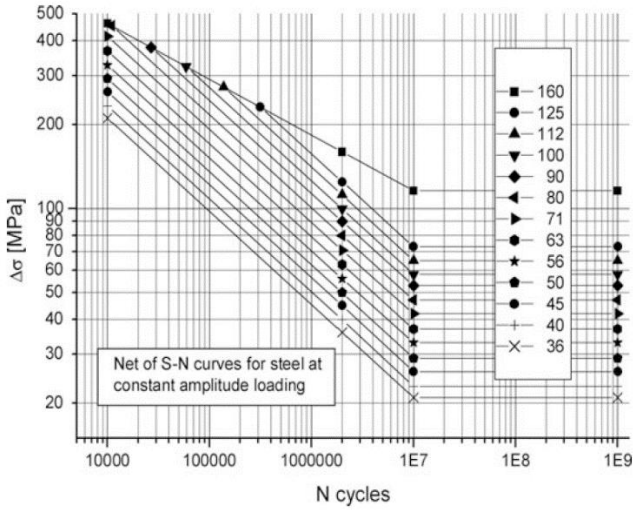

Figure 2.6: Bilinear *S-N* curves for normal stresses in steel elements, standard applications (Figure © IIW, 2016).

The slope of the fatigue strength *S-N* curves for details assessed on the basis of normal stresses is again $m = 3$, while the constant amplitude knee point is assumed to correspond to $N_L = 10^7$ cycles (cut-off).

The slope of the fatigue strength curves for details assessed on the basis of shear stresses is $m = 5$, but in this case the knee point is assumed to correspond to $N_L = 10^8$ cycles.

The conventional assumption is that the *S-N* curves terminate at a fatigue limit, below which failure will not occur, or in which case the *S-N* curve becomes a horizontal line. Traditionally, this constant amplitude fatigue limit remains the most common assumption, even if new experimental data indicate that

a cut-off limit does not exist and the *S-N* curve should continue on the basis of a further decline in stress range of about 10% per decade in terms of cycles, which corresponds to a slope of $m = 22$.

This issue is only relevant if a design is expected to withstand very large numbers of stress cycles, such as for example at rotating welded machine parts. The matter is still under development and users should consult the latest relevant literature.

Meanwhile, the cases of steel subjected to very high cycles applications and of aluminium details are proposed with the extrapolation beyond 10^7 cycles at a slope of $m = 22$.

If structural details of these two materials are classified in such a consistent document, details made of other materials are often not classified and generally studied case by case. Composite elements are often approximated by straight line *S-N* curves with high slope values.

2.2.3. Cycles counting methods

Cycle counting is the process of converting a variable amplitude stress sequence into a series of constant amplitude stress range cycles that are equivalent in terms of damage to the original sequence.

The use of a cumulative damage model, such as the linear Palmgren-Miner rule, and of experimental *S-N* fatigue curves requires the decomposition of the actual loading time-history into a sequence of constant amplitude cycles. Starting from the loading time-history, cycles amplitudes can be identified using a suitable cycle counting method. Several definitions of cycle counting procedures have been proposed in literature, but only Rainflow count leads to good predictions of the actual fatigue life (Dowling, 1972).

One possible loading cycles representation is the range histogram, which represents a series of blocks proportional to the number of cycles of constant amplitude, varying the amplitude level. Histogram representation does not retain any information about the order in which cycles have been counted. However, this is suitable with the cumulative damage model used, the Miner law.

Fatigue loading due to environmental actions is very often represented by a random process. In this case, total accumulated damage and predicted fatigue life also vary randomly. The problem can be dealt with using two different approaches, well developed in research literature. The first requires the application of time-domain cycles counting methods to simulated samples of the loading process. Assuming the process as stationary, the second approach describes fatigue damage starting from the spectral properties of the loading process. For Gaussian narrow-band processes amplitude and peak distributions coincide and the mean total damage can be obtained in closed form. For different types of processes, the hypothesis of coincidence between the probability densities of amplitudes and peaks can give rise to great errors.

A parallel approach to fatigue analysis derives from fracture mechanics. Its key ingredients are the initial crack side, crack driving force solution, applied stress and material properties describing the crack

growth characteristics (Paris and Erdogan, 1963). The most popular analytical formulation is the Paris law (Paris, 1964). The advanced methods of fracture mechanics for prediction of subcritical growth of cracks and final crack instability are analysed by many authors (Kanninen and Popelar, 1985; Anderson, 1991; Spencer, 1993; Fricke, 2003).

In this Section 2.2.3, firstly deterministic loadings and then random loadings are taken into account: some definitions of cycles counting procedures are presented, since the concept of these methods, used to transform a loading time history into a set of cycles, will be helpful in the following steps of this thesis.

- *Deterministic loadings*

Loads and the resulting fatigue actions (i.e. stresses) in real structures usually fluctuate in an irregular manner and give rise to variable amplitude loading. The stress range may vary in both magnitude and period from cycle to cycle. The stress history is a record and/or a representation of the fluctuations of the fatigue actions in the anticipated service time of the component. It is described in terms of successive maxima and minima of the stress caused by the fatigue actions (Fig. 2.7). It should aim to cover all loading events and the corresponding induced dynamic response in a conservative way.

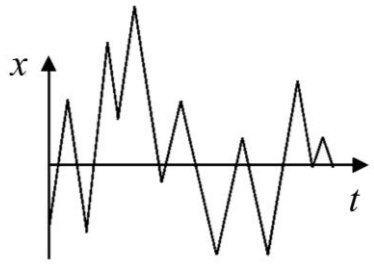

Figure 2.7: Example of stress fluctuations time history.

Therefore, a cycle is completely defined by its highest and lowest points and by the time t at which the cycle is counted. The amplitude of the cycle is then defined as the difference between the highest and lowest values, the mean value is the half of their sum. It is worth notice that the registration of time t allows to know the loading sequence.

Let $x(t)$, $t \in [0,T]$, be a continuous function representative of the input to fatigue analysis (e.g. stress time history $s(t)$). Among all the methods proposed in literature, the Rainflow Counting (RFC), the Peak-Valley Counting (PVC) and the Peak Counting (PC) are frequently used. The Rainflow or similar 'Reservoir' methods are recommended for counting stress ranges (Endo et al., 1967, 1974).

The Rainflow counting method defines a one-to-one correspondence between the sequences of the local maxima and minima of the loading time history. The definition proposed by Endo et al. (1967) has a

sequential structure to identify cycles ranges. The time-history is first converted into a series of peak and troughs. The time axis is oriented vertically, with the positive direction downward. The time series is then viewed as a sequence of roofs with rain falling on them. The stress cycles are defined in terms of the distances travelled by water flowing down the roof. A Rainflow path is started at each peak and trough; each path stops when it falls down from the roof without encountering a new roof. If the rain flowing down a roof intercepts flow from a previous path, the present path is stopped. A new path is not started until the path under consideration is stopped. Half-cycles are thus identified, whose amplitude is the projection of the rain flow path on the *x* axis. Figure 2.8 illustrates this procedure, showing the Rainflow paths and the correspondent half-cycles amplitudes.

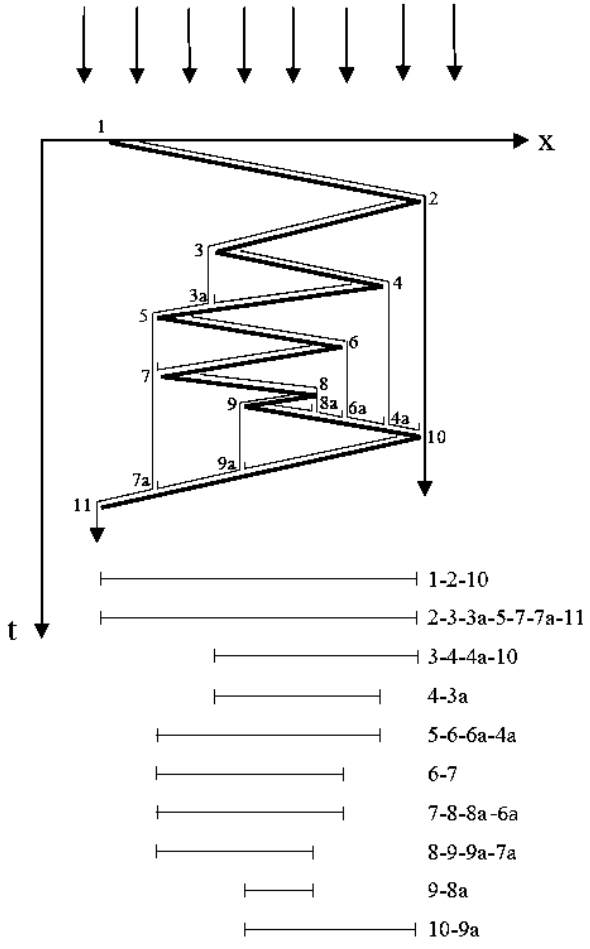

Figure 2.8: Rainflow counting method.

An alternative mathematical definition is given by Rychlik (1987), namely the Reservoir counting method, well explained by using the analogy of the flow of water from a reservoir, the boundary of which is the stress-time. Let t_i be a sequence of time points corresponding to the local maxima $x(t)$. For each local maximum, an appropriate cycle is analytically defined. The same results are obtained from each

method. These two methods treat the small cycles as interruptions of the larger cycles. In this way, both slowly varying large amplitude cycles and more rapid small reversals on the top or bottom of these are identified.

The Peak-Valley counting method (Rychlik, 1993) identifies each cycle as the difference between two successive local extremes, i.e. between the local maximum of x occurring at time t_i and the following local minimum. Thus, the PVC method uses only local information about the loading time history, as each local extreme is combined with the following one. In this way, the PVC has the characteristic that, if all small reversals are counted, the larger cycles are broken up and counted as several smaller ones.

The Peak counting method (Rychlik, 1993) takes into account all local maxima above the mean value of the time history and pairs them with fictitious local minima of the same size under the mean value. Thus, the PC method ignores a number of reversals corresponding to local maxima below the mean value. Furthermore, the method has the characteristic that all small reversals above the mean value are counted as much larger cycles.

The set of cycles obtained from a cycle counting method can be represented by counting distribution and histogram functions. The counting distribution function enumerates the cycles whose highest and lowest points are greater and lower than two thresholds values, respectively. It corresponds to the cumulative probability of stress range expressed in terms of stress range level exceedances versus the number of cycles. The counting histogram function enumerates the cycles whose highest and lowest points fall into small ranges of two thresholds values. The counting distribution and histogram functions are frequently defined in terms of amplitude, disregarding the mean value.

In the applications, the distribution and histogram functions in terms of amplitude are defined in discrete form, by a table of discrete blocks of cycles of amplitude included in stress ranges, typically up to 20 different stress levels. The assumed magnitude of the stress range in a given block would then depend on the conservatism required. Typical values would be the maximum or the mean of the stress range in the block.

The fatigue damage induced in a structure by a set of cycles can be evaluated in connection with a cumulative damage model, e.g. the Miner rule presented in Section 2.2.1, see Eqs. (2.3), (2.4), (2.5). The definition of the cycle counting methods highlights some differences in the resulting set of cycles; such differences lead to different estimations of the total accumulated damage and of the fatigue life prediction. Based on Dowling (1972) and Rychlick (1993) studies, it results that, under the Palmgren-Miner hypothesis, the total accumulated damage obtained using the Peak-Valley counting method is lower than the total damage obtained using the Rainflow counting method, which is in turn lower than the total damage provided by the Peak counting method (PVC $\leq$ RFC $\leq$ PC).

- *Random loadings*

Fatigue loading due to environmental actions is very often represented by a random process. In this case, the total accumulated damage and the predicted fatigue life also vary randomly. A complete probabilistic approach requires the knowledge of the probability distribution of the fatigue damage or of the fatigue life. The choice of the probabilistic model can be dealt with using two different approaches.

The first requires the application of time-domain cycles counting methods to simulated samples of the loading process or to measured time-histories. A cycles histogram is built for each simulated time-history, from which a sample of the total accumulated damage can be obtained. In order to assure accurate results, the evaluation of the damage must involve a large number of stress samples, extended to a representative time interval, thus the simulation procedure requires particular attention. This approach is well established and independent from random process characteristics, but it is very burdensome and time-consuming, both for the numerical simulation and for the fatigue analysis of samples. Many studies in scientific literature are based on this approach, analysing different structural types such as guyed mast (Clobes and Willecke, 2014), wind turbines (Benedetti et al., 2013), bridges (Klinger et al., 2014), tubular structures (Jia, 2011), marine structures (Wang et al., 2015), etc. Time-domain analysis is not suitable to basic standards verifications, except for wind turbines, that are structures precisely designed according to wind-induced fatigue.

Assuming the process as stationary, the second approach describes fatigue damage starting from the spectral properties of the loading process. The frequency-domain analysis requires definition of cycle counting for random loads and definition of the mean fatigue damage or mean fatigue life. It is synthetic and directly connected with spectral parameters, thus it would be suitable to be at the basis of codes methods, but it implies some simplifying hypotheses and it is dependent on random process characteristics. Most of research works are addressed in counting methods definitions.

The correlation between the power spectral density and the cycles amplitude distribution is known only for Gaussian narrow-banded processes. With these hypotheses, amplitude and peak distributions coincide and follow the Rayleigh model; so the mean total damage can be obtained in closed form. For different types of processes, the hypothesis of coincidence between the probability densities of amplitudes and peaks is unrealistic and it can give rise to great errors in fatigue damage evaluation. In general, the expected number of cycles per unit time, whose amplitude lies between Δ and $\Delta+d\Delta$, is given by:

$$n(\Delta) = \nu_{\Delta} p_{\Delta}(\Delta) \mathrm{d}\Delta \tag{2.10}$$

where $p_{\Delta}(\Delta)$ is the probability density function of amplitudes of the random process and ν_{Δ} is the expected frequency of amplitude. The problem is the knowledge of the probability density function of the

amplitudes $p_\Delta(\Delta)$ of the loading random process. This is in general unknown, except for narrow-band stationary Gaussian processes.

- Narrow-band processes

Let $S_x(n)$ be the one-sided power spectral density function of the stationary random process $X(t)$, expressed in the domain of frequency n. If the process is stationary, narrow-band and Gaussian, the power spectral density $S_x(n)$ provides an exhaustive description of the statistical properties of the process and its spectral content is concentrated around one value of the frequency. Under these hypotheses, the probability density function of the semi-amplitudes coincides with the probability density function of the peaks, following the Rayleigh distribution (Rice, 1944). Without loss of generality, if the process is assumed to have the mean value equal to zero, the mean rate of zero up-crossing ν_0 coincides with the mean rate of the total peaks and with the mean rate of the cycles ν_Δ. In this case, Eq. (2.10) assumes the form:

$$n(\Delta) = \nu_0 \frac{\Delta}{(2\sigma_x)^2} exp\left\{-\frac{\Delta^2}{2(2\sigma_x)^2}\right\} \mathrm{d}\Delta \tag{2.11}$$

where σ_x is the standard deviation of the process X and $2\sigma_x$ represents the standard deviation of the cycle amplitude process. The mean damage intensity $\bar{D}(1)$ can be solved in closed form when the fatigue curve is a straight line in the whole *S-N* diagram, therefore when a_k and m_k are fixed constants in Eq. (2.2), a and m. In order to use different forms of fatigue curves or different cumulative damage models, it could be useful to define the cycles histogram in discrete form. In this case, the mean number of cycles per unit time with amplitude Δ_j, which is representative of the interval $2x_{j-1} \le \Delta_j \le 2x_j$ where $x_j = j\delta x$ (j = 0, 1, 2, …) is a succession of thresholds, is given by the expression (Repetto, 2003):

$$n(\Delta_j) = \nu_0 \left[exp\left\{-\frac{(j-1)^2(\delta x)^2}{2\sigma_x^2}\right\} - exp\left\{-\frac{(j\delta x)^2}{2\sigma_x^2}\right\}\right] \tag{2.12}$$

where δx is an appropriate interval. These definition of the number of cycles n are equivalent and correspond to the application of the Peak counting method, which coincides with the PVC and the RFC under the hypothesis of narrow-band process.

- Broad-band processes

A common approach is the so called narrow-band approximation: the stationary Gaussian zero mean process is dealt with as an equivalent ideal narrow-band process, with the same values of ν_0 and σ_x. Under

this hypothesis, the mean damage intensity $\bar{D}(1)$ can be obtained in closed form by using the PC or the PVC, disregarding both the bandwidth and the shape of the spectral density function. The two results furnish two bounds for the fatigue damage estimation of stationary Gaussian processes. Depending on the spectral properties of the processes, the gap between the two bounds may be small or large. A general expression approximating the amplitude distribution obtained from the Rainflow cycles counting method is at present unknown. Wirsching and Light (1980) proposed to approximate the damage intensity $\bar{D}(1)$, under the Palmgren-Miner assumption for the cumulative damage rule, as a modification of the narrow-band approximation obtained applying PC, in the form:

$$\bar{D}(1)^{\mathrm{RFC}} = \lambda \cdot \bar{D}(1)^{\mathrm{PC}} \tag{2.13}$$

in which λ is a damage correction factor depending on the fatigue curve and on a bandwidth parameter. Many authors tried to define this factor but it seems to be very difficult to develop feasible theoretical models generally applicable to Gaussian processes with various spectral shape. Lutes et al. (1984) maintained that spectral bandwidth parameter is not sufficient to define correction of the narrow-band solution. Dirlik (1985) proposed a method based on the description of the amplitude PDF (power density function) as the combination of an Exponential and two Rayleigh PDFs, weighted by empirical coefficients dependent on the spectral moments $\tilde{m}_0$, $\tilde{m}_1$, $\tilde{m}_2$, $\tilde{m}_4$. Dirlik empirical formula derivation is based on extensive Monte-Carlo simulations and, as a PSD based cycle counting method, the formula derived from Dirlik often leads to reliable approximations of the Rainflow results. Many following research works are based on Dirlik solution; nevertheless, Rychlik (1992) showed that it is not possible to describe Rainflow damage only on the base of spectral moments. Therefore, the Rainflow approximation must be studied more closely for a given spectral shape.

- Broad-band processes with bi-modal spectrum

Attention is focused on a family of Gaussian processes which are the combinations of two narrow-band processes with well separated spectral components. Such types of processes are referred to as bi-modal processes, can be found in many problems, and can be schematised as the sum of two independent narrow-band Gaussian processes:

$$X(t) = X_{LF}(t) + X_{HF}(t) \tag{2.14}$$

where X_{LF} and X_{HF} are the low frequency component and the high frequency component, respectively. The sum of the power spectral density functions of the two components is equal to the spectral density function of X, $S_X(n)$. Without loss of generality, let us consider the normalised process

$X^*(t) = X^*_{LF}(t) + X^*_{HF}(t)$ (Fig. 2.9), obtained by scaling the original process *X* with respect to its standard deviation value. The number of cycles induced by *X* and *X** are equal, the amplitudes of *X* are obtained by re-scaling suitably the normalised amplitudes of *X**.

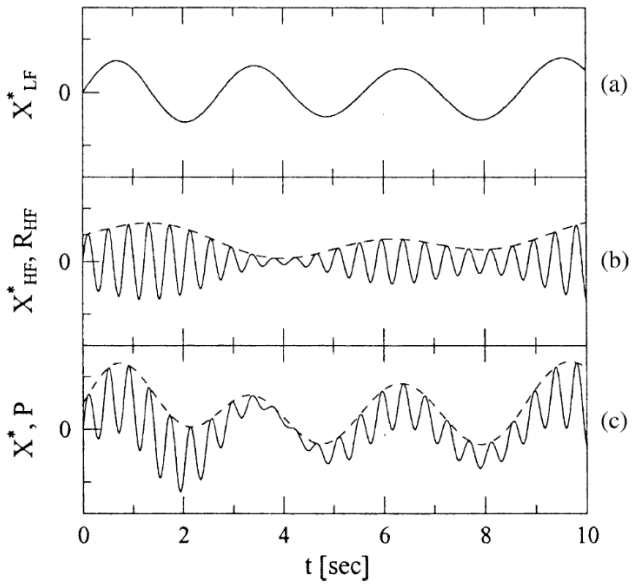

Figure 2.9: Sample of normalised bi-modal process: (a) low frequency component X^*_{LF}; (b) high frequency component X^*_{HF} (solid line) and its envelope R_{HF} (dashed line); (c) bi-modal process X^* (solid line) and its pseudo-envelope *P* (dashed line) (Figures © Repetto, 2003, 2005).

By applying the Rainflow counting principle to the process, it can be shown that there are two distinct cycles groups. One includes the large amplitude cycles, related to the envelope of the process. The other includes the small reversals related to the high frequency component (Fig. 2.9). The methods proposed in literature try to approximate their two contributions to the total accumulated damage.

The large cycles contribution is related to the pseudo-envelope *P* of the process *X** (Fig. 2.9), which is a stationary process defined as (Toro GR, Cornell CA, 1986):

$$P(t) = X^*_{LF}(t) + R_{HF}(t) \tag{2.15}$$

where X^*_{LF} is the normalised low frequency component, R_{HF} is the envelope of the normalised narrow-band high frequency component X^*_{HF} (Fig. 2.9). They follow a Gaussian and Rayleigh distribution, respectively.

The amplitude of small cycles is related to the high frequency component, so it follows the Rayleigh distribution.

Under these hypothesis, Jiao and Moan (1992) expressed the damage correction factor, but the simple addition of the two contributions from the two groups of cycles is not correct, as a number of small cycles have been already included in the large amplitude cycle evaluation. Repetto (2003, 2005) made advances in bi-modal processes induced fatigue, proposing the cycle histogram of a bi-modal stationary Gaussian zero mean process, written in analytical form.

By applying the Rainflow counting technique to the process X^*, the mean number of cycles characterised by the normalised amplitude Δ_j^* associated with the bi-modal process X^* per unit time is assumed as the sum of two separate contributions:

$$n\left(\Delta_j^*\right) = \hat{n}\left(\Delta_j^*\right) + \breve{n}\left(\Delta_j^*\right) \tag{2.16}$$

where $\hat{n}\left(\Delta_j^*\right)$ enumerates the number of the large cycles related to the pseudo-envelope of the process; $\breve{n}\left(\Delta_j^*\right)$ enumerates the number of the small cycles related to the high frequency component, taking into account the portion of cycles included into the first contribution.

The number of large amplitude cycles is evaluated by applying the PC method to the pseudo-envelope process P of the process X^* (Eq. (2.15)), assumed as narrow-band. This assumption leads to overestimate the contribution of large cycles thus it results always on the safe side. The mean number of large cycles can be written as equal to the mean number of cycles with normalised amplitude Δ_j^* due to the process P per unit time:

$$\hat{n}\left(\Delta_j^*\right) = n_P\left(\Delta_j^*\right) = \left[\nu_P\left(x_{j-1}\right) - \nu_P\left(x_j\right)\right] \mathrm{H}\left[\nu_P\left(x_{j-1}\right) - \nu_P\left(x_j\right)\right] \tag{2.17}$$

where $\nu_P(x)$ is the mean up-crossing rate of P and $\mathrm{H}[\cdot]$ is the Heavyside's function.

The number of small amplitude cycles is evaluated by applying the PC method to the high frequency process X_{HF} and by correcting the results considering the cycles related to the envelope process R_{HF}. This correction removes the error due to the mean number of cycles related to the high frequency component already counted in the large cycles histogram. The mean number of small cycles is then given by:

$$\breve{n}\left(\Delta_j^*\right) = n_{HF}\left(\Delta_j^*\right) - n_{R_{HF}}\left(\Delta_j^*\right) \tag{2.18}$$

knowing that X_{HF} is a stationary, Gaussian and narrow-band process, and applying the PC method to the envelope process R_{HF}, the mean number of cycles can be evaluated.

Substituting Eqs. (2.17) and (2.18) into Eq. (2.16) furnishes the mean number of normalised amplitude cycles per unit time of a bi-modal Gaussian process. The solution represents generally a good

approximation of the Rainflow counting method, always on the safe side. Thus, an approximated closed form of the mean number of normalised amplitude cycles of a bi-modal Gaussian process is provided by Repetto (2005).

2.3. BASIS OF ALONGWIND-INDUCED FATIGUE METHODS

The realization of more and more slender and low-damped structures exposed to wind, such as poles, masts, towers, signal supports, chimneys, lattice towers or wind turbines, increases their susceptibility to wind actions, leading to large amplitude structural vibrations.

Wind-structure interaction implies complex aerodynamic phenomena which result in alongwind, crosswind and torsional actions. The mean part of the structural response, in the alongwind direction, is linked with the mean wind velocity; the fluctuating part of the response is caused by the joint action of the oncoming wind turbulence and of the vortex wake.

As large vibrations may occur at moderate and frequent wind velocities, structures may undergo a great number of repeated stress cycles that lead to damage accumulation. Fatigue damages produced by these situations can be discerned from damages of other nature because of their micro and macro characteristics.

Several damages and collapses due to wind loading are attributed to fatigue, which have been observed for different kinds of slender structures, such as guyed masts (van Staalduinen, 1993), chimneys (Pritchard, 1984; Verwiebe and Glockner, 2003), cranes (Klinger et al., 1996), cantilever steel structures (Gilani and Whittaker, 2000; Hamilton et al., 2000) and poles (Robertson et al., 2001; Peil and Behrens, 2002; Caracoglia and Jones, 2006; Das et al., 2006; Alexander and Wood, 2009).

The literature attests in particular a great sensitivity to fatigue damage of the two latter structural types: Hamilton et al. (2000) reported that, after the failure of two traffic signal structures, an inspection of the Wyoming Department of Transportation indicated that roughly 1/3 of the poles inspected showed visible fatigue cracks; Caracoglia and Jones (2006) reported a multiple collapse of 140 tapered aluminum light poles in Illinois, 4–6 years after installation. All the authors highlight the complexity of the problem, involving meteorological, aerodynamic and mechanical aspects, and attest the lack of reliable engineering methods of analysis. Moreover, it is very hard to find complete sets of data on structural failures to use as a benchmark for fatigue analyses and studies (Repetto and Solari, 2010).

In previous Section 2.2 two possible approaches to analyse fatigue due to random processes, such as wind actions, are described. Time-domain analysis is carried out by Monte Carlo simulations of turbulence histories or by processing pressures measured in wind tunnel tests. The cycle counting applied to each time history of the stress process adopts classical deterministic criteria, such as the Rainflow counting method. Frequency-domain theoretical formulations depend on spectral characteristics of the

stress process, therefore alongwind and crosswind-induced fatigue analysis are usually dealt with separately.

Despite a wide research literature addressed to this issue, standards and codes related to wind-induced fatigue are still fragmentary. Eurocode 1 (2005) provides an expression for cycle histogram in alongwind fatigue assessment based on very simplified assumptions (Kemper and Feldmann, 2011). This code also provides reliable methods for evaluating the amplitude and number of load cycles due to vortex shedding. Other international standards are addressed to special kinds of structures, such as chimneys (CICIND, 1999), poles (AASHTO, 2015 – 2018) and wind turbine (IEA, 1990), adopting different approaches.

As concerns alongwind-induced fatigue, Wyatt (1984) analysed the problem of alongwind-induced fatigue on lattice towers, evaluating the number of cycles at an equivalent stress range estimated at a given reference wind velocity value and direction and introducing suitable parameters in order to take into account the effective probabilities of wind velocities and directions. Patel and Freathy (1984) introduced a normalized damage, evaluated numerically, and formulated a denormalizing factor depending on the wind data and on the structural parameters. Dionne and Davenport (1988) introduced a simple relationship between the alongwind gust factor and fatigue damage. Mikitarenko and Perelmuter (1998) and Petrov (1998) dealt with wind-induced fatigue by frequency domain probabilistic criteria that are quite difficult to apply in the engineering sector. Holmes (2002) derived a closed form solution of the alongwind fatigue based on semiempirical formulas of the stress state, taking into account the bandwidth of the stress processes by means of the approximated method proposed by Wirsching and Light (1980). Kemper (2019) suggests an approach based on spectral methods which uses damage equivalence factors, taking into account an individual and realistic shape of the cycle count distribution. All the cited methods involve a Palmgren–Miner linear accumulation law.

Repetto and Solari (2012) carried out a wide research project aimed at formulating and calibrating a procedure for determining alongwind-induced fatigue. Two are the problems they faced: the first one concerns the definition of a suitable bi-modal counting method in order to obtain in closed form the cycle histogram knowing the structural response at a large number of wind velocity values (Repetto and Solari, 2006); the second problem is to overcome the requirement of huge computations of structural response at every value of wind velocity by integrating the damage on the whole range of velocities in closed form (Repetto and Solari, 2012). In this Section 2.3, according to Repetto and Solari approach, alongwind loading and response of slender structures are presented and simplifying hypotheses adopted in order to obtain closed form solutions of the fatigue problem are introduced.

2.3.1. Wind field, loading and induced response model

A structure immersed in a wind field distorts the flow, giving rise to complex aerodynamic phenomena which cause a change of the pressure field on the structural surface. If the structure is slender enough, such pressure field can be represented by a set of generalized forces per unit length along a suitable structural axis: a couple of drag and lift forces, respectively in the alongwind and crosswind directions, and a torsional moment around the vertical axis. Each component of actions can in turn be divided into a mean part, mainly associated with the mean wind velocity, and a nil mean fluctuation. Each fluctuating component depends on three distinct excitation mechanism: the longitudinal turbulence, the lateral turbulence and the vortex wake at the back of the structure.

Based on the knowledge of the external forces and of the structural mechanical properties the response may be evaluated, using classical structural dynamics, by identifying the deformed configuration with the initial non-deformed one.

According to the Davenport Chain (1962) (Fig. 2.10a), the undisturbed oncoming wind field, represented by the wind velocity *u*, is the input of a filter characterized by a transfer function χ, generally referred to as aerodynamic admittance, taking into account bluff-body aerodynamics. The output furnishes the wind-induced resultant forces *r* acting on the structure. They constitute the input of a new filter characterized by a transfer function *H*, referred to as mechanical admittance, representing the structural mechanical properties. Its output provides the wind-induced structural response *x* (Fig. 2.10b).

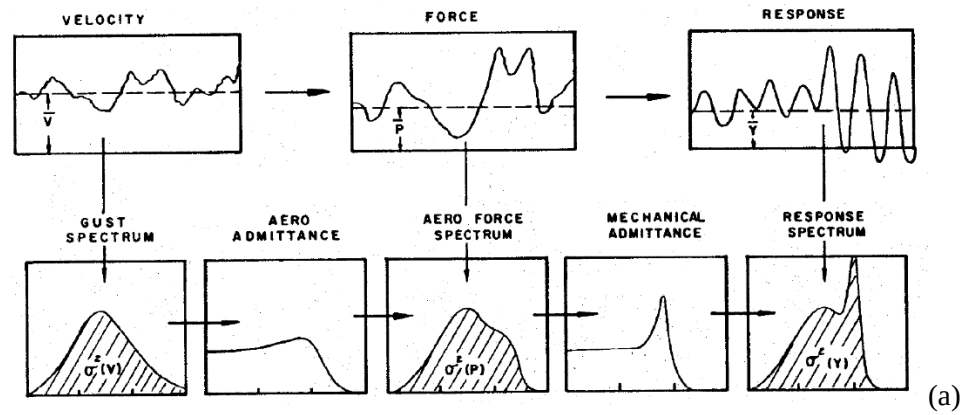

Figure 2.10: Wind-induced dynamic response: (a) © Davenport Chain; (b) conventional scheme.

Since the structure undergoes displacements and velocities, fluid-structure interaction phenomena actually occur and aeroelastic effects can not be disregarded. The response is then function of motion.

Aeroelastic effects can be interpreted as an additional set of generalized forces, representing the motion-induced actions. The global force is thus the sum of the aerodynamic forces and the aeroelastic forces. It is worth notice that aeroelastic forces are usually treated by means of two levels of simplifications: the first considers aeroelastic forces as a linear function of the structural response, the second considers aeroelastic forces as negligible.

- *Wind field*

The atmosphere is conventionally subdivided, vertically, into four strata (troposphere, stratosphere, mesosphere, thermosphere). The lowest layer (troposphere, form 0 to 10 km high on average), contains almost all the clouds and precipitation of the atmosphere. About 90% of the mass of the atmosphere and 75% of the water vapour is located there. In this stratum, the atmospheric phenomena and atmospheric motions are due to the solar radiation, which in fact produces a complex circulation system. It is convenient to classify such atmospheric circulation according to the horizontal scale criterion, identifying a primary circulation, at the planetary scale, a secondary circulations, at the synoptic scale, and local circulations, at the mesoscale.

The secondary circulation causes the local weather. In this group of atmospheric phenomena the extra-tropical cyclones represent the most typical wind that determine the design wind velocity of structures for the European mid-latitude areas and in particular for Italy. The models developed for schematizing the extra-tropical cyclone provide sound idealizations of the physical reality and are widely diffused in both the meteorological and engineering sectors.

To represent the wind configuration in an extratropical cyclone two atmospheric layers having different properties are considered, the atmospheric boundary layer and the free atmosphere. In the atmospheric boundary layer, the presence of frictional forces due to surface roughness opposed to the wind velocity creates a particular profile of the mean wind velocity; furthermore, they generate random fluctuations of the velocity called atmospheric turbulence. The atmospheric boundary layer develops up to the gradient (or geostrophic) height z_g, defined as the height above which the wind is no longer affected by the ground friction force; this height is between 1000 m and 3000 m depending on the wind velocity and on the roughness length of the terrain, which is expressed by a roughness parameter z_0.

Structures and constructions raise within the atmospheric boundary layer, whose schematization is described by Fig. 2.11. The mean wind velocity growths from the ground to the top of the atmospheric boundary layer, where the gradient or geostrophic velocity occurs, u_g, then it remains constant in free

atmosphere. The vertical profile of the mean wind velocity in the site of interest is expressed by means of a deterministic function of the terrain roughness and its local topography. Consider a flat ground of uniform roughness length z_0, the atmospheric boundary layer is divided into two regions called the inner layer and the outer layer. The inner layer lies between the ground surface and an altitude of approximately 200 m; the average velocity has a logarithmic profile that is a function of the roughness length z_0. In the outer layer, which is located above up to the gradient height z_g, the mean velocity tends toward the geostrophic velocity u_g following a spiral shaped profile. The wind direction is parallel to the isobars and the intensity is the greater the more closely are spaced the isobars. This vertical mean profile is referred to as the Ekman spiral. The atmospheric turbulence, which represents the random fluctuations of the velocity due to frictional forces, is maximum close to the ground and diminishes with height up to result as nul at the top of the atmospheric boundary layer. Also the direction of these fluctuations varies randomly.

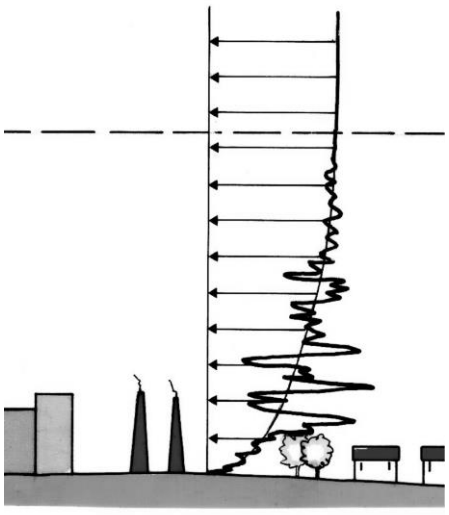

Figure 2.11: Wind mean profile and turbulence fluctuations within the atmospheric boundary layer (Figure © CNR, 2008, 2018).

Summarising, the typical model developed to spatially schematize the wind field in which engineering structures are immersed represents a tapering mean velocity profile overlaid by a three-dimensional fluctuation with zero mean, designated atmospheric turbulence (Figure 2.11).

As concerns the wind field schematization on time varying, the wind field is a 3-variate 4-dimensional random process. It is 3-variate because it is described by a three vector components and it is 4-dimensional because each of these components depends on four independent parameters, x, y, z (spatial coordinates) and t (time).

Starting from long-period measurements over open terrain, the obtained power spectral density function of the wind velocity presents two main peaks, separated by a spectral gap (Fig. 2.12). The harmonic content at high periods is referred to as the macro-meteorological peak (4 - 1 days), corresponding to the weather system; the harmonic content at rather low periods (5 minutes – few seconds) is referred to as the micro-meteorological peak, corresponding to the atmospheric turbulence. The spectral gap, which separates the macro-meteorological and the micro-meteorological peaks, covers the periods between 10 minutes and 1 hour, in which the harmonic content is almost negligible.

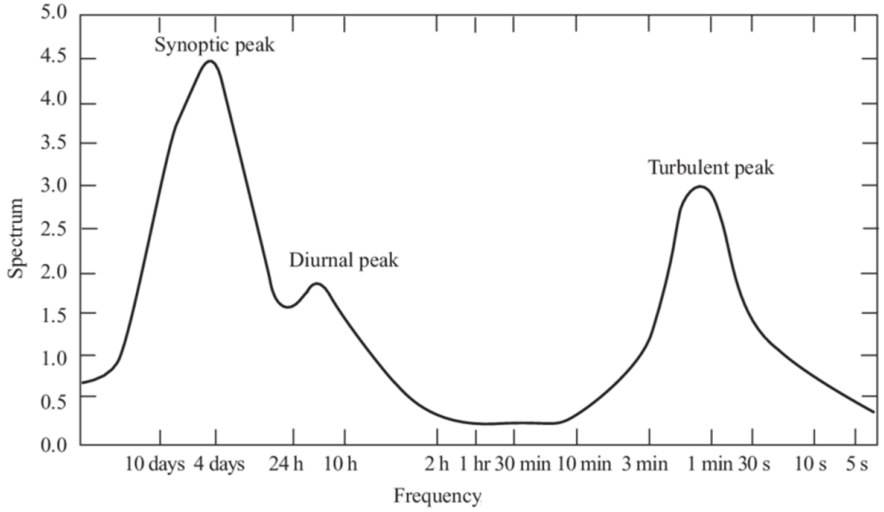

Figure 2.12: Long-term spectrum based on Van der Hoven (1957).

Time is conventionally subdivided into successive ΔT time intervals of 10 minutes – 1 hour, falling in the spectral gap, consequently the wind field can be interpreted as the superimposition of two independent components, corresponding to the macro-meteorological and micro-meteorological peaks of the power spectral density function. These two independent components are related to different generating mechanism, the mean wind velocity and the turbulence field, respectively. The former varies slowly in time and it can be considered as constant in each ΔT interval within the spectral gap, the latter varies rapidly in time. Wind velocity at a fixed height above the ground is schematized, in each ΔT interval, through its constant mean value $\bar{u}$, its direction, and the three zero-mean fluctuating orthogonal components, u', v', w', referred to, respectively, as longitudinal, lateral and vertical turbulence; these are modelled as stochastic stationary Gaussian processes.

Referring to the mean wind velocity profile $\bar{u}$, it is in general a complex function of terrain orography, terrain roughness and temperature distribution. The latter influences atmospheric stratification: if an air element, dealt with as an ideal gas with initial temperature $T°$ and pressure p, is moved adiabatically up to

reach the pressure p_0, it assumes a new temperature $T°_0$; the potential temperature θ is the $T°_0$ value related to p_0 = 1000 mb. In a stably stratified atmosphere the potential temperature has a positive gradient, the natural convection tends to suppress the turbulence, the heat flux is negative (directed downwards) and air particles tend to return to their trajectory. In an unstably stratified atmosphere the potential temperature has a negative gradient, the natural convection tends to exalt the turbulence, the heat flux is positive (directed upwards) and air particles tend to move further away from their trajectory. It is worth notice that atmosphere in atmospheric boundary layer tends to stable conditions during nights and unstable conditions during days, balancing the respective effects in long periods. Within a neutrally stratified atmosphere the potential temperature has a nil gradient, the natural convection disappears and the turbulence is totally due to the mechanical convection, the heat flux is zero and air particles tend to retain their trajectory. Under this condition the atmosphere is characterized by high wind velocity, large shear forces, large turbulent fluctuations, rapid atmospheric mixing and adiabatic atmospheric conditions. In such situation, wind velocity is independent of temperature. Atmospheric thermal stratification may be classified in accordance with two parameters, namely the Richardson number *Ri* and the Obukhov length *L*. Neutral atmospheric thermal stratification corresponds to $Ri = 0$ and $1/L \rightarrow 0$. Field measurements of the inverse of the Obukhov length as function of mean wind velocity show that high mean wind velocity (more than 10 m/s on average) can be associated with neutral conditions (Fig. 2.13).

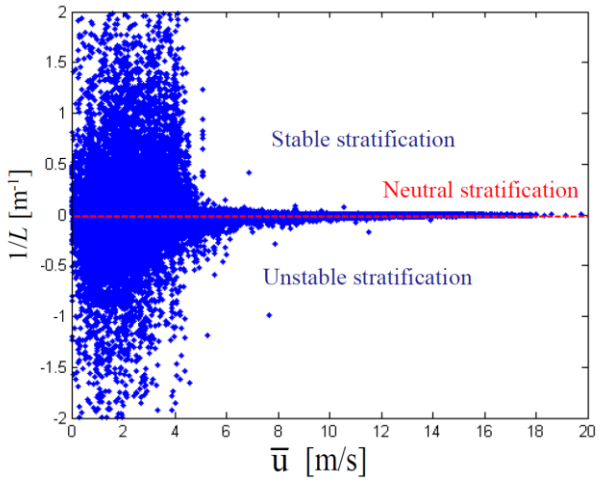

Figure 2.13: Field measurements of the inverse of the Obukhov length.

The mean wind profile description can be obtained by numerical models such as Computational Fluid Dynamics (CFD), experimental tools such as boundary-layer wind tunnels and, limitedly to simple conditions, analytical methods. Under the condition of neutral atmosphere, and therefore the condition of wind velocity independent of temperature, the analytical models describing the mean wind velocity profile in proximity of the ground express $\bar{u}(z)$ by means of suitable functions. The variation of the mean

wind velocity $\bar{u}$ with the height z is suitable described by the logarithmic law (Eq. 2.19) or by the simpler power law (Davenport, 1960), which has no physical foundation though.

$$\bar{u}(z) = \frac{1}{\tilde{k}} u_* \ln \frac{z}{z_0} \tag{2.19}$$

where $\tilde{k}$ is the Von Karman constant, approximately equal to 0.4, u_* is the frictional velocity, z_0 is the roughness length. In design codes, the mean wind velocity at the structural site is linked with the mean wind velocity at a reference site $\bar{u}_{ref}$, namely the mean wind velocity at a reference height z_{ref} on a reference terrain characterized by the roughness length $z_{0,ref}$:

$$\bar{u}(z) = \bar{u}_{ref} \left(\frac{z_0}{z_{0,ref}} \right)^p \frac{\ln(z/z_0)}{\ln(z_{ref}/z_{0,ref})} \tag{2.20}$$

where $p \approx 0.07$.

The mean wind velocity is usually treated as a 2-dimensional random vector including the mean wind intensity and the direction. The knowledge of their joint probability distribution is fundamental for structural reliability analyses and, in particular, for fatigue assessment.

Wind climate analyses generally involves three phases: the first is concerned with the collection, control, correction and transformation of the meteorological data; the second phase deals with the analysis of the probability distribution of the mean wind velocity population; the third phase further develops the treatment in order to obtain the probability distribution of the maximum value of the mean wind velocity over a fixed period of time. An Aeolic data base should be representative, reliable and homogeneous (Solari, 1996a). The probabilistic analysis of the parent population involves the choice of a suitable distribution. The Weibull model (1951) is often used to represent the wind velocity distribution aloft and at ground level. The distribution parameters are two, k and c, the shape parameter and the scale parameter, respectively. The Weibull distribution can be corrected in order to take into account the problem of the wind calms. The hybrid technique (Takle and Brown, 1978) accepts the instrumental response and modifies the Weibull density and distribution functions as:

$$\mathrm{p}_{\mathrm{U}}(\bar{u}) = F_0 \delta(\bar{u}) + (1 - F_0) \frac{k}{c} \left(\frac{\bar{u}}{c} \right)^{k-1} \exp\left\{ -\left(\frac{\bar{u}}{c} \right)^k \right\}; \qquad (\bar{u} \geq 0) \tag{2.21}$$

$$\mathrm{P}_{\mathrm{U}}(\bar{u}) = F_0 + (1 - F_0) \left[1 - \exp\left\{ -\left(\frac{\bar{u}}{c} \right)^k \right\} \right]; \qquad (\bar{u} \geq 0) \tag{2.22}$$

in which $\delta(\bullet)$ is the Dirac operator; F_0 is the probability that wind velocity value is zero, identified by the ratio between the number of values $\bar{u}$ = 0 and the total number of data; *k* and *c* are the Weibull model parameters, regressed solely on the basis of only the values greater than zero. The hybrid technique furnishes good results (Solari, 1996a). Some advanced models have been proposed to improve the outcomes quality, such as the composite models (Solari, 1996a), which are obtained by assembling Weibull distribution families individually applied to uniform data portions. Finally, the third phase concerns the probability distribution of the maximum wind velocity over a fixed period $T >> \Delta T$. Usually the distribution of the maximum value of wind velocity is evaluated over a long time period (e.g. 50 years) referring to annual maxima values of the mean wind velocity (yearly maximum distribution). The evaluation of such distribution is carried out on the basis of different procedures: asymptotic extreme distributions analysis (Gumbel, 1958); generalized extreme distributions analysis (Jenkinson, 1955); penultimate distributions analysis (Cook and Harris, 2004, 2009); process analysis or parent population method (Gomes and Vickery, 1977; ESDU, 1990); peak over threshold (POT) method or generalized pareto distributions analysis (Pickands, 1975; Simiu and Heckert, 1996; Holmes and Moriarty, 1999).

Wind climate is modelled by the joint density function of the mean wind velocity intensity and direction, therefore directional distribution analysis results as a major issue. In each ΔT interval the mean wind velocity is schematized with constant intensity and constant direction (rotated with respect to *x*). Subdividing space in a set of directional sectors around a considered position, the joint probability that the mean wind velocity belongs to the *i*-th velocity interval Δu_i and the wind blows from the *h*-th sector is usually expressed by Weibull distribution in which distribution parameters depend on *h*-th directional sector (k_h and c_h).

The turbulence field is generally schematized by a zero mean stationary Gaussian 3-variate (*u*', *v*', *w*') and 4-dimensional (*x*, *y*, *z*, *t*) random process whose spatial-temporal properties are expressed, in the frequency-domain, by cross-power spectral density functions, defined as:

$$S_{\varepsilon\eta}(M,M';n) = \sqrt{S_{\varepsilon}(z;n)S_{\eta}(z';n)}\,\mathrm{Coh}_{\varepsilon\eta}(M,M';n) \qquad (\varepsilon,\eta = u',v',w') \tag{2.23}$$

where *n* is the frequency; *M'* is a point of coordinates *x'*,*y'*,*z'*; $S_{\varepsilon\eta}(M,M';n)$ is the cross-power spectral density function of $\varepsilon(M;t)$ and $\eta(M';t)$; $S_{\varepsilon}(z;n) = S_{\varepsilon\varepsilon}(M,M;n)$ is the power spectral density function of $\varepsilon(M;t)$; $\mathrm{Coh}_{\varepsilon\eta}(M,M';n)$ is the coherence function of $\varepsilon(M;t)$ and $\eta(M';t)$. Turbulent fluctuations can be interpreted as a superposition of eddies in periodic motion, whose large eddies are associated with low frequency kinetic energy and, in the inertial subrange, transfer energy to smaller ones, which in turn, in

high frequency range, dissipate viscous energy. This energy cascade furnishes a physical interpretation of the power spectral density function and of the coherence function of turbulence.

The power spectral density function of the ε turbulence component may be expressed by (Piccardo and Solari, 2001):

$$\frac{nS_\varepsilon(z;n)}{\sigma_\varepsilon^2} = \frac{d_\varepsilon n L_\varepsilon(z)/\bar{u}(z)}{\left[1+1.5 d_\varepsilon n L_\varepsilon(z)/\bar{u}(z)\right]^{5/3}} \tag{2.24}$$

where d_u = 6.868, $d_v = d_w$ = 9.434, L_ε is the integral length scale of ε in the x direction, σ_ε^2 is the variance of ε. Eq. (2.24) represents an effective, simple and conservative approximation of the formulae given by ESDU (1993a) in the inertial subrange. The turbulence standard deviation σ_ε quantifies the turbulence intensity; close to the ground it is nearly independent of z. The turbulence integral length scale L_ε defines the position of the turbulence spectral content; it increases with z and decreases with z_0. Focusing attention on slender structures, only the effects of *u'* and *v'* are relevant. In the following, they are considered as uncorrelated.

- *Wind loading*

A fixed structure immersed in the wind distorts the flow field giving rise to a pressure variation on its surface. If the structure is slender, the resultant of pressures on the perimeter of a generic perpendicular cross-section is normally expressed as a couple of drag and lift forces, in the alongwind and crosswind directions respectively, and a torsional moment around the structural axis. Aerodynamic wind actions depend, in general, on the wind flow characteristics, on the shape and size of the structure and its orientation with respect to the wind, and on the properties of the vortex wake at the back of the structure.

Let us consider a slender structure or structural element whose length l is much greater than the reference size b of its cross-section. Let x, y, and z be a local Cartesian reference system with origin at o (Fig. 2.14); z coincides with the structural axis, x is aligned with the mean wind direction, o lies on the face of the structure with z = 0, at height h above the ground. Let X, Y, and Z be a global Cartesian reference system with origin at O; the X- and Y-axes are coplanar with ground; Y and Z are coplanar with y and z; X is parallel to x; Z is directed upward and passes through o; z is rotated ϕ with respect to Z. The wind loading is schematized as a three-variate two-dimensional random stationary Gaussian process, whose ω-th component ($\omega = x, y, \theta$) is given by:

$$F_\omega(z,t) = \bar{F}_\omega(z) + F'_\omega(z,t) \qquad (\omega = x, y, \theta) \tag{2.25}$$

where $0 \le z \le l$; t = time; F_x, F_y, F_θ = alongwind force, crosswind force and torsional moment around z per unit length; $\bar{F}_\omega$ = mean value of F_ω; and F'_ω = nil mean fluctuation of F_ω around $\bar{F}_\omega$. These quantities can be defined using physical modelling, numerical methods or analytical approaches.

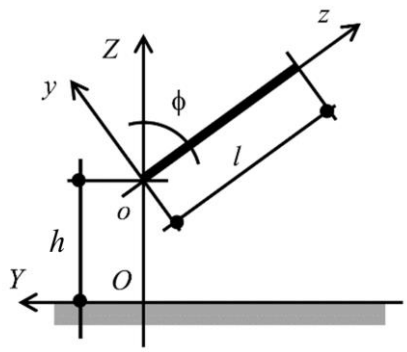

Fig. 2.14: Structural model and reference systems (X, x entering the page).

Focusing on analytical approaches to define mean and fluctuating aerodynamic forces, they are limited to isolated constructions of suitable shape and they can be developed at various level in accordance with the characteristics and the importance of the structure analysed. Eurocode model is based on the one proposed by Piccardo and Solari (2000, 2002), by making use of aerodynamic coefficients, namely drag, lift and torsional moment coefficients, and of turbulence intensities.

Furthermore, a slender structure or structural element immersed in a wind field is also subjected to a regular alternating shedding of vortices which causes asymmetries of the velocity and pressure fields of the fluid, responsible for transversal and longitudinal forces that vary in time with frequency respectively equal and twice that of vortex shedding. The longitudinal forces are usually small and they may be neglected. The transversal forces are often essential for the study of the behaviour of structures in respect of the wind. According to commonly used models, only fluctuating crosswind force F'_y is due to both turbulence and vortex wake-induced loads. Speaking of the oscillating force only induced by vortex shedding, the frequency of this almost periodic action depends on the mean wind velocity and the cross-section shape and size. When the vortex shedding frequency is close to a natural frequency of vibration, resonance occurs, causing on lightweight and low damped structures or components large amplitude vibrations. This resonant phenomenon happens in correspondence of a wind velocity called critical velocity.

When the structure oscillates, the fluid-structure interaction gives rise to aeroelastic effects, whose importance depends on the structural shape and the mechanical properties. Such effects can be interpreted as the result of aeroelastic or motion-induced actions, additional to the aerodynamic wind actions. In

general they are non-linear function of the structural motion. Under the hypothesis of small structural displacements and velocities, wind engineering frequently adopts a linearized approximation. Moreover, using quasi-steady and quasi-static theory, aeroelastic forces can be obtained schematising the moving structure into the actual wind field as a fixed structure into a relative wind field. The dependence on the structural motion (deflection and velocity) means that linearized aeroelastic actions can be described through parameters that modify the mechanical properties of the structure, in particular damping, when the self-excited action is proportional to velocity, and stiffness when the self-excited action is proportional to deflection. As the mean wind velocity increases, the above phenomena are such as to reduce and possibly cancel the total stiffness and/or the damping of the structure, generating critical conditions of incipient instability (aeroelastic instability). The values of mean wind velocity at which instability arises are defined as critical and depend on the geometric and mechanical characteristics of the structure.

In the following, only mean and fluctuating aerodynamic forces due to mean wind velocity and atmospheric turbulence are taken into account. The bases of alongwind-induced fatigue methods are then provided. Nevertheless, lightweight, flexible and low damped structures are prone to phenomena such as vortex-induced vibrations (VIV) and aeroelastic effects. Therefore, the former is introduced and analysed in Chapter 5 as regards VIV-induced fatigue. The latter is neglected in this research work because of the complexity of the problem to be dealt with in terms of standards procedures. Design codes maintain that, apart from those associated with vortex shedding, all critical velocities of the structure and its components associated with aeroelastic instability phenomena must be considerably higher than the design wind velocity. As a rule, it is important to ensure that the probability of critical velocities is extremely small.

- *Wind induced response*

The wind-induced fatigue on structures is determined by the structural vibrations during the whole structural life; the wind-induced structural response definition is a main topic in the research. Considering a general formulation of the wind-induced dynamic response of a slender structure under aerodynamic wind actions, the following provides response parameters definition according to the influence function technique (ESDU, 1976; Holmes, 1994).

Using a quasi-steady theory and dealing with the structure as a linear system, the wind-induced stress at a coordinate z of the structure in a ΔT time interval is a stochastic stationary Gaussian process given by the sum of the mean static stress caused by the mean wind action and the fluctuating stress components, caused by the buffeting and vortex shedding actions.

Therefore, the wind-induced stress at a coordinate z of the structure in a ΔT time interval is given by:

$$s_\omega(z,t) = \bar{s}_\omega(z) + s'_\omega(z,t) \tag{2.26}$$

where $\bar{s}_\omega$ is the mean static stress and s'_ω is the fluctuating stress.

Considering the latter quantity as only caused by the buffeting actions due to turbulence, it can be schematized as a bi-modal process (Repetto, 2005; Repetto and Solari, 2006):

$$s'_\omega(z,t) = s'_{\omega,Q}(z,t) + s'_{\omega,R}(z,t) \tag{2.27}$$

where $s'_{\omega,Q}$ is the low frequency quasi-static part of s'_ω; $s'_{\omega,R}$ is the high frequency resonant part of s'_ω, considered here as related to only one mode of vibration whose natural frequency $n_{\omega 1}$ is much greater than the expected frequency $\nu_{\omega,Q}$ of $s'_{\omega,Q}$. Therefore, the quasi-static part and the resonant part of the stress may be considered as uncorrelated. It follows that the variance and the expected frequency of the wind-induced stress can be expressed as:

$$\sigma_\omega^2 = \sigma_{\omega,Q}^2 + \sigma_{\omega,R}^2 \tag{2.28}$$

$$\nu_\omega = \sqrt{\nu_{\omega,Q}^2 \lambda_{\omega,Q} + n_{\omega 1}^2 \lambda_{\omega,R}} \tag{2.29}$$

where $\sigma_{\omega,Q}$ and $\sigma_{\omega,R}$ are the standard deviations of $s'_{\omega,Q}$ and $s'_{\omega,R}$, respectively; $\lambda_{\omega,Q}$ and $\lambda_{\omega,R}$ are the normalized variances of the quasi-static and resonant parts of the stress, respectively, defined as:

$$\lambda_{\omega,Q} = \frac{\sigma_{\omega,Q}^2}{\sigma_\omega^2} \tag{2.30}$$

$$\lambda_{\omega,R} = \frac{\sigma_{\omega,R}^2}{\sigma_\omega^2} \tag{2.31}$$

The previous description of fluctuating stress parameters is valid for both alongwind and crosswind stress processes due to only turbulence, neglecting here the combined effect of the crosswind dynamic loading attributable to gust buffeting and to critical vortex shedding conditions (Eqs. 2.27-2.31). The impact of this choice is discussed in Chapter 5, as previously mentioned.

2.3.2. Alongwind induced-fatigue analyses in frequency domain

The study of the wind-induced fatigue necessarily starts from the knowledge of the wind climate at the structural site, and passes through the evaluation of the stress cycle histogram, of the mean total damage and of the mean fatigue life induced by wind during the structure's whole life.

Some frequency-domain formulations were established by Repetto and Solari for determining the wind-induced fatigue of slender vertical structures subjected to alongwind (Repetto and Solari, 2001), crosswind (Repetto and Solari, 2002), and simultaneous alongwind and crosswind vibrations (Repetto and Solari, 2004). Such procedures take into account the joint probability distribution of the mean wind velocity and direction, and furnish the cycles histogram, the mean fractions of damage, the mean total accumulated damage, and the mean fatigue life under the hypothesis of narrow band stress processes. Comparison between theoretical and time-domain numerical results points out that the narrow band hypothesis is usually appropriate for the crosswind-induced fatigue analysis, but can lead to large overestimates of the alongwind-induced fatigue, when the quasi-static part of the response is not negligible. Based on these and analogous remarks, the role of the spectral bandwidth of the stress processes in the alongwind-induced fatigue has been the matter of some more research.

Holmes (2002) derived two closed form solutions of the alongwind fatigue representing an upper and a lower bound of the total damage, under some simplifying assumptions. In particular, Holmes assumed that the mean wind velocity is a random variable described by a Weibull distribution, neglecting the presence of the wind calms; the stress standard deviation is a power law of the mean wind velocity; the expected frequency of the response is constant, and does not take into account the actual spectral content of the stress. In contrast to the classic curves provided by standards, the fatigue curve is a straight line in a log-log scale; the Palmgren–Miner damage accumulation law is adopted without taking into account the mean stress state. The proposed limit solutions were obtained correcting the narrow-band solution by the damage correction factor derived from the method of Wirsching and Light (1980). The upper bound of the total damage was obtained assuming the damage correction factor to be a unit, thus representing the stress process as narrow banded. The lower bound was related to the lower bound of the Wirshing and Light damage correction factor, therefore becoming independent of the bandwidth of the stress processes. The proposed expressions showed good agreement with the observed damage rates on a light pole. However, as proved by Lutes et al. (1984), the damage correction factor proposed by Wirsching and Light (1980) can give inaccurate results depending on the spectral shape of the process. As a consequence, Holmes' lower bound can underestimate or overestimate the real damage, depending on the spectral properties of the stress processes.

Consequent steps towards a pertinent method to evaluate damage accumulation due to alongwind actions was made by Repetto and Solari (2006), taking into account the bandwidth spectral properties of the stress processes. This aim was pursued by establishing an advanced broadband formulation, improving the level of approximation compared to previous methods. Applying the cycle counting method based on the narrow-band assumption, two discrete cycles histogram expressions are first suggested, which approximate the Peak counting and the Peak-Valley counting methods (Repetto 2003, 2005), and lead to an upper and lower bound of the fatigue damage, respectively. As the gap between the

two bounds may be very large, starting from the bi-modal formulation developed by Jiao and Moan (1992), a more refined counting method is formulated (Repetto 2003, 2005), based on a bi-modal representation of the alongwind induced stress power spectral density functions; the low- and high-frequency spectral contents are associated, respectively, with the quasi-static and the resonant parts of the response related to the first mode. This method involves a closed form solution of the cycles histogram, from which the mean total damage and the mean fatigue life can be derived. The proposed procedure showed good agreement between the bi-modal approach and the numerical results obtained through Monte Carlo simulations analyzed by means of the Rainflow counting method.

Considering a time interval T much greater than ΔT, the time variation of the mean wind velocity shall be dealt with probabilistically. For this aim, a series of $\bar{u}_{ref,i}$ values is considered, where i-index represents a velocity step. The probability that $\bar{u}_{ref,i}$ belongs to the i-th velocity interval is defined as P_i, which can be expressed adopting a Weibull distribution corrected by the hybrid technique (Eqs. (2.21), (2.22)) (Takle and Brown, 1978). Wind directionality is neglected for sake of simplicity (Repetto and Solari, 2004). The wind loading effects induced on a structure during the time interval T are treated as a series of loading conditions each corresponding to a ΔT step. A structure is said to undergo the i-th loading condition when $\bar{u}_{ref}$ belongs to i-th interval of mean wind velocity values. The i-th loading condition is characterized by the probability of occurrence P_i. Thus, the structure undergoes the i-th loading condition for an effective duration time $T_i=TP_i$.

$$P_i = (1-F_0)\left(\exp\left\{ -\left[\frac{(i-1)\delta\bar{u}}{c} \right]^k \right\} - \exp\left[-\left(\frac{i\delta\bar{u}}{c} \right)^k \right] \right); \qquad (i=1,2,...) \tag{2.32}$$

Considering a linear behavior of the structure, the wind loading effect associated to the i-th loading condition is given by $e_i = \bar{e}_i + e'_i$, where $\bar{e}_i$ and e'_i are the mean and the nil mean fluctuating loading effects, respectively, evaluated under the condition $\bar{u} = \bar{u}_{ref,i}$. Disregarding the effects of the original load cycle sequence, the damage induced by all the wind loading conditions during the whole structure's life is evaluated collecting the wind loading cycles into a discrete cycles histogram. Adopting the *S-N* approach, the fatigue analysis is carried out based on the nominal alongwind-induced stress s_x, i.e., assuming $e_i = s_{xi}$. Thus, a series of stress amplitude cycles Δ_j, and a related stress amplitude step $\delta\Delta$ are considered. The mean number of cycles $\bar{n}_{ij}$ with amplitude Δ_j around the mean stress $\bar{s}_{xi}$ is given adopting the bi-modal approach (Jiao and Moan, 1990) as modified in Repetto (2003; 2005). The cycle histogram furnished by the Rainflow counting method is approximated by two distinct cycles groups: the first includes the large amplitude cycles and is related to the pseudoenvelope P_{si} of the alongwind stress process s'_{xi}; the second

includes the small reversals, related to the high frequency component s'_{Rxi} and the envelope R_{Ri} of the process s'_{Rxi} (Fig. 2.9; Fig. 2.15).

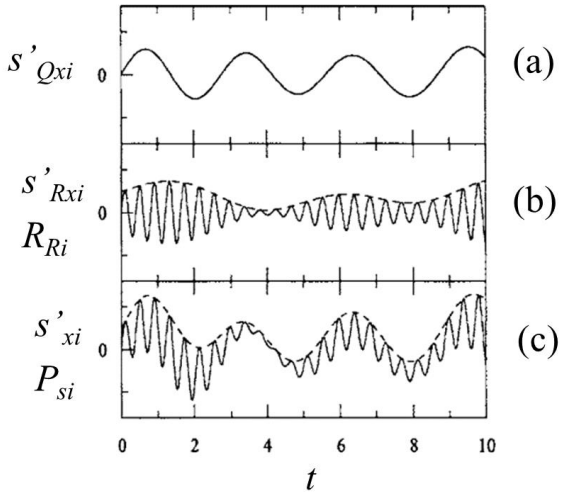

Fig. 2.15: Sample of stress bi-modal process: (a) low frequency component s'_{Qxi}; (b) high frequency component s'_{Rxi} (solid line) and its envelope R_{Ri} (dashed line); and (c) bi-modal process s'_{xi} (solid line) and its pseudoenvelope P_{si} (dashed line).

The mean number of cycles $\bar{n}_{ij}$ with amplitude Δ_j around the mean stress $\bar{s}_{xi}$ in the point *M* during the time interval *T* is given by:

$$\bar{n}_{ij}(T) = \hat{n}_{ij}(T) + \check{n}_{ij}(T) \tag{2.33}$$

where $\hat{n}_{ij}(T)$ and $\check{n}_{ij}(T)$ enumerate, respectively, the large and small amplitude cycles induced by the *i*-th stress process (see Eq. (2.16) and following).

Adopting the model proposed in Repetto (2003; 2005), the mean number of the large amplitude cycles is obtained by applying the Peak counting method to the pseudoenvelope P_{si} of the process s'_{xi}, treated as narrow band; it can be expressed by:

$$\hat{n}_{ij}(T) = TP_i\sqrt{2\pi\left(\lambda^*_{Rxi}\lambda^*_{Qxi}\nu^2_{0,Qxi} + q^2_{Rxi}\lambda^{*\,2}_{Rxi}n^2_{x1}\right)}\nu_{[Pij]}H\left(\nu_{[Pij]}\right) \tag{2.34}$$

where λ^*_{Rxi}, λ^*_{Qxi} = the normalized variances of the resonant and quasi-static parts of the stress process induced by the *i*-th loading condition, respectively; $\nu_{0,Qxi}$ = expected frequency of the quasi-static part of the stress process induced by the *i*-th loading condition (Repetto and Solari, 2006); q_{Rxi} = the spectral bandwidth of the resonant part of the stress process, which can be approximated by (Vanmarke, 1972),

depending only on the first modal damping in the *x* direction (it depends on the loading condition when including the aerodynamic damping); n_{x1} = fundamental frequency; $H(\bullet)$ = Heavyside's function; $v_{[Pij]}$ is given by:

$$v_{[Pij]} = \left\{ \frac{(j-1)\delta s}{\sigma_{xi}} \exp\left[-\frac{(j-1)^2 \delta s^2}{2(\sigma_{xi})^2} \right] - \frac{j\delta s}{\sigma_{xi}} \exp\left[-\frac{j^2 \delta s^2}{2(\sigma_{xi})^2} \right] \right\} \tag{2.35}$$

where σ_{xi} is the standard deviation of the wind-induced stress in the *i*-th loading condition.

The mean number of the small amplitude cycles is evaluated by applying the Peak counting method to the high frequency component s'_{Rxi}, and by correcting the results considering the cycles related to the envelope R_{Ri}; it can be expressed by:

$$\breve{n}_{ij}(T) = TP_i n_{x1} \left\{ \left[\exp\left(-\frac{(j-1)^2 \delta s^2}{2\lambda^*_{Rxi}(\sigma_{xi})^2} \right) - \exp\left(-\frac{j^2 \delta s^2}{2\lambda^*_{Rxi}(\sigma_{xi})^2} \right) \right] - \sqrt{\frac{2\pi}{\lambda^*_{Rxi}}} q_{Rxi} v_{[Rij]} H\left(v_{[Rij]}\right) \right\} \tag{2.36}$$

where $v_{[Rij]}$ is given by:

$$v_{[Rij]} = \left\{ \frac{(j-1)\delta s}{\sigma_{xi}} \exp\left[-\frac{(j-1)^2 \delta s^2}{2\lambda^*_{Rxi}(\sigma_{xi})^2} \right] - \frac{j\delta s}{\sigma_{xi}} \exp\left[-\frac{j^2 \delta s^2}{2\lambda^*_{Rxi}(\sigma_{xi})^2} \right] \right\} \tag{2.37}$$

Knowing the mean number of cycles $\bar{n}_{ij}$ (Eq. (2.33)), the fractions of the mean damage result in closed form. Moreover, the mean total damage and the mean fatigue life can be estimated (Fig. 2.16).

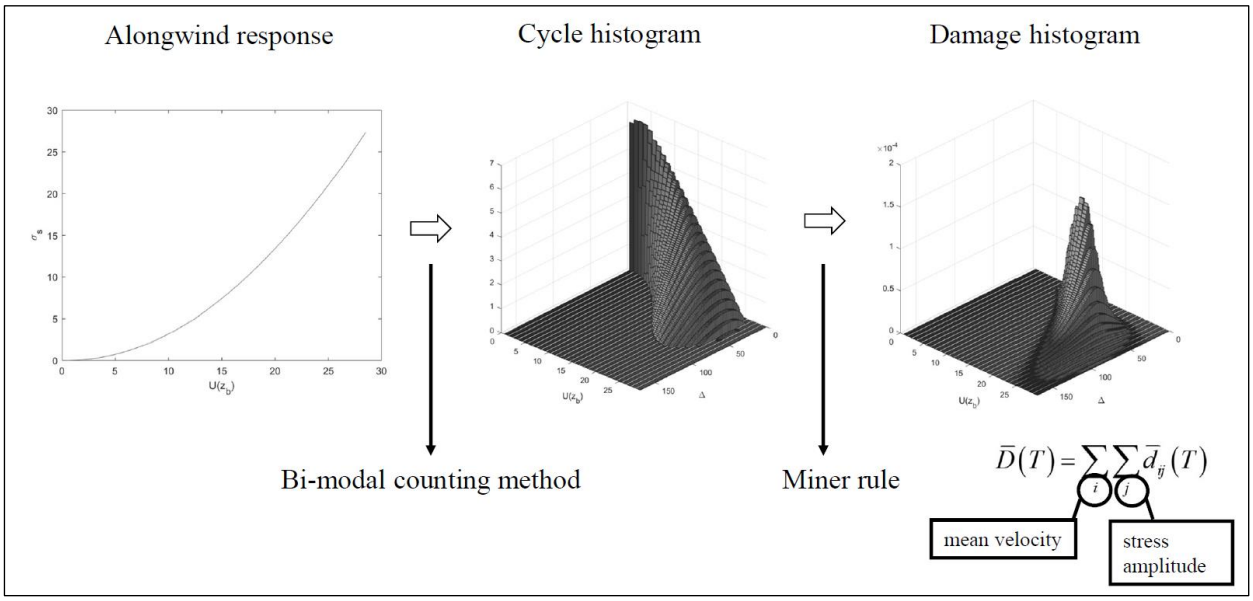

Fig. 2.16: Representation of the alongwind-induced fatigue analysis procedure: the structural response is evaluated for every *i*-th loading condition; the cycle histogram can be evaluated by means of the bi-modal counting method; the fractions of the mean damage and the consequent mean total damage result applying Miner linear rule.

Bi-modal approach validation overview

The bi-modal approach by Repetto and Solari is at the base of the current research work.

Repetto, in her work of 2005, reported a comparison between different cycle counting methods, by applying them to some bi-modal processes. Starting from the power spectral density functions of the processes, a series of time histories were simulated by the Monte Carlo technique, adopting the random phase method (Shinozuka and Jan, 1972). Each time-history was analysed by a numerical algorithm based on the Rainflow counting method RFC (Rychlik, 1987), determining numerically the mean cycles histogram of each process.

The first step of her analysis was the comparison of the results of the RFC numerical estimation with the proposed bi-modal method, the proposed bounds and with other methods presented in literature. The bi-modal method, with respect to RFC numerical benchmark, results the most effective because it follows in a more closer way the numerical tendencies, while remaining on the safe side. Moreover, differently from other methods presented in literature, the bi-modal method allows to extend the above fatigue analysis to different fatigue curves and damage models, as it furnishes the cycles histogram in analytical form.

The second step of the analysis by Repetto considered three selected bi-modal processes, characterised by different power spectral density functions. Figure 2.17 shows the comparison between the cycles histograms, on varying the normalised amplitude, obtained by the numerical RFC applied to the simulated time histories (solid lines), the Peak counting method (dashed lines), the Peak-Valley counting method (dash-dotted lines) and the bi-modal counting method (dotted lines) (called BMC); the latter follows more closely the numerical path, on the upper side. The logarithmic scale on the ordinate points out that relevant differences occur in the tails. The comparison between the fatigue predictions corresponding to the three counting methods was completed by further developing the fatigue analysis of the three processes, assuming the fatigue procedure analysis prescribed by Eurocode 3 (2005), adopting the linear Miner damage law and the fatigue curve for Category 50. Assuming the standard deviation of all the processes as $\sigma_x = \sqrt{50}$ MPa, Figure 2.18 shows the fractions of the damage induced by the processes obtained by the numerical RFC applied to the simulated time histories (solid lines), the PC method (dashed lines), the PVC method (dash-dotted lines) and the BMC method (dotted lines). The differences apparently small in the cycles histograms, considerably increase when dealing with the fractions of damage. The predicted fatigue life values of the three processes, according to the considered methods, confirmed that the PC method leads to lower bound solutions (safe side), the PVC method leads to unsafe overestimated values of the fatigue life, and the bi-modal method leads to good approximations of the fatigue life of the three processes, however on the safe side.

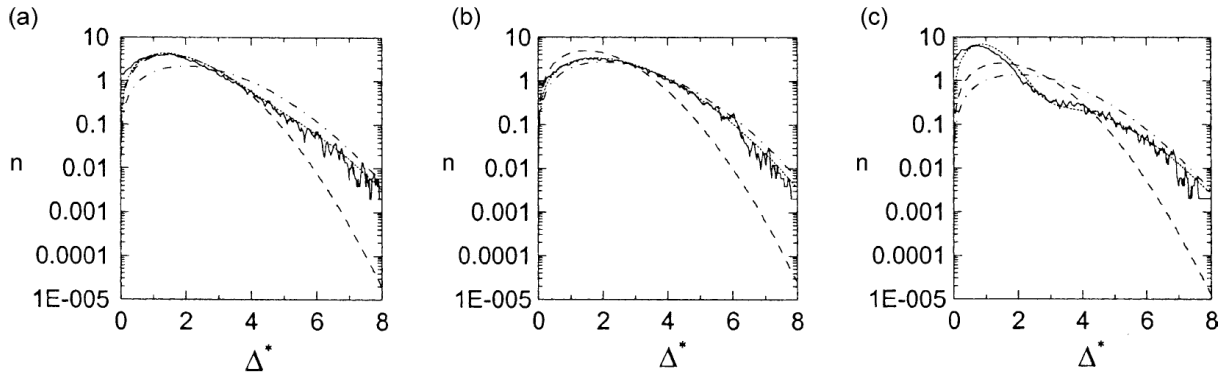

Fig. 2.17: Comparison of cycles histograms of the bi-modal processes by different cycles counting methods: (a) Process 1; (b) Process 2; (c) Process 3; (solid lines, numerical RFC; dashed lines, PC; dash-dotted lines, PVC; dotted lines, BMC) (© Repetto, 2005).

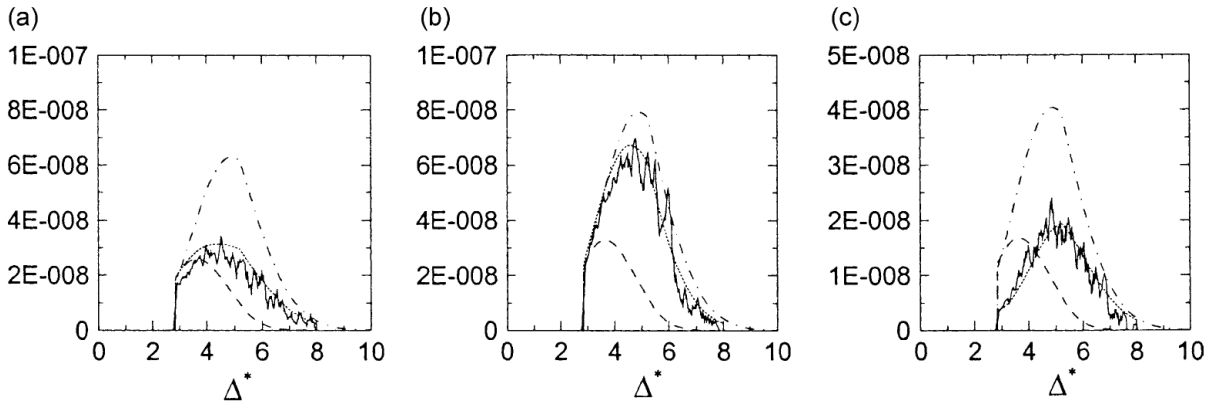

Fig. 2.18: Comparison of damage distribution of the bi-modal processes by different cycles counting methods: (a) Process 1; (b) Process 2; (c) Process 3; (solid lines, numerical RFC; dashed lines, PC; dash-dotted lines, PVC; dotted lines, BMC) (© Repetto, 2005).

Later on, in 2006, Repetto and Solari compared their bi-modal method with the method proposed by Holmes in 2002. Three cases were analysed, characterized by three stress power spectral density functions with different quasi-static and resonant parts. Again the considered benchmark was the result of the Rainflow counting method applied to time histories obtained by Monte Carlo numerical simulations. The comparison between analytical and numerical results highlighted again that the bi-modal method furnishes excellent approximations of the numerical results in all the three cases, always on the safe side. Holmes' method does not depend on the actual bandwidth of the processes, so the results were more approximated and not always on the safe side.

In the same paper, Repetto and Solari showed the application of the proposed procedure to evaluate the alongwind induced fatigue of a slender urban light pole, which was a real structure sensitive to this phenomenon. The main characteristics of the structure are shown in the paper and the fatigue damage was analysed in the critical cross-section at the base of the structure, classified as Category 36 according to the Eurocode 3 (2005). By applying the Peak counting method, the predicted fatigue life was 20 years, corresponding to the lower bound solution; by applying the Peak-Valley counting method, the predicted fatigue life was 63 years, corresponding to the upper bound solution; more precise and reliable results can be obtained by the bi-modal counting method, according to which the predicted fatigue life was 35 years.

The above solutions were compared with the results of a numeric analysis carried out by Monte Carlo simulations. The power spectral density function of the maximum stress at the critical cross-section of the pole was first obtained as the result of a buffeting analysis taking into account the multi-correlated nature of the turbulence field. Then, 30 stress histories of the maximum stress, associated with 30 loading conditions, have been generated by the random phase method (Shinozuka and Jan, 1972). The simulated stress histories showed that the alongwind-induced stress process is not narrow banded and the bi-modal

property of the stress process is more evident at low and moderate wind velocities, where the fatigue damage is concentrated. Each history was analysed by means of a cycles counting algorithm based on the Rainflow counting method (Rychlik, 1987); the number of cycles was obtained over a period of 10 min and extended to the reference period T=1 year by taking into account the occurrence probability of each loading condition (Weibull model). The fatigue life obtained by this procedure was 40 years. The agreement between the bi-modal solution (35 years of predicted fatigue life) and the Monte Carlo simulation was very good.

Figure 2.19 shows the fractions of the damage associated with each loading condition, evaluated with the analytical methods and with the Rainflow method applied to the simulated stress histories. The dash-dotted line represents the damage evaluated according to the Rainflow counting method applied to the simulated stress time histories; the solid line represents the damage evaluated by the proposed bi-modal counting method; the dashed line represents the damage evaluated with the Peak counting method; and the dotted line represents the damage evaluated with the Peak-Valley counting method. The bi-modal counting damage evaluation was in excellent agreement with the Rainflow results on varying the wind velocity, providing very good approximations on the safe side; the Peak counting method furnished an upper bound of the damage, very conservative with respect to the numerical results; and the Peak-Valley counting method furnished a lower bound of the damage, leading to non-conservative results.

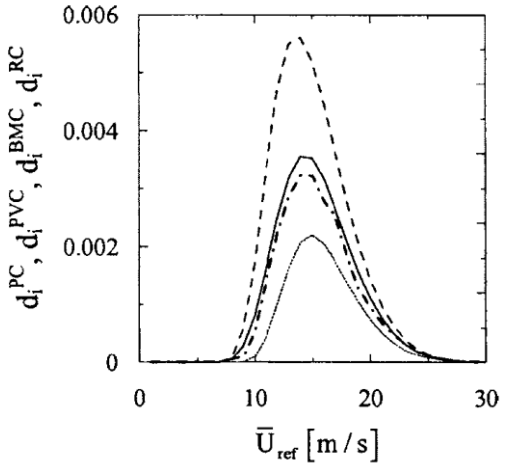

Fig. 2.19: Example of the urban light pole: analysis of alongwind-induced damage for different counting methods: solid line, BMC; dashed line, PC; dotted line, PVC; dash-dotted line, numerical RFC (© Repetto and Solari, 2006).

In (Repetto and Solari, 2010) other two real slender structures fatigue collapse due to wind-induced vibrations was analysed. The two real cases were a ten-meter anemometric pole and a thirty-meter antenna tower, which were both characterized by a very simple structural scheme and satisfied the

national and international Structural Codes from the ultimate limit state point of view. However, they both exhibited premature collapses due to wind-induced fatigue damage. The comparison between the predicted and the exhibited fatigue life confirmed the reliability of the method proposed by the authors.

The first case study was the anemometric pole. This simple structure exhibited a premature collapse one year after its installation, caused by a fatigue crack in the base welding joint. During its short life, the anemometer continuously registered the ten-minute mean wind velocity. The statistical analysis of the measured mean wind velocity was based on this database, adopting the Weibull probability distribution model. It was observed that the site was an exposed ridge characterized by local windy conditions well above those prescribed by the Italian code. The alongwind and crosswind responses were evaluated numerically, on varying the top mean wind velocity, showing that they were mainly due to turbulence and grew with the mean wind velocity, while the vortex shedding action provided limited effects. Adopting the bi-modal procedure, the fatigue damage associated with the wind loading conditions was examined. The fatigue resistance was described by the *S-N* curve of the critical section. Since no standard detail matched the actual geometry of the joint, a hot spot analysis (IIW, 2016) was carried out, starting from the FEM models of the actual joint and of a reference joint reported in Standards (Eurocode 3, 2005). The predicted fatigue life resulted very critical: according to the alongwind analysis 740 days and according to the crosswind analysis 270 days. Its collapse was associated with the particularly windy condition of the site. The safety factor adopted in structural design covers this anomalous situation from the ultimate limit state point of view, while it is completely inadequate from the fatigue point of view. The analysis also highlighted the key role of lateral turbulence, currently disregarded in structural standards, and the critical choice of the *S-N* curve for non-standardized welded joints.

The second structure examined, the antenna tower, was composed of a steel shaft above which there was a steel circular bar. The bar at the top can support different configurations of telecommunication antennas. Moreover, sometimes antennas are covered by a fiberglass cylinder. The configuration with the cover cylinder exhibited a premature collapse after a few months of structural life, caused by a fatigue crack at the shaft-bar joint. After the collapse, an extensive in-situ inspection revealed that other similar antenna towers were subject to fatigue damage, showing a critical behaviour with similar characteristics. Adopting the procedure by Repetto and Solari, the evolution of the stress state and fatigue damage of the tower without the cover cylinder and with the cover cylinder was examined. The structure was schematized as a cantilever beam, taking into account the different stiffness of the shaft and of the upper bar, and the different mass distribution of the configurations considered. The structural response was analysed numerically, considering three modes of vibrations in x and y directions. The results highlighted two potentially critical sections, at the base of the tower and at the base of the supporting bar, respectively. In both alongwind and crosswind analyses and in both configurations, with or without the cover cylinder, the latter cross-section resulted as more critical in terms of fatigue damage. The antenna's

tower damage and collapse were mainly linked with the aerodynamic effects generated by the vortex shedding actions resonant with the top cover cylinder, the predicted fatigue life was less than one year, as expected from the real collapse. Avoiding the use of such a cylinder, or removing it, the vortex shedding effects were drastically reduced and the maximum stress value was linked with alongwind actions. However, even in this case, the crosswind actions due to turbulence and vortex shedding actions on the shaft were responsible for the main fatigue damage. In this configuration, the predicted fatigue life is 115 years in alongwind analysis and 45 years in crosswind analysis.

From a general point of view, the analyses based on the procedure proposed, compared with the real cases examined, leads to accurate fatigue life predictions. Furthermore, they highlight the limits of Standards and Codes in preventing wind-induced damage. Thus, the subsequent aim of the authors was to introduce an engineering simplified procedure concerning the alongwind-induced fatigue.

In conclusion, Repetto and Solari compared successfully their bi-modal approach with numerical simulations (Rainflow couting method on stress time histories; Repetto, 2005; Repetto and Solari, 2006) and with real case studies which exhibited fatigue damage due to wind (Repetto and Solari, 2006, 2010). Taking this into account, it can be stated that the bi-modal approach proposed to investigate the gust induced fatigue of slender structures is valid and reliable, being the basis of the whole present dissertation.

2.3.3. Hypothesis and analytical assumptions

Section 2.3.2 deals with wind induced-fatigue analyses in frequency domain and, in particular, with alongwind induced-fatigue method proposed by Repetto and Solari in 2006. These authors obtained the previously described closed form solution of the alongwind induced-fatigue cycles histogram by adopting some hypotheses. Assuming *S*-*N* nominal approach and disregarding the effects of the original load cycle sequence, wind-induced nominal stress processes associated with the *i*-th loading conditions are considered. The *i*-th loading condition probability of occurrence is expressed by the hybrid Weibull distribution. Wind directionality is neglected, considering a constant direction *x*.

A hierarchy of further hypotheses was then introduced and critically discussed by Repetto and Solari (2007; 2009; 2012), which have led to a progressive simplification of the basic formulation. Focusing attention on alongwind-induced fatigue, they developed a novel, precise and reliable closed form solution for predicting total damage and fatigue life. This aim was pursued by retaining the fundamental approach of previous work and indeed introducing the hypotheses that progressively simplified the basic formulation. Two levels of formulae were derived, namely a closed form solution and an approximated closed form expression of the wind-induced damage; these represented a solid base from which to derive suitable methods for engineering calculations and standards. Again, the application of the proposed method highlighted good agreement with the numerical results obtained with Monte Carlo simulations

analysed by the Rainflow Counting method. Crosswind-induced fatigue and simultaneous alongwind and crosswind-induced fatigue were not taken into account.

- Wind directionality is neglected.

One major issue is that of directionality. Section 2.3.2 introduces the strong underlying assumption of an omnidirectional behaviour. The method under consideration treats the mean wind velocity as a Weibull random variable, disregarding directionality effects. Alongwind and crosswind buffeting forces are represented, by quasisteady theory, as a linear combination of the longitudinal and lateral turbulence components. Actually, wind climate is suitably modelled by the joint density function of the mean wind velocity intensity and direction, therefore directional distribution analysis results as a major issue.

Repetto and Solari (2004) discussed this matter, pointing out that disregarding wind directionality implies the concentration of the most severe stress conditions in the same structural plane, instead of spreading the damage accumulation around the entire fatigue sensitive detail. They carried out a research on this topic, deriving histogram of the stress cycles, the accumulated damage, and the fatigue life of slender vertical structures exposed to simultaneous alongwind and crosswind vibrations, applying a reformulated model which considered the joint density function of the mean wind velocity and direction. At this stage of their research, the probabilistic accumulation of damage due to aerodynamic actions on stationary structures was estimated by a counting cycle method inspired by narrow band processes and the damage in lock-in conditions was superimposed. Their analyses and results focused on the role of wind directionality.

In each ΔT interval the mean wind velocity is schematized with constant intensity and constant direction (rotated with respect to x). Subdividing space in a set of directional sectors around a considered position, the joint probability P_{ih} that the mean wind velocity belongs to the i-th velocity interval and the wind blows from the h-th sector is usually expressed by Weibull distribution in which distribution parameters depend on h-th directional sector (k_h and c_h). This enables the estimation of the four dimensional histogram that underlines the distribution of the stress cycles with varying mean wind velocity, mean wind direction, and stress amplitude. Incorporating these improvements into the original proposed method, using S-N fatigue curves and the Palmgren–Miner linear accumulation law, the fatigue damage can be estimated.

Conclusions of this work were that if the wind direction is considered as constant during the structure's whole life, the estimated mean fatigue life is minimum, representing a lower bound on the safe side, as it corresponds to concentrate the damage in the most stressed point of the analysed structural detail. Assuming that the wind blows from any direction with uniform probability, the resulting fatigue life represents an upper bound that corresponds to spread the damage over the critical sections uniformly. In the case of a slender structure very sensitive to crosswind-induced fatigue but almost insensitive to

alongwind-induced fatigue, the gap between the two bounds may be large. On the contrary, for slender structures almost equally sensitive to both alongwind and crosswind-induced fatigue, the gap between the two bounds may be narrow. Therefore, the importance of wind directionality is linked with structural sensitivity to alongwind and crosswind actions. If a structure is sensitive to both actions, wind directionality seems not to be determinant; in such cases, wind directionality has a marginal role. On the contrary, if a structure is sensitive to only one of these actions, disregarding wind directionality can lead to fundamental underestimation of the mean fatigue life, remaining on the safe side.

It is worth notice that directional probability P_h, namely the probability that the wind blows from the h-th sector with nonzero velocity, is normally linked with the territorial position and with the local site properties. Codes does not provide standard recommendations regarding the assessment of directional probability at present. In order to develop a method to evaluate wind-induced fatigue in engineering practice, the unidirectional hypothesis results safe and fit for purpose.

- Neutral atmospheric thermal stratification is assumed for any wind condition.

One other major issue is that of atmospheric stratification. As introduced in Section 2.3.1, the atmosphere may be stably stratified (this condition generally occurs during nights and it is characterized by suppressed turbulence), unstably stratified (this condition generally occurs during days and it is characterized by exalted turbulence) or neutrally stratified (this condition is characterized by high wind velocity and large turbulent fluctuations). Under neutral condition wind velocity is independent of temperature, therefore the mean wind velocity profile is a function of terrain orography and terrain roughness and it is suitable described by the logarithmic law (Eqs. (2.19), (2.20)). Since high mean wind velocity (more than 10 m/s on average) can be associated with neutral conditions, hypothesising the wind field as neutrally stratified is typical of evaluations addressed to ultimate loading conditions. However, fatigue problems arise from damage cumulating over the entire range of wind velocities, being sensitive to moderate wind velocities for which stable or unstable atmospheric conditions can occur (Panofsky and Dutton, 1984); such occurrences may result very important especially with reference to critical vortex shedding effects.

Despite this, neutral stratification is one of the underlying hypotheses of the method under consideration; this strong assumption is required for expressing the mean wind velocity by the logarithmic law, allowing to develop closed form equations. This aspect was properly discussed by Repetto and Solari (2007) in order to analyse the impact of the assumption on the quality of the results. The procedures previously established have been extended to non-neutral thermal stratifications. The mean wind velocity profile and the cross-power spectral density functions of the atmospheric turbulence are expressed in terms of the Monin–Obukhov length (Monin and Obukhov, 1954). The occurrence of stable, unstable and neutral conditions is taken into account by means of the joint probability distribution

of the mean wind velocity and direction and of the Monin–Obukhov length. The joint probability that the mean wind velocity belongs to the *i*-th velocity interval, that the wind blows from the *h*-th directional sector, and that (1/L = Obukhov length) belongs to the *l*-th interval is defined as P_{ihl}, a quantity linked with the territorial position, with the local site properties and with the thermal atmospheric stratification. The *ihl*-th loading condition is characterised by the probability P_{ihl}, and the structure undergoes such a condition for an effective duration time $T_{ihl} = TP_{ihl}$. The damage induced by all the wind loading conditions during the whole structure's life is evaluated, based on the spectral bi-modal counting method (Repetto and Solari, 2006), collecting the wind loading cycles into a discrete cycles histogram. The total mean damage is given by the sum of all the fractions of the mean damage induced by every block of the cycles histogram, each associated to a *j*-th cycle amplitude, a *i*-th velocity interval, a *h*-th directional sector and *l*-th Monin–Obukhov length.

Conclusive observations are that, as expected, the alongwind and crosswind-induced response significantly changes at low mean wind velocities, depending on the thermal stratification. Under stable conditions or unstable conditions, the stress cycles histogram and the fractions of damage, very sensitive to the most frequent low mean wind velocities, completely change. However, the changes compensate each other such that the mean total damage and the mean fatigue life under neutral and stratified conditions are almost the same. This is in accordance with the day-night alternation of non-neutral atmospheric conditions, which probably produces a balance of the respective effects in long periods. Sound statistical models of the joint distribution of the mean wind velocity and of the Monin–Obukhov length require to be elaborated.

Furthermore, three simplifying hypotheses (Repetto and Solari, 2009; 2012) were necessary in order to obtain the mean total damage analytically rather than by means of double summations of every loading condition and every stress amplitude (Fig. 2.16):

- Power law approximation of stress parameters;
- Hybrid Weibull model for mean wind velocity density function (Section 2.3.1; Eq. (2.21));
- Trilinear *S-N* fatigue curves (Section 2.2.2; Eq. (2.8); Fig. 2.5).

Hybrid Weibull model for mean wind velocity density function is introduced in Section 2.3.1 and it is often adopted in wind engineering procedures; trilinear *S-N* fatigue curves typical of steel details under normal stress conditions is introduced in Section 2.2.2 and it is often adopted in fatigue engineering procedures; the essential power law approximation is introduced and discussed below.

The solution of the mean total damage in closed form solution requires expression of the statistical parameters of the wind-induced stress range on varying the mean wind velocity $\bar{u}$. Standards generally

furnish suitable methods for evaluating the standard deviation and the expected frequency of the stress process at a reference wind velocity $\bar{u}_{ref}$ (e.g. the mean wind velocity with a 50-year return period, at 10 m height on a flat homogeneous terrain with roughness length 0.05 m). Limited to cantilever slender structures, the model proposed in (Piccardo and Solari, 2002) furnishes closed form solutions of all the stress parameters introduced in Section 2.3.1 (Eqs. (2.26)-(2.31)), for any value of mean wind velocity $\bar{u}$. Stress parameters vary with the mean wind velocity $\bar{u}$ as a function of many quantities characterizing the site (e.g. the reference wind velocity $\bar{u}_{ref}$ and the roughness length z_0), the geometry of the structure (e.g. the length l and the reference size b), and its dynamic properties (e.g. the natural frequency n_1 and the damping ratio ξ).

The basic stress parameters – namely, the mean value $\bar{s}$, the standard deviation σ, the expected frequency ν, the expected frequency of the quasi-static part ν_Q, and the normalized variance of the resonant part λ_R – are linked with the mean wind velocity $\bar{u}$ by the approximate power law:

$$\kappa(\bar{u}) = \kappa_{ref}\left(\frac{\bar{u}}{\bar{u}_{ref}}\right)^{\alpha_\kappa} \tag{2.38}$$

where κ is a generic stress parameter ($\kappa = \bar{s}, \sigma, \nu, \nu_Q, \lambda_R$), $\bar{u}_{ref}$ is the design mean wind velocity, i.e. the reference wind velocity associated with the design return period R (e.g. R = 50 years), $\kappa_{ref} = \kappa(\bar{u}_{ref})$. The first diagram of Fig. 2.20, which represents a generic alongwind stress status, can be approximated by power laws (Eq. (2.38)) because it grows with the mean wind velocity following an exponential trend, thus maximum ultimate condition occurs at high velocities. In the second diagram of Fig. 2.20, which represent a relevant wind-induced damage histogram, it is evident that the maximum fatigue damage condition occurs instead in the middle range of the mean wind velocity.

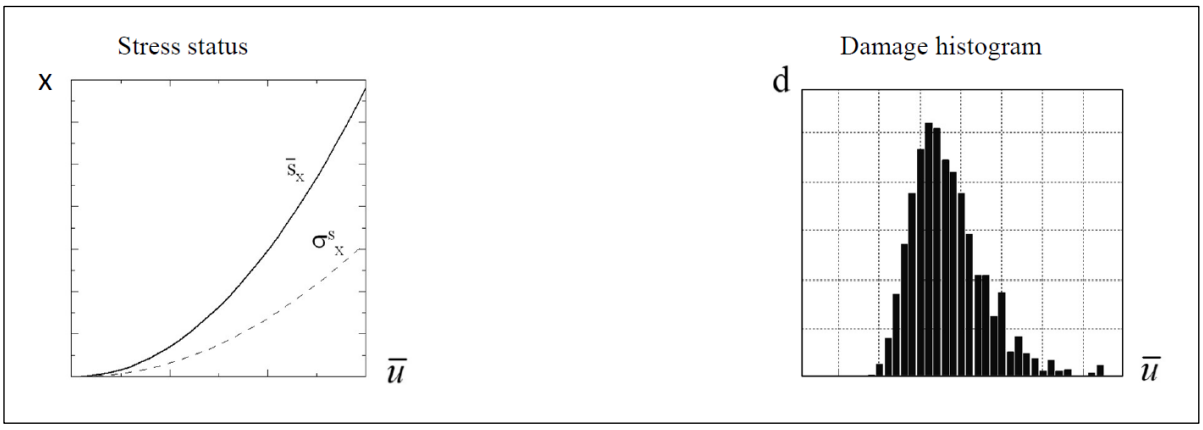

Fig. 2.20: Diagram of some basic stress response parameters in x direction (alongwind), namely the mean value and the standard deviation, on varying mean wind velocity; related damage histogram on varying mean wind velocity.

Eq. (2.38) was first introduced by Holmes (2002) limited to the standard deviation, suggesting a power value between 2 and 2.5. This expression is simple, but the proposed range of the power value leads to great uncertainties in the middle range of the wind velocity, greatly affecting the fatigue damage estimate. Bearing this in mind, Repetto and Solari (2009; 2012) generalized the approximated power law to any stress parameter due to alongwind loadings, defining a general effective expression to estimate the exponent of the power law α_κ in function of two different values of wind velocity. Therefore, the fatigue velocity $\bar{u}_{fat}$ has been defined as representative of the range where the fatigue damage is maximum. Its value strictly depends on the probability density function of the mean wind velocity at the site (Eq. (2.21)). An appropriate value for territory in Italy is the half of the reference velocity $\bar{u}_{fat}(Z) = 0.5 \cdot \bar{u}_{ref}(Z)$; an appropriate value of $\bar{u}_{fat}$ may be estimate for any other country following the procedure described by Repetto and Solari (2009). In this way, the approximation of the power law is optimized in the middle and high wind velocity ranges, since they turn out to be influential in determining the alongwind induced fatigue damage.

Calibration of power law functions was made taking into account a set of slender vertical structures, varying l in the range 10 m to 100 m, n_1 in the range 0.5 Hz to 1.5 Hz, and ξ in the range 0.005 to 0.05, and producing curves of the stress parameters as a function of $\bar{u} / \bar{u}_{ref}$. The maximum spread occurs in the middle range of the mean wind velocity, in correspondence with the typical range of the maximum fatigue damage. Thus, simple expressions providing good approximations of these parameters in the middle range of the wind velocity were proposed. The power law proposed by Holmes for the stress standard deviation has been adopted also for the other stress parameters and the exponent of the function was defined as:

$$\alpha_\kappa = \frac{\ln\left(\kappa_{fat} / \kappa_{ref}\right)}{\ln\left(\bar{u}_{fat} / \bar{u}_{ref}\right)} \tag{2.39}$$

The approximations are optimized in the middle and high wind velocity ranges. In the low wind velocity range errors are very large but they turn out not to be influential in determining the alongwind induced fatigue damage (Repetto and Solari, 2008, 2009).

As regards the quantity $\bar{u}_{fat}$, it was identified in correspondence of the maximum value of the mean total damage, strictly depending on the probability density function of the mean wind velocity at the site of the structure $p_U(\bar{u})$. Thus, in principle, evaluating $\bar{u}_{fat}$ requires ad hoc analyses for each local condition. In order to furnish general indications about $\bar{u}_{fat}$, Repetto and Solari (2009) developed a two-step analysis. The first step expresses the mean total damage in an approximated form as the integral of a

function proportional to $p_U(\bar{u})\bar{u}^6$ and $\bar{u}_{fat}$ is defined as the abscissa of the maximum of that function. The second step concerns a specific country, for example Italy, by evaluating the velocity associated to the maximum fatigue damage condition according to data provided by meteorological stations and by making the average. Their analyses led to the relationship $\bar{u}_{fat} \cong 0.5\bar{u}_{ref}$ in Italian territory.

Summarizing, the approximate equation (2.38) basically allows to express analytically the basic buffeting response parameters variation on wind velocity. Therefore, evaluating structural response at only two different values of wind speed is sufficient to apply the proposed fatigue model and estimate a reliable fatigue life. The structural response can be evaluated at the reference mean velocity, $\bar{u}_{ref}$, and at the fatigue velocity, $\bar{u}_{fat}$, in the area where the structure is located. As the reference mean velocity $\bar{u}_{ref}$ is the wind velocity corresponding to the maximum wind ultimate conditions, the choice for defining the fatigue velocity $\bar{u}_{fat}$ is the wind velocity corresponding to the maximum wind-induced fatigue damage conditions.

In this thesis wind directionality and thermal stratification are disregarded, assuming the wind direction as constant and the atmosphere as neutrally stratified for any wind condition. These assumptions are commonly used in wind engineering ultimate analyses. It is noted that no information on directional distribution and on thermal stratification suitable for engineering practice is currently available (Repetto and Solari, 2004; 2007).

Power law approximation of stress parameters and hybrid Weibull model for mean wind velocity density function are also assumed in the present research thesis (Repetto and Solari, 2009; 2012).

As regards the hypothesis of trilinear *S-N* fatigue curves, Chapter 3 goes beyond this assumption providing an improved model of analysis.

CHAPTER 3 - FATIGUE RESISTANCE CURVES GENERALIZATION

3.1. INTRODUCTION

Structural elements often experience fatigue process in critical joints, which may lead to damage or even failure. Assessment and design procedures involves the knowledge of resistance and actions. Resistance *S-N* curves are obtained experimentally for different materials and structural details. In civil engineer field, the cyclic loadings that stress the structures may be stochastic processes and require suitable cycle counting methods application.

Slender structures may be subject to wind-induced fatigue, this turning out to be a common and critical event. Since standards and codes were still lacking of a reliable general method (Eurocode 1, 2005), many research investigations deal with this issue, trying to come to a closed form-solution.

Holmes made a distinction between narrow and wide-banded time series (Holmes, 2002; Robertson et al., 2004; Holmes, 2008). This author used the level crossing formula from Rice (1944) for a closed form solution of narrow band stress responses; for a wide band response, typical for alongwind actions, he suggested a formula according to Wirsching and Light (1980), which lead to useful approximations of the lower and upper lifetime. A limiting assumption of this solution is that a linear *S-N* relation (in the bi-logarithmic diagram) is taken into account.

Kemper proposed a closed-form solution applicable for random wide-banded responses and for arbitrary *S-N* curves (Kemper and Feldmann, 2011). In this approach remains the distinction between the nature of the response, the fatigue resistance definition and the damage accumulation hypothesis. Based on the power spectral density of the response with arbitrary bandwidth, these authors proposed to apply a frequency based cycle counting method from Dirlik (1985) in order to obtain a cycle histogram under extreme wind. Taking into account the Weibull distribution for the parent population of mean wind velocity, a design-life can be determined, adopting one of all the common approaches of the damage theory. The procedure directly allows the usage of *S-N* curves with arbitrary shapes. The following challenge has been to introduce simplifications in order to make this method suitable in the codification sector. Recent developments present a simplified approach, which suggests damage equivalence factors, taking into account an individual and realistic shape of the cycle count distribution (Kemper, 2019). According to this concept, realistic stress distributions for gust excited structures may be derived without a need of a detailed structural calculation.

Among the other proposals, a wide research project aimed at formulating and calibrating a general procedure for determining wind-induced fatigue was carried out between 2001 and 2012 by Repetto and Solari (2001, 2002, 2004, 2006, 2007, 2008, 2009, 2010, 2012; Repetto, 2003, 2005). A refined closed-form solution of the alongwind-induced fatigue damage has been obtained, from which a simplified procedure suitable for engineering evaluation and code provisions has been derived (Repetto and Solari, 2012).

The bases of this method have been introduced in Chapter 2 (Section 2.3) and its description is here resumed and analysed. Then, some advancements are proposed in the present and following Chapters.

In order to obtain the cycle histogram, structural response must be evaluated at a large number of wind velocity values, usually at intervals of 1 m/s up to the reference mean velocity with 50 years return period, then the number of cycles that stresses the structure is identified by the bi-modal counting method (Repetto, 2003, 2005; Repetto and Solari, 2001, 2002, 2004, 2006, 2010). This counting method involves expressing the stress associated with the mean velocity as a sum of the quasi-static and the resonant part of the structural response. Following this consideration, the mean damage derives from a sum of two narrow band contributions. The total cumulative damage is expressed by means of the linear accumulation law (Miner, 1945) and the fatigue life is estimated from the mean total damage in the unit time.

Furthermore, a refined closed-form solution of the alongwind turbulence-induced fatigue has been obtained (Repetto and Solari, 2009, 2012). The achievement is that the mean total damage obtained, which usually requires huge computations of structural response at every value of wind velocity, is allowed to be evaluated in closed-form computing the structural response just for two values of wind velocity. To this aim, three hypotheses are assumed. The first main simplifying hypothesis is that basic stress parameters of the random process (the mean value, the standard deviation, the expected frequency, the expected frequency of the quasi-static part and the normalized variance of the resonant part) are linked with the mean wind velocity by the power law approximation. This rule was first introduced by Holmes (2002) limited to the standard deviation and later generalized by Repetto and Solari (2009, 2012) to any stress parameter due to alongwind loadings. It is possible to estimate the exponent of the power law in function of only two different values of wind velocity, conventionally the reference mean wind velocity, that is the velocity with 50 years return period in the site at a fixed reference height adopted for ULS analysis, and fatigue velocity, which represents velocity that produces maximum fatigue damage. The second hypothesis is that the density function of the mean wind velocity is represented by the hybrid Weibull model (Takle and Brown, 1978). Third, the considered *S-N* resistance curve follows the trilinear trend adopted in the mechanical and structural practice for steel details subjected to normal stresses, according to the nominal approach (Eurocode 3, 2005).

This method to evaluate alongwind-induced fatigue damage have two main limitations: it is valid only for bi-modal response processes, so induced by alongwind turbulence excluding a crosswind-induced fatigue analysis; its applicability is limited to fatigue due to normal stresses in steel elements, whose *S-N* fatigue curve in standards has a fixed trilinear trend. Objective of the present research thesis is to overcome this two important limitations, contributing in make this method suitable and reliable for standard engineering verifications.

The present Chapter 3 proposes a new generalization of this procedure at engineering level, covering buffeting-induced fatigue for a wide range of resistance fatigue curve types, suitable for different materials. In order to develop these purposes, the formulation proposed in 2012 has been revised and discussed, in complete accordance with Eurocode standards format for wind induced Ultimate Limit State (ULS) analysis. The hypothesis of trilinear *S-N* curve in a bi-logarithmic diagram, typical of normal stresses in steel details, is overcome, generalizing the whole formulation for different possible shapes of fatigue curves. This is the first original contribution of this thesis to the effective existing method proposed in 2012. This intent is proving to be crucial since fatigue arises in different materials as well as in steel, and the damage may be the result of normal or tangential stresses.

Section 3.2 introduces the whole derivation of the closed-form solution of buffeting-induced fatigue damage. Firstly, it introduces the basic hypotheses of the methods and its fundamentals. The mean total damage is expressed as the product of a *0 level solution* multiplied by three corrective factors. Then Paragraphs 3.2.1, 3.2.2, 3.2.3 and 3.2.4 resume the analytical steps to obtain the all factors in closed-form (Repetto and Solari, 2009, 2012).

In particular, Paragraph 3.2.4 deals with the Generalized fatigue curve factor, a novelty reached with the purpose of generalizing the method as regards fatigue resistance curves. In this paragraph an important contribution of this thesis to the original method can be found.

Section 3.3 simplifies the generalized formulation in order to make the procedure suitable for engineering evaluation and code provisions. This Section introduces the simplifying hypotheses needed to this aim and it presents the final formulation directly. All analytical steps are reported in Appendix A: the derivation of the simplified Generalized fatigue curve factor, although it purposely leads to an equation in compliance with the old solution, is completely new.

3.2. CLOSED-FORM SOLUTION OF MEAN DAMAGE

The proposed fatigue assessment approach takes into account the buffeting response and it considers, for safety's sake, that the incoming wind has always the worst direction for the structural response (unidirectional analysis) (Repetto and Solari, 2004). The formulation considers the joint effect of the turbulence-induced variable loadings, of the wind-induced static actions and other permanent loads on the

structure; it does not consider the joint effect due to other variable loadings on the structure, such as mobile loads, vehicular traffic, waves; it does not consider vortex shedding effects as well. As the fatigue damage phenomenon is strongly non-linear, superposition effect does not apply; therefore, when different types of variable actions affect the structure, the current model is no longer applicable.

Adopting the *S-N* approach, the fatigue damage is evaluated by the Palmgren-Miner linear rule referred to the nominal stress. Thus, the fractions of the mean damage induced in the unit time at a fixed mean wind velocity $\bar{u}$ can be expressed as:

$$d\bar{\delta}\left(1,\Delta,\bar{u}\right)=\frac{d\bar{n}\left(1,\Delta,\bar{u}\right)}{N\left(\Delta,\bar{s}_t,\bar{u}\right)}=\frac{\nu_{\Delta}\left(\bar{u}\right)p\left(\Delta\,|\,\bar{u}\right)d\Delta}{N\left(\Delta_e;\bar{u}\right)} \tag{3.1}$$

where $d\bar{n}$ = mean number of cycles related to $\bar{u}$ with stress range between Δ and $\Delta + d\Delta$; ν_{Δ} = expected frequency of the stress cycles; $p(\Delta|\bar{u})$ = probability density function of Δ, conditional to the occurrence of $\bar{u}$; N = number of cycles that causes the collapse for a stress range Δ and a mean stress $\bar{s}_t=\bar{s}+\bar{s}_p$, $\bar{s}$ and $\bar{s}_p$ = static stresses because of the mean wind velocity $\bar{u}$ and the permanent and variable static loads, respectively. Standards usually furnish the *S-N* curves providing the number of cycles $N(\Delta)$ that causes the collapse for a stress range Δ and $\bar{s}$ =0. A non-null mean stress can be considered to replace Δ by an equivalent stress range Δ_e, evaluated by Goodman's relationship (Goodman 1930), $\Delta_e = \Delta\, s_u / (s_u - \bar{s}_t)$, where s_u is the ultimate stress of the material (see Section 2.2.1; Eq. (2.1)).

The fraction of damage because of $\bar{u}$ in the unit time is obtained by integrating Eq. (3.1) on Δ:

$$\bar{d}\left(1,\bar{u}\right)=\int_0^{\infty}\frac{\nu_{\Delta}\left(\bar{u}\right)p\left(\Delta\,|\,\bar{u}\right)}{N\left(\Delta_e;\bar{u}\right)}d\Delta \tag{3.2}$$

Considering the mean wind velocity variation, the mean total damage in the unit time results in:

$$\bar{D}(1)=\int_0^{\infty}\bar{d}\left(1,\bar{u}\right)p\left(\bar{u}\right)d\bar{u} \tag{3.3}$$

where $p(\bar{u})$ = the density function of $\bar{u}$.

In order to obtain a closed-form solution to Eqs. (3.2) and (3.3), three simplifying hypotheses are introduced, previously discussed in Section 2.3.3. First, the basic stress parameters are linked with $\bar{u}$ by the approximate power law in Eq. (2.38) (Holmes, 2002; Repetto and Solari, 2012); second, the density function of $\bar{u}$ is given by the hybrid Weibull model (Takle and Brown, 1978; Repetto and Solari, 2012), expressed by Eq. (2.21) in Section 2.3.1; third, in accordance with the code provisions usually adopted in the mechanical and structural practice, the fatigue resistance is expressed by a *S-N* fatigue curve (Section 2.2.2). Differently than Repetto and Solari (2012) solution, this third hypothesis is here more general,

concerning general *S-N* curves in a log-log diagram, identified by the detail category Δ_C, corresponding to $N_C = 2 \times 10^6$. These curves are characterized by a first line slope named m_1, which remains implicit in this new formulation.

The mean total damage in a period T is $\bar{D}(T) = T\bar{D}(1)$. Collapse conventionally occurs after a mean time $T=T_F$ such that $\bar{D}(T_F) = 1$. Therefore, the so called fatigue life T_F, defined as the time in which total damage reaches the unit, is provided by:

$$T_F = \frac{1}{\bar{D}(1)} \tag{3.4}$$

Based on these three hypotheses, Repetto and Solari (2009, 2012) demonstrated that the annual mean damage in the unit time $\bar{D}(1)$, provided by Eq. (3.3), may be reasonably expressed by the product of an approximated closed-form solution of the mean damage $\bar{D}_0(1)$, referred to as the *0 level solution*, multiplied by three suitable corrective factors:

$$\bar{D}(1) = \bar{D}_0(1) C_{BM} C_M C_{SN} \tag{3.5}$$

where C_{BM}, C_M and C_{SN} are the corrective factors obtained analytically, called the bi-modal factor, the mean stress factor and the fatigue curve factor, respectively.

The 0 level solution, $\bar{D}_0(1)$, is inspired by a similar method proposed by Holmes (2002), and adopts three classic simplifications traditionally used in the technical literature: 1) the stress process is narrow band; 2) the stress process is zero mean; 3) the fatigue curve is a straight line on a log (stress range) – log (number of cycles that cause the collapse) diagram, with constant slope m_1.

The bi-modal factor C_{BM} reduces the 0 level damage taking into account the quasi-static part of the response spectrum; in buffeting-induced response the quasi-static part of the response may have a high role, which can not be neglected (Section 2.3.1).

The mean stress corrective factor C_M increases the total damage, taking into account the non-zero value of the mean response to wind loading.

Finally, the fatigue curve factor C_{SN} reduces the damage, taking into account the actual fatigue resistance curve related to the analysed structural detail.

In the following of this Section 3.2, all the factors that appears in Eq. (3.5), needed to calculate the total mean damage in the unit time, are derived and discussed.

3.2.1. Zero level solution of damage

The 0 level solution of damage, $\bar{D}_0(1)$, adopts three classic simplifications.

1) Assuming that the wind-induced stress process at the mean wind velocity $\bar{u}$ is a narrow band Gaussian stationary process, each peak of the stress time history $\hat{s}$ is associated with a cycle of double range of the peak value $\Delta = 2\hat{s}$; thus, according to the Peak counting method, the expected frequency of the stress range Δ is equal to the expected frequency of the process $v_{\Delta}(\bar{u}) = v(\bar{u})$ and the stress range Δ follows a Rayleigh distribution with standard deviation $\sigma_{\Delta}(\bar{u}) = 2\sigma(\bar{u})$ and probability density function, conditional to the occurrence of $\bar{u}$:

$$p(\Delta \mid \bar{u}) = \frac{\Delta}{\left[2\sigma(\bar{u})\right]^2} \exp\left(-\frac{\Delta^2}{2\left[2\sigma(\bar{u})\right]^2}\right) \mathrm{d}\Delta \tag{3.6}$$

2) The 0 level solution $\bar{D}_0(1)$ derives from the assumption that the mean stress due to permanent and variable actions are neglected, assuming the stress process as a zero mean one with $N(\Delta_e; \bar{u}) = N(\Delta; \bar{u})$.

3) The 0 level solution $\bar{D}_0(1)$ is obtained considering the fatigue curve as a straight line on the bi-logarithmic *S-N* diagram:

$$N = \frac{a_1}{\Delta^{m_1}} \tag{3.7}$$

where N is the number of cycles that causes the failure, Δ is the stress range of the cycles, a_1 and m_1 are constants depending on the material and the structural component.

Taking into account all these considerations, the 0 level solution of damage is provided starting from Eq. (3.2) rewritten as:

$$\bar{d}_0(1, \bar{u}) = \int_0^{\infty} \frac{v(\bar{u})}{a_1} \frac{\Delta^{m_1+1}}{\left[2\sigma(\bar{u})\right]^2} \exp\left(-\frac{\Delta^2}{2\left[2\sigma(\bar{u})\right]^2}\right) \mathrm{d}\Delta \tag{3.8}$$

Considering the gamma Function (Davis 1965):

$$\Gamma(n) = \int_0^{\infty} t^{n-1} \exp(-t) \mathrm{d}t \tag{3.9}$$

the integral in Eq. (3.8) can be solved in closed-form, giving as result:

$$\bar{d}_0(1, \bar{u}) = \frac{v(\bar{u})}{a_1} \left[2\sqrt{2}\sigma(\bar{u})\right]^{m_1} \Gamma\left(\frac{m_1}{2} + 1\right) \tag{3.10}$$

This expression represents the mean damage in the unit time at a fixed mean wind velocity $\bar{u}$ on varying cycles amplitude. The total mean damage in the unit time on varying mean wind velocity, with

the three simplifications, is given by Eq. (3.3), in which $\bar{d}(1,\bar{u})$ multiplied by the density function of $\bar{u}$, $p(\bar{u})$, is integrating on $\bar{u}$.

Substituting Eq. (3.10) and Eq. (2.21) (hybrid Weibull) into Eq. (3.3), the 0 level solution of the mean total damage per unit time is given by:

$$\bar{D}_0(1)=\int_0^{\infty}\frac{\nu(\bar{u})}{a_1}\left[2\sqrt{2}\sigma(\bar{u})\right]^{m_1}\Gamma\left(\frac{m_1}{2}+1\right)\left[F_0\delta(\bar{u})+(1-F_0)\frac{k}{c}\left(\frac{\bar{u}}{c}\right)^{k-1}\exp\left\{-\left(\frac{\bar{u}}{c}\right)^{k}\right\}\right]d\bar{u} \tag{3.11}$$

This integral is the sum of two integrals, one equal to zero, therefore:

$$\bar{D}_0(1)=\int_0^{\infty}\frac{\nu(\bar{u})}{a_1}\left[2\sqrt{2}\sigma(\bar{u})\right]^{m_1}\Gamma\left(\frac{m_1}{2}+1\right)(1-F_0)\frac{k}{c}\left(\frac{\bar{u}}{c}\right)^{k-1}\exp\left\{-\left(\frac{\bar{u}}{c}\right)^{k}\right\}d\bar{u} \tag{3.12}$$

Approximating $\sigma(\bar{u})$ and $\nu(\bar{u})$ by the power laws (from Eq. (2.38)):

$$\sigma(\bar{u})=\sigma_{ref}\left(\frac{\bar{u}}{\bar{u}_{ref}}\right)^{\alpha_\sigma} \tag{3.13}$$

$$\nu(\bar{u})=\nu_{ref}\left(\frac{\bar{u}}{\bar{u}_{ref}}\right)^{\alpha_\nu} \tag{3.14}$$

and considering again the gamma Function (Eq. (3.9)), Eq. (3.12) becomes:

$$\bar{D}_0(1)=\frac{\left(2\sqrt{2}\right)^{m_1}}{a_1}\left(\frac{\sigma_{ref}}{\bar{u}_{ref}^{\alpha_\sigma}}\right)^{m_1}\frac{\nu_{ref}}{\bar{u}_{ref}^{\alpha_\nu}}(1-F_0)c^{(\alpha_\nu+m_1\alpha_\sigma)}\Gamma\left(\frac{m_1}{2}+1\right)\Gamma\left(\frac{\alpha_\nu+m_1\alpha_\sigma+k}{k}\right) \tag{3.15}$$

which is the 0 level closed-form solution of mean damage.

3.2.2. Bi-modal factor

The result obtained in Section 3.2.1 derives from the assumption that the wind-induced stress at the mean wind velocity $\bar{u}$ is a narrow-band Gaussian stationary process. This usual hypothesis in random fatigue analyses leads to conservative results. The overestimation involved in turbulence-induced fatigue can be very large when the quasi-static part of the response is non-negligible.

The bi-modal factor, C_{BM}, corrects the 0 level solution, removing the first simplifying hypothesis that the stress process is narrow band and taking into account the actual bi-modal spectrum of the dynamic response process at turbulent wind actions, with quasi-static and resonant contents (Fig. 3.1). It satisfies the condition $C_{BM} \leq 1$.

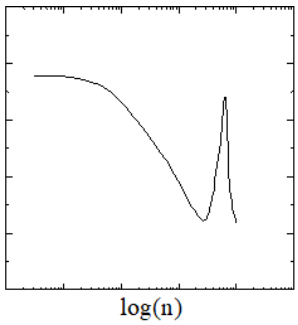

Figure 3.1: Spectrum of the dynamic response process at turbulent wind actions.

The expression of this corrective factor is obtained analytically considering that the stress process, in the conventional ΔT = 10 minutes – 1 hour time interval, is bi-modal, which means that the fluctuating stress $s'(\bar{u})$ is the sum of two independent components: the quasi-static (low frequency) and the resonant (high frequency) parts of the response, $s'_Q(\bar{u})$ and $s'_R(\bar{u})$, respectively. The quasi-static part of the harmonic content is characterized by large cycles, related to the pseudo-envelope process, approximated as a zero mean, gaussian, narrowband process, with attended frequency equal to $\nu_Q(\bar{u})$ and standard deviation $\sigma(\bar{u})$. The resonant part of the harmonic content is characterized by small cycles, related to the resonant process and its envelope, with attended frequency n_1 and standard deviation $\sigma(\bar{u})\cdot\sqrt{\lambda_R(\bar{u})}$ (Section 2.3.1; 2.3.2). C_{BM} tends to 1 when the stress process tends to be narrowband and it reduces the 0 level solution according to the actual stress spectral content (this issue is further discussed in Section 4.3.4).

Taking into account all these considerations and starting again from Eq. (3.2), the mean damage related to $\bar{u}$ is the sum of two distinct narrow-band contributions:

$$\bar{d}_{BM}(1,\bar{u}) = \int_0^\infty \frac{\nu_Q(\bar{u})}{a_1} \frac{\Delta^{m_1+1}}{\left[2\sigma(\bar{u})\right]^2} \exp\left(-\frac{\Delta^2}{2\left[2\sigma(\bar{u})\right]^2}\right) d\Delta + \int_0^\infty \frac{n_1}{a_1} \frac{\Delta^{m_1+1}}{\left[2\sigma(\bar{u})\right]^2 \lambda_R(\bar{u})} \exp\left(-\frac{\Delta^2}{2\left[2\sigma(\bar{u})\right]^2 \lambda_R(\bar{u})}\right) d\Delta \qquad (3.16)$$

Considering the gamma Function (Eq. (3.9)), the integrals in Eq. (3.16) can be solved in closed-form, giving as result:

$$\bar{d}_{BM}(1,\bar{u}) = \frac{\nu(\bar{u})}{a_1}\left[2\sqrt{2}\sigma(\bar{u})\right]^{m_1} \Gamma\left(\frac{m_1}{2}+1\right)\left\{\frac{\nu_Q(\bar{u})}{\nu(\bar{u})} + \frac{n_1}{\nu(\bar{u})}\lambda_R^{m_1/2}(\bar{u})\right\} \qquad (3.17)$$

Comparing Eq. (3.17) with Eq. (3.10), the bi-modal correction is equivalent to replacing the expected frequency of the narrow-band cycles by a weighted value of the expected frequencies of the quasi-static and resonant components. The expression in curly brackets represents the correction of the zero level

solution at a fixed mean wind velocity $\bar{u}$. The total mean damage in the unit time on varying mean wind velocity, with bi-modal correction, is given by Eq. (3.3), in which $\bar{d}(1,\bar{u})$ is given substituting Eq. (3.17) and $p(\bar{u})$ is given substituting Eq. (2.21):

$$\bar{D}_{BM}(1)=\int_0^{\infty}\frac{\nu(\bar{u})}{a_1}\left[2\sqrt{2}\sigma(\bar{u})\right]^{m_1}\Gamma\left(\frac{m_1}{2}+1\right)\left\{\frac{\nu_Q(\bar{u})}{\nu(\bar{u})}+\frac{n_1}{\nu(\bar{u})}\lambda_R^{m_1/2}(\bar{u})\right\}\left[F_0\delta(\bar{u})+(1-F_0)\frac{k}{c}\left(\frac{\bar{u}}{c}\right)^{k-1}\exp\left\{-\left(\frac{\bar{u}}{c}\right)^{k}\right\}\right]d\bar{u} \tag{3.18}$$

and it is rewritten as follows:

$$\bar{D}_{BM}(1)=\int_0^{\infty}\left\{\frac{\nu_Q(\bar{u})}{\nu(\bar{u})}+\frac{n_1}{\nu(\bar{u})}\lambda_R^{m_1/2}(\bar{u})\right\}\frac{\nu(\bar{u})}{a_1}\left[2\sqrt{2}\sigma(\bar{u})\right]^{m_1}\Gamma\left(\frac{m_1}{2}+1\right)(1-F_0)\frac{k}{c}\left(\frac{\bar{u}}{c}\right)^{k-1}\exp\left\{-\left(\frac{\bar{u}}{c}\right)^{k}\right\}d\bar{u} \tag{3.19}$$

This integral is the sum of two integrals that can be solved in closed-form. Considering the gamma Function (Eq. (3.9)) and assuming the power law approximation (Eqs. (2.38), (3.13), (3.14)):

$$\nu_Q(\bar{u})=\nu_{Q,ref}\left(\frac{\bar{u}}{\bar{u}_{ref}}\right)^{\alpha_{\nu,Q}}\cong\nu_{Q,ref}\left(\frac{\bar{u}}{\bar{u}_{ref}}\right)^{\alpha_\nu} \tag{3.20}$$

$$\lambda_R(\bar{u})=\lambda_{R,ref}\left(\frac{\bar{u}}{\bar{u}_{ref}}\right)^{\alpha_\lambda} \tag{3.21}$$

Eq. (3.19) results:

$$\bar{D}_{BM}(1)=\frac{\left(2\sqrt{2}\right)^{m_1}}{a_1}\left(\frac{\sigma_{ref}}{\bar{u}_{ref}^{\alpha_\sigma}}\right)^{m_1}(1-F_0)\Gamma\left(\frac{m_1}{2}+1\right) \tag{3.22}$$
$$\times\left\{\frac{\nu_{Q,ref}}{\bar{u}_{ref}^{\alpha_\nu}}c^{(\alpha_\nu+m_1\alpha_\sigma)}\Gamma\left(\frac{\alpha_\nu+m_1\alpha_\sigma+k}{k}\right)+n_1\left(\frac{\lambda_{R,ref}}{\bar{u}_{ref}^{\alpha_\lambda}}\right)^{\frac{m_1}{2}}c^{\left(\frac{m_1}{2}\alpha_\lambda+m_1\alpha_\sigma\right)}\Gamma\left(\frac{\frac{m_1}{2}\alpha_\lambda+m_1\alpha_\sigma+k}{k}\right)\right\}$$

Collecting together the terms related to the 0 level solution (Eq. (3.15)), the bi-modal factor is obtained:

$$\bar{D}_{BM}(1)=\frac{\left(2\sqrt{2}\right)^{m_1}}{a_1}\left(\frac{\sigma_{ref}}{\bar{u}_{ref}^{\alpha_\sigma}}\right)^{m_1}\frac{\nu_{ref}}{\bar{u}_{ref}^{\alpha_\nu}}\left(1-F_0\right)c^{(\alpha_\nu+m_1\alpha_\sigma)}\Gamma\left(\frac{m_1}{2}+1\right)\Gamma\left(\frac{\alpha_\nu+m_1\alpha_\sigma+k}{k}\right)$$
$$\times\left\{\frac{\nu_{Q,ref}}{\nu_{ref}}+\frac{n_1}{\nu_{ref}}\bar{u}_{ref}^{\left(\alpha_\nu-\frac{m_1}{2}\alpha_\lambda\right)}\lambda_{R,ref}^{\left(\frac{m_1}{2}\right)}c^{\left(\frac{m_1}{2}\alpha_\lambda-\alpha_\nu\right)}\frac{\Gamma\left(\dfrac{\frac{m_1}{2}\alpha_\lambda+m_1\alpha_\sigma+k}{k}\right)}{\Gamma\left(\dfrac{\alpha_\nu+m_1\alpha_\sigma+k}{k}\right)}\right\} \tag{3.23}$$

$$\bar{D}_{BM}(1)=\bar{D}_0(1)\cdot C_{BM} \tag{3.24}$$

$$C_{BM}=\frac{\nu_{Q,ref}}{\nu_{ref}}+\frac{n_1}{\nu_{ref}}\bar{u}_{ref}^{\left(\alpha_\nu-\frac{m_1}{2}\alpha_\lambda\right)}\lambda_{R,ref}^{\left(\frac{m_1}{2}\right)}c^{\left(\frac{m_1}{2}\alpha_\lambda-\alpha_\nu\right)}\frac{\Gamma\left(\dfrac{\frac{m_1}{2}\alpha_\lambda+m_1\alpha_\sigma+k}{k}\right)}{\Gamma\left(\dfrac{\alpha_\nu+m_1\alpha_\sigma+k}{k}\right)} \tag{3.25}$$

3.2.3. Mean stress factor

The 0 level solution of damage obtained in Section 3.2.1 derives from the assumption that the mean stress due to permanent and variable actions has a negligible role in fatigue damage. This hypothesis can lead to unsafe results (Repetto and Solari, 2008). The mean stress factor, C_M, corrects the 0 level solution, removing the second simplifying hypothesis. It takes into account the non-null value of the mean stress due to static wind actions and to other static loadings on the structure adopting the Goodman approach, which allows to replace the stress range Δ by an equivalent stress range Δ_e, expressed by Eq. (2.1), rewritten as $\Delta_e = \Delta\, s_u / (s_u - \bar{s}_t)$, see Section 3.2. The mean stress $\bar{s}_t$ is given by the sum of the mean stress due to the static loads $\bar{s}_p$ plus the mean stress due to the mean wind velocity $\bar{s}$. This corrective factor satisfies the condition $C_M \geq 1$, tending to 1 when the mean stress is null and increasing the 0 level solution depending on the mean stress value.

The equivalent stress range Δ_e is:

$$\Delta_e=\Delta\frac{s_u}{s_u-\bar{s}_t}=\Delta\frac{s_u}{s_u-\left(\bar{s}_p+\bar{s}\right)} \tag{3.26}$$

Expressing the mean stress due to the mean wind velocity $\bar{s}(\bar{u})$ by the power law (from Eq. (2.38)), with $\alpha_{\bar{s}}$=2:

$$\bar{s}\left(\bar{u}\right)=\bar{s}_{ref}\left(\frac{\bar{u}}{\bar{u}_{ref}}\right)^2 \tag{3.27}$$

and expanding Eq. (3.26) in Taylor series and disregarding higher order terms, the equivalent stress range Δ_e becomes:

$$\Delta_e=\Delta\frac{s_u}{s_u-\left[\bar{s}_p+\bar{s}_{ref}\left(\frac{\bar{u}}{\bar{u}_{ref}}\right)^2\right]}\cong\Delta\frac{s_u}{s_u-\bar{s}_p}\left[1+\frac{\bar{s}_{ref}}{\left(s_u-\bar{s}_p\right)\bar{u}_{ref}^2}\bar{u}^2\right] \tag{3.28}$$

Considering the non-null value of the mean stress, Eq. (3.2) results:

$$\bar{d}_M\left(1,\bar{u}\right)=\int_0^\infty\frac{v_\Delta\left(\bar{u}\right)p\left(\Delta\,|\,\bar{u}\right)}{N\left(\Delta_e;\bar{u}\right)}d\Delta=\int_0^\infty\frac{v\left(\bar{u}\right)}{a_1}\frac{\Delta\cdot\Delta_e^{m_1}}{\left[2\sigma\left(\bar{u}\right)\right]^2}\exp\left(-\frac{\Delta^2}{2\left[2\sigma\left(\bar{u}\right)\right]^2}\right)\mathrm{d}\Delta \tag{3.29}$$

which can be solved in closed-form, taking into account Eqs. (3.9) (gamma Function) and (3.28):

$$\bar{d}_M\left(1,\bar{u}\right)=\frac{v\left(\bar{u}\right)}{a_1}\left[2\sqrt{2}\sigma\left(\bar{u}\right)\right]^{m_1}\Gamma\left(\frac{m_1}{2}+1\right)\left(\frac{s_u}{s_u-\bar{s}_p}\right)^{m_1}\left[1+\frac{\bar{s}_{ref}}{\left(s_u-\bar{s}_p\right)\bar{u}_{ref}^2}\bar{u}^2\right]^{m_1} \tag{3.30}$$

This expression represents the mean damage associated with $\bar{u}$; substituting Eqs. (2.21) (hybrid Weibull) and (3.30) into Eq. (3.3), the total damage with non-zero mean stress can be expressed by:

$$\begin{aligned}\bar{D}_M\left(1\right)=&\int_0^\infty\frac{v\left(\bar{u}\right)}{a_1}\left[2\sqrt{2}\sigma\left(\bar{u}\right)\right]^{m_1}\Gamma\left(\frac{m_1}{2}+1\right)\left(\frac{s_u}{s_u-\bar{s}_p}\right)^{m_1}\left[1+\frac{\bar{s}_{ref}}{\left(s_u-\bar{s}_p\right)\bar{u}_{ref}^2}\bar{u}^2\right]^{m_1}\\&\times\left[F_0\delta\left(\bar{u}\right)+\left(1-F_0\right)\frac{k}{c}\left(\frac{\bar{u}}{c}\right)^{k-1}\exp\left\{-\left(\frac{\bar{u}}{c}\right)^k\right\}\right]d\bar{u}\end{aligned} \tag{3.31}$$

and it is rewritten as follows:

$$\bar{D}_M\left(1\right)=\Gamma\left(\frac{m_1}{2}+1\right)\left(\frac{s_u}{s_u-\bar{s}_p}\right)^{m_1}\left(1-F_0\right)\frac{k}{c}\int_0^\infty\left[1+\frac{\bar{s}_{ref}}{\left(s_u-\bar{s}_p\right)\bar{u}_{ref}^2}\bar{u}^2\right]^{m_1}\frac{v\left(\bar{u}\right)}{a_1}\left[2\sqrt{2}\sigma\left(\bar{u}\right)\right]^{m_1}\left(\frac{\bar{u}}{c}\right)^{k-1}\exp\left\{-\left(\frac{\bar{u}}{c}\right)^k\right\}d\bar{u} \tag{3.32}$$

The binomial expansion (Davis, 1965) is introduced:

$$\left[1+\frac{\bar{s}_{ref}}{\left(s_u-\bar{s}_p\right)\bar{u}_{ref}^2}\bar{u}^2\right]^{m_1}\cong1+m_1\frac{\bar{s}_{ref}\bar{u}^2}{\left(s_u-\bar{s}_p\right)\bar{u}_{ref}^2} \tag{3.33}$$

therefore:

$$\bar{D}_M(1)=\Gamma\left(\frac{m_1}{2}+1\right)\left(\frac{s_u}{s_u-\bar{s}_p}\right)^{m_1}(1-F_0)\frac{k}{c}\int_0^{\infty}\left[1+m_1\frac{\bar{s}_{ref}\bar{u}^2}{(s_u-\bar{s}_p)\bar{u}_{ref}^2}\right]\frac{v(\bar{u})}{a_1}\left[2\sqrt{2}\sigma(\bar{u})\right]^{m_1}\left(\frac{\bar{u}}{c}\right)^{k-1}\exp\left\{-\left(\frac{\bar{u}}{c}\right)^k\right\}d\bar{u} \tag{3.34}$$

This integral is the sum of two integrals that can be solved in closed-form. Considering the gamma Function (Eq. (3.9)) and assuming the power law approximation (Eqs. (2.38), (3.13), (3.14)), Eq. (3.34) results:

$$\bar{D}_M(1)=\frac{\left(2\sqrt{2}\right)^{m_1}}{a_1}\left(\frac{\sigma_{ref}}{\bar{u}_{ref}^{\alpha_\sigma}}\right)^{m_1}\frac{v_{ref}}{\bar{u}_{ref}^{\alpha_v}}\left(\frac{s_u}{s_u-\bar{s}_p}\right)^{m_1}(1-F_0)\Gamma\left(\frac{m_1}{2}+1\right)c^{\alpha_v+m_1\alpha_\sigma}$$

$$\times\left[\Gamma\left(\frac{\alpha_v+m_1\alpha_\sigma+k}{k}\right)+\frac{m_1\bar{s}_{ref}}{(s_u-\bar{s}_p)\bar{u}_{ref}^2}c^2\Gamma\left(\frac{\alpha_v+m_1\alpha_\sigma+k+2}{k}\right)\right] \tag{3.35}$$

Collecting together the terms related to the 0 level solution (Eq. (3.15)), the mean stress factor is obtained:

$$\bar{D}_M(1)=\bar{D}_0(1)\cdot C_M \tag{3.36}$$

$$C_M=\left(\frac{s_u}{s_u-\bar{s}_p}\right)^{m_1}\left[1+\frac{m_1\bar{s}_{ref}}{(s_u-\bar{s}_p)\bar{u}_{ref}^2}c^2\frac{\Gamma\left(\frac{\alpha_v+m_1\alpha_\sigma+k+2}{k}\right)}{\Gamma\left(\frac{\alpha_v+m_1\alpha_\sigma+k}{k}\right)}\right] \tag{3.37}$$

3.2.4. Generalized fatigue curve factor

The result of damage obtained in Section 3.2.1 derives from assuming that the fatigue *S-N* curve is a straight line on a log-log scale (Eq. (3.7)). The fatigue curve factor, C_{SN}, corrects the 0 level solution, removing this simplifying hypothesis and taking into account the actual *S-N* fatigue curve trend on the bi-logarithmic diagram, furnished by codes and provisions. It satisfies the condition $C_{SN} \leq 1$.

The expression of this corrective factor is obtained analytically, in an approximated form. The current Paragraph 3.2.4 represents the first original contribution of this thesis to the 2012 method by Repetto and Solari, carrying out the derivation of the generalized C_{SN} expression.

Differently from the old fatigue curve factor, which was obtained referring to a fixed *S-N* fatigue resistance curve (trilinear, for normal stresses in steel structural details), this new generalized one is obtained assuming different possible shapes of fatigue curves.

Based on codes and standards, fatigue *S-N* curves may be grouped in three families on the bi-logarithmic diagram:

1) Linear (slope = m_1);
2) Bilinear (first slope = m_1 and then the curve has a cut-off limit or a second slope = m_2, Fig. 3.2a and 3.2b, respectively);
3) Trilinear (first slope = m_1; second slope = m_2 and then the curve has a cut-off limit).

The fatigue curve factor is considered equal to one if the considered *S-N* curve is linear (case 1), because the hypotheses on the 0 level solution of mean damage is that the fatigue curve is a straight line on the log – log diagram, with constant slope m_1; the hypotheses is in fact verified without the need for a corrective factor.

The fatigue curve factor has never been considered in this method with regard to bilinear *S-N* curves (case 2), which are very common for estimating fatigue resistance of different materials and different loading conditions. These bilinear curves can have different shapes, to varying of the first line slope named m_1, the second line slope named m_2 and the position of the knee of the curve identified by Δ_L, which corresponds to a specific number of cycles of collapse N_L (IIW Recommendations, 2016).

The 2012 fatigue curve factor was calibrated to a fixed trilinear *S-N* curve (case 3). It represents fatigue resistance of steel elements subjected to normal stress cycles of loading. Slopes m_1, m_2 and the position of the knees of the curve, which presents a cut-off limit, are represented by constant values (Eurocode 3, 2005). Trilinear *S-N* curves are still adopted in current Eurocode, regarding to steel details, but international recommendations and codes recently tend to standardize the trend (IIW Recommendations, 2016). In recent times, the use of bilinear *S-N* curves is indeed well developed also for steel structural details.

Due to these observations, it is decided to generalize the expression of C_{SN} for different types of bilinear *S-N* curves (case 2, Fig.3.2). Then, semiempirical approximations are used to simplify the equation which defines C_{SN} by eliminating the explicit presence of the Incomplete gamma Function.

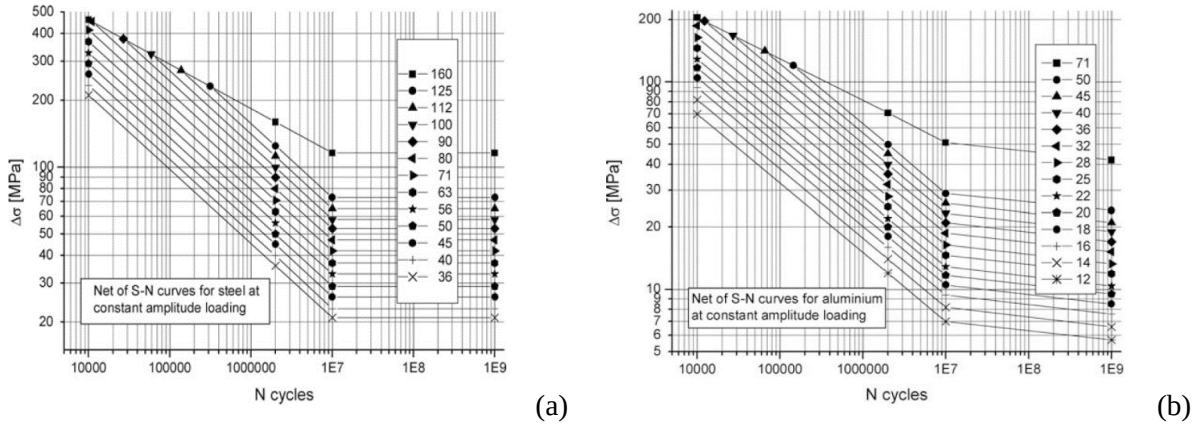

(a) (b)

Fig. 3.2: Bilinear *S-N* curves proposed by © IIW Recommendations of 2016 for steel (a) and aluminum (b) structural components.

Fig. 3.2a shows the scheme of a typical bilinear fatigue *S-N* curve with cut-off limit for a structural detail. The curve is identified by the stress range of the detail category, Δ_C, corresponding to $N = 2 \times 10^6$; the stress range Δ_L is the cut-off limit. Fig. 3.2b, instead, shows the scheme of a typical bilinear fatigue *S-N* curve with two different slopes m_1 and m_2, for a structural detail. It does not present any cut-off limit. The curve is identified by the detail category, Δ_C, corresponding to $N = 2 \times 10^6$, as well; the stress range Δ_L is the knee of the curve, which separates straight lines with different slopes.

The expression of the fatigue curve factor C_{SN} is obtained removing the simplification that the fatigue curve is a straight line on the log – log diagram, with constant slope m_1. Therefore, the relationship $N = a_1/\Delta^{m_1}$ assumes the form:

$$\begin{aligned} N &= a_2/\Delta^{m_2} \quad \text{for} \quad \Delta \le \Delta_L \\ N &= a_1/\Delta^{m_1} \quad \text{for} \quad \Delta \ge \Delta_L \end{aligned} \tag{3.38}$$

When the bilinear curve has only one slope m_1 and then a cut-off limit (Fig. 3.2a), a_2 and m_2 tend to infinite with different orders and the relationship $N = a_1/\Delta^{m_1}$ in this case assumes the form:

$$\begin{aligned} N &\to \infty \quad \text{for} \quad \Delta \le \Delta_L \\ N &= a_1/\Delta^{m_1} \quad \text{for} \quad \Delta \ge \Delta_L \end{aligned} \tag{3.39}$$

In the following Eq. (3.39) is considered as a particular case of the more general Eq. (3.38). Substituting Eqs. (3.6) (Rayleigh distribution) and (3.38) into Eq. (3.2), the mean damage associated with $\bar{u}$ can be expressed by:

$$\bar{d}_{SN}\left(1,\bar{u}\right)=\int_{0}^{\Delta_L}\frac{v\left(\bar{u}\right)}{a_2}\frac{\Delta^{m_2+1}}{\left[2\sigma\left(\bar{u}\right)\right]^2}\exp\left(-\frac{\Delta^2}{2\left[2\sigma\left(\bar{u}\right)\right]^2}\right)\mathrm{d}\Delta+\int_{\Delta_L}^{\infty}\frac{v\left(\bar{u}\right)}{a_1}\frac{\Delta^{m_1+1}}{\left[2\sigma\left(\bar{u}\right)\right]^2}\exp\left(-\frac{\Delta^2}{2\left[2\sigma\left(\bar{u}\right)\right]^2}\right)\mathrm{d}\Delta \tag{3.40}$$

These two integrals can be solved in closed-form using gamma Function (Eq. (3.9)) and $\Gamma_{inc}(\bullet)$ = Incomplete gamma Function (Davis, 1965; Repetto and Solari, 2009):

$$\Gamma_{inc}\left(L,n\right)=\frac{\int_{0}^{L}t^{n-1}\exp\left(-t\right)\mathrm{d}t}{\Gamma\left(n\right)}=\frac{\int_{0}^{L}t^{n-1}\exp\left(-t\right)\mathrm{d}t}{\int_{0}^{\infty}t^{n-1}\exp\left(-t\right)\mathrm{d}t} \tag{3.41}$$

Eq. (3.40) can be therefore solved:

$$\bar{d}_{SN}\left(1,\bar{u}\right)=\frac{v\left(\bar{u}\right)}{a_1}\left[2\sqrt{2}\sigma\left(\bar{u}\right)\right]^{m_1}\Gamma\left(\frac{m_1}{2}+1\right)\chi_{SN}\left[\sigma\left(\bar{u}\right);m_1;m_2;\Delta_L\right] \tag{3.42}$$

where:

$$\chi_{SN}\left[\sigma\left(\bar{u}\right);m_1;m_2;\Delta_L\right]=1-\Gamma_{inc}\left(L\left(\bar{u}\right),\frac{m_1}{2}+1\right)+\frac{a_1}{a_2}\left[2\sqrt{2}\sigma\left(\bar{u}\right)\right]^{m_2-m_1}\frac{\Gamma\left(\frac{m_2}{2}+1\right)}{\Gamma\left(\frac{m_1}{2}+1\right)}\Gamma_{\mathrm{inc}}\left(L\left(\bar{u}\right),\frac{m_2}{2}+1\right) \tag{3.43}$$

in which $L\left(\bar{u}\right)=\Delta_L{}^2\Big/\left\{2\left[2\sigma\left(\bar{u}\right)\right]^2\right\}$. It is worth noting that the *Chi factor* χ_{SN} depends on the stress standard deviation and on the actual *S-N* curve of the structural detail. Assuming the particular case of bilinear trend with slope m_1 and a cut-off limit on N_L, χ_{SN} has a simpler form:

$$\chi_{SN}\left[\sigma\left(\bar{u}\right);m_1;\Delta_L\right]=1-\Gamma_{inc}\left(L\left(\bar{u}\right),\frac{m_1}{2}+1\right) \tag{3.44}$$

because the last term in Eq. (3.43) tends to 0 and indeed χ_{SN} is no longer dependent on m_2. This may also be proved starting the derivation of the fatigue curve factor C_{SN} substituting Eq. (3.39) into Eq. (3.2).

Therefore semiempirical approximations are needed to settle the matter of the explicit presence of the Incomplete gamma Function, which are not convenient for the engineering practical use of C_{SN} equation. Following what Repetto and Solari already did for the old C_{SN} formulation, the Chi factor χ_{SN} is suitable to be approximated to a trilinear function with respect to the normalized standard deviation $\sigma\left(\bar{u}\right)/\Delta_C$. The complication is that there is one specific Chi function χ_{SN} for every *S-N* curve trend, whereas the old investigation was only on the χ_{SN} corresponding to the selected *S-N* curve (Repetto and Solari, 2009).

In the present thesis the following choices are made, in order to have a wide and reliable scenario of bilinear *S-N* fatigue curves.

In the first case (Eq. (3.43)), slopes m_1 scale from 3 to 6, slopes m_2 scale from 16 to 22 and N_L equal to 10^7 or 10^8 are chosen. In the second case Eq. (3.44), slopes m_1 scale from 3 to 11 and cut-off limits on N_L equal to 10^7 or 10^8 are assumed instead. The factor χ_{SN} is evaluated for so many different fatigue *S-N* curves with respect to the ratio $\sigma(\bar{u})/\Delta_C$. This is shown in Fig. 3.3 with the continuous lines, for the cases with cut-off at $N_L = 10^7$ as examples. Every continuous line represents the χ_{SN} coefficient for a fatigue curve with a particular bilinear trend, characterized by fixed fatigue curve parameters.

Every curve involves three distinct ranges. The first corresponds to low $\sigma(\bar{u})/\Delta_C$ values; the probability density function of the stress range is shifted towards values lower than Δ_L (Eqs. (3.38)-(3.39)); thus, both the induced damage and χ_{SN} are low and they tend to zero. The second range corresponds to intermediate $\sigma(\bar{u})/\Delta_C$ values; the probability density function of the stress range is shifted towards values quite higher than Δ_L (Eqs. (3.38)-(3.39)); thus, $0< \chi_{SN} < 1$. The third range corresponds to high $\sigma(\bar{u})/\Delta_C$ values; the probability density function of the stress range is shifted towards values much higher than Δ_L (Eqs. (3.38)-(3.39)); thus, $\chi_{SN} = 1$.

In order to determine a closed form solution of the total mean damage, it is appropriate to choose a suitable approximate expression of χ_{SN}. A reasonable choice with such a requirement is given by trilinear curves which can approximate the Chi factor (Fig. 3.3, dashed lines).

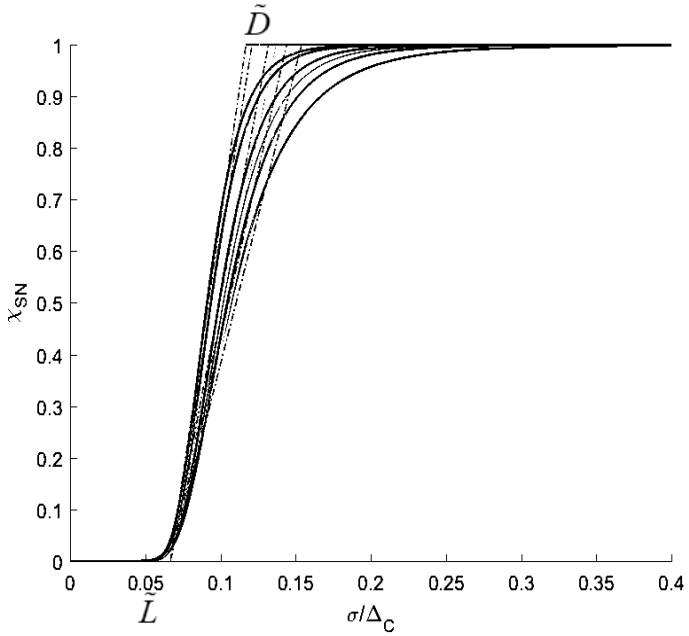

Fig. 3.3: χ_{SN} factor for different bilinear *S-N* curves with $N_L = 10^7$ (continuous lines) and proposed approximations (dashed lines).

The broken lines, which approximate χ_{SN}, are expressed by:

$$\chi_{SN}\left(\frac{\sigma(\bar{u})}{\Delta_C}\right)=\begin{cases}0 & \text{if} \quad \dfrac{\sigma(\bar{u})}{\Delta_C}\le \tilde{L}\\ \dfrac{1}{\left(\tilde{D}-\tilde{L}\right)}\left(\dfrac{\sigma(\bar{u})}{\Delta_C}-\tilde{L}\right) & \text{if} \quad \tilde{L}<\dfrac{\sigma(\bar{u})}{\Delta_C}<\tilde{D}\\ 1 & \text{if} \quad \dfrac{\sigma(\bar{u})}{\Delta_C}\ge \tilde{D}\end{cases} \tag{3.45}$$

where $\tilde{D}$ and $\tilde{L}$ are constant values selected for every combination of m_1, m_2 and N_L in order to minimize the errors involved by this trilinear approximation. Comparing to Repetto and Solari formulation, they found a couple of values ($\tilde{D}$; $\tilde{L}$) for the selected *S-N* curve, here a set of couples of values ($\tilde{D}$; $\tilde{L}$)$_i$ are defined, one for each *i*-th *S-N* curve under investigation.

Substituting Eqs. (2.21) (hybrid Weibull) and (3.42) into Eq. (3.3), the mean total damage per unit time (under the hypothesis of a fatigue curve in the form of Eqs. (3.38) or (3.39)) is given by:

$$\bar{D}_{SN}(1)=\int_0^{\infty}\frac{\nu(\bar{u})}{a_1}\left[2\sqrt{2}\sigma(\bar{u})\right]^{m_1}\Gamma\left(\frac{m_1}{2}+1\right)\chi_{SN}\left[\sigma(\bar{u});m_1;m_2;\Delta_L\right]\left[F_0\delta(\bar{u})+(1-F_0)\frac{k}{c}\left(\frac{\bar{u}}{c}\right)^{k-1}\exp\left\{-\left(\frac{\bar{u}}{c}\right)^{k}\right\}\right]d\bar{u} \tag{3.46}$$

and using Eq. (3.45) to approximate the Chi factor χ_{SN}:

$$\begin{aligned}\bar{D}_{SN}(1)=&\int_{u_L}^{u_D}\frac{\nu(\bar{u})}{a_1}\left[2\sqrt{2}\sigma(\bar{u})\right]^{m_1}\Gamma\left(\frac{m_1}{2}+1\right)\frac{1}{\left(\tilde{D}-\tilde{L}\right)}\left(\frac{\sigma(\bar{u})}{\Delta_C}-\tilde{L}\right)\left[F_0\delta(\bar{u})+(1-F_0)\frac{k}{c}\left(\frac{\bar{u}}{c}\right)^{k-1}\exp\left\{-\left(\frac{\bar{u}}{c}\right)^{k}\right\}\right]d\bar{u}\\ &+\int_{u_D}^{\infty}\frac{\nu(\bar{u})}{a_1}\left[2\sqrt{2}\sigma(\bar{u})\right]^{m_1}\Gamma\left(\frac{m_1}{2}+1\right)\left[F_0\delta(\bar{u})+(1-F_0)\frac{k}{c}\left(\frac{\bar{u}}{c}\right)^{k-1}\exp\left\{-\left(\frac{\bar{u}}{c}\right)^{k}\right\}\right]d\bar{u}\end{aligned} \tag{3.47}$$

in which:

$$u_L=\bar{u}_{ref}\left(\frac{\tilde{L}\Delta_C}{\sigma_{ref}}\right)^{\frac{1}{\alpha_\sigma}};\qquad u_D=\bar{u}_{ref}\left(\frac{\tilde{D}\Delta_C}{\sigma_{ref}}\right)^{\frac{1}{\alpha_\sigma}} \tag{3.48}$$

Eq. (3.47) is rewritten as follows:

$$\begin{aligned}\bar{D}_{SN}(1)=&\int_{u_L}^{u_D}\frac{\nu(\bar{u})}{a_1}\left[2\sqrt{2}\sigma(\bar{u})\right]^{m_1}\Gamma\left(\frac{m_1}{2}+1\right)\frac{1}{\left(\tilde{D}-\tilde{L}\right)}\left(\frac{\sigma(\bar{u})}{\Delta_C}-\tilde{L}\right)(1-F_0)\frac{k}{c}\left(\frac{\bar{u}}{c}\right)^{k-1}\exp\left\{-\left(\frac{\bar{u}}{c}\right)^{k}\right\}d\bar{u}\\ &+\int_{u_D}^{\infty}\frac{\nu(\bar{u})}{a_1}\left[2\sqrt{2}\sigma(\bar{u})\right]^{m_1}\Gamma\left(\frac{m_1}{2}+1\right)(1-F_0)\frac{k}{c}\left(\frac{\bar{u}}{c}\right)^{k-1}\exp\left\{-\left(\frac{\bar{u}}{c}\right)^{k}\right\}d\bar{u}\end{aligned} \tag{3.49}$$

These two integrals can be solved in closed-form considering the gamma Function (Eq. (3.9)), the Incomplete gamma Function (Eq. (3.41)) and assuming the power law approximation (Eqs. (2.38), (3.13), (3.14)):

$$\begin{aligned}\bar{D}_{SN}(1) = {} & \frac{\left(2\sqrt{2}\right)^{m_1}}{a_1}\left(\frac{\sigma_{ref}}{\bar{u}_{ref}^{\alpha_\sigma}}\right)^{m_1}\frac{\nu_{ref}}{\bar{u}_{ref}^{\alpha_\nu}}(1-F_0)c^{(\alpha_\nu+m_1\alpha_\sigma)}\Gamma\left(\frac{m_1}{2}+1\right)\Gamma\left(\frac{\alpha_\nu+m_1\alpha_\sigma+k}{k}\right) \\ \times\Bigg\{ & \left(\frac{1}{\tilde{D}-\tilde{L}}\right)\frac{\sigma_{ref}c^{\alpha_\sigma}}{\Delta_C\bar{u}_{ref}^{\alpha_\sigma}}\frac{\Gamma\left(\frac{\alpha_\nu+(m_1+1)\alpha_\sigma+k}{k}\right)}{\Gamma\left(\frac{\alpha_\nu+m_1\alpha_\sigma+k}{k}\right)}\left[\Gamma_{inc}\left(t_D,\frac{\alpha_\nu+(m_1+1)\alpha_\sigma+k}{k}\right)-\Gamma_{inc}\left(t_L,\frac{\alpha_\nu+(m_1+1)\alpha_\sigma+k}{k}\right)\right] \\ & -\left(\frac{\tilde{L}}{\tilde{D}-\tilde{L}}\right)\left[\Gamma_{inc}\left(t_D,\frac{\alpha_\nu+m_1\alpha_\sigma+k}{k}\right)-\Gamma_{inc}\left(t_L,\frac{\alpha_\nu+m_1\alpha_\sigma+k}{k}\right)\right]+1-\Gamma_{inc}\left(t_D,\frac{\alpha_\nu+m_1\alpha_\sigma+k}{k}\right)\Bigg\}\end{aligned} \tag{3.50}$$

in which:

$$t_L = \tilde{L}^{\frac{k}{\alpha_\sigma}}\left(\frac{\bar{u}_{ref}^{\alpha_\sigma}\Delta_C}{c^{\alpha_\sigma}\sigma_{ref}}\right)^{\frac{k}{\alpha_\sigma}}; \qquad t_D = \tilde{D}^{\frac{k}{\alpha_\sigma}}\left(\frac{\bar{u}_{ref}^{\alpha_\sigma}\Delta_C}{c^{\alpha_\sigma}\sigma_{ref}}\right)^{\frac{k}{\alpha_\sigma}} \tag{3.51}$$

Collecting together the terms related to the 0 level solution (Eq. (3.15)), the fatigue curve factor is obtained:

$$\bar{D}_{SN}(1) = \bar{D}_0(1)\cdot C_{SN} \tag{3.52}$$

$$\begin{aligned}C_{SN} = {} & \frac{1}{\tilde{D}-\tilde{L}}\Bigg\{\frac{\sigma_{ref}c^{\alpha_\sigma}}{\Delta_C\bar{u}_{ref}^{\alpha_\sigma}}\frac{\Gamma\left(\frac{\alpha_\nu+(m_1+1)\alpha_\sigma+k}{k}\right)}{\Gamma\left(\frac{\alpha_\nu+m_1\alpha_\sigma+k}{k}\right)}\left[\Gamma_{inc}\left(t_D,\frac{\alpha_\nu+(m_1+1)\alpha_\sigma+k}{k}\right)-\Gamma_{inc}\left(t_L,\frac{\alpha_\nu+(m_1+1)\alpha_\sigma+k}{k}\right)\right] \\ & +\tilde{D}\left[1-\Gamma_{inc}\left(t_D,\frac{\alpha_\nu+m_1\alpha_\sigma+k}{k}\right)\right]-\tilde{L}\left[1-\Gamma_{inc}\left(t_L,\frac{\alpha_\nu+m_1\alpha_\sigma+k}{k}\right)\right]\Bigg\}\end{aligned} \tag{3.53}$$

3.3. FROM THE CLOSED-FORM SOLUTION TO THE FINAL FORMULATION

The 0 level solution, bi-modal factor, mean stress factor and fatigue curve factor are provided by Eqs. (3.15), (3.25), (3.37), (3.53), respectively. The product of these four terms allows to estimate a reliable mean damage in the unit time (one year), from which the fatigue life can be predicted (Eqs. (3.5) and (3.4)). In the following Table 3.1 the whole complete analytical solution is summarized:

Buffeting-induced fatigue analysis (closed-form solution)	*Eq.*

$$T_F = \frac{1}{\bar{D}(1)} \tag{3.4}$$

$$\bar{D}(1) = \bar{D}_0(1) C_{BM} C_M C_{SN} \tag{3.5}$$

$$\bar{D}_0(1) = \frac{\left(2\sqrt{2}\right)^{m_1}}{a_1} \left(\frac{\sigma_{ref}}{\bar{u}_{ref}^{\alpha_\sigma}}\right)^{m_1} \frac{\nu_{ref}}{\bar{u}_{ref}^{\alpha_\nu}} \left(1 - F_0\right) c^{(\alpha_\nu + m_1 \alpha_\sigma)} \Gamma\left(\frac{m_1}{2} + 1\right) \Gamma\left(\frac{\alpha_\nu + m_1 \alpha_\sigma + k}{k}\right) \tag{3.15}$$

$$C_{BM} = \frac{\nu_{Q,ref}}{\nu_{ref}} + \frac{n_1}{\nu_{ref}} \bar{u}_{ref}^{\left(\alpha_\nu - \frac{m_1}{2}\alpha_\lambda\right)} \lambda_{R,ref}^{\left(\frac{m_1}{2}\right)} c^{\left(\frac{m_1}{2}\alpha_\lambda - \alpha_\nu\right)} \frac{\Gamma\left(\dfrac{\frac{m_1}{2}\alpha_\lambda + m_1\alpha_\sigma + k}{k}\right)}{\Gamma\left(\dfrac{\alpha_\nu + m_1\alpha_\sigma + k}{k}\right)} \tag{3.25}$$

$$C_M = \left(\frac{s_u}{s_u - \bar{s}_p}\right)^{m_1} \left[1 + \frac{m_1 \bar{s}_{ref}}{\left(s_u - \bar{s}_p\right)\bar{u}_{ref}^2} c^2 \frac{\Gamma\left(\dfrac{\alpha_\nu + m_1\alpha_\sigma + k + 2}{k}\right)}{\Gamma\left(\dfrac{\alpha_\nu + m_1\alpha_\sigma + k}{k}\right)}\right] \tag{3.37}$$

$$C_{SN} = \frac{1}{\tilde{D} - \tilde{L}} \left\{ \frac{\sigma_{ref} c^{\alpha_\sigma}}{\Delta_C \bar{u}_{ref}^{\alpha_\sigma}} \frac{\Gamma\left(\dfrac{\alpha_\nu + \left(m_1 + 1\right)\alpha_\sigma + k}{k}\right)}{\Gamma\left(\dfrac{\alpha_\nu + m_1\alpha_\sigma + k}{k}\right)} \left[\Gamma_{inc}\left(t_D, \frac{\alpha_\nu + \left(m_1+1\right)\alpha_\sigma + k}{k}\right) - \Gamma_{inc}\left(t_L, \frac{\alpha_\nu + \left(m_1+1\right)\alpha_\sigma + k}{k}\right)\right] \right.$$
$$\left. + \tilde{D}\left[1 - \Gamma_{inc}\left(t_D, \frac{\alpha_\nu + m_1\alpha_\sigma + k}{k}\right)\right] - \tilde{L}\left[1 - \Gamma_{inc}\left(t_L, \frac{\alpha_\nu + m_1\alpha_\sigma + k}{k}\right)\right] \right\} \tag{3.53}$$

Tab. 3.1: Complete formulation to evaluate buffeting-induced fatigue.

This closed form solution derived in the previous Section 3.2 can be further simplified, in order to be more suitable with standard format, by considering the following points:

(I) fatigue *S-N* curve parameters may be express in function of Δ_C, N_C and m_1, thanks to the relationship $a_1=N_C \cdot \Delta_C^{m_1}$; N_C is conventionally considered equal to 2×10^6;

(II) the simplification $\alpha_v = 0$ lends to slightly conservative estimates (Repetto and Solari, 2009; 2012);

(III) the gamma Function is approximated by simple analytical formulas (Davis 1965; Repetto and Solari 2009, 2012): fractional values of the gamma Function, for any positive integer *n*, are given by Eq. (3.54) and for positive real *x*, the asymptotic Stirling approximation can be applied to the gamma Function; retaining only the first term of the series, this is given by Eq. (3.55);

$$\Gamma\left(n+\frac{1}{2}\right)=\frac{1\cdot 3\cdot 5\cdot\cdots\cdot(2n-1)}{2n}\sqrt{\pi} \tag{3.54}$$

$$\Gamma(x)=\left(\frac{x}{e}\right)^x\sqrt{\frac{2\pi}{x}} \tag{3.55}$$

$$\Gamma(az+x)=\sqrt{2\pi}\cdot \mathrm{e}^{-az}(az)^{az+x-\frac{1}{2}} \tag{3.56}$$

(IV) as regards synoptic events it may be considered $F_0 = 0$ (Gomes and Vickery 1977; Repetto and Solari 2012); furthermore, a simplification may be applied by selecting suitable wind parameters that are related to the local wind climate. In particular, some research on Italian territory showed interesting relationships linking the Weibull parameters *k* and *c* with the reference velocity: in Italian territory $c=(0.2k-0.12)\bar{u}_{ref}$ (Pagnini and Solari, 2016). Such relationships make the above formulation more explicit. In any case further studies are needed for different areas.

These considerations allow to obtain simplified expressions of the 0 level solution, bi-modal factor and mean stress factor by means of simple analytical passages. For the fatigue curve factor the simplification of Eq. (3.53) is more complex and it needs again some semiempirical approximations in order to overcome the presence of the Incomplete gamma Function.

The whole simplification is outlined in Appendix A.

Final formulae are summarized in Table 3.2: they are convenient for the engineering practical use and perfectly coherent with standard format. The new generalized fatigue curve factor C_{SN} expression (Eq. (3.60)) is perfectly consistent with the specific one introduced by Repetto and Solari (2009, 2012) for the particular *S-N* fatigue resistance curve which was taken into consideration. This thesis contribution to the method allows to apply the analysis to structural details whose fatigue resistance is characterized by

different *S-N* curve trends. The expressions are suitable to be introduced in engineering and codification fields.

Buffeting-induced fatigue analysis (simplified solution)	*Eq.*
$T_F = \frac{1}{\bar{D}(1)}$	(3.4)
$\bar{D}(1) = \bar{D}_0(1) C_{BM} C_M C_{SN}$	(3.5)
$\bar{D}_0(1) = 31.536 \cdot 2^{\left(\frac{3m_1-1}{2}\right)} \sqrt{\pi}\Gamma\left(\frac{m_1}{2}+1\right) \frac{\sigma_{ref}^{m_1}}{\Delta_C^{m_1}} v_{ref} (0.2k-0.12)^{m_1\alpha_\sigma} \left(\frac{m_1\alpha_\sigma}{k}+1\right)^{\left(\frac{m_1\alpha_\sigma}{k}+0.5\right)} \left(\frac{1}{e}\right)^{\left(\frac{m_1\alpha_\sigma}{k}+1\right)}$	(3.57)
$C_{BM} = \frac{v_{Q,ref}}{v_{ref}} + \frac{n_1}{v_{ref}} \lambda_{R,ref}^{\frac{m_1}{2}} (0.2k-0.12)^{\frac{m_1\alpha_\lambda}{2}} \left(\frac{m_1\alpha_\sigma}{k}+1\right)^{\frac{m_1\alpha_\lambda}{2k}}$	(3.58)
$C_M = \left[\frac{s_u}{(s_u - \bar{s}_P)}\right]^{m_1} \left[1 + \frac{\bar{s}_{ref}}{(s_u - \bar{s}_P)} m_1 (0.2k-0.12)^2 \left(\frac{m_1\alpha_\sigma}{k}+1\right)^{\left(\frac{2}{k}\right)}\right]$	(3.59)
$C_{SN} = 1 - \exp\left\{-\left\{\left[\left(a^I\left(m_1 + \frac{N_L - 10^7}{45\cdot 10^6}\right) + a^{II}\right)^{\frac{1}{k}} (0.2k-0.12)\right]^{\alpha_\sigma} \left(\frac{\sigma_{ref}}{\Delta_C}\right)\right\}^{\left[\frac{k}{\alpha_\sigma}\left(0.15\left(m_1 + \frac{N_L-10^7}{45\cdot 10^6}\right)+1.55\right)\right]}\right\}$	(3.60)
$a^I = +7.44\,;\ a^{II} = -3.81$	bilinear with cut-off
$a^I = +6.33\,;\ a^{II} = +2$	bilinear without cut-off

Tab. 3.2: Final generalized formulation to evaluate buffeting-induced fatigue.

CHAPTER 4 – ALONGWIND AND CROSSWIND GUST – INDUCED FATIGUE

4.1. INTRODUCTION

Slender vertical structures exposed to wind may experience crosswind vibrations which may be even more critical than alongwind vibrations and however characterised by different properties. In fact, the mean part of the crosswind response is usually negligible. The fluctuating part is due to the lateral turbulence and to the vortex wake. This constitutes a complex physical phenomenon that is often the main source of the vibration mechanism.

According to a large set of experimental measurements (Solari and Piccardo, 2001), it can be assumed that the lateral turbulence standard deviation is equal to 75% of the longitudinal turbulence one. Crosswind buffeting actions and effects due to lateral turbulence are again schematized as bi-modal random processes, but in this case with zero mean. Identifying the wind loading with the gust buffeting attributable to the oncoming turbulence, the wind loading model adopted is simplified by neglecting the vortex shedding. This simplification is possible far from resonance conditions, where the loading caused by the vortex shedding is almost negligible in comparison with the gust buffeting.

Of course the vortex shedding deserves accurate evaluations in correspondence to the wind velocities that cause crosswind resonant vibrations. The vortex wake produces aerodynamic actions perpendicular to the wind direction, whose frequency depends on the mean wind velocity and on the shape and the size of the structural section. The worst situation happens in correspondence of the critical wind velocities, which cause a resonant shedding with a natural frequency. In these conditions aeroelastic forces may exalt the motion up to realise an extremely dangerous synchronisation mechanism well known as lock-in.

As regards fatigue analysis and frequency-domain theoretical formulations, literature is mostly focused on alongwind-induced fatigue (Chapter 2). Crosswind fatigue analysis still represents a fully open matter, as very few contributions have been proposed in literature. The Eurocode 1 (2005) codifies a method to take vortex-induced fatigue into account, using a pseudo-deterministic approach based on the vortex-resonance model (Ruscheweyh, 1994). An analogous method is introduced in the CICIND Model Code (1999). Simultaneous 3-D wind-induced fatigue as not been yet investigated completely (Repetto Solari 2004).

It is apparent that neither research literature nor international recommendations have been deeply involved in defining crosswind turbulence-induced fatigue assessment procedures, this being a lacking in structural engineering field. Even if some cases of typical slender structures are mainly sensitive to alongwind loading and vortex shedding effects, in some other situations crosswind actions on slender

structures and structural elements caused by the buffeting loading may exceed the alongwind buffeting loading and the crosswind loading caused by critical vortex shedding. In addition, provided that crosswind actions attributable to the buffeting loading do not prevail on the alongwind ones, their evaluation cannot be ignored and their load effects have to be analysed (Solari, 2018).

In the current Chapter 4, the model proposed previously (Chapters 2 and 3) to evaluate the total mean damage in the unit time due to alongwind turbulence effect is generalized regarding both longitudinal and lateral turbulence effects. Proposed equations to evaluate fatigue damage and fatigue life consider response input parameters referred to alongwind or crosswind stresses. Two prediction of fatigue life may be done, starting from alongwind or crosswind buffeting response in a critical structural detail. This is possible at engineering level thanks to new formulas proposed by Solari (2018) of generalized static, quasi-static, and resonant parameters for slender structures, used for evaluating the 3-D gust effect factor (Piccardo and Solari, 2002), taking into account buffeting actions.

Section 4.2 deals with buffeting-induced fatigue analytical model, concerning both alongwind and crosswind turbulence effects. It includes the whole final general formulation and two particular formulations derived from the general one, regarding the case of cyclic normal stresses in structural steel details and the case of cyclic shear stresses in structural steel details, as examples. In closing of this part, Paragraph 4.2.1 defines two different levels of calculations, simplified and detailed, effective for standards format.

Section 4.3 provides all input parameters discussion and definition, consistently with Eurocode. Paragraph 4.3.1 deals with resistance and structural parameters, Paragraph 4.3.2 deals with climatological parameters, Paragaraph 4.3.3 deals with response parameters, in particular alongwind response parameters and crosswind response parameters are subdivided in Paragaraph 4.3.4 and 2.3.5, respectively.

Summarizing the novel contributions to the existing method, the whole analytical formulation presented here is generalized with regard to different bilinear *S-N* fatigue resistance curves (Chapter 3) and with regard to alongwind and crosswind buffeting response (Chapter 4). As regard vortex-shedding-induced fatigue, since this is a complex phenomenon which produces a completely different effect on structures it can not be easily adapted to the proposed generalized analytical model. Therefore, its contribution is neglected at this stage and discussed in Chapter 5, at the completion of the crosswind-induced fatigue analysis.

4.2. TURBULENCE-INDUCED FATIGUE ANALYTICAL MODEL

Considering alongwind response, stress parameters follow a monotonic increasing trend, while crosswind response is due to turbulence contribution as well as vortex shedding effects. The peak related to critical velocity has an important impact on total damage estimation (Fig. 4.1).

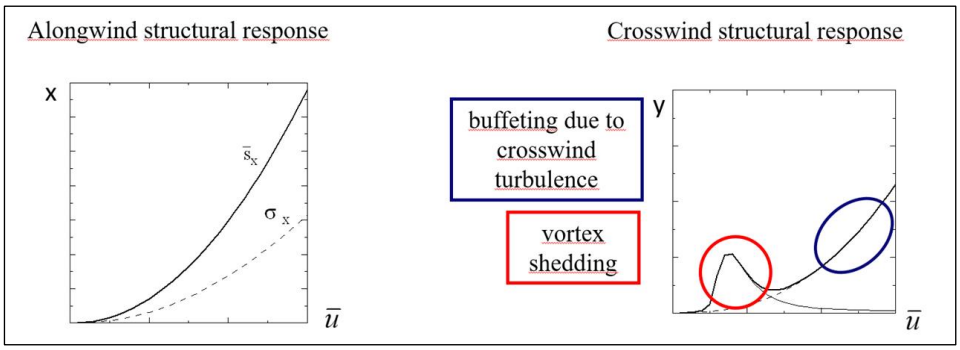

4.1: Diagrams of alongwind and crosswind response parameters on varying of mean wind velocity.

Neglecting the vortex shedding effect and considering only longitudinal and lateral turbulence effects, the power law approximation of response parameters, which has been introduced previously only concerning alongwind response parameters (Section 2.3.3), remains effective (Fig. 4.2). However, neglecting vortex shedding contribution to response and to fatigue is a really strong assumption, which will be deeply and critically analysed in the whole following part of this thesis (Chapter 5).

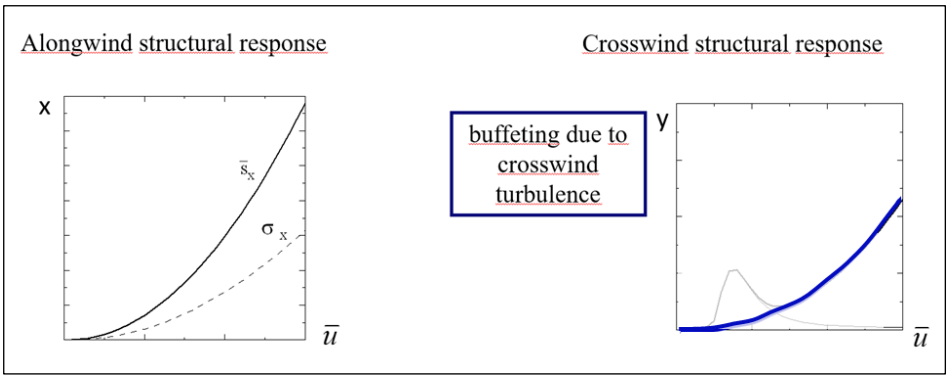

4.2: Diagrams of alongwind and crosswind response parameters on varying of mean wind velocity, highlighting response parameters due to crosswind turbulence.

Since the power law approximation for the basic stress input parameters is effective for alongwind and crosswind turbulence induced response, if vortex shedding contribution is neglected, the analytical formulation is formally equal for alongwind and crosswind buffeting-induced fatigue analysis. Coherently, the closed-form solution of wind-induced cumulated mean damage in the unit time can be again expressed as the product of the "0 level" solution, multiplied by the corrective factors (Eq. (3.5)). The generalized formulation of terms in Eq. (3.5) is then given by Eqs. (3.57) – (3.60) (Section 3.3, Table 3.2). Alongwind and crosswind fatigue analyses are both taken into account by distinguishing response input parameters with a directional index.

Buffeting-induced fatigue analysis	*Eq.*
$$T_F = \frac{1}{\bar{D}(1)}$$	(3.4)
$$\bar{D}(1) = \bar{D}_0(1) C_{BM} C_M C_{SN}$$	(3.5)
$$\bar{D}_0(1) = 31.536 \cdot 2^{\left(\frac{3m_1-1}{2}\right)} \sqrt{\pi}\,\Gamma\left(\frac{m_1}{2}+1\right) \frac{\sigma_{\omega,ref}^{m_1}}{\Delta_C^{m_1}} \nu_{\omega,ref} \left(0.2k-0.12\right)^{m_1\alpha_{\sigma,\omega}} \left(\frac{m_1\alpha_{\sigma,\omega}}{k}+1\right)^{\left(\frac{m_1\alpha_{\sigma,\omega}}{k}+0.5\right)} \exp\left[-\left(\frac{m_1\alpha_{\sigma,\omega}}{k}+1\right)\right]$$	(3.57)
$$C_{BM} = \frac{\nu_{\omega,Q,ref}}{\nu_{\omega,ref}} + \frac{n_{\omega 1}}{\nu_{\omega,ref}} \lambda_{\omega,R,ref}^{\frac{m_1}{2}} \left(0.2k-0.12\right)^{\frac{m_1}{2}\alpha_{\lambda,\omega}} \left(\frac{m_1\alpha_{\sigma,\omega}}{k}+1\right)^{\frac{m_1\alpha_{\lambda,\omega}}{2k}}$$	(3.58)
$$C_M = \left[\frac{s_u}{\left(s_u - \bar{s}_P\right)}\right]^{m_1} \left[1 + \frac{\bar{s}_{\omega,ref}}{\left(s_u - \bar{s}_P\right)} m_1 \left(0.2k-0.12\right)^2 \left(\frac{m_1\alpha_{\sigma,\omega}}{k}+1\right)^{\left(\frac{2}{k}\right)}\right]$$	(3.59)
$$C_{SN} = 1 - \exp\left\{-\left\{\left[\left(a^I\left(m_1 + \frac{N_L - 10^7}{45\cdot 10^6}\right) + a^{II}\right)^{\frac{1}{k}} \left(0.2k-0.12\right)\right]^{\alpha_{\sigma,\omega}} \left(\frac{\sigma_{\omega,ref}}{\Delta_C}\right)\right\}^{\left[\frac{k}{\alpha_{\sigma,\omega}}\left(0.15\left(m_1 + \frac{N_L-10^7}{45\cdot 10^6}\right)+1.55\right)\right]}\right\}$$	(3.60)
$a^I = +7.44\,;\ a^{II} = -3.81$	bilinear with cut-off
$a^I = +6.33\,;\ a^{II} = +2$	bilinear without cut-off

Tab. 3.2 (second version): Generalized formulation to evaluate alongwind and crosswind buffeting-induced fatigue.

where "ω" is the directional index, with $\omega = D, L$ for alongwind and crosswind structural response parameters, respectively (red color in second version of Tab. 3.2); m_1, Δ_C and N_L are parameters of the considered *S-N* fatigue curve; a^I, a^{II} are constant values depending on the shape of the considered *S-N* fatigue curve, in particular $a^I = +7.44$, $a^{II} = -3.81$ for bilinear *S-N* curves with cut-off limit, $a^I = +6.33$, $a^{II} = +2$ for bilinear *S-N* curves without cut-off limit; $\Gamma(\bullet)$ is the gamma function (Davis, 1965); k is the shape parameter of the Weibull probability distribution of the current values of the wind velocity in situ (Pagnini and Solari, 2016); $n_{\omega 1}$ is the first mode of vibration frequency in the ω-direction; s_u is the material failure characteristic stress; $\overline{s}_p$ is the permanent loadings-induced stress in the examined section (calculated at serviceability); parameters of the response process in ω-direction at reference wind velocity are $\overline{s}_{\omega,ref}$, $\sigma_{\omega,ref}$, $\nu_{\omega,ref}$, $\nu_{\omega,Q,ref}$, $\lambda_{\omega,R,ref}$, which are the mean value, standard deviation, expected frequency, expected frequency of the quasi-static part and normalized variance of the resonant part of the process in the critical section, respectively; $\alpha_{\sigma,\omega}$ is the exponent of the power law expressing the standard deviation of the fluctuating stress, σ_ω, on varying wind velocity; $\alpha_{\lambda,\omega}$ is the exponent of the power law expressing the normalized variance of the stress resonant part, $\lambda_{\omega,R}$, on varying wind velocity (Repetto and Solari, 2012; Solari, 2018). Only the exponents of power laws parameters, $\alpha_{\sigma,\omega}$ and $\alpha_{\lambda,\omega}$, require the calculation of the structural response at reference and fatigue wind velocity values.

These many input parameters are fairly simple to evaluate (see Section 4.3). Most critical ones to estimate may be the Weibull shape parameter k and the power law exponents $\alpha_{\sigma,\omega}$ and $\alpha_{\lambda,\omega}$. It is possible to reformulate Eqs. (3.57) - (3.60) in order to separate these three parameters from the others. The 0 level solution of mean fatigue damage and the three corrective factors may be expressed in function of five non dimensional quantities A_0, A_{BM}, A_M, A_{SN} and B_{SN}, which depend only on the three parameters, k, $\alpha_{\sigma,\omega}$ and $\alpha_{\lambda,\omega}$. By way of example, two particular formulations derived from the general one, regarding the case of cyclic normal stresses in structural steel details and the case of cyclic shear stresses in structural steel details, are introduced below. When a structural detail that has to be analysed is defined, the first step is to establish the *S-N* fatigue curve which represent fatigue resistance of that structural detail subjected to that loading conditions. When the type of *S-N* curve is fixed, and therefore m_1, N_L, a^I and a^{II} are associated to known values, it is possible to rewrite all factors in function of quantities A_0, A_{BM}, A_M, A_{SN} and B_{SN} (Table 4.1).

The case of *steel structural details subjected to normal stress status* is the one examined by Repetto and Solari (2009, 2012). They actually considered only trilinear fatigue curves provided by Eurocodes for steel elements (Eurocode 3, 2005; Section 2.2.2: Fig. 2.5). Now, starting from the generalized formulation proposed in the current thesis (Table 3.2), the same case can be dealt with considering bilinear fatigue curves provided by IIW Recommendations (2016) for steel structural details subjected to normal stresses (Section 2.2.2: Fig. 2.6). Therefore, replacing $m_1 = 3$, $N_L = 10^7$ cycles, $a^I = +7.44$ and $a^{II} = -3.81$ in the

general formulation, the same particular case of formulation derived by Repetto and Solari in 2012 is obtained indeed (Table 4.1, first column).

The second case concerns *steel structural details subjected to shear stress status* and it is discussed in this thesis for the first time, as a particular example derived from the generalized formulation. The *S-N* fatigue resistance curves taken into account in this case are the bilinear ones provided by Eurocode 3 (2005) (Fig. 4.3a) or by IIW Recommendations (2016) (Fig.4.3b).

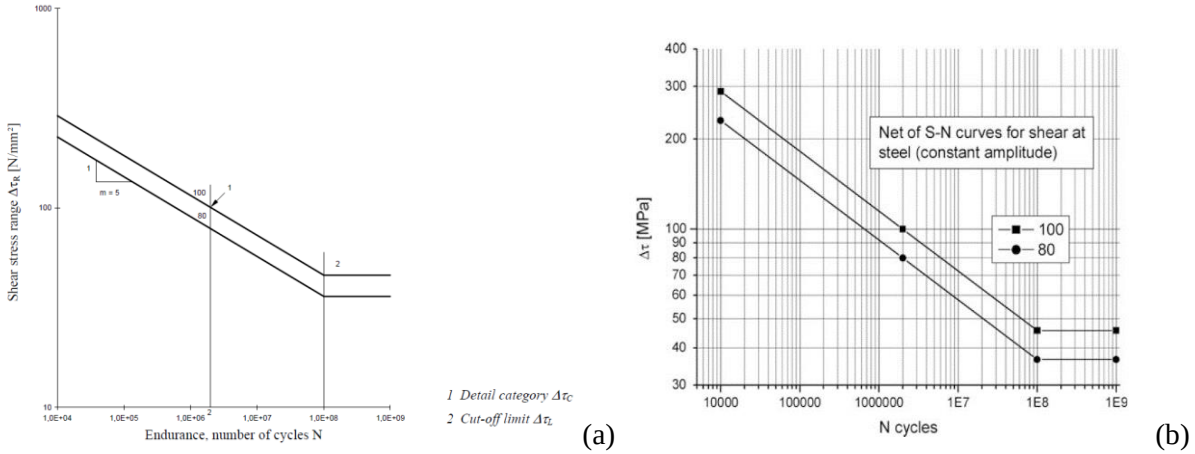

Figure 4.3: Standard set of *S-N* curves for shear stresses in steel elements provided by Eurocodes (a) and by the International Institute of Welding (b).

The slope of the fatigue strength curves for details assessed on the basis of shear stresses is $m_1 = 5$ and in this case the knee point is assumed to correspond to $N_L = 10^8$ cycles. Due to the presence of a cut-off limit at N_L, $a^I = +7.44$ and $a^{II} = -3.81$. By substituting these values in the generalized formulation proposed in Table 3.2 and by separating parameters k, $\alpha_{\sigma,\omega}$ and $\alpha_{\lambda,\omega}$ so that they are included in A_0, A_{BM}, A_M, A_{SN}, B_{SN} quantities, the particular formulation is obtained (Table 4.1, second column).

Normal stresses in steel details	*Eq.*	Shear stresses in steel details	*Eq.*
$\bar{D}_0(1) = 15.77 \frac{\sigma^3_{\omega,ref}}{\Delta^3_C} v_{\omega,ref} A_0$	(4.1a)	$\bar{D}_0(1) = 315.36 \frac{\sigma^5_{\omega,ref}}{\Delta^5_C} v_{\omega,ref} A_0$	(4.1b)
$C_{BM} = \frac{v_{\omega,Q,ref}}{v_{\omega,ref}} + \frac{n_{\omega 1}}{v_{\omega,ref}} \lambda^{3/2}_{\omega,R,ref} A_{BM}$	(4.2a)	$C_{BM} = \frac{v_{\omega,Q,ref}}{v_{\omega,ref}} + \frac{n_{\omega 1}}{v_{\omega,ref}} \lambda^{5/2}_{\omega,R,ref} A_{BM}$	(4.2b)
$C_M = \left[\frac{s_u}{(s_u - \bar{s}_P)}\right]^3 \left[1 + \frac{\bar{s}_{\omega,ref}}{(s_u - \bar{s}_P)} A_M\right]$	(4.3a)	$C_M = \left[\frac{s_u}{(s_u - \bar{s}_P)}\right]^5 \left[1 + \frac{\bar{s}_{\omega,ref}}{(s_u - \bar{s}_P)} A_M\right]$	(4.3b)
$C_{SN} = 1 - \exp\left\{-A_{SN}\left(\frac{\sigma_{\omega,ref}}{\Delta_C}\right)^{B_{SN}}\right\}$	(4.4a)	$C_{SN} = 1 - \exp\left\{-A_{SN}\left(\frac{\sigma_{\omega,ref}}{\Delta_C}\right)^{B_{SN}}\right\}$	(4.4b)
$A_0 = 24\pi(0.2k - 0.12)^{3\alpha_{\sigma,\omega}} \left(\frac{3\alpha_{\sigma,\omega}}{k} + 1\right)^{\left(\frac{3\alpha_{\sigma,\omega}}{k} + 0.5\right)} \exp\left[-\left(\frac{3\alpha_{\sigma,\omega}}{k} + 1\right)\right]$	(4.5a)	$A_0 = 24\pi(0.2k - 0.12)^{5\alpha_{\sigma,\omega}} \left(\frac{5\alpha_{\sigma,\omega}}{k} + 1\right)^{\left(\frac{5\alpha_{\sigma,\omega}}{k} + 0.5\right)} \exp\left[-\left(\frac{5\alpha_{\sigma,\omega}}{k} + 1\right)\right]$	(4.5b)
$A_{BM} = (0.2k - 0.12)^{\frac{3}{2}\alpha_{\lambda,\omega}} \left(\frac{3\alpha_{\sigma,\omega}}{k} + 1\right)^{\frac{3\alpha_{\lambda,\omega}}{2k}}$	(4.6a)	$A_{BM} = (0.2k - 0.12)^{\frac{5}{2}\alpha_{\lambda,\omega}} \left(\frac{5\alpha_{\sigma,\omega}}{k} + 1\right)^{\frac{5\alpha_{\lambda,\omega}}{2k}}$	(4.6b)
$A_M = 3(0.2k - 0.12)^2 \left(\frac{3\alpha_{\sigma,\omega}}{k} + 1\right)^{\frac{2}{k}}$	(4.7a)	$A_M = 5(0.2k - 0.12)^2 \left(\frac{5\alpha_{\sigma,\omega}}{k} + 1\right)^{\frac{2}{k}}$	(4.7b)
$A_{SN} = 342.25(0.2k - 0.12)^{2k}$	(4.8a)	$A_{SN} = 23828(0.2k - 0.12)^{2.6k}$	(4.8b)
$B_{SN} = \frac{2k}{\alpha_{\sigma,\omega}}$	(4.9a)	$B_{SN} = 2.6 \frac{k}{\alpha_{\sigma,\omega}}$	(4.9b)

Tab. 4.1: Particular formulations to evaluate buffeting-induced fatigue.

The five quantities, A_0, A_{BM}, A_M, A_{SN} and B_{SN} (Eqs. (4.5)-(4.9)), which depend on structural response at wind velocities lower than or equal to reference velocity $\bar{u}_{ref}$ and on the probability distribution of the wind velocity in situ, may be evaluated by *simplified* or *detailed calculations*.

4.2.1. Simplified and detailed calculations

Two different levels of calculations, simplified and detailed, are defined. This is useful to possibly introduce the method in standards and codes, since it suits with their format and it becomes effective for engineering applications.

The only input parameters that are usually not available and deserve specific evaluations or provisions is limited to three non dimensional coefficients, the Weibull shape parameter k and the power law exponents $\alpha_{\sigma,\omega}$ and $\alpha_{\lambda,\omega}$. Furthermore, these input parameters small variation gives rise to a wide spread of results, thus an appropriate choice of them, especially of k and $\alpha_{\sigma,\omega}$, is crucial for a reliable estimate of the mean fatigue damage and the mean fatigue life. It seems to be important to define a simple method to understand if a structure or a structural element is sensitive or not to fatigue phenomenon without requiring their evaluation. To this aim, particular formulations should be expressed separating these three parameters from the others, making use of the five quantities, A_0, A_{BM}, A_M, A_{SN} and B_{SN} (Eqs. (4.1)-(4.9)).

Knowing the typical ranges of values of these three parameters, it is possible to assign values on the safe side one by one, in order to have five constant values of A_0, A_{BM}, A_M, A_{SN} and B_{SN}, for a particular case. This might provide a first level of calculation, that is very simple to apply, because Eqs. (4.5)-(4.9) are avoided and replaced by fixed constant quantities, but far too on the safe side. Applying such calculation provides preventive values of fatigue damage and fatigue life just to understand if the structural element examined is sensitive or not to fatigue due to turbulence. If the structural element is sensitive to fatigue, it is necessary to evaluate k, $\alpha_{\sigma,\omega}$ and $\alpha_{\lambda,\omega}$ in a more extensive manner and, therefore, it is necessary to apply Eqs. (4.5)-(4.9).

These levels of calculation may be defined as *simplified calculation*, that provides preventive values, and *detailed calculation*, that provides reliable values of fatigue damage and fatigue life in the examined structural detail.

In the particular case of normal stresses repeated in a cross-section of a steel structural detail, the *simplified* level of calculation, already discussed by Repetto and Solari (2012), gives constant values to k, $\alpha_{\sigma,\omega}$ and $\alpha_{\lambda,\omega}$ so that $A_0 = 0.085$, $A_{BM} = 0.9$, $A_M = 1.4$, $A_{SN} = 2.2$ and $B_{SN} = 0.8$ (Table 4.2, first column).

On the other hand, the particular case of cyclic shear stresses in a steel detail is defined here as a novelty, according to both levels of calculation, simplified and detailed.

For this case, Fig. 4.4 shows A_0, A_{BM}, A_M, A_{SN} and B_{SN} as functions of the typical values of the parameters k, $\alpha_{\sigma,\omega}$ and $\alpha_{\lambda,\omega}$.

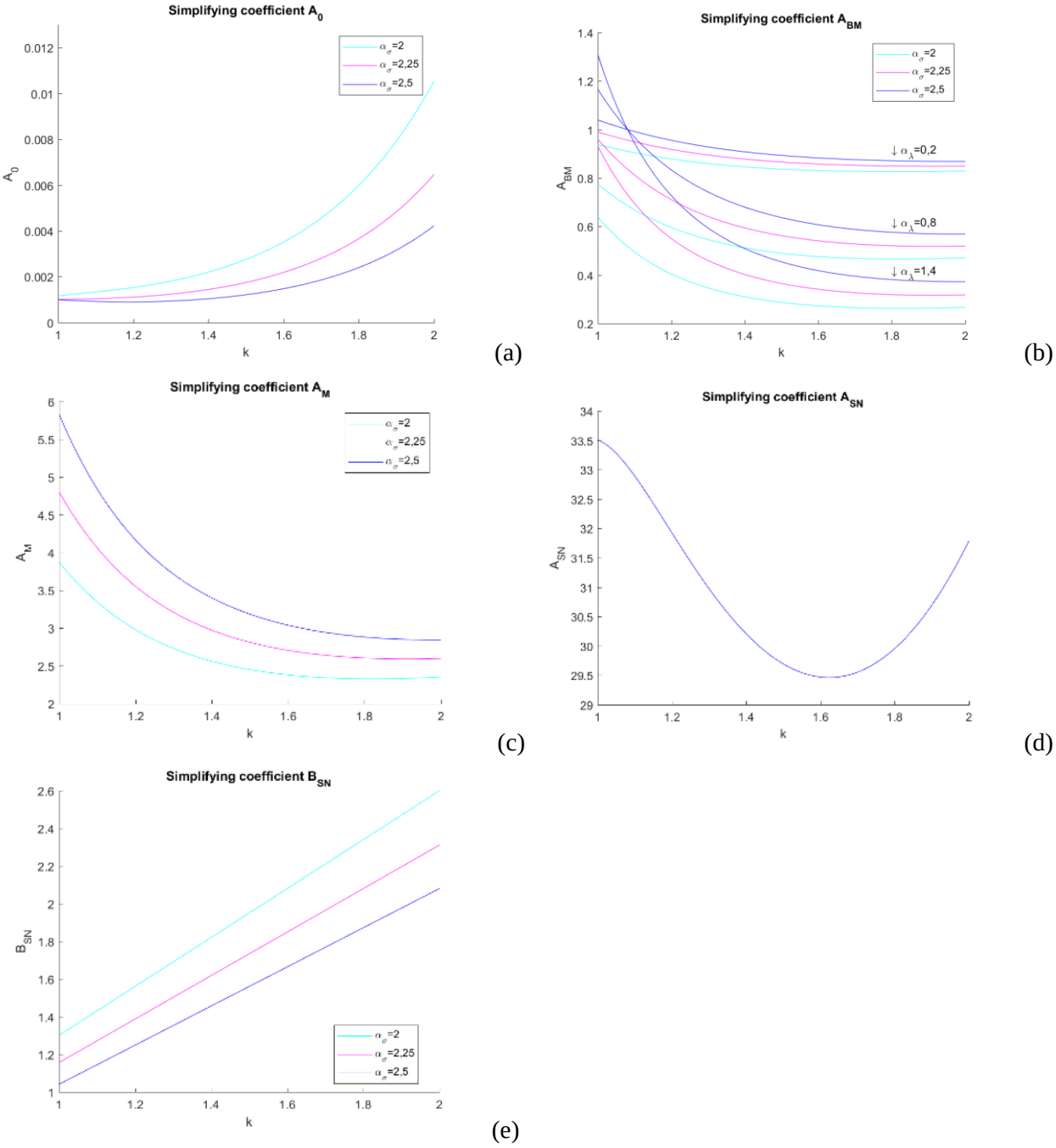

Figure 4.4: Non-dimensional quantities A_0 (a), A_{BM} (b), A_M (c), A_{SN} (d) and B_{SN} (e) as functions of k, $\alpha_{\sigma,\omega}$ and $\alpha_{\lambda,\omega}$.

The figures show the five quantities on varying k between 1 and 2, highlighting the dominant role of this parameter. Light blue, pink and purple lines correspond to $\alpha_{\sigma,\omega}$ = 2, 2.25, 2.5, respectively, which has a dominant role as well. The parameter $\alpha_{\lambda,\omega}$ only influences A_{BM} coefficient. Summarizing, $\alpha_{\sigma,\omega}$ usually varies in a limited range but it gives rise to a wide spread of results; on the contrary, $\alpha_{\lambda,\omega}$ usually varies in a wide range but it gives rise to a limited spread of results; k has a dominant role particularly in B_{SN}.

Following the same approach used for the previous particular case, it is possible to assign values on the safe side to the parameters k, $\alpha_{\sigma,\omega}$ and $\alpha_{\lambda,\omega}$, one by one, in order to have five constant values of A_0, A_{BM}, A_M, A_{SN} and B_{SN}. This leads to the definition of the *simplified calculation* for this particular case, in which Eqs. (4.5)-(4.9) are avoided, replaced by constant values. This level of calculation results far too on the safe side, providing preventive values of fatigue damage and fatigue life just to understand if the structural element examined is sensitive or not to fatigue due to turbulence. As in the other particular case, if the structural element is sensitive to fatigue by applying the *simplified calculation*, it is necessary to evaluate k, $\alpha_{\sigma,\omega}$ and $\alpha_{\lambda,\omega}$ in a more extensive manner and, therefore, it is necessary to apply Eqs. (4.5)-(4.9). This levels of calculation, namely the *detailed calculation*, provides reliable values of fatigue damage and fatigue life in the examined structural detail.

To reach this aim, parameters $\alpha_{\sigma,\omega}$ and $\alpha_{\lambda,\omega}$ are assigned on the safe side, disregarding the possibility that their values may result conflicting with each other for different parameters. Also k is assigned on the safe side, adopting the same approach (Fig. 4.5).

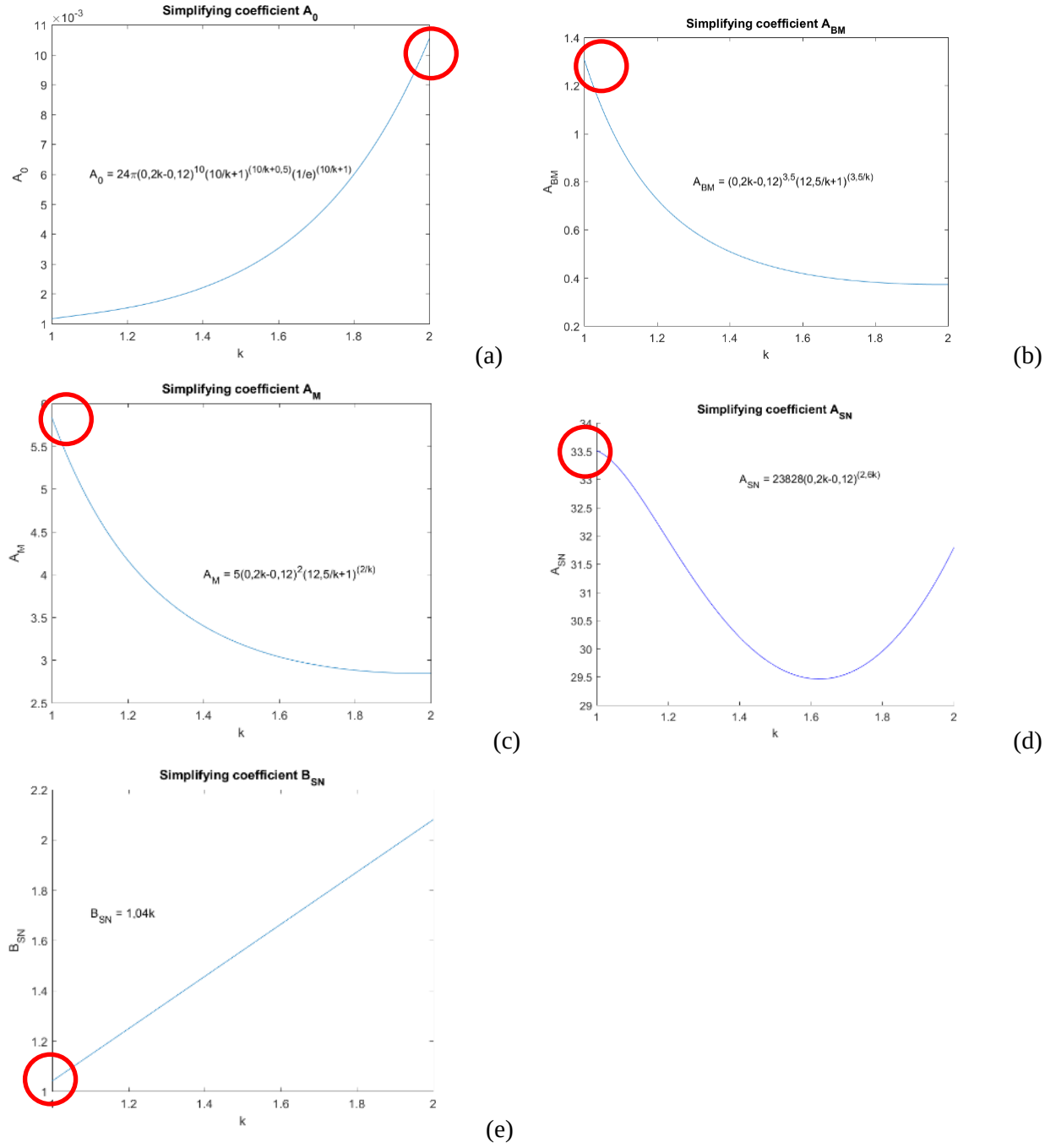

Figure 4.5: Conservative estimates of non-dimensional quantities A_0 (a), A_{BM} (b), A_M (c), A_{SN} (d) and B_{SN} (e), choosing values of k, $\alpha_{\sigma,\omega}$ and $\alpha_{\lambda,\omega}$ on the safe side.

The *simplified* level of calculation, discussed here in accordance with Repetto and Solari manner (2012), gives constant values to k, $\alpha_{\sigma,\omega}$ and $\alpha_{\lambda,\omega}$ so that $A_0 = 0.0105$, $A_{BM} = 1.3$, $A_M = 5.8$, $A_{SN} = 33.5$ and $B_{SN} = 1.04$ (Table 4.2, second column).

Normal stresses in steel details	Shear stresses in steel details
$A_0 = 0.085$	$A_0 = 0.0105$
$A_{BM} = 0.9$	$A_{BM} = 1.3$
$A_M = 1.4$	$A_M = 5.8$
$A_{SN} = 2.2$	$A_{SN} = 33.5$
$B_{SN} = 0.8$	$B_{SN} = 1.04$

Tab. 4.2: Simplified calculation constant quantities on the safe side.

4.3. INPUT PARAMETERS DEFINITION

It is evident that the proposed analytical model requires the assessment of many input parameters in order to be applied. When such parameters, in particular the ones related to wind loadings and effects on constructions, can not be evaluated by measurement, experimental tests or numerical simulations, analytical procedures are needed. Useful instructions is the document provided by Italian CNR. Coherently with Eurocode and CNR format, all input parameters are defined and discussed in the following Section 4.3, expressing them in a simplified format suitable with analytical engineering verifications.

4.3.1. Resistance and structural input parameters

Fatigue resistance parameters concerns parameters of the considered *S-N* fatigue curve according to nominal approach, as described in Sections 2.2.1 and 2.2.2 (Eurocode 3, 2005, part 1-9; IIW, 2016). In bi-logarithmic diagram m_1 = slope value of the first line; Δ_C = detail category defining the structural detail geometry, material and loading conditions, expressed in MPa or N/mm^2, it is the reference value of fatigue resistance of the analyzed structural detail for 2 million cycles; N_L = number of cycles corresponding to the knee of the curve. These parameters are referred to bilinear curves with or without a

cut-off limit; in the first case constants $a^{I} = +7.44$, $a^{II} = -3.81$, while in the second one $a^{I} = +6.33$, $a^{II} = +2$. The *S-N* fatigue curve can be provided by standards and recommendations or by experimental tests.

Knowing m_1 value, the gamma function in Eq. (3.57) can be solved finding its numerical solution (Eqs. (3.54), (3.55). This calculation is easy using Bohr-Mollerup Theorem, 1922:

$$\Gamma(1) = 1; \qquad \Gamma(x+1) = x\Gamma(x) \tag{4.10}$$

and the property:

$$\Gamma\left(\frac{1}{2}\right) = \sqrt{\pi} \tag{4.11}$$

Another resistance parameter is s_u, in MPa or N/mm^2, which is the material failure characteristic stress; it depends on the material and it is provided by the supplier of the structural elements that create the structural detail.

A parameter which depends on structural properties is $n_{\omega 1}$, which is the first mode of vibration frequency in the ω-direction, expressed in Hz (or s^{-1}). For slender structures with polar symmetric cross-section, this parameter usually has the same value in the alongwind and crosswind directions. It can be estimated by means of Finite Element Methods or of simplified approaches proposed by standards and codes (Eurocode 1, 2005; CNR, 2008, 2018).

4.3.2. Climatological input parameters

Local meteorological conditions are expressed by *k*, which is the shape parameter of the Weibull probability distribution of the current values of the wind velocity in situ (Section 2.3; Eq. (2.21); Pagnini and Solari, 2016). Estimation of this parameter is critical because it depends on the probabilistic local meteorological conditions, which is not regularly provided for every geographic area. Assuming $F_0 = 0$, in Italian territory the Weibull parameters *k* and *c* are linked with the reference mean wind velocity $\bar{u}_{ref}$ by means of the relationship (Pagnini and Solari, 2016) $c = (0.2k - 0.12)\bar{u}_{ref}$. Two relevant aspects follow: first, the representation of the density function of mean wind velocity is limited to only the parameter *k* and in a country or in a region this parameter is usually more stable than the companion parameter *c*; second, one of the quantities that are usually not available and deserve specific evaluations or provisions is limited to only *k* as regards meteorological parameters. Pagnini and Solari provided *k* values for different Italian zones (Pagnini and Solari, 2009, 2016; CNR 2018) (Fig. 4.6; Tab 4.3).

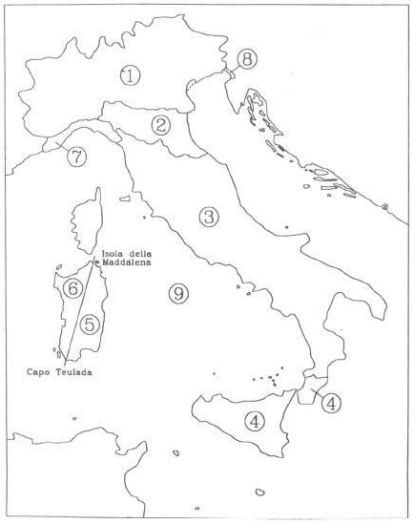

Fig. 4.6: Italian geographical zones defined in CNR code.

Zones	u_{ref} (m/s)	k
1	25	1.00
2	25	1.15
3	27	1.20
4	28	1.35
5	28	1.50
6	28	1.35
7	28	1.35
8	30	1.50
9	31	1.15

Tab. 4.3: Italian zones and related $\bar{u}_{ref}$ and k parameter values.

Further considerations concerning the parent population distribution model of the mean wind velocity at the site will be presented and discussed in Chapter 5. The choice proposed here, which follows the cited research studies, is compared with the Weibull distribution implicitly proposed by Eurocode 1 (2005) with regard to vortex shedding induced fatigue.

4.3.3. Response input parameters

The permanent loadings-induced stress in the examined section (calculated at serviceability) is expressed by $\bar{s}_P$, in MPa or N/mm^2; usually this stress is due to the dead weight of the construction and it can be evaluated thanks to approaches proposed by codes (Eurocode 1, 2005).

All other stress input parameters are due to wind loading and they are defined for alongwind and crosswind analysis, respectively. They have been obtained analytically starting from the method recently proposed by Solari (2018), which allows to determine the simultaneous alongwind, crosswind, and torsional loading and response of slender structures by means of calculations suitable for standard verifications, within the gust factor technique framework (Piccardo and Solari, 2000, 2001, 2002).

The formulations described below (Sections 4.3.4 and 4.3.5) are based on a schematization commonly used in wind engineering international procedures, according to which the wind field is characterized by the mean wind velocity, the turbulence intensities and the integral length scales calculated at a sole reference height, Z_{eq} = a fixed reference height for evaluating external wind action on a structure in the wind flow. Fig. 4.7 shows the scheme of three standard reference models widely used in structural engineering: (1) the vertical cantilever structure, used for instance to schematize chimneys and towers; (2) the inclined element of an industrial framework, for instance representative of an angular or double T cross-section member of a crane, a lattice frame, or a truss tower; and (3) the horizontal structure, adopted for instance with regard to bridges and footbridges. For each structural scheme Fig. 4.7 also provides the reference local coordinate, z_{eq}, also called equivalent coordinate, and its value in the global reference system, Z_{eq}, namely the reference height above ground (Solari, 2018).

Vertical Model	Inclined Model	Horizontal Model
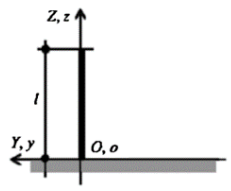	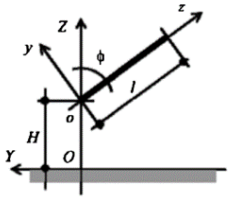	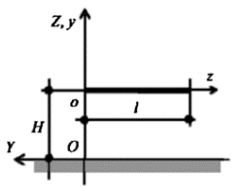
$z_{eq} = 0.6 \cdot l$	$z_{eq} = 0.5 \cdot l$	-
$Z_{eq} = 0.6 \cdot l$	$Z_{eq} = H + 0.5 \cdot l \cdot \cos\phi$	$Z_{eq} = H$

Fig. 4.7: Structural standard models, reference local coordinates, and reference heights (Figure © Solari, 2018).

Parameters of the response process in ω-direction at reference wind velocity are $\bar{s}_{\omega,ref}$, $\sigma_{\omega,ref}$, $\nu_{\omega,ref}$, $\nu_{\omega,Q,ref}$, $\lambda_{\omega,R,ref}$, which are the mean value, standard deviation, expected frequency, expected frequency of

the quasi-static part and normalized variance of the resonant part of the process in the critical section, respectively. The exponents of the power laws are $\alpha_{\sigma,\omega}$, which is the exponent of the power law expressing the standard deviation of the fluctuating stress, σ_ω, on varying wind velocity; and $\alpha_{\lambda,\omega}$, which is the exponent of the power law expressing the normalized variance of the stress resonant part, $\lambda_{\omega,R}$, on varying wind velocity. These response input parameters are discussed in Sections 4.3.4 as concerns *Drag*-direction ($\omega = D$) and in Section 4.3.5 as concerns *Lift*-direction ($\omega = L$).

4.3.4. Alongwind response input parameters

Alongwind turbulence-induced stress input parameters are defined by considering $\omega = D$, which means that fatigue damage due to drag aerodynamic forces is evaluated.

The alongwind response parameters are referred to the alongwind stress process in the critical section produced by the drag aerodynamic loading on the structure due to a wind velocity process induced by $\bar{u}_{ref}$. $\bar{u}_{ref}$ is the reference mean wind velocity in the site with 50 years return period at a fixed reference height adopted for ULS analysis, namely z_{ref}, on a reference terrain characterized by a reference roughness length (CNR 2008, 2018).

The mean value of the alongwind stress process in the critical section, evaluated at reference wind velocity $\bar{u}_{ref}$, is $\bar{s}_{D,ref}$. It is the maximum alongwind mean stress in the analyzed critical section, obtained applying the static aerodynamic force induced by reference mean velocity along the structure length, expressed by:

$$\bar{f}_D(z) = \frac{1}{2}\rho \bar{u}^2(z) b(z) c_D(z) \tag{4.12}$$

where z is the coordinate along the axis of the slender structure; ρ is the air density, usually assumed as 1.25 kg/m^3; b is the reference size related to the aerodynamic coefficient; c_D is the drag aerodynamic coefficient. Standards and codes often assumes b and c_D as constants. The mean wind velocity profile $\bar{u}(z)$ is evaluated starting from $\bar{u}_{ref}$ and taking into account the actual geographic, topographic, terrain and roughness conditions of the site of the construction.

The standard deviation value of the alongwind stress process in the critical section, evaluated at reference wind velocity $\bar{u}_{ref}$, is $\sigma_{D,ref}$. The mean stress $\bar{s}_{D,ref}$ defined previously is the mean value of a stress process characterized by a constant mean value and fluctuations around this value. The alongwind

fluctuating stress process is bi-modal and, at the reference velocity, it is characterized by the standard deviation $\sigma_{D,ref}$:

$$\sigma_{D,ref} = \gamma_F \overline{s}_{D,ref} 2 I_u \left(Z_{eq}\right) \sqrt{B_D^2 + R_D^2} \tag{4.13}$$

where γ_F is the safety factor for fatigue analysis (Eurocode 3, 2005, part 1-9); $I_u\left(Z_{eq}\right)$ is the longitudinal turbulence intensity at reference height; B_D is the quasi-static response factor, which considers the non-perfect correlation of the pressure acting on the structure; R_D is the resonant response factor, which considers the resonance between the turbulent excitement and the first mode of vibration of the structure (Piccardo and Solari, 2002; Solari, 2018; CNR, 2008, 2018). These two response factor are associated to $\overline{u}_{ref}$ and Z_{eq}.

The expected frequency value of the alongwind stress process in the critical section, evaluated at reference wind velocity $\overline{u}_{ref}$, is $\nu_{D,ref}$. It can be expressed in a simple form (Piccardo and Solari, 2002; Solari, 2018; CNR, 2008, 2018):

$$\nu_{D,ref} = n_{D1} \sqrt{\frac{R_D^2}{B_D^2 + R_D^2}} \geq 0.08 Hz \tag{4.14}$$

where n_{D1} is the first mode of vibration frequency in alongwind direction.

The expected frequency of the quasi-static part of the alongwind stress process in the critical section, evaluated at reference wind velocity $\overline{u}_{ref}$, is $\nu_{D,Q,ref}$. It is assumed equal to the expected frequency of the alongwind component of turbulence *u* and it can be expressed in a simple form:

$$\nu_{D,Q,ref} = 0.179 \frac{\overline{u}_{ref}}{L_u\left(Z_{eq}\right)} \left[\frac{L_u\left(Z_{eq}\right)}{\tau \cdot \overline{u}_{ref}}\right]^{0.72} \tag{4.15}$$

where $L_u\left(Z_{eq}\right)$ is the integral length scale of the longitudinal turbulence component at reference height; τ is the averaging time for the peak wind velocity, much less than the interval ΔT = 10 min, usually assumed equal to 1 - 3 s (Piccardo and Solari, 2002; Solari, 2018; CNR, 2008, 2018).

This parameter results to be crucial, then a wider discussion is carried out in the following.

The expected frequency of the quasi-static part of the response appears only in Eq. (3.58) of the proposed formulation (Table 3.2), which expresses the bi-modal corrective factor C_{BM} introduced in Chapter 3. This factor reduces the 0 level damage, which is evaluated considering a narrow-band stress

process, taking into account the quasi-static part of the response spectrum. It is corresponding to the Wirsching and Light (1980) wide band parameter. They proposed an empirical formula to estimate it in function of the slope of the *S-N* fatigue curve and the moments of the spectral density. On the other hand, C_{BM} factor is here obtained in closed form (Chapter 3) in function of the parameters defined in the current Chapter 4.

Since 0 level damage is estimated in correspondence of the expected frequency the stress process, C_{BM} factor is composed of two addends which "bring" the damage on the quasi-static and resonant harmonic contents of the response spectrum, respectively. When the quasi-static part of the response has an high role and the resonant part can be neglected, C_{BM} tends to be equal to the first addend ($\nu_{\omega,Q,ref}/\nu_{\omega,ref}$) because $\lambda_{\omega,R,ref}$ tends to 0. This might be a critical situation because C_{BM} corrective factor may be really small, depending on $\nu_{\omega,Q,ref}/\nu_{\omega,ref}$ ratio, hugely reducing the damage estimation. Figure 4.8 shows C_{BM} corrective factor on varying reference wind velocity and on varying input parameters; different curves in every diagram are related to example slender structures with different characteristic stiffness; τ is assumed equal to 3 s.

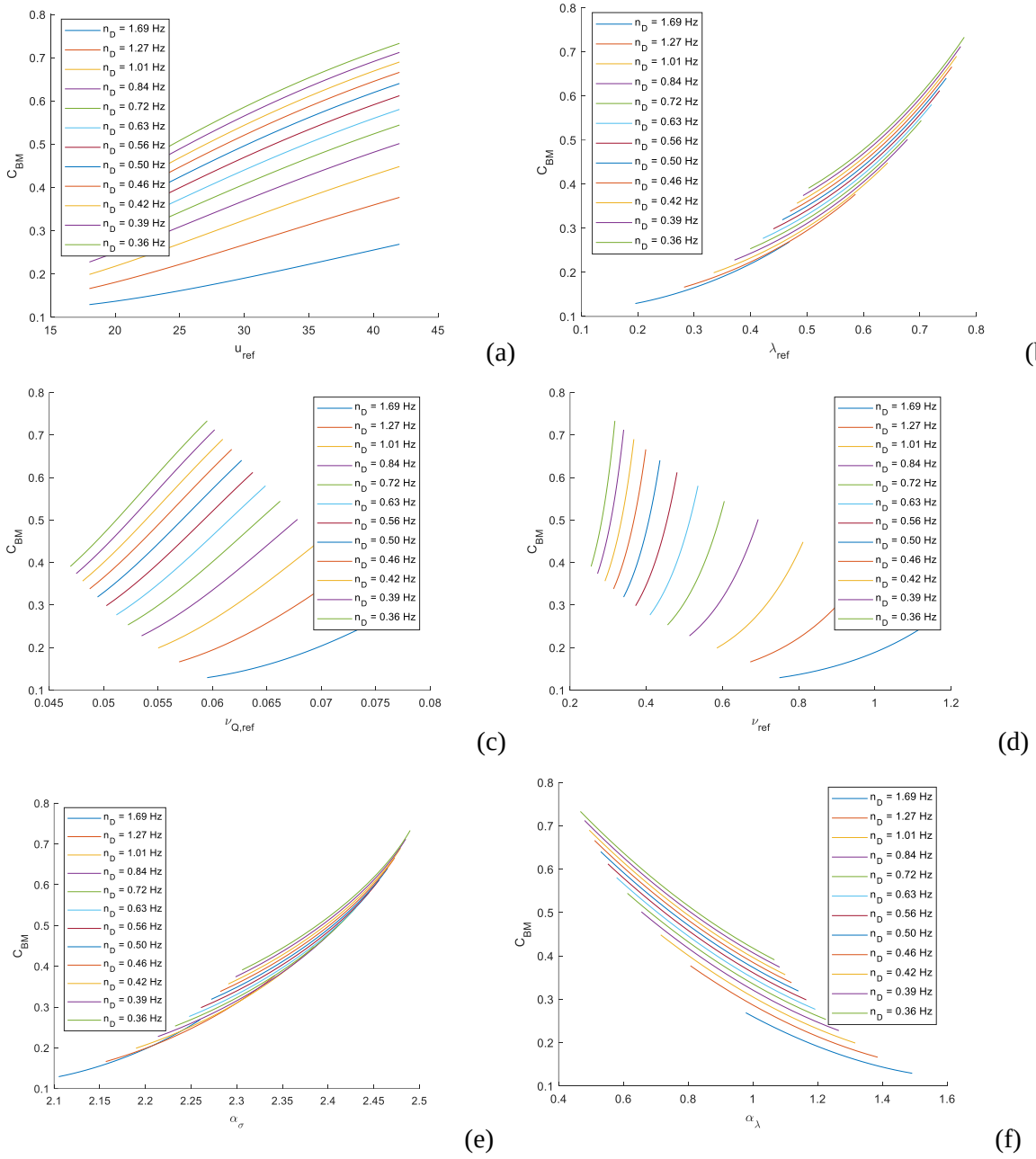

Fig. 4.8: C_{BM} variation for different slender structures on varying reference wind velocity (a), normalized variance of the resonant part of the stress process (b), expected frequency of the quasi-static part of the stress process (c), expected frequency of the stress process (d), exponent of the standard deviation power law (e) and exponent of the normalized variance power law (f); it is assumed τ = 3 s.

It is worth notice that, when a slender structure is characterized by higher stiffness, C_{BM} factor range is really low, this producing a reduction of the 0 level damage that can easily be more than 50%. In order to have a fatigue prediction on the safe side, hence, it is a good choice to fix τ = 1 s (Fig. 4.9).

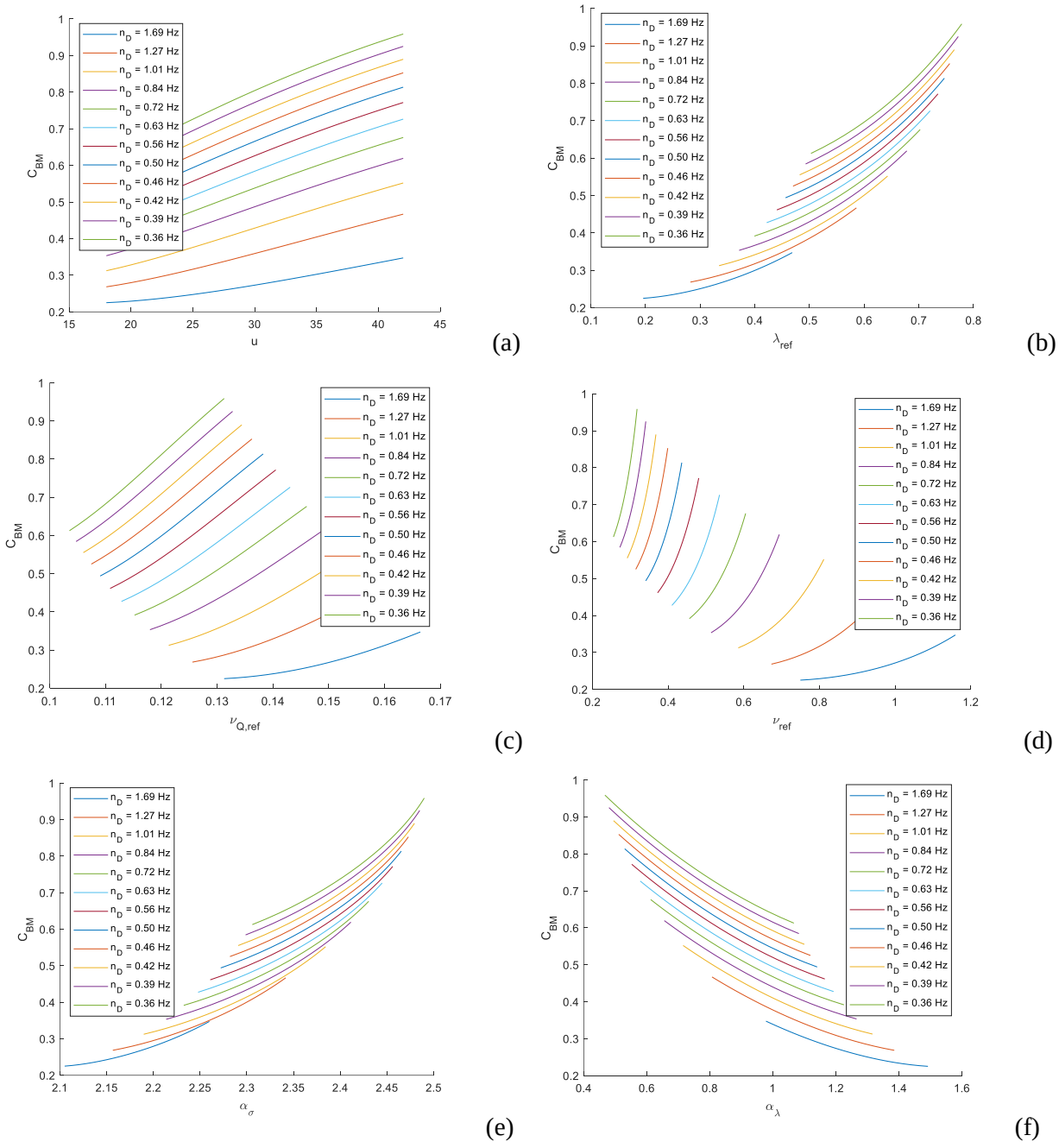

Fig. 4.9: C_{BM} variation for different slender structures on varying reference wind velocity (a), normalized variance of the resonant part of the stress process (b), expected frequency of the quasi-static part of the stress process (c), expected frequency of the stress process (d), exponent of the standard deviation power law (e) and exponent of the normalized variance power law (f); it is assumed τ = 1 s.

Diagrams are really similar, but the ones obtained assuming τ = 1 s are on the safe side with slightly higher ranges of C_{BM} factor, so this is the recommendable choice. To confirm this choice, it can be observed both in Figures 4.8c and 4.9c that C_{BM} increases when the expected frequency of the quasi-static

part of the stress process increases. By assuming τ = 1 s rather than τ = 3 s, $v_{\omega,Q,ref}$ and then C_{BM} results safely slightly higher.

The normalized variance of the resonant part of the alongwind stress process in the critical section, evaluated at reference wind velocity $\bar{u}_{ref}$, is $\lambda_{D,R,ref}$:

$$\lambda_{D,R,ref} = \frac{R_D^2}{B_D^2 + R_D^2} \tag{4.16}$$

The power law expressing the standard deviation of the alongwind fluctuating stress, σ_D, on varying wind velocity, is given by (see Eqs. (2.38), (3.13)):

$$\sigma_D(\bar{u}) = \sigma_{D,ref}\left(\frac{\bar{u}}{\bar{u}_{ref}}\right)^{\alpha_{\sigma,D}} \tag{4.17}$$

in which the exponent of the power law $\alpha_{\sigma,D}$ is given by (Repetto and Solari, 2009, 2012):

$$\alpha_{\sigma,D} = 2 - 0.721 \cdot ln\left[\frac{B_D^2 + R_{Dfat}^2}{B_D^2 + R_D^2}\right] \tag{4.18}$$

where R_{Dfat} is the resonant response factor evaluated with respect to the fatigue velocity $\bar{u}_{fat}$ (Repetto and Solari, 2012; Section 2.3.3), which in Italian territory can be conventionally assumed as $\bar{u}_{fat}(Z_{eq}) = 0.5 \cdot \bar{u}_{ref}(Z_{eq})$. This Equation (4.18) is obtained from Equation (2.39) by substituting $\sigma_D(z) = \bar{s}_D(z) 2 I_u(Z_{eq}) \sqrt{B_D^2 + R_D^2}$.

The power law expressing the normalized variance of the alongwind fluctuating stress resonant part, $\lambda_{D,R}$, on varying wind velocity, is given by (see Eqs. (2.38), (3.21)):

$$\lambda_{D,R}(\bar{u}) = \lambda_{D,R,ref}\left(\frac{\bar{u}}{\bar{u}_{ref}}\right)^{\alpha_{\lambda,D}} \tag{4.19}$$

in which the exponent of the power law $\alpha_{\lambda,D}$ is given by (Repetto and Solari, 2009, 2012):

$$\alpha_{\lambda,D} = -1.443 \cdot ln\left[\frac{B_D^2 + R_D^2}{B_D^2 + R_{Dfat}^2} \cdot \frac{R_{Dfat}^2}{R_D^2}\right] \tag{4.20}$$

This Equation (4.20) is obtained from Equation (2.39) by substituting Equation (4.16).

These two input parameters, exponents of the power laws approximations $\alpha_{\sigma,D}$ and $\alpha_{\lambda,D}$, are quantities that deserve specific evaluations; they are not available by applying provisions for ULS analysis, because they need the calculation of the resonant response factor both at reference and fatigue wind velocities. Together with the meteorological parameter *k*, these are the most critical input parameters to be evaluated.

4.3.5. Crosswind response input parameters

The whole analytical model, generalized with regard to different bilinear *S-N* fatigue resistance curves (Chapter 3) and with regard to alongwind and crosswind buffeting response (Chapter 4), is synthetized in six equations. The fatigue life of a structural element and the total mean damage in the unit time are predicted by Eqs. (3.4) and (3.5); terms in these expressions are evaluated by Eqs. (3.57)-(3.60), which are expressed in a simplified and a general format, suitable with standards and recommendations (see Table 3.2 in Section 3.3 and reported in Section 4.2). Section 4.3 discussed input parameters definition. As regards fluctuating response input parameters, there are two separated discussions. In Section 4.3.4, alongwind turbulence-induced fatigue analysis is considered, therefore alongwind response parameters are defined. In the current Section 4.3.5, crosswind turbulence-induced fatigue analysis is considered, therefore crosswind response parameters are defined.

Considering only lateral turbulence effect, thus crosswind buffeting response of slender structures, the 3-D generalized gust factor technique is taken into account (Piccardo and Solari, 2002). Within this approach, Solari (2018) proposes new simple formulas to evaluate the response at engineering level, and in particular equations to calculate generalized static, quasi-static, and resonant response parameters for slender structures. The proposed model takes into account these references to define crosswind response input parameters according to standards format. This allows to carry out the prediction of fatigue life starting from crosswind buffeting response in a critical structural detail.

Considering $\omega = L$ in the general model, which means that fatigue damage due to lift aerodynamic forces is evaluated, neglecting vortex induced vibrations contribution, response input parameters are introduced. The response parameters are referred to the crosswind stress process in the critical section produced by the lateral turbulence associated to the mean alongwind velocity $\bar{u}_{ref}$. $\bar{u}_{ref}$ is the reference mean wind velocity in the site with 50 years return period at a fixed reference height adopted for ULS analysis, namely z_{ref}, on a reference terrain characterized by a reference roughness length (CNR 2008, 2018).

The mean value of the crosswind stress process in the critical section, evaluated at reference wind velocity $\bar{u}_{ref}$, is $\bar{s}_{L,ref}$. It is the maximum crosswind mean stress in the analyzed critical section, obtained

applying the static aerodynamic force induced by reference mean velocity along the structure length. A simplified and reliable method to obtain this quantity is to multiply the maximum alongwind mean stress $\overline{s}_{D,ref}$ in the critical section by the crosswind static response factor μ_L (Solari, 2018):

$$\overline{s}_{L,ref} = \overline{s}_{D,ref}\mu_L \tag{4.21}$$

where:

$$\mu_L = \frac{c_L}{c_D} \tag{4.22}$$

assuming μ_L as constant on the safe side, according to standards provisions as concerns slender structures. c_D is the drag aerodynamic coefficient and c_L is the lift aerodynamic coefficient.

The standard deviation value of the crosswind stress process in the critical section, evaluated at reference wind velocity $\overline{u}_{ref}$, is $\sigma_{L,ref}$. This parameter represents the amplitude of the fluctuations around the mean value in the crosswind stress process. Neglecting vortex shedding effects on the response, this fluctuating process is bi-modal as the alongwind one and, at the reference velocity, it is characterized by the standard deviation $\sigma_{L,ref}$:

$$\sigma_{L,ref} = \gamma_F \overline{s}_{D,ref} 2 I_u\left(Z_{eq}\right)\sqrt{B_L^2 + R_L^2} \tag{4.23}$$

where γ_F is the safety factor for fatigue analysis (Eurocode 3, 2005, part 1-9); $I_u\left(Z_{eq}\right)$ is the longitudinal turbulence intensity at reference height; B_L is the quasi-static response factor in crosswind direction, which considers the non-perfect correlation of the pressure acting on the structure along its axis; R_L is the resonant response factor in crosswind direction, which considers the resonance between the turbulent excitement and the first mode of vibration of the structure in crosswind direction (Piccardo and Solari, 2002; Solari, 2018; CNR, 2008, 2018). These two response factor are associated to $\overline{u}_{ref}$ and Z_{eq}.

The expected frequency value of the crosswind stress process in the critical section, evaluated at reference wind velocity $\overline{u}_{ref}$, is $\nu_{L,ref}$. It can be expressed in a simple form (Piccardo and Solari, 2002; Solari, 2018; CNR, 2008, 2018):

$$\nu_{L,ref} = n_{L1}\sqrt{\frac{R_L^2}{B_L^2 + R_L^2}} \geq 0.08Hz \tag{4.24}$$

where n_{L1} is the first mode of vibration frequency in crosswind direction.

The expected frequency of the quasi-static part of the crosswind fluctuating stress process in the critical section, evaluated at the reference wind velocity $\bar{u}_{ref}$ and at the reference height Z_{eq}, can be reasonably assumed equal to the expected frequency of the crosswind component of turbulence *v*, evaluated at the same velocity and at the same height. Differently than the expected frequency of the alongwind component of turbulence *u*, whose simplified equation is already provided in standard format in CNR Recommendations (2008, 2018), the crosswind parameter is obtained with reference to Piccardo and Solari (2002). They defined the equation of the expected frequency of the quasi-static part of the nil mean fluctuation of the generic structural effect e_ω, as:

$$\nu^{e}_{Q\omega\varepsilon}(r)=\frac{d_u\bar{u}\left[z^{e}_{\omega\varepsilon}(r)\right]}{d_\varepsilon L_\varepsilon\left[z^{e}_{\omega\varepsilon}(r)\right]}\cdot\frac{1}{\sqrt{31.25\left[\tilde{\tau}^{e}_{\omega\varepsilon}(r)\right]^{1.44}+0.74\left[\tilde{l}^{e}_{\omega\varepsilon}(r)\right]^{0.64}+5.41\left[\tilde{\tau}^{e}_{\omega\varepsilon}(r)\right]^{0.93}\left[\tilde{l}^{e}_{\omega\varepsilon}(r)\right]^{0.71}}} \tag{4.25}$$

in which ω = generalized direction (*x*,*y*,*θ*); ε = loading indices (*u*,*v*,*s*) associated with the two turbulence components and with the wake excitation; *z* = vertical Cartesian axis, along the vertical slender structure, $0 \le z \le l$; $z(r)$ = reference coordinate at height *r*, $0 \le r \le l$; d_ε = coefficient derived from the closed form solution of the 3-D gust effect factor (d_u = 6.868; d_v = 9.434); $\bar{u}$ = mean wind velocity; L_ε = the integral length scale of the ε turbulence component in *x* direction;

$$\tilde{\tau}^{e}_{\omega\varepsilon}(r)=\frac{\tau d_u\bar{u}\left[z^{e}_{\omega\varepsilon}(r)\right]}{d_\varepsilon L_\varepsilon\left[z^{e}_{\omega\varepsilon}(r)\right]} \tag{4.26}$$

$$\tilde{l}^{e}_{\omega\varepsilon}(r)=\frac{k^{e}_{\omega\varepsilon}(r)\,d_u C_{z\varepsilon} l}{d_\varepsilon L_\varepsilon\left[z^{e}_{\omega\varepsilon}(r)\right]}\to 0 \tag{4.27}$$

τ = averaging time for the peak wind velocity, much less than the interval ΔT = 10 min, usually assumed equal to 1 - 3 s; $k^{e}_{\omega\varepsilon}$ = equivalent correlation factor for the effect *e* at height *r*; $C_{z\varepsilon}$ = exponential decay coefficient of the ε turbulence component along *z* (Piccardo and Solari, 2002).

Replacing constant values of d_u and d_v, assuming $\tilde{l}^{e}_{\omega\varepsilon}(r)=0$, considering $L_v(z)$ = 0.25 $L_u(z)$ and naming $z^{e}_{\omega\varepsilon}(r)=Z_{eq}$ it is possible to obtain the expected frequency of the quasi-static part of the nil mean fluctuation of the structural stress in crosswind direction, at the reference wind velocity $\bar{u}_{ref}$, expressed in a simplified form:

$$\nu_{L,Q,ref}=0.241\frac{\bar{u}_{ref}}{L_u(Z_{eq})}\left[\frac{L_u(Z_{eq})}{\tau\cdot\bar{u}_{ref}}\right]^{0.72} \tag{4.28}$$

The simplification $\tilde{l}^{e}_{\omega\varepsilon}(r)=0$, adopted to obtain the same format proposed by codes for the alongwind corresponding parameter, is on the safe side for both cases, causing a slight increase of $\nu_{\omega,Q,ref}$.

Equation (4.28) differs from the corresponding alongwind one (4.15) only for the numerical coefficient, then it is apparent that $v_{D,Q,ref} < v_{L,Q,ref}$ (Fig. 4.10).

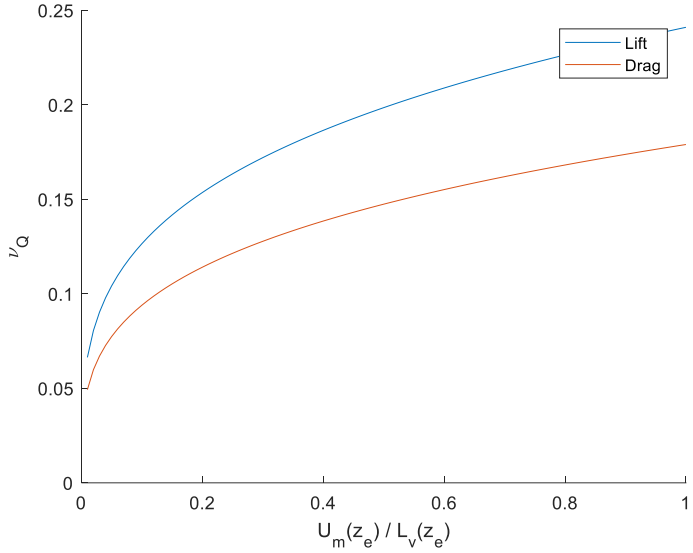

Fig. 4.10: $v_{D,Q,ref}$ and $v_{L,Q,ref}$ parameters trends.

The normalized variance of the resonant part of the crosswind stress process in the critical section, evaluated at reference wind velocity $\bar{u}_{ref}$, is $\lambda_{L,R,ref}$:

$$\lambda_{L,R,ref} = \frac{R_L^2}{B_L^2 + R_L^2} \tag{4.29}$$

The power law expressing the standard deviation of the crosswind fluctuating stress, σ_L, on varying wind velocity, is given by (see Eqs. (2.38), (3.13)):

$$\sigma_L(\bar{u}) = \sigma_{L,ref}\left(\frac{\bar{u}}{\bar{u}_{ref}}\right)^{\alpha_{\sigma,L}} \tag{4.30}$$

in which the exponent of the power law $\alpha_{\sigma,L}$ is given by:

$$\alpha_{\sigma,L} = 2 - 0.721 \cdot ln\left[\frac{B_L^2 + R_{Lfat}^2}{B_L^2 + R_L^2}\right] \tag{4.31}$$

where R_{Lfat} is the crosswind resonant response factor evaluated with respect to the fatigue velocity $\bar{u}_{fat}$ (Repetto and Solari, 2012; Section 2.3.3), which in Italian territory can be conventionally assumed as

$\bar{u}_{fat}\left(Z_{eq}\right)=0.5\cdot\bar{u}_{ref}\left(Z_{eq}\right)$. This Equation (4.31) is obtained from Equation (2.39) by substituting $\sigma_L\left(z\right)=\bar{s}_D\left(z\right)2I_u\left(Z_{eq}\right)\sqrt{B_L^2+R_L^2}$.

The power law expressing the normalized variance of the crosswind fluctuating stress resonant part, $\lambda_{L,R}$, on varying wind velocity, is given by (see Eqs. (2.38), (3.21)):

$$\lambda_{L,R}\left(\bar{u}\right)=\lambda_{L,R,ref}\left(\frac{\bar{u}}{\bar{u}_{ref}}\right)^{\alpha_{\lambda,L}} \tag{4.32}$$

in which the exponent of the power law $\alpha_{\lambda,L}$ is given by:

$$\alpha_{\lambda,L}=-1.443\cdot ln\left[\frac{B_L^2+R_L^2}{B_L^2+R_{Lfat}^2}\cdot\frac{R_{Lfat}^2}{R_L^2}\right] \tag{4.33}$$

This Equation (4.33) is obtained from Equation (2.39) by substituting Equation (4.29).

These two input parameters, exponents of the power laws approximations $\alpha_{\sigma,L}$ and $\alpha_{\lambda,L}$, are quantities that deserve specific evaluations; they are not available by applying provisions for ULS analysis, because they need the calculation of the resonant response factor both at reference and fatigue wind velocities. Together with the meteorological parameter *k*, these are the most critical input parameters to be evaluated.

CHAPTER 5 – CROSSWIND RESPONSE IN FATIGUE ANALYSIS

5.1. INTRODUCTION

The general method of wind-induced fatigue analysis of slender structures proposed in this thesis is based on a closed form solution of damage obtained analytically starting from fluctuating structural response due to oncoming wind turbulence. In previous Chapters in fact, only mean wind velocity and atmospheric turbulence effects are taken into account. Nevertheless, lightweight, flexible and low damped structures are prone to phenomena such as vortex-induced vibrations (VIV) and aeroelastic effects. Crosswind-induced fatigue damage is actually caused by the combined effect of the crosswind dynamic loading attributable to gust buffeting and to critical vortex shedding conditions, which has been neglected so far (Sections 2.3, 4.1 and 4.2). The impact of this choice is discussed in the current Chapter.

Slender vertical structures exposed to wind may experience critical crosswind vibrations, whose mean part is usually negligible and whose fluctuating part is due to the joint action of the lateral turbulence and to the vortex wake. The vortex wake produces aerodynamic actions in crosswind direction, whose frequency depends on the mean wind velocity, on the shape and on the size of the cross-section. Resonant response to vortex shedding actions occur at critical wind velocity, corresponding to the condition in which the shedding frequency is equal to the fundamental mode of vibration of the structure. Diagram representing crosswind response parameters with respect to mean wind velocity is not monotonic since it is characterized by the superposition of buffeting and vortex shedding contributions (Section 4.2, Fig. 4.1); it is worth noting that vortex shedding peak corresponds to moderate values of mean wind speed. In resonant conditions, aeroelastic forces may exalt the motion up to realise an extremely dangerous synchronisation mechanism well known as lock-in. Far from resonance conditions the dynamic response caused by the vortex shedding is almost negligible in comparison with the gust buffeting. In correspondence to the wind velocities that cause resonance, the vortex shedding deserves accurate evaluations.

As regards crosswind fatigue analysis, the peak related to critical velocity has an important impact on total damage estimation. Since large vibrations occur at moderate and frequent wind speeds, structures sensitive to this phenomenon usually undergo a large number of stress cycles. It is impossible to obtain a closed form solution of damage by following the same approach used in previous Chapters, because the power law approximation of response parameters is not effective if the combined effect of lateral turbulence and vortex shedding is considered (Section 4.2, Fig. 4.1, Fig. 4.2). Since VIV is a complex

phenomenon which produces a completely different effect on structures, it can not be easily adapted to a simple analytical function of wind velocity.

Engineering procedures estimates separately crosswind maximum response to gust buffeting and crosswind response to critical vortex shedding conditions. This is reasonable for ULS analysis, but there's no guarantee such assumption would provide reliable outcomes in fatigue analysis. The fatigue damage phenomenon is strongly non-linear, then superposition effect does not apply. Frequency-domain theoretical formulations are still open matters in the state of the art. Eurocode 1 (2005) codifies a method to take vortex-induced fatigue into account, using an approach based on the vortex-resonance model (Ruscheweyh, 1994). It provides an expression for evaluating the number of load cycles due to vortex shedding, neglecting lateral turbulence contribution. Therefore, the current regulations and state of the art take into account vortex shedding induced fatigue as an independent loading condition with respect to buffeting induced fatigue, even if this is a non-linear problem.

The present Chapter develops an in-depth analysis regarding the possibility of separating turbulence and vortex shedding effects. For sake of simplicity, at this stage, it is assumed that only the first mode of vibration in crosswind direction is taken into account.

Section 5.2 introduces vortex shedding phenomenon (Section 5.2.1), the induced response according to spectral model (Section 5.2.2), “forced” and “lock-in” regimes (Section 5.2.3) and fatigue standard procedure (Section 5.2.4).

Then, in Section 5.3, some example chimneys (Sections 5.3.1, 5.3.2, 5.3.3 and 5.3.4) and a pole (Section 5.3.5) are numerically analysed, evaluating crosswind dynamic response on varying wind velocity, calculating the cycle and the damage histograms, in order to predict a reliable value of fatigue life. Using such results as benchmark, the proposed crosswind turbulence-induced fatigue method and the engineering verification of VIV-induced fatigue (Eurocode 1, 2005) are applied separately. Resulting fatigue lives are compared and critically discussed.

Once the possibility of separating crosswind effects in fatigue analysis is considered, in Section 5.4 VIV-induced fatigue standard method is critically analysed, because it seems to provide too much preventive results compared with numerical simulations. In particular, the first main problem concerns the equation that estimates the number of cycles due to VIV, which does not consider properly the local climatology. The number of cycles associated to the maximum amplitude due to vortex shedding is really sensitive to the mean wind velocities Weibull distribution (Section 5.4.1). The second issue concerns the fact that maximum response is estimated in correspondence of one specific wind velocity, the critical one, even if the peak of the structural response corresponds to a range of wind velocity (Section 5.4.2). The role of parameters uncertainties has been discussed as regards response evaluation to VIV (Section 5.4.3).

The propagation of the produced error is exponentially significant in fatigue estimation, therefore some preventive suggestions to improve the calculation are proposed (Section 5.4.4).

5.2. VORTEX SHEDDING-INDUCED VIBRATIONS

Vortex induced vibrations (VIV) represent one of the most important issues concerning wind excited slender structures and elements. Although its great significance, the engineering description of this phenomenon mainly comes from the experimental evidence and uses empirical models.

Key parameters are the Strouhal number *St* and the Scruton number *Sc*. The Strouhal number determines the frequency of vortex shedding from the structure and, therefore, rules the critical velocity at resonant conditions. It is related to the cross-section shape and, in the case of structures with rounded surfaces, it is Reynolds number dependent, since the *Re* directly rules the vortex shedding topology. The Scruton number governs the synchronization region at lock-in. At high *Sc* values, a structure undergoes low amplitude linear vibrations in random forcing regime. Conversely, at low *Sc*, non-linear resonant vibrations arise in lock-in conditions. When dealing with structural verifications this is the discriminating quantity that allows either to exclude or to highlight possible critical VIV. However, the scientific literature on this topic does not supply specific quantitative limits in terms of Scruton number; technical applications refer to high enough values for excluding synchronous vibrations (e.g., $Sc > 30$ for circular cross-sections according to CNR, 2008, 2018).

According to Païdoussis et al. (2011), the description of crosswind VIV comes from three families of phenomenological models of increasing complexity. Forced system models consider a cylinder excited by a force independent from its motion, therefore only depending on time (e.g., Ruscheweyh, 1994; Blevins, 2001). In fluid-elastic system models, the vortex-induced force also depends on the cylinder motion through an equivalent fluid-structure interactive term (e.g., Vickery and Basu, 1983a; Goswami et al., 1993). Coupled system models are a further evolution that considers explicitly the interaction with the wake dynamics; in case of crosswind VIV they are described by two degree of freedom systems, including the dependence on both the cylinder motion and the wake oscillation (e.g., Hartlen and Currie, 1970; Skop and Griffin, 1973; Tamura and Matsui, 1979; Facchinetti et al., 2004). At present, coupled system models are quite diffused in hydrodynamics whereas they have limited technical applications in aerodynamics (e.g., Farshidianfar and Zanganeh, 2010; Violette et al., 2010).

The different opinions on how to represent the phenomenon mathematically are reflected in the variety of procedures used in practical designs to determine structural response. Dealing with wind engineering verifications, two calculation procedures are commonly used, respectively of forced and fluid-elastic type (e.g., Eurocode 1, 2005). The first method, referred to as the harmonic model, was proposed by Ruscheweyh (1994) who supplied a heuristic vortex-induced force based on the correlation length parameter, which increases with increasing vibration amplitude. The second method, referred to as the

spectral model, was proposed by Vickery and Basu (1983a) who supplied an analytical expression for the equivalent aerodynamic damping, derived from a modified van der Pol oscillator, accounting for the intrinsic non-linearity of the problem and its self-limiting features. The method proposed by ESDU 96030 (1998) can be considered as a hybrid of the two previously described approaches (Holmes, 1998). It adopts a random excitation model, similar to the spectral model, at low amplitudes and assumes a harmonic model at large amplitude. All these formulations lead to evaluations that may involve considerable uncertainties compared to measured data (e.g., ESDU 96030; Hansen, 1999; Kawecki and Zuranski, 2007). The spectral formulation is commonly considered more sound and more prudential. Moreover, it is considered more reliable at sufficiently high Scruton numbers, when the response tends to be in the so-called "forced vibration" regime.

The Vickery and Basu complete analytical solution still remains not easy to use and, for this reason, it is seldom applied (e.g., Verboom and van Koten, 2010; Pagnini and Piccardo, 2017). The reworking of the spectral model in terms of simplified analytical coefficients (e.g., Hansen, 1999, 2007) makes it possible including this procedure into codes and guidelines. However, engineering applications often adopt extreme simplifications, the reliability of which has not been adequately explored yet. Contradictory outcomes can be found compared to the experimental results (e.g., Hansen, 1999; Ruscheweyh and Sedlaceck, 1988). Moreover, extended comparisons between complete and approximate solutions are lacking. Especially, there are no broad-range analyses of the sensitivity to the model parameters whose uncertainties are the greatest hindrance to the analytical prediction of VIV. At this purpose, Pagnini and Piccardo (2017) highlighted the fundamental role of the limiting amplitude, in both transition and lock-in regime, in order to find realistic value of the VIV maximum amplitude. Working in the frame of the Vickery and Basu model, Pagnini, Piccardo and Solari (2020) proposed calculation developments suitable for engineering applications, trying to maintain the rigor of the initial formulation.

This thesis focuses on the spectral model included in Eurocode and CNR provisions for predicting vortex-induced vibrations of structures and it focuses on the equation provided by these documents for determining the number of cycles that the structure undergoes.

5.2.1. The vortex-shedding on slender structures

A slender structure or structural element immersed in a wind field is subjected to a regular alternating shedding of vortices which causes asymmetries of the velocity and pressure fields of the fluid, responsible for transversal forces that vary in time with frequency equal that of vortex shedding (Fig. 5.1). Such transversal forces are often essential for the study of the behaviour of structures in respect of the wind.

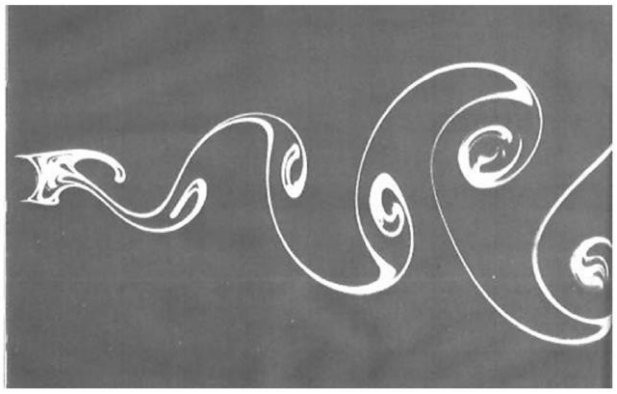

Fig. 5.1: Vortex shedding for a circular cylinder immersed in a fluid.

The frequency of this almost periodic action depends on the mean wind velocity and the cross section shape and size. Strouhal in 1878 observed that the regular phenomenon of vortex shedding can be described by a dimensionless number *St* provided by the relationship:

$$St = \frac{n_s b(z)}{\bar{u}(z)} \tag{5.1}$$

in which n_s is the vortex shedding frequency or loading frequency, b is the crosswind size of the structure, $\bar{u}$ is the mean wind velocity and z is the location coordinate. When the vortex shedding frequency is close to a natural frequency of vibration, resonance occurs, causing on lightweight and low damped structures or components large amplitude vibrations. This resonant phenomenon happens in correspondence of a wind velocity called critical velocity:

$$\bar{u}_{cr} = \frac{n_L b}{St} \tag{5.2}$$

where n_L is the natural frequency in crosswind direction and b is the characteristic size. The vortex-induced vibrations calculated do not depend on the choice of reference quantities, e.g. the characteristic size. The reference quantities chosen often refer to the point at which the structural vibrations are largest. *St* depends on the shape of the cross-section and, in the case of structures with rounded surfaces, on the Reynolds number *Re*. Figure 5.2a shows *St* values provided for cylinders with circular section by CNR recommendation, while Figure 5.2b provides *St* for different cross-sections according to Eurocode 1.

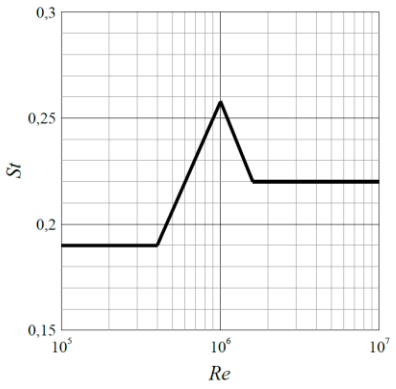

(a)

Cross-section		*St*
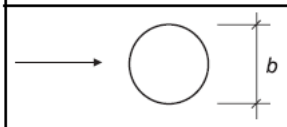 for all *Re*-numbers		0,18
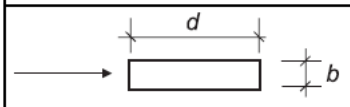 $0,5 \le d/b \le 10$		from Figure E.1
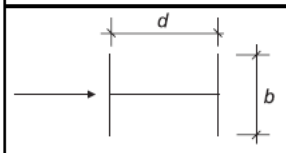 linear interpolation	*d*/*b* = 1 *d*/*b* = 1,5 *d*/*b* = 2	0,11 0,10 0,14
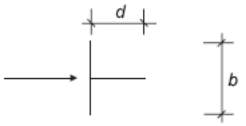 linear interpolation	*d*/*b* = 1 *d*/*b* = 2	0,13 0,08
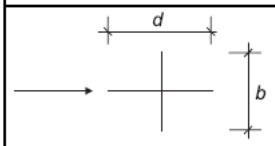 linear interpolation	*d*/*b* = 1 *d*/*b* = 2	0,16 0,12
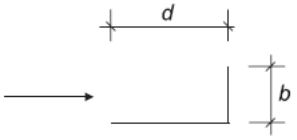 linear interpolation	*d*/*b* = 1,3 *d*/*b* = 2,0	0,11 0,07
NOTE Extrapolations for Strouhal numbers as function of *d*/*b* are not allowed.		

(b)

Fig. 5.2: Strouhal number values for circular cylinders (a) and for different cross-sections (b) according to codes.

Buffeting and vortex shedding processes are very different, the former is a broad band process, in particular bi-modal when only the first mode of vibration is taken into account, and the latter is a narrow band one. The pulsation of the loading process at fixed mean wind velocity is constant, equal to $2\pi n_s$.

Developing the equation of motion, Scruton and Flint (1964) defined one of the crucial parameters for the vortex-induced vibrations of structures, namely the Scruton number *Sc*:

$$Sc = \frac{4\pi m_e \xi_s}{\rho b^2} \tag{5.3}$$

where m_e is the equivalent mass per unit length, ξ_s is the structural damping ratio and ρ is the air density (the recommended value is 1,25 kg/m^3). Therefore, *Sc* is proportional to the structural damping and to the ratio between the vibrating mass and the mass of the air displaced by the structure.

If *Sc* corresponds to a high value, such as 30 or more, the probability of lock-in is quite low and vortex shedding is not the critical load case. If *Sc* corresponds to an intermediate value, such as between 5 and 30, vortex shedding is very sensitive to different parameters, first of all turbulence intensity. High values of turbulence intensity reduce the risk of strong vibrations; small values of turbulence intensity, usually associated with small values of critical velocities, may amplify the critical vortex shedding. If *Sc* corresponds to a low value, such as 5 or less, vibrations induced by vortex shedding may be very large and dangerous; a lock-in regime has quite high probability of occurrence.

Lock-in is an aeroelastic effect produced by the fluid-structure interaction. The aeroelastic or motion-induced actions are added to the aerodynamic wind actions, producing critically large oscillations of the structure and aeroelastic instability. When the vortex shedding frequency or loading frequency n_s, proportional to $\bar{u}$, is in the proximity of the natural frequency of the elastic system n_L (constant), the periodicity in the wake is synchronized or captured by that of the mechanical system. This happens over a certain range of wind speeds, for which the detuning or separation of these two frequencies is close to zero. The shedding abruptly deviates from the linear Strouhal dependence and stays constant at the mechanical natural frequency n_L (Fig. 5.3). This condition is referred to as lock-in. Under such a state, the feedback from the synchronized wake to the cylinder is intensified, leading to large response amplitudes of the elastically supported cylinder (Goswami et al., 1993).

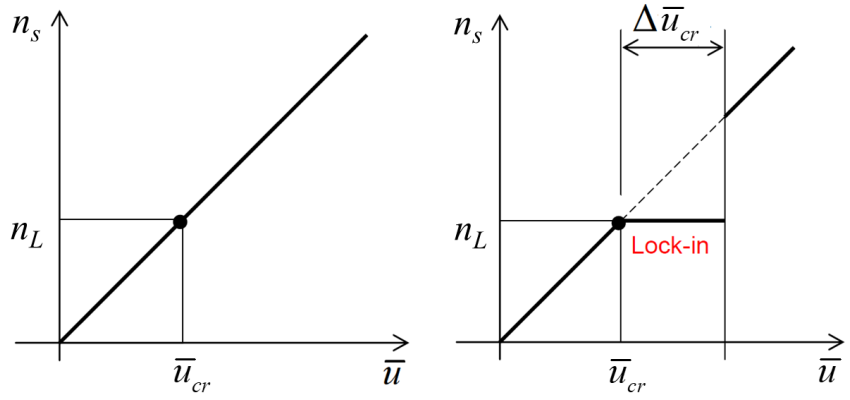

Fig. 5.3: Different conditions produced by high Scruton number and small Scruton number, respectively.

The slender structure or structural element is subjected to a vortex-induced force $f_{Ls}(z,t)$ varying over time *t* and space *z*. Assuming a lack of correlation between the vortex-shedding forces induced on the

stationary cylinder and the motion-induced actions, the lift force per unit length $f_{Ls}(t)$ is given by the sum of an external fluctuating lift force and an aerodynamic lift force, which in turn is the sum of a displacement-dependent term and a velocity-dependent term:

$$f_{Ls}(t) = f_s(t) + f_a(t) = \left[\frac{1}{2}\rho\bar{u}^2 b c_{Ls}\sin(2\pi n_s t)\right] + \left[h_a y(t) + k_a \dot{y}(t)\right] \tag{5.4}$$

where c_{Ls} is the lift coefficient, actually a space- and time-dependent coefficient classically described in the frequency domain by its standard deviation; h_a and k_a are coefficients for the in-phase and out-of-phase components, respectively, of the aerodynamic force; y is the crosswind structural displacement; $\dot{y}$ is the crosswind structural velocity.

The second squared brackets in Equation (5.4) represents motion-induced forces. This contribution is a nonlinear function of parameters of both the fluid (e.g., the Reynold number *Re*) and the structure (e.g., the structural displacement y and its derivatives). The influence of turbulence is implicit in the formulation (e.g., it influences the values of aerodynamic and aeroelastic coefficients) but it does not appear explicitly in the equations, as usual in the literature. The aerodynamic lift force per unit length is classically expressed as the sum of a displacement-dependent term and a velocity-dependent term. The former, which is representative of the aerodynamic force in phase with the motion (and, therefore, modifies the structural stiffness) is usually negligible compared with the structure elastic force (Vickery and Basu, 1983a). The latter is representative of the aerodynamic damping force, which will reduce the effective damping of the vibrations when k_a is positive. As this occurs for wind velocities close to the critical wind velocity it is a very essential parameter when calculating the response.

The linear dependence between loading and velocity indicated in Equation (5.4) is sufficiently accurate for small vibrations of up to approx. 5-10% of the structural width. For larger vibration amplitudes non-linear damping terms become important.

Assuming $k_a = 4\pi n_L \rho b^2 K_a$, in which K_a is the aerodynamic damping parameter determining the linear term of the motion-induced wind loads on the structure, the total damping of the system becomes:

$$\xi_{eq} = \xi_s + \xi_a = \frac{\rho b^2}{4\pi m_e}\left(Sc - 4\pi K_a\right) \tag{5.5}$$

in which *Sc* is the parameter representing the structural damping ξ_s and K_a is the parameter representing the aerodynamic damping, which may become negative.

The effect of turbulence on vortex-induced vibrations has been considered experimentally by Vickery (1998), and Krenk and Nielsen (1999) include turbulence in their theoretical lift-oscillator model. The basic influence of air turbulence concerns the fact that an increase in oscillations amplitude for a slender structure occurs with low turbulence flow. This happens in correspondence of the critical wind velocity.

When the mean wind velocity for a short period of time is equal to the resonance wind velocity, the amplitudes will grow slowly, but as soon as the mean wind velocity has changed away from the resonance wind velocity, large amplitudes will not grow up. The actual amplitudes will be of stochastic nature, i.e. increase when the wind velocity is close to the resonance wind velocity and reduce when this is not the case. These observations refer to structures not having extremely low Scruton numbers. At low Scruton numbers large vibrations may develop even in turbulent flow.

The influence of large-scale turbulence may be estimated approximately by integrating the aerodynamic damping parameter K_a measured for different mean wind velocities and weighed with a Gaussian distribution describing the variation of the longitudinal turbulent component. A more accurate approach will be to analyse the differential equation describing the variations of the lift coefficient in time. Measurements of aerodynamic damping terms in turbulent flow may also be used.

The aerodynamic damping depends on turbulence intensity and not on the absolute variations of the wind velocity. The critical Scruton number, at which the jump from small to large vibrations occurs, depends strongly on the low frequency turbulence with large scales, but not on the high frequency turbulence with small scales.

5.2.2. The spectral model

Originally, Vickery and Clark (1972) proposed the spectral model used to predict vortex-induced vibrations of line-like structures. They express the power spectral density function of the vortex induced force on the stationary structure $S(n)$ through:

$$\frac{nS(n)}{c_{Ls}^2} = \frac{n}{\sqrt{\pi}\beta n_s}\exp\left\{-\frac{1}{\beta^2}\left(1-\frac{n}{n_s}\right)^2\right\}; \quad \beta = \sqrt{\beta_0^2 + 2I_u^2}; \quad \beta_0 \approx 0.08 \tag{5.6}$$

In their formulation of the power spectral density function of the vortex shedding (Eq. (5.6)) the longitudinal turbulence intensity I_u is taken into account (Fig. 5.4). Then the formulation and aerodynamic parameters used in the model have been analysed in several papers and text books.

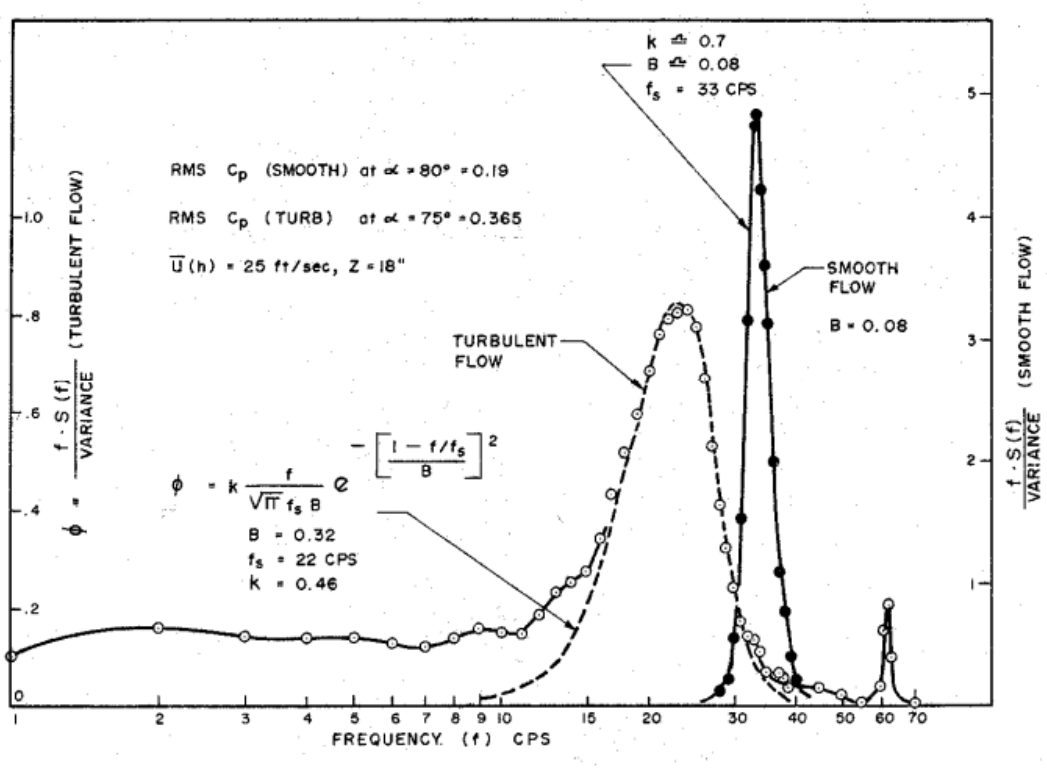

Fig. 5.4: Power spectral density function of the vortex shedding proposed by © Vickery and Clark (1972).

Using the spectral model developed in the framework of linear random dynamics, following Basu and Vickery (1983) and Vickery and Basu (1983a), three assumptions are made: a) the forcing "stationary" term is described in the frequency domain by the lift coefficient standard deviation, through the power spectral density function of $c_{Ls}(z,t)$ in the classic form proposed by Vickery and Clark (1972); (b) the motion-induced excitation concerns a single mode at a time, then the model is able to include fluid-structure interaction for (sufficiently) well-separated modes only; (c) the physical nonlinearity of the motion-induced forces term (second squared brackets in Equation (5.4)) is considered in a statistical form only, through a suitable ratio of crosswind displacements standard deviations. Therefore, the motion-induced force can be expressed as (Marris 1964):

$$f_a(t) = 4\pi n_s \rho b^2 K_a \left[1 - \frac{\sigma_s^2(t)}{\sigma_{Lim}^2}\right] \dot{y}(t) \tag{5.7}$$

where σ_s is the displacement standard deviation and σ_{Lim} is the standard deviation of the limiting amplitude of VIV displacements, being the phenomenon self-limited in nature.

K_a is the aerodynamic damping parameter for small oscillation amplitudes (i.e., when $\sigma_s \rightarrow 0$); its values and shape are strongly influenced by the longitudinal turbulence intensity I_u (e.g., Verboom and

van Koten, 2010). On the other hand, the dependence on the turbulence integral length scale is not included; this parameter seems to have a modest influence on VIV-induced displacements in both low-amplitude and high-amplitude regimes (Acebedo et al., 2016; Daniels et al., 2016; Vickery and Basu, 1983a).

Basu and Vickery (1983) express the limiting amplitude of the full-scale element as a function of the characteristic size (e.g., the diameter of a circular cross-section), $\sigma_{Lim} = b/\kappa$, b being the characteristic size and $1/\kappa$ being a suitable fraction of b, often assumed by codes equal to 0,4 ($\kappa = 2.5$). This choice appears, however, more suitable for a bi-dimensional description, rather than for a full-scale modelling, because it does not account for the geometric boundary conditions of the element.

Unfortunately, there are no physical models for the prevision of K_a and σ_{Lim} that can only be estimated on experimental and/or empirical basis. In front of a number of factors that may influence these parameters (turbulence in particular), available measures are still scanty and mainly referred to vertical circular cylinders. Experimental or numerical estimates for other structural typologies are restricted (e.g., Vickery, 1995; Hansen, 2013; Pagnini and Piccardo 2017).

The spectral model developed by Vickery and Basu (1983a) and Basu and Vickery (1983) presumes an equivalent aerodynamic damping ξ_{eq}, accounting for both the mechanical ξ_s and the aerodynamic ξ_a contribution. This coefficient ξ_{eq} can be considered able to approximate the non-linearity induced by the aerodynamic interaction; the aerodynamic damping is indeed composed by two terms, the first linear term introduces negative aerodynamic damping and the last non-linear term gives positive damping ensuring that the response is self-limiting. For small amplitudes of up to approx. 5-10% of the structural width, the aerodynamic damping is described sufficiently accurate by the first, linear term.

Starting from the equation of motion, in the spectral model framework, the equivalent aerodynamic damping ratio is given by:

$$\xi_{eq} \cong \frac{\rho b^2}{4\pi m_e}\left\{Sc - 4\pi K_a\left[1-\frac{\sigma_s^2}{a_L^2 b^2}\right]\right\} \tag{5.8}$$

in which $a_L = 1/\kappa$ and the standard deviation of the crosswind structural deflection σ_s, which follows the mode shape, is defined in the frequency domain (Vickery and Basu, 1983a):

$$\frac{\sigma_s}{b} = \sqrt{\frac{-a_L^2\left(Sc - 4\pi K_a\right) + \sqrt{a_L^4\left(Sc - 4\pi K_a\right)^2 + 16\pi K_a A^2}}{8\pi K_a}} \tag{5.9}$$

where:

$$A = \frac{bc_{Ls}}{8\pi St^2}\sqrt{\frac{\rho}{m_e\beta}} \tag{5.10}$$

5.2.3. "Forced vibration" and "lock-in" regimes

The possible regimes to which the fluid-structure system may belong are "forced vibration" regime, "transition" regime and "lock-in" regime (Fig. 5.5; 5.6 and 5.7).

The so-called "forced vibration" regime corresponds to high Scruton numbers, larger than $4\pi K_a$, and also high structural damping ξ_s. It is a condition in which structural vibrations are produced by the vortex shedding force and therefore it is also called vortex-excited regime. It is less critical because it leads to smaller amplitude oscillations of the structure. The response process related to the "excited" regime is a narrow-band random process.

The so-called "lock-in" regime corresponds to small Scruton numbers, smaller than $4\pi K_a$, and also low structural damping ξ_s. It is a condition in which structural vibrations are produced by the motion-induced aeroelastic force. It is more critical because it leads to larger amplitude oscillations of the structure. The response process related to the "lock-in" regime is a deterministic process (almost sinusoidal).

The transition regime is intermediate between the previous two regimes, corresponding to Scruton numbers approximately equal to $4\pi K_a$. Turbulence intensity strongly influences this regime.

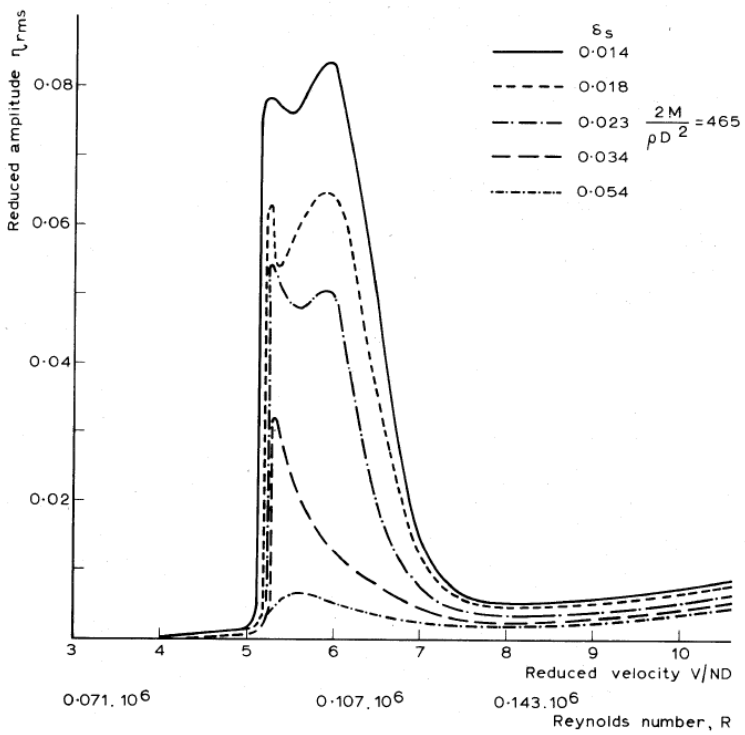

Fig. 5.5: Diagram of the structural response on varying mean wind velocity (© Wootton, 1969); lower structural damping, therefore smaller *Sc*, increases the response in correspondence of the critical velocity range (lock-in region); higher structural damping, therefore larger *Sc*, decreases the response in correspondence of the critical velocity range (forced vibration region).

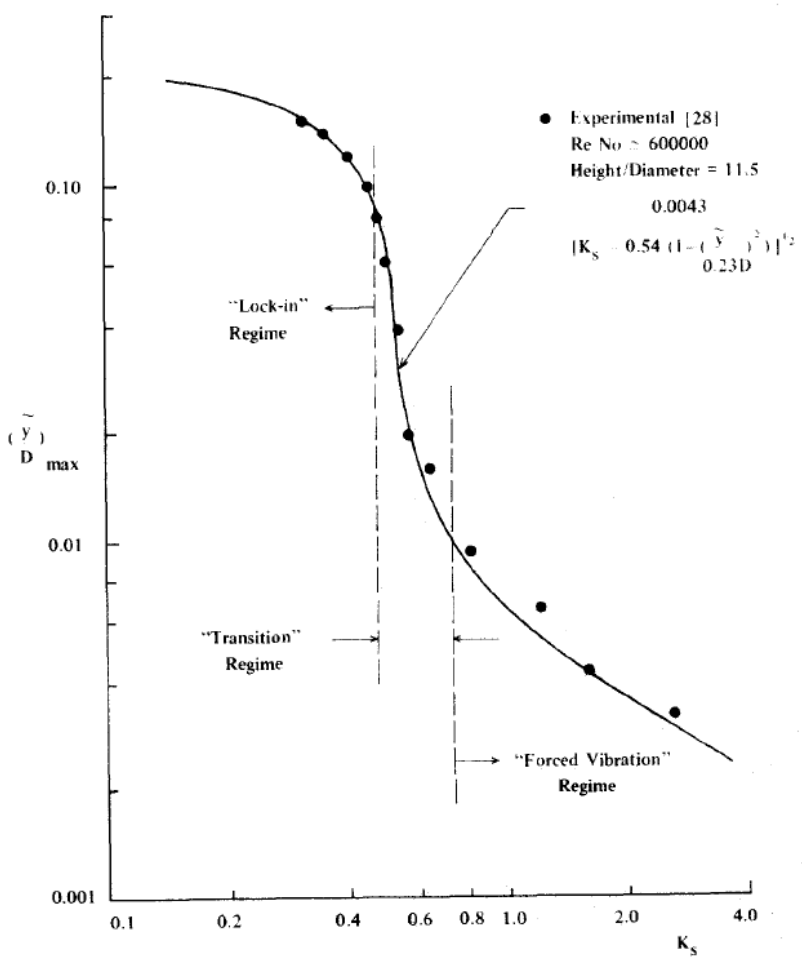

Fig. 5.6: Diagram of the structural response on varying structural damping parameter (© Vickery and Basu, 1983); lower structural damping, therefore smaller *Sc*, increases the response ("lock-in" regime); higher structural damping, therefore larger *Sc*, decreases the response ("forced vibration" regime); intermediate values of structural damping and *Sc* corresponds to a high slope of the curve with abrupt variations of the response depending on *Sc* ("transition" regime).

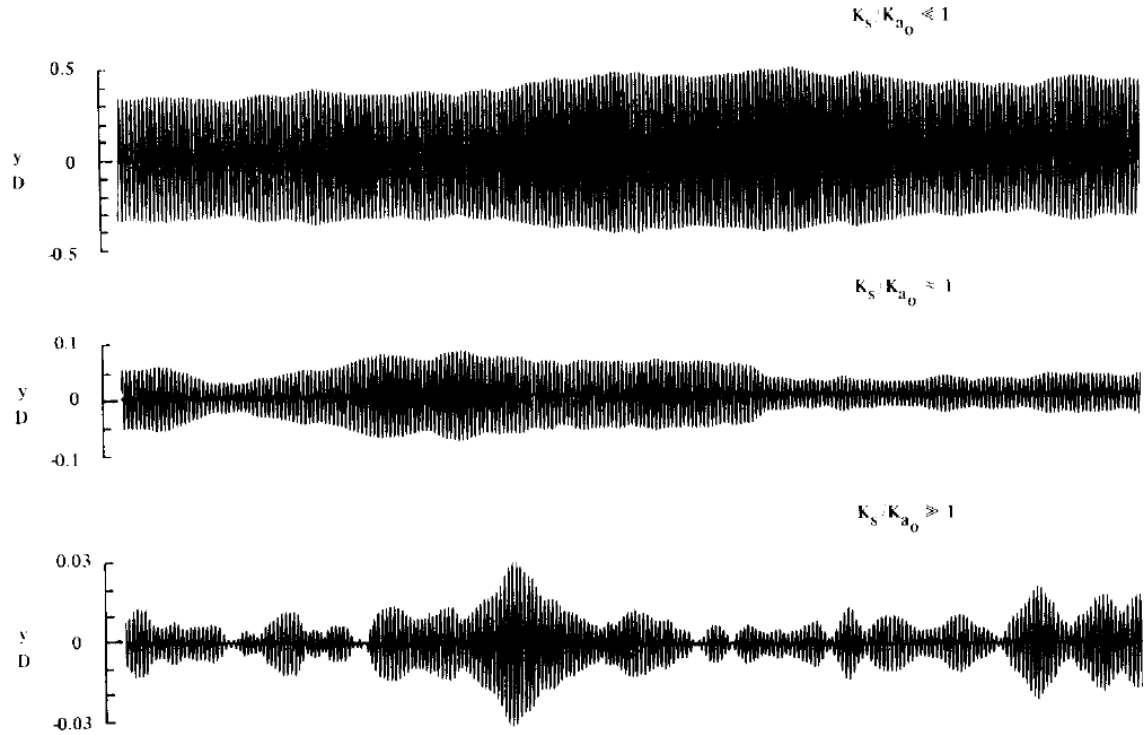

Fig. 5.7: Response processes (displacements histories) for high, moderate and low structural damping (© Vickery and Basu, 1983); the first process (low *Sc*) corresponds to lock-in deterministic regime; the second process (intermediate *Sc*) corresponds to transition regime; the third process (high *Sc*) corresponds to vortex-excited random regime.

Turbulence intensity strongly affects vortex shedding response. In previous Sections 5.2.1 and 5.2.2 it is explained how I_u influences aerodynamic damping parameter K_a and how the response became critical with low turbulence flow and small *Sc*. Vickery and Basu (1983) studied how I_u influences structural response on varying structural damping parameter (Fig 5.6 and 5.8):

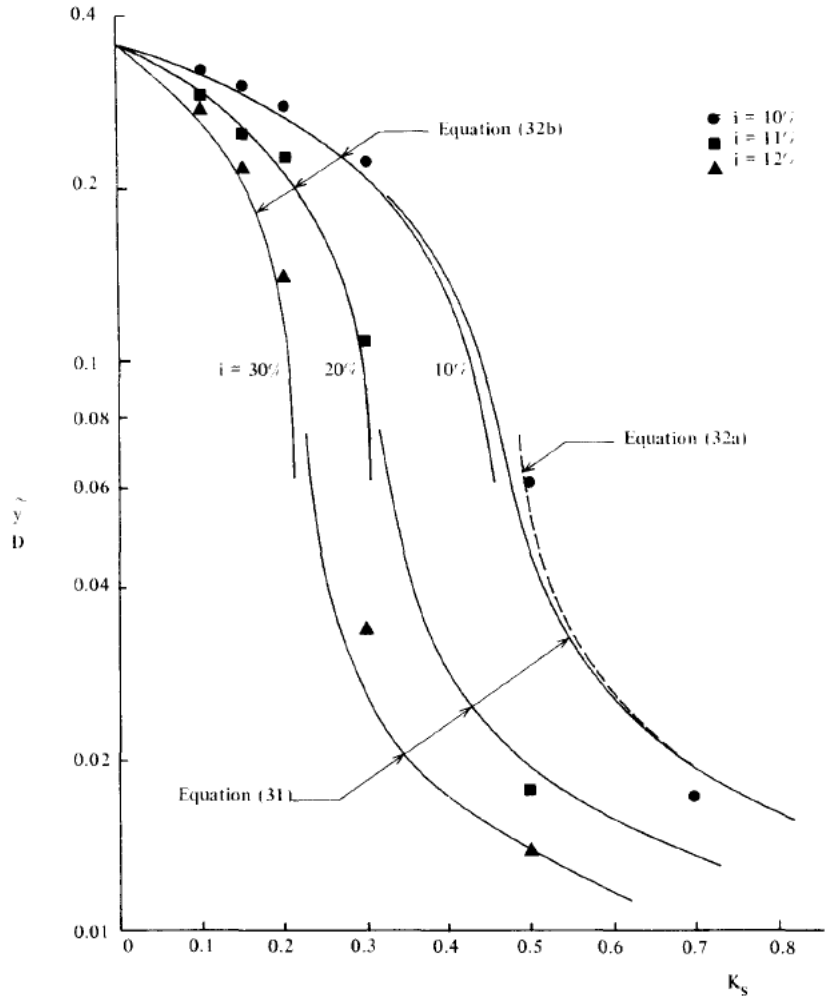

Fig. 5.8: Diagrams of the structural response on varying structural damping parameter (© Vickery and Basu, 1983); large I_u moves the curve on the left, this being a safer condition; small I_u moves the curve on the right, this being a less safe condition.

It is worth notice that for the same *Sc* (abscissa), when turbulence intensity is small, amplitudes are larger, being in an unsafe region of the diagram; on the other hand, when turbulence intensity is large, amplitudes are smaller, being in a safe region of the diagram. Moreover, small values of I_u are usually associated with small values of critical velocity, this may be really critical in terms of fatigue damage because critical large vibrations are associated with frequent occurrence.

The maximum crosswind response, or the peak deflection value, is given by the standard deviation of the deflection multiplied by the peak deflection factor:

$$\bar{y}_{max}=g_s\sigma_s \tag{5.11}$$

where g_s (Fig.5.9) follows a different trend in vortex excited random regime (Eq. (5.12)), lock-in deterministic regime (Eq. (5.13)) and transition regime (Eq. (5.14)):

$$g_s=\sqrt{2ln(n_L T)}+\frac{0.5772}{\sqrt{2ln(n_L T)}} \tag{5.12}$$

$$g_s=\sqrt{2} \tag{5.13}$$

$$g_s=\sqrt{2}\left\{1+1.2\text{arctg}\left[\frac{0.75\cdot Sc^4}{(4\pi K_a)^4}\right]\right\} \tag{5.14}$$

where T is the time interval during which expected maximum value occurs.

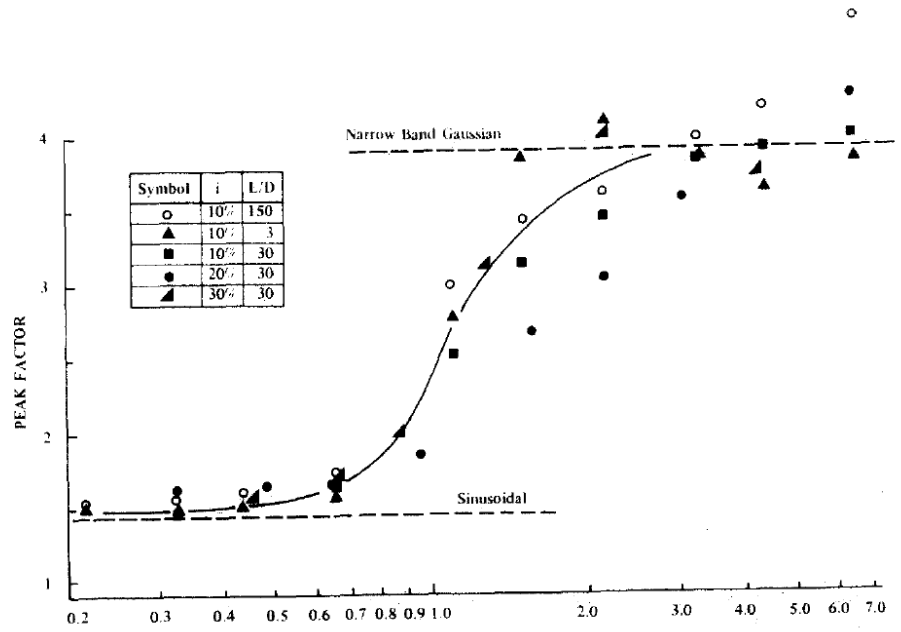

Fig. 5.9: Diagram of the peak deflection factor on varying structural and aerodynamic damping parameters ratio (© Vickery and Basu, 1983); lower bound is $g_s=\sqrt{2}$ (lock-in regime); upper bound is $g_s=4$ (forced regime).

5.2.4. Code design procedure: response and fatigue calculation

The different opinions on how to represent the phenomenon mathematically are reflected in the variety of procedures used in practical designs to determine structural response. The present Eurocode 1 on wind

actions includes both the spectral model and the vortex-resonance model for predicting vortex-induced vibrations of structures (Eurocode 1, 2005; CNR, 2018). These two models have complementary strengths and weaknesses, and none may be considered fully shared and approved. The present Section 5.2.4 focuses only on the spectral method included in this document to estimate vortex-induced response and furthermore on the fatigue calculation proposed in the same international code. The whole Chapter 5 takes into account only the spectral model to predict vortex-shedding effect, this is due to the fact that it is recommended for slender cantilevered structures with regular variation of the cross-section along the structural axis and with oscillations resonant with the first vibration mode in "forced vibration" regime; moreover, this model is commonly considered more sound and more prudential.

The effect of vortex-induced vibrations may be calculated through application of an equivalent static force per unit length, acting perpendicular to the mean wind direction and to the axis of the structure or structural element. This is given by:

$$F_{L,eq}(z) = m(z)\left(2\pi n_L\right)^2 \Phi_L(z)\,\bar{y}_{max} C_R \tag{5.15}$$

where $m(z)$ is the mass per unit length of the structure with z as the coordinate along the structure axis; n_L is the crosswind natural frequency of the structure; Φ_L is the crosswind structural mode shape, normalized such as to be 1 at the position z of maximum displacement; $\bar{y}_{max}$ is the peak deflection of the structure, evaluated at the position z of maximum displacement; C_R is a dimensionless parameter associated with the critical values of the mean wind velocity for long return periods R.

Expressing the mass in kg/m, the frequency in Hz and the peak deflection value in m, the force $F_{L,eq}$ is obtained in N/m (being the mode shape of the structure dimensionless).

Coefficient C_R is a dimensionless parameter introduced only in the CNR document (2008, 2018) for two purposes: to consider critical phenomena at mean wind velocities with a return period larger than the design return period used for standard safety assessments; to reduce the calculated response for high values of the mean wind velocity, for which the flow tends to become significantly turbulent and therefore to attenuate vortex shedding. It varies from 0 to 1 depending on the ratio between the critical vortex shedding mean wind velocity, in the most unfavourable position, and the mean wind velocity, evaluated at the height at which the critical velocity occurs, in correspondence with different design return periods. When the critical mean wind velocity is equal or lower than the mean wind velocity in correspondence with the reference return period, C_R is equal to 1. When the critical mean wind velocity is equal or higher than the mean wind velocity in correspondence with a design return period equal to 10 times the reference one, C_R is equal to 0. This dimensionless parameter is considered as varying linearly between these two conditions.

The peak deflection of the structure, $\bar{y}_{max}$, can be evaluated according to the spectral model described previously. Codes give simple formula and assumption to calculate it. Equation (5.11) is applied, whose input parameters are given by:

$$g_s = \sqrt{2}\left\{1+\left[\operatorname{arctg}\left(0.7\left(\frac{Sc}{4\pi K_a}\right)^{2.5}\right)\right]^{1.4}\right\} \tag{5.16}$$

$$\frac{\sigma_s}{b} = \sqrt{c_1 + \sqrt{c_1^2 + c_2}} \tag{5.17}$$

$$c_1 = \frac{a_L^2}{2}\left(1 - \frac{Sc}{4\pi K_a}\right) \tag{5.18}$$

$$c_2 = \frac{a_L^2}{K_a}\frac{\rho b^3}{m_e h}\frac{C_c^2}{St^4} \tag{5.19}$$

where g_s is the peak deflection factor; Sc is the Scruton number; K_a is the aerodynamic damping parameter; σ_s is the standard deviation of the crosswind deflection; b is the characteristic size; $a_L = 1/\kappa$ is the normalized (dimensionless) limiting amplitude, i.e. the maximum deflection divided by the corresponding reference size b, for Sc going to zero; ρ is the air density, usually assumed as 1.25 kg/m^3; m_e is the equivalent mass per unit length; h is the height of the structure; C_c is a dimensionless parameter, function of the shape of the cross-section and possibly of the Reynolds number; St is the Strouhal number.

It may be noticed that Equation (5.16) (CNR, 2008, 2018) is slightly different from Equation (5.14), which is the one previously introduced referring to spectral model and included in classic literature and Eurocode 1 (incorporating corrigendum January 2010) (Fig 5.10). Equation supplied by CNR is based on advanced numerical simulations (Vickery and Basu, 1983a; Chen, 2014a; Pagnini and Piccardo, 2017), considering only the prototypes with slenderness values h/b=30, that are typical of real chimneys, and ignoring the other measures obtained for slenderness values of no practical interest (h/b=3 and h/b=150). Estimates supplied by Equation (5.16) (CNR, 2008, 2018) match very well with numerical results for h/b=30, while Equation (5.14) provides a curve which lies above almost all values, highlighting that its derivation was actually influenced by values of slenderness of minor interest for technical applications. In conclusion, Equation (5.16) (CNR, 2008, 2018) seems more reliable.

It is noted that the peak deflection factor g_s assumes values tending to $\sqrt{2}$ in lock-in regime and it assumes values tending to 4 in forced regime.

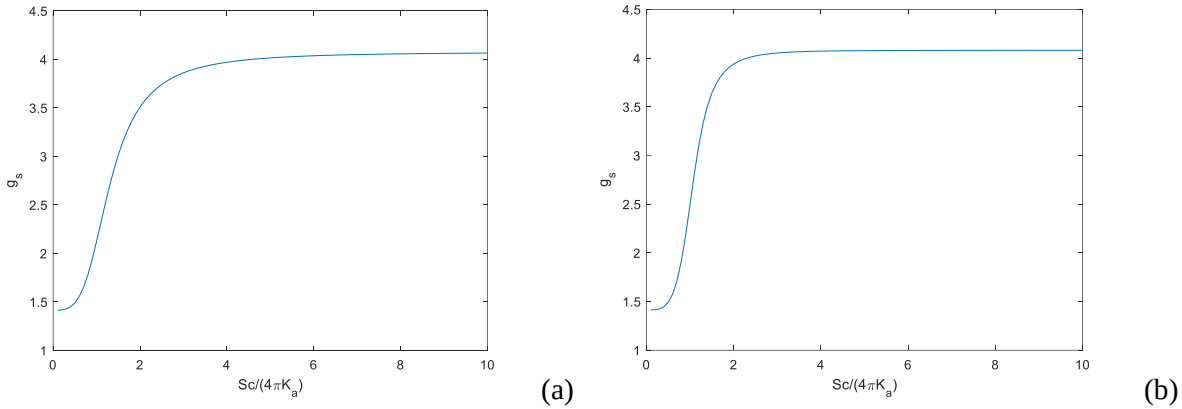

Fig. 5.10: Peak deflection factor according to CNR (a) and Eurocode 1 (b).

Standards provide input parameters in Equations (5.16)-(5.19) in really simplified manner.

The dimensionless aerodynamic damping parameter K_a is obtained multiplying $K_{a,max}$ and C_I. $K_{a,max}$ is the maximum value of the aerodynamic damping parameter, that is the value of K_a corresponding to the absence of atmospheric turbulence. $K_{a,max}$ is given by codes only for circular and square cross-sections; in the first case, four different ranges of Reynolds number *Re* are considered (CNR, 2018). C_I is the turbulence factor, less than or equal to 1, and it is given for three different ranges of critical velocity of vortex shedding.

As regards the normalised limiting amplitude, giving the deflection of structures with very low damping, it is suggested to take $a_L = 0.4$.

The dimensionless parameter C_c is provided only for circular and square cross-sections; in the first case, three different ranges of Reynolds number *Re* are considered. Although a recent study (Pagnini, Piccardo and Solari, 2020) provides a new formulation of C_c, valid also for different cross-section shapes, codes and standards are still scanty.

It is worth notice that, in addition to a very simplified formulation to predict the structural response, two most critical parameters, K_a and a_L, which strongly influence the equivalent damping (Eq. (5.8)) and consequently the structural response, are given in very simplified manner. Little variations of these two parameters, especially K_a, will give largely different values of crosswind response to vortex shedding (Fig. 5.11).

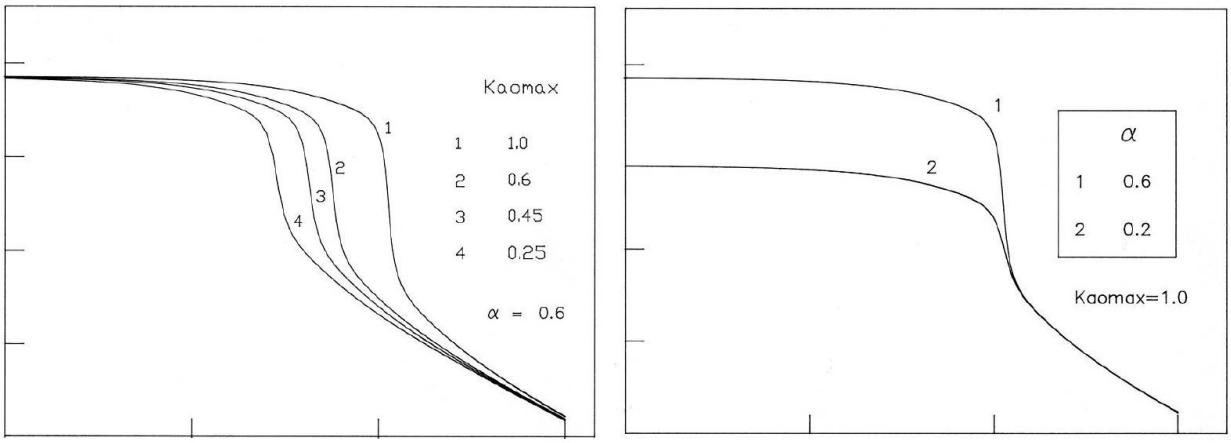

Fig. 5.11: Crosswind response on varying structural damping parameter (© Vickery and Basu, 1983); the first diagram shows the influence of K_a and the second diagram shows the influence of a_L.

Concerning fatigue calculation, the European codes give a simple formula to evaluate the number of load cycles N caused by vortex excited oscillation:

$$N = 2V_N n_L \varepsilon_0 \left(\frac{\bar{u}_{cr}}{\bar{u}_0}\right)^2 \exp\left[-\left(\frac{\bar{u}_{cr}}{\bar{u}_0}\right)^2\right] \tag{5.20}$$

where V_N is the life-time in seconds, namely the nominal life-time of the structure or structural element; n_L is the natural frequency of crosswind mode; ε_0 is the bandwidth factor describing the band of wind velocities with vortex-induced vibrations, which is in the range 0.1 – 0.3 (0.3 is the value recommended by the code); $\bar{u}_{cr}$ is the critical wind velocity of vortex shedding (see Eq. (5.2)); $\bar{u}_0$ is a reference value of the wind velocity, indicatively equal to 0.2 times the mean wind velocity with a design return period R = 50 years, calculated in the cross-section where the critical vortex shedding phenomenon occurs. A recommended minimum value of N is given by the code, $N \geq 10^4$.

This expression derives from the correlation length method by Ruscheweyh (1988). By adopting this approach, it is considered as all the load cycles are counted in correspondence of the critical mean wind velocity (Fig. 5.12), taking into account a Weibull probability density function of mean wind velocity implicit in Equation (5.20). N is equal to the number of times in which $\bar{u} = \bar{u}_{cr}$ during the nominal life-time of the structure. To this number of cycles is associated the maximum stress cycle amplitude $\Delta_{s,max} = 2\,\bar{y}_{s,max}$ in the considered critical cross-section. It is worth notice this is maybe a reasonable assumption when the stress response is a sinusoidal deterministic process, in lock-in regimes, while it is not reliable when the stress response is a narrow-band random process, in forced regimes, because the cycle amplitudes follow a Rayleigh distribution (Rice, 1944).

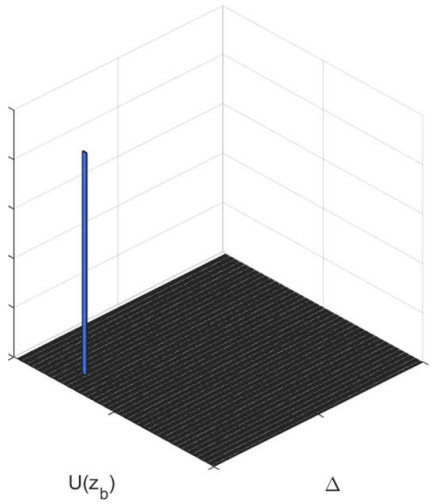

Fig. 5.12: Qualitative representation of the number of load cycles associated with vortex shedding, corresponding to $\bar{u}_{cr}$ and $\Delta_{s,max}$.

According to the linear Miner rule (1945), fatigue damage is equal to the ratio of N to N_C, that is the number of cycles leading to collapse associated to $\Delta_{s,max}$, estimated from a suitable S-N curve.

Further considerations concerning Equation (5.20) are included in Section 5.4. The parent population distribution model of the mean wind velocity implicit in the formula is discussed; a new formula is proposed, which considers local climatology at the site where the analysed structure is located and which considers a more appropriate factor ε_0 describing the wind velocities range with vortex-induced vibrations; an extensive comparison between the two approaches is carried out.

5.3. CROSSWIND TURBULENCE AND VIV-INDUCED FATIGUE

Numerical simulation is applied on different case studies to obtain the structural crosswind responses according to a generalized gust factor technique proposed by Pagnini and Piccardo (2017) based on the classic Vickery and Basu (1983) spectral approach. This model provide a reliable and unified procedure for dealing with gust-excited vibrations and aeroelastic phenomena on slender structures, allowing to evaluate the wind–induced response of structures sensitive to vortex-induced vibrations. The effectiveness of the procedure has been verified over an extensive experimental measurements. The model is fully suitable to reproduce the effective structural aeroelastic behavior, also in the synchronization region at lock-in (Pagnini and Piccardo, 2017).

Then suitable counting methods are applied to produce cycles histograms. The approach is that the bi-modal counting method is used over a range of velocity which produces gust-excited vibrations, where VIV is negligible (Section 2.3.2; Repetto and Solari, 2006). On the other hand, the range of velocity

which produces vortex-induced vibrations is characterized by response processes of the type Gaussian narrow-banded, then amplitude and peak distributions coincide and follow the Rayleigh model. In this second case, the expected number of cycles per unit time, whose amplitude lies between Δ and Δ+dΔ, is given by (Repetto and Solari, 2001, 2002):

$$n_{NB,ij} = P_i \nu_{si} \left\{ \exp\left[-\frac{(j-1)^2 \delta s^2}{2(\sigma_{si})^2} \right] - \exp\left[-\frac{j^2 \delta s^2}{2(\sigma_{si})^2} \right] \right\} \tag{5.21}$$

where $n_{NB,ij}$ is the number of cycles of the narrow-band process associated with the *i*-th wind velocity interval $\Delta\bar{u}_i$ and with the *j*-th stress cycles amplitude Δ_j; s_i is the stress fluctuation associated with the *i*-th loading condition, which is a nil mean Gaussian stationary random process, whose standard deviation is σ_{si} and expected frequency is ν_{si}; P_i is the occurrence probability of the *i*-th loading condition, which is provided by Equation (2.32) adopting a Weibull distribution corrected by the hybrid technique (Section 2.3.2).

Finally, for all the case studies, damage histograms are obtained according to Miner approach (1945). For each *i*-th wind velocity interval and *j*-th stress cycles amplitude, the fractional damage d_{ij} is calculated by the ratio of n_{ij} to the number of cycles leading to collapse associated to Δ_j according to the suitable *S-N* curve.

Thank to these numerical analyses, for every case study is estimated a reliable fatigue life value in years which is considered as a benchmark for the subsequent considerations.

1) The first step is to repeat the simulations neglecting the number of cycles associated with gust-excited vibrations, considering just the cycles associated with VIV. The fatigue life is estimated and compared with the actual one. Also the opposite study, neglecting the number of cycles associated with VIV, is carried out.
2) After this numerical analysis, the same examples have been analytically discussed. The crosswind turbulence-induced fatigue method proposed in the present thesis is applied. Then, separately, the engineering verification of VIV-induced fatigue (Eurocode 1, 2005; CNR 2008, 2018) is conducted. The spectral approach is recommended to calculate the response for vibrations in the first mode of cantilevered structures with a regular distribution of cross wind dimensions along the main axis of the structure and typically structures covered are chimneys or masts, that are the analysed cases. This approach allows for the consideration of different turbulence intensities, which may differ due to meteorological conditions.

By comparing the results, it is possible to confirm that, since fatigue occurs for moderate values of mean wind velocity, i.e. when vortex shedding resonant response is relevant, in most of the examples the damage accumulation diagram results completely dominated by this only contribution.

In the cases when VIV is at least not negligible, neglecting the crosswind turbulence contribution produces no error. For the other cases, the vortex shedding effect is totally negligible both in response and fatigue analyses, therefore fatigue damage is due only to crosswind buffeting.

These considerations mean that applying two separated fatigue procedures at engineering level seems to be reliable.

5.3.1. Case study: Chimney 1

The structure examined in this Section is a tapered steel chimney, 100 m tall. The structural steel is Fe510 so the yielding limit stress of the structural material is f_y = 355 Mpa. The tapered portion at the base is 34 m high; the external diameters at the base and at z = 34 m are respectively 7,00 m and 3,80 m. The constant-section portion is 66 m tall and has an external diameter of 3,80 m. The structure is entirely welded and has no internal or external lining/cladding. Figure 5.13 gives the vertical profiles of mass per unit height, m, and the moment of inertia of the cross section J_f. Table 5.1 gives the shell thicknesses t at the various sections, between heights z_i and z_s.

This case study is referred to the steel chimney examined in CNR document (2008, 2018) as one of the example applications.

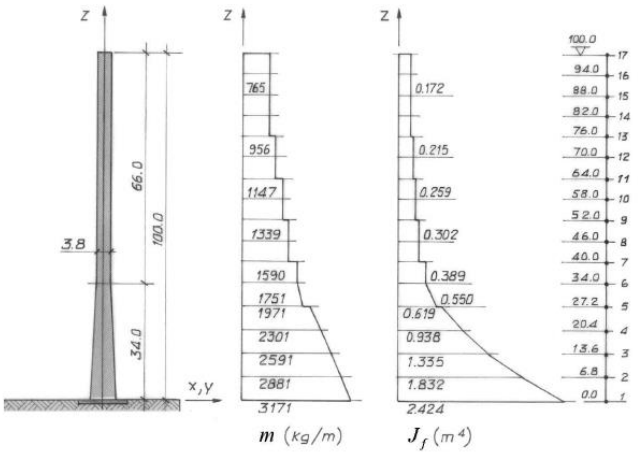

Fig. 5.13: Steel chimney (Figure © CNR, 2008, 2018).

Section	z_i(m)	z_s(m)	t(mm)
1	0.0	27.2	18
2	27.2	40.0	16
3	40.0	52.0	14
4	52.0	64.0	12
5	64.0	76.0	10
6	76.0	100.0	8

Tab. 5.1: Shell thicknesses of the steel chimney (CNR, 2008, 2018).

The construction is located in central Italy at sea level. Applying the rules given in Italian code, this corresponds to Zone 3 (see Section 4.3.2, Fig. 4.6, Tab. 4.3). The roughness class is C, the exposure category is III, so k_r = 0.20, z_0 = 0.10 m, z_{min} = 5 m; furthermore, admitting that terrain is flat, c_t = 1. Thus, in correspondence with a mean return period of 50 years, $\bar{u}_{ref}$ = 27 m/s (with ΔT = 10 min).

The dynamic response of the structure is determined for 44 loading conditions, assuming wind velocity intervals of 1 m/s. The occurrence probability of each loading condition is given by Equation (2.32) using the parameters F_0 = 0, k = 1.2, c = 3.24 m/s (Fig. 5.14).

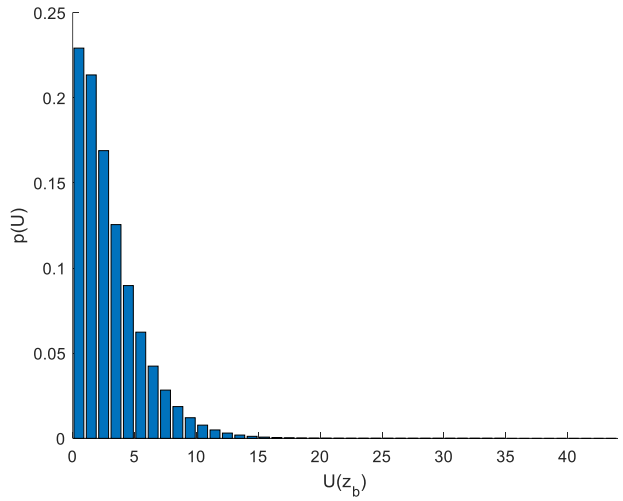

Fig. 5.14: Occurrence probability of the loading conditions.

According to the code, some input parameters are defined. The drag coefficient is c_D = 0.54; the lift wake coefficient is c_{Ls} = 0.1; the reference cross size is b = 3.8 m. Given the polar symmetry, the vibration mode occur in pairs. The natural frequency of the structure is n_D = n_L = 0.77 Hz; the parameter

that defines the shape of the mode is $\zeta_D = \zeta_L = 2$; the equivalent mass per unit length is m_e = 821 kg/m; the structural damping is $\xi_{sD} = \xi_{sL} = 0.002$. Moreover, the Strouhal number is St = 0.22.

The normalised limiting amplitude is assumed equal to a_L = 0.2; the aerodynamic damping parameter K_a varies on wind velocity, depending on turbulence intensity I_u and the Reynolds number Re according to Pagnini and Piccardo (2017) model.

The numerical simulation estimates some other critical parameters. The critical velocity is $\bar{u}_{cr}$ = 15.5 m/s; the Scruton number is Sc = 1.14 ; the peak deflection factor is g_s = 1.42.

The critical section which is subjected to fatigue verification is at the base of the chimney (z = 0).

The numerical simulation provides the crosswind structural response, in terms of displacements at the top of the structure or bending moment at the base, which can be translated into crosswind stress in the critical cross-section (Fig. 5.15).

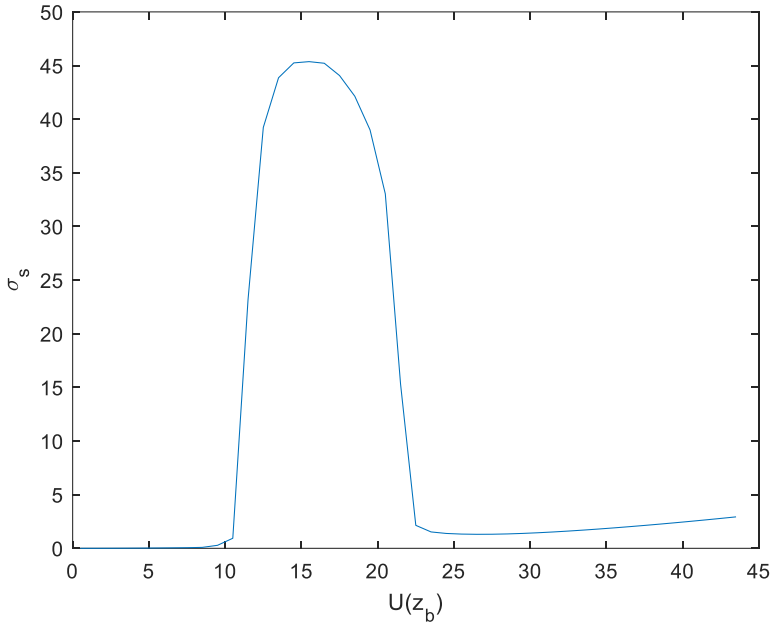

Fig. 5.15: Crosswind response in terms of normal stress at the base of the structure.

The standard deviation of the maximum displacement at the top of the structure is $\sigma_{d,max}$ = 0.654 m, the peak deflection value is $\bar{y}_{d,max}$ = 0.930 m. The standard deviation of the normal stress at the base of the structure, in correspondence of $\bar{u}_{cr}$, is $\sigma_{s,max}$ = 45.36 N/mm^2 and the maximum stress is $\bar{y}_{s,max}$ = 64.51 N/mm^2, then the maximum stress cycles amplitude correspondent with $\bar{u}_{cr}$ is $\Delta_{s,max} = 2\,\bar{y}_{s,max}$ = 129.02 N/mm^2.

By applying the suitable counting methods described at the beginning of Section 5.3, the cycle histogram can be obtained (Fig. 5.16). This diagram shows numerous blocks at low wind velocity due to vortex shedding and few blocks at high wind velocity due to lateral turbulence.

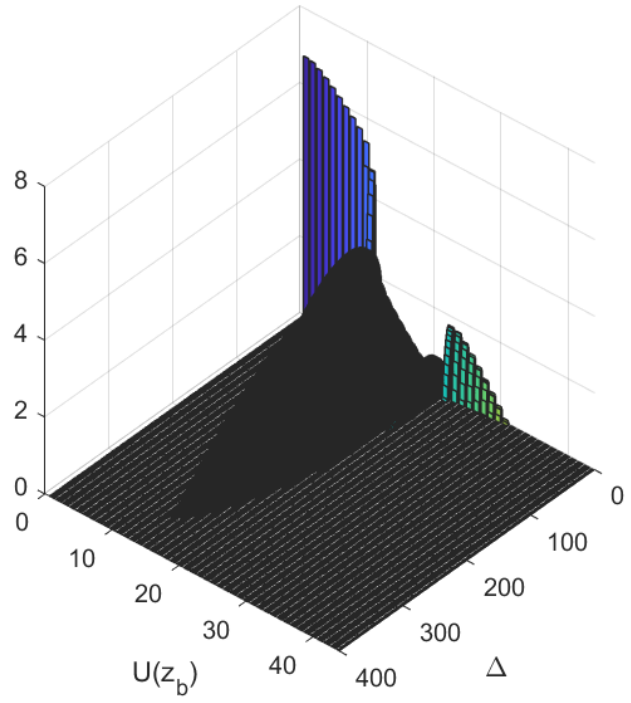

Fig. 5.16: Histogram of the stress cycles .

Fatigue damage is analysed in the critical structural section according to the Eurocode 3 (2005). The cross-section is classified as Category 71 and the number of cycles that causes the failure at different values of amplitude Δ_{sj} is provided by the concerning *S-N* fatigue curve. The damage histogram is obtained calculating the fractional damages d_{ij} (Fig. 5.17). The damage is concentrated in the intermediate range of the wind velocity, where great amplitude cycles due to vortex shedding arise. The fatigue phenomenon is dominated by the vortex shedding.

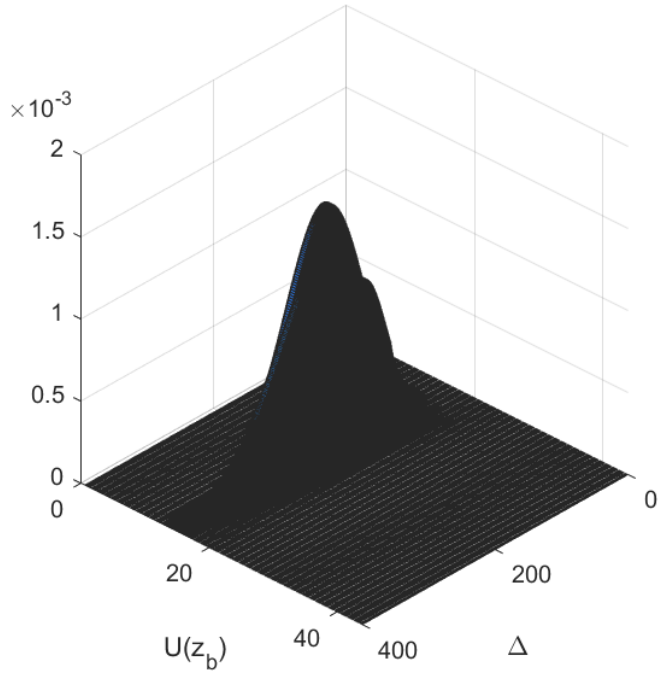

Fig. 5.17: Histogram of the fractions of damage.

These two histograms (Figures 5.16 and 5.17) refer to 1 year life-time of the structure. Then, making the sum of all fractional damages the annual total damage is calculated D = 0. 6849 and then the predicted fatigue life T_F = 1.46 years.

The standard deviation of the fluctuating stress in the critical section on varying the reference mean velocity is shown in Fig. 5.15. It can be observed that the diagram is due to two different contributions: the one due to the lateral turbulence and the one due to the vortex shedding. The latter is definitely dominant with respect to the former. In fact, the crosswind response is characterised by a lock-in phenomenon in correspondence of a wide range of wind velocity, around the critical one. This is confirmed by the low value of the Scruton number Sc = 1.14 and by the peak deflection factor is g_s = 1.42, which tends to $\sqrt{2}$. Due to such phenomenon, vortex shedding effects in the low wind velocity range are larger than lateral turbulence effects at high wind velocity values. In addition to a large crosswind structural response, there is also a high probability of occurrence of wind velocities that causes such response. For this reason, fatigue life is critically low. The value of T_F = 1.46 years is considered as an actual and reliable prediction.

The procedure is repeated neglecting the number of cycles associated with gust-excited vibrations, considering just the cycles associated with VIV. The estimated fatigue life is again T_F = 1.46 years. No error is committed.

The procedure is repeated neglecting the number of cycles associated with VIV, considering just the cycles associated with gust-excited vibrations. The estimated fatigue life is T_F tends to ∞ because gust-excited vibrations do not produce detectable fatigue damage.

In this case it is possible to analyse separately lateral turbulence-induced fatigue and vortex shedding-induced fatigue, since only the second of these two contributions influences the fatigue life prediction.

At engineering level, two separated methods can be applied in crosswind fatigue: the crosswind turbulence-induced fatigue method proposed in the present thesis and, separately, the standard verification of VIV-induced fatigue (Eurocode 1, 2005; CNR 2008, 2018). Results of these two analytical methods are presented and discussed below.

- Following code provisions, the mean wind profile and the mean wind velocity pressure can be obtained in function of *z*; the aerodynamic coefficients and the reference size are defined, so the mean alongwind aerodynamic force per unit height is calculated. By applying this force along the structural axis in alongwind direction, the mean maximum bending moment at the base of the chimney can be estimated, being equal to 7881 kNm. It is calculated the mean value of the alongwind stress process $\bar{s}_{D,ref}$ = 11.464 N/mm^2. The permanent loadings-induced stress in the examined section is calculated as $\bar{s}_P$ = 3.727 N/mm^2.

The longitudinal turbulence intensity I_u and the longitudinal turbulence length scale L_u at the site are obtained in function of *z*. It is defined the reference height above ground, Z_{eq} = 60 m, at which $I_u(Z_{eq})$ = 0.1563 and $L_u(Z_{eq})$ = 154.72.

Therefore, the standard deviation of the alongwind nominal stress in the section of the considered structural detail, $\sigma_{D,ref}$, is evaluated by means of Equation (4.13), in which γ_F = 1.35, the quasi-static response factor B_D^2 = 0.5883 and the resonant response factor R_D^2 = 0.3042. $\sigma_{D,ref}$ = 4.571 N/mm^2 is obtained. The expected frequency value of the alongwind stress process in the critical section, evaluated at reference wind velocity $\bar{u}_{ref}$, is $\nu_{D,ref}$ = 0.450 Hz, calculated by Equation (4.14). The expected frequency of the quasi-static part of the alongwind stress process in the critical section, evaluated at reference wind velocity $\bar{u}_{ref}$, is $\nu_{D,Q,ref}$ = 0.118 Hz, calculated by Equation (4.15) assuming τ = 1 s. The normalized variance of the resonant part of the alongwind stress process in the critical section, evaluated at reference wind velocity $\bar{u}_{ref}$, is $\lambda_{D,R,ref}$ = 0.341, calculated by Equation (4.16). The exponent of the power law $\alpha_{\sigma,D}$ = 2.205 is given by Equation (4.18) where R_{Dfat}^2 = 0.084. The exponent of the power law $\alpha_{\lambda,D}$ = 1.456 is given by Equation (4.20).

On the other hand, the mean value of the crosswind stress process $\bar{s}_{L,ref}$ = 0 N/mm^2, according to Equation (4.21), in which μ_L = 0/0.54 = 0. The standard deviation of the crosswind nominal stress in the

section of the considered structural detail, $\sigma_{L,ref}$, is evaluated by means of Equation (4.23), in which γ_F = 1.35, the quasi-static response factor B_L^2 = 0.0859 and the resonant response factor R_L^2 = 1.3422. $\sigma_{L,ref}$ = 5.782 N/mm^2 is obtained. The expected frequency value of the crosswind stress process in the critical section, evaluated at reference wind velocity $\bar{u}_{ref}$, is $\nu_{L,ref}$ = 0.747 Hz, calculated by Equation (4.24). The expected frequency of the quasi-static part of the crosswind stress process in the critical section, evaluated at reference wind velocity $\bar{u}_{ref}$, is $\nu_{L,Q,ref}$ = 0.158 Hz, calculated by Equation (4.28) assuming τ = 1 s. The normalized variance of the resonant part of the crosswind stress process in the critical section, evaluated at reference wind velocity $\bar{u}_{ref}$, is $\lambda_{L,R,ref}$ = 0.940, calculated by Equation (4.29). The exponent of the power law $\alpha_{\sigma,L}$ = 2.663 is given by Equation (4.31) where R_{Lfat}^2 = 0.483. The exponent of the power law $\alpha_{\lambda,L}$ = 0.147 is given by Equation (4.33).

Dealing with alongwind and crosswind detailed calculation, Equations (3.4), (3.5), (3.57)-(3.60) (see Tab. 3.2 in Sections 3.3 and 4.2) are applied obtaining values in Tab. 5.2. As concerns alongwind fatigue (first column of Tab. 5.2), the analytical procedure leads to a mean total damage in the unit time equal to $\bar{D}(1)$ = $5 \cdot 10^{-7}$ (Eq. (3.5)), therefore the fatigue life of the structure is predicted as $2 \cdot 10^6$ years (Eq. (3.4)). On the other hand, dealing with crosswind fatigue analysis, values in the second column of Tab. 5.2 are obtained, leading to a mean total damage in the unit time equal to $\bar{D}(1)$ = $5 \cdot 10^{-6}$ (Eq. (3.5)), therefore the fatigue life of the structure is predicted as $2 \cdot 10^5$ years (Eq. (3.4)).

	Alongwind buffeting-induced fatigue analysis	Crosswind buffeting-induced fatigue analysis
$\bar{D}_0(1)$	$1 \cdot 10^{-5}$	$2 \cdot 10^{-5}$
C_{BM}	0.3622	1.000
C_M	1.0450	1.0222
C_{SN}	0.1012	0.1978
$\bar{D}(1)$	$5 \cdot 10^{-7}$	$5 \cdot 10^{-6}$
T_F	$2 \cdot 10^6$ years	$2 \cdot 10^5$ years

Tab. 5.2: Calculation of the fatigue life induced by alongwind and crosswind turbulence.

In both analyses, the 0 level solutions $\bar{D}_0(1)$ results comparable, with a slightly larger value in crosswind direction, due to larger standard deviation of crosswind response. The bi-modal factor C_{BM}

reduces the 0 level damage taking into account the quasi-static part of the response spectrum; in alongwind assessment the quasi-static part of the response has a high role, strongly reducing the total damage; on the contrary, in crosswind assessment the role of quasi-static part of the response is nul, prevailing the resonant contribution, $\lambda_{L,R,ref}$ = 0.940. In this case, the simplified formula to estimate the input parameters and the simplifying assumptions at the basis of the method cause a bi-modal factor slightly higher than the unit. By assuming τ = 1 s in the expected frequency of the quasi-static part of the crosswind stress process calculation, C_{BM} = 1.0684, while by assuming τ = 3 s C_{BM} = 0.9525. Consistently with the choice in alongwind fatigue analysis, it is taken τ = 1 s, however considering C_{BM} = 1 as an upper limit of this corrective factor; thus it does not influence the total damage. The mean stress corrective factor C_M slightly increases the total damage in both analysis, meaning that the mean response to wind loading is not all that important. Finally, the fatigue curve factor C_{SN} strongly reduces the damage in both cases, taking into account the cut-off limit of fatigue resistance in steel details. The very low values of C_{SN} mean that almost all cycles are considered under this limit so they do not influence fatigue damage. All these considerations highlight that in both alongwind and crosswind analyses, turbulence-induced fatigue is completely negligible. In general, the chimney under consideration does not suffer fatigue phenomenon due to atmospheric turbulence.

- In addition, the standard calculation of VIV-induced fatigue (Eurocode 1, 2005; CNR 2008, 2018) is applied, independently from the previous turbulence verification.

Following code provisions, the equivalent static force per unit length $F_{L,eq}(z)$, given by Eq. (5.15), is applied perpendicular to the mean wind direction and to the axis of the structure or structural element. The equivalent static action is associated with vortex shedding in resonance with the structure. It is therefore necessary to firstly determine the critical velocity, that is the mean wind velocity that cause resonance, and the relative Scruton number.

The critical wind velocity $\bar{u}_{cr}$ is given by Equation (5.2), where n_L = 0.77 Hz is the natural frequency in crosswind direction; b = 3.8 m is the characteristic size, namely the diameter at the tip of the chimney where the mode shape is maximum; St is the Strouhal number. The Strouhal number is a function of the Reynolds number and therefore of the critical wind velocity; in principle, the solution of Equation (5.2) thus requires an iterative calculation. It is possible to proceed as follows: 1) initially set St = 0.2, followed by $\bar{u}_{cr}$ = 14.63 m/s; 2) determine the Reynolds number through $Re(z) = \left[b \cdot \bar{u}(z)\right] / \upsilon$, where υ is the kinematic viscosity of the air taken equal to 15 10^{-6} m^2/s, therefore Re = 3.7 10^6; 3) calculate the Strouhal number St using Figure 5.2, St = 0.22; 4) the final value of the critical velocity $\bar{u}_{cr}$ = 13.3 m/s corresponds to Re = 3.37 10^6 (considering the level of convergence achieved, further iterations are not necessary).

Thus, the Strouhal number is St = 0.22 and $\bar{u}_{cr}$ = 13.3 m/s. According to provisions, the verification related to the critical wind velocity is required provided that $\bar{u}_{cr}$ is lower than the mean wind velocity at the tip of the structure, with return period R = 500 years (13.3 m/s < 45.02 m/s).

The Scruton number is given by the Equation (5.3), where m_e = 821 kg/m is the equivalent mass per unit length and the damping factor is ξ_L = 0.002, non-including aerodynamic damping; then Sc = 1.14, a very critical low value.

Now, calculation of the static equivalent crosswind force per unit length $F_{L,eq}(z)$ caused by critical vortex shedding is carried out by using Eq. (5.15). The mass per unit length of the structure $m(z)$ and the crosswind normalized structural mode shape $\Phi_L(z)=(z/h)^{\zeta}$, h = 100 m and ζ_L = 2, are calculated in function of the coordinate along the structure axis z; the crosswind natural frequency of the structure is n_L = 0.77 Hz; the dimensionless parameter C_R, which depends on the critical velocity $\bar{u}_{cr}$ = 13.3 m/s, on the tip mean wind velocity $\bar{u}(R=50\,years)$ = 37.3 m/s and on the tip mean wind velocity $\bar{u}(R=500\,years)$ = 45.02 m/s, is estimated equal to 1 according to CNR provisions; then, it is required the calculation of the peak tip deflection $\bar{y}_{max}$, which is performed by using the spectral method.

The peak deflection value is given by Equation (5.11), multiplying the standard deviation of the deflection σ_s, here called $\sigma_{d,max}$ in order to indicate the kind of response (d = displacement) and the correspondence to the critical velocity which produce a peak response (max), by the peak deflection factor g_s.

The parameter g_s (Eq. (5.16)) depends on the Scruton number Sc = 1.14 and on the aerodynamic damping parameter $K_a = K_{a,max}\, C_I$. Since Re = 3.37 10^6, $K_{a,max}$ = 1; moreover, since $\bar{u}_{cr}$ = 13.3 m/s, z_{cr} = 100 m and $I_u(z_{cr})$ = 0.1448, the turbulence factor C_I = 0.64; then K_a = 0.64. Therefore, by using Equation (5.16), g_s = 1.415 (CNR, 2018).

The parameter $\sigma_{d,max}$ is given by Equations (5.17)-(5.19) for a_L = 0.4, Sc = 1.14, K_a = 0.64, thus c_1 = 0.06866 (Eq. (5.18)); ρ = 1.25 kg/m^3, b = 3.8 m, h = 100 m, m_e = 821 kg/m, K_a = 0.64, C_c = 0.01, St = 0.22, then c_2 = 8.916 10^{-6} (Eq. (5.19)). Therefore, $\sigma_{d,max}/b$ = 0.371 (Eq. (5.17)), so $\sigma_{d,max}$ = 1.408 m.

Lastly, by applying the Equation (5.11), $\bar{y}_{max}$ = 1.415 · 1.408 = 1.993 m is obtained, a quite large value.

Therefore, the standard deviation of the maximum displacement at the top of the structure is $\sigma_{d,max}$ = 1.408 m, the peak deflection value $\bar{y}_{d,max}$ = 1.993 m. The large difference between these values and the ones obtained by the numerical simulation is mainly due to differences in input parameters, especially a_L.

The limiting amplitude is crucial in the response prediction, both in the transition and in the lock-in regime. It is Reynolds dependent and it is probably related to structural scale factors, although it does not

seem to depend on the aspect ratio as tentatively discussed by Basu (1983). Despite this, it is usually assumed according to purely tentative values. Regarding circular cylinders, all the literature seems crystallized on the limiting value of 0.4*b*, although Basu (1983) indicates different possibilities in his pioneering work. Estimates inferred from wind-tunnel measures for various cross-sections (e.g., Hansen, 2007, 2013) are extremely interesting but not yet useful in predictive assessments, because they are hardly generalizable (Pagnini and Piccardo, 2017).

The static equivalent crosswind force $F_{L,eq}(z)$ (Eq. (5.15)) associated with resonant vortex shedding can be applied to the structure, expressing z in m, m in kg/m obtaining the force in N/m. The mean maximum bending moment obtained at the base of the chimney is estimated equal to 1.04 10^5 kNm. Then, it is calculated the mean maximum normal stress at the base of the structure, $\bar{y}_{s,max}$ = 151.23 N/mm^2, which is multiplied by the safety factor for fatigue analysis γ_F = 1.35, so $\bar{y}_{s,max}$ = 204.2 N/mm^2. The maximum stress cycles amplitude correspondent with $\bar{u}_{cr}$ is $\Delta_{s,max} = 2\ \bar{y}_{s,max}$ = 408.4 N/mm^2.

Fatigue analysis can be carried out. The number of load cycles which lead to collapse are given by $N_C = a_1 / \Delta_{s,max}^{m_1}$ considering the first straight line of the *S-N* curve. The detail category is 71, m_1 = 3, $a_1 = 2 \cdot 10^6 \cdot 71^3 = 715822000000$. It is estimated N_C = 10507.4. Calculation of the number of load cycles caused by resonant vortex shedding during the nominal lifetime of the structure, 50 years, is performed by applying Equation (5.20), where V_N = 1576800000 s is the life-time; n_L = 0.77 Hz is the natural frequency of crosswind mode; ε_0 = 0.3 is the bandwidth factor describing the band of wind velocities with vortex-induced vibrations; $\bar{u}_{cr}$ = 13.3 m/s is the critical wind velocity of vortex shedding; $\bar{u}_0 = 0.2 \cdot 37.3$ = 7.46 m/s is a reference value of the wind velocity. It is estimated $N = 9.65 \cdot 10^7$, so it is verified $N \geq 10^4$.

The total damage in 50 years is given by the ratio $D = N/N_C = 9.18 \cdot 10^3$, which corresponds to a fatigue life $T_F = 50/D = 5.45 \cdot 10^{-3}$ years.

The prediction of the fatigue life according to VIV-induced fatigue procedure proposed by code (Eurocode 1, 2005; CNR 2008, 2018) gives a very low value, much less than 1 year. The value of T_F = 1.46 years is considered as the reliable prediction, so this method is hugely on the safe side. Table 5.3 presents a comparison between results of simulation and CNR procedure. The latter is considered in three different possibilities: with all input parameters given according to the code, with a_L value equal to the one used in the simulation, with the response from the simulation.

Response calculation method	Numerical model a_L = 0.2	Standard method (Eurocode/CNR) a_L = 0.4	Standard method (Eurocode/CNR) a_L = 0.2	Numerical model a_L = 0.2
$\sigma_{d,max}$	0.654 m	1.408 m	0.705 m	0.654 m
$\Delta_{s,max}$	129.02 N/mm^2	408.4 N/mm^2	204.4 N/mm^2	129.02 N/mm^2
Fatigue prediction approach	Histograms calculation	Standard method (Eurocode/CNR)	Standard method (Eurocode/CNR)	Standard method (Eurocode/CNR)
T_F	1.46 years	$5.45 \cdot 10^{-3}$ years	$4.35 \cdot 10^{-2}$ years	0.17 years

Tab. 5.3: Outcomes comparison.

It is possible to notice from Tab. 5.3 that input parameters uncertainties have an important role in response estimation. Moreover, errors exponentially propagate in fatigue analysis. Starting from the same response estimation, fatigue standard method is simplified in a manner that provides values further on the safe side. It considers all the load cycles in correspondence of the critical mean wind velocity (Fig. 5.12), taking into account a Weibull probability density function of mean wind velocity implicit in Equation (5.20) and taking into account a sinusoidal deterministic stress process with cycle amplitude equal to $\Delta_{s,max} = 2\ \bar{y}_{s,max}$ during the whole time in which $\bar{u} = \bar{u}_{cr}$.

In conclusion, VIV-induced fatigue standard procedure tends to hugely underestimate the fatigue life value.

5.3.2. Case study: Chimney 2a

The structure examined in this Section is a steel chimney, 100 m tall, tapered again in its first 34 m above the ground. Its main characteristics are shown in Fig. 5.18, where R is the radius and t is the thickness of the shell. The chimney is composed by two trunks connected at z = 34 m; in order to decrease its tendency to lock-in, an inner layer of 5 cm of gunite is realised, which furnishes an added mass and increases the structural damping. The structural steel is Fe510 so the yielding limit stress of the structural material is f_y = 355 Mpa. The external diameters at the base and at z = 34 m are respectively 7.00 m and 5.00 m. The thickness is, respectively in the three portions in Fig. 5.18, 18 mm, 15 mm and 12 mm. The mass per unit height, m, and the moment of inertia of the cross section J_f are calculated.

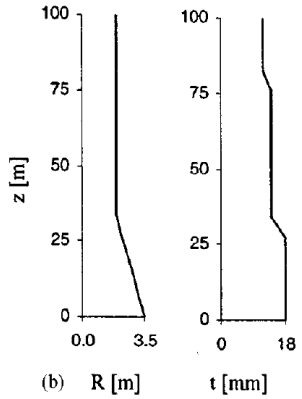

Fig. 5.18: Radius and thickness.

The construction is placed in Italy, Liguria, at sea level. The roughness class is C, the exposure category is III, so k_r = 0.20, z_0 = 0.10 m, z_{min} = 5 m; furthermore, admitting that terrain is flat, c_t = 1.

Climatological analyses provide, in correspondence with a mean return period of 50 years, $\bar{u}_{ref}$ = 29 m/s (with ΔT = 10 min). The dynamic response of the structure is determined for 31 loading conditions, assuming wind velocity intervals of 1 m/s. The occurrence probability of each loading condition is given by Equation (2.32) using the parameters F_0 = 0.1943, k = 1.549, c = 4.629 m/s (Fig. 5.19).

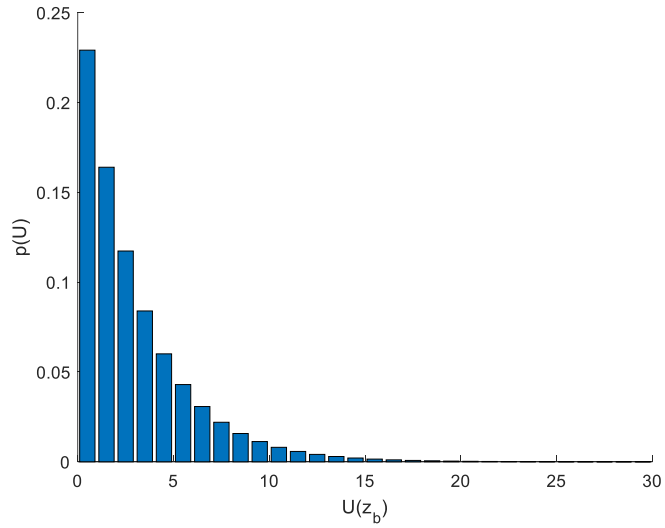

Fig. 5.19: Occurrence probability of the loading conditions.

Input parameters are defined. The drag coefficient is c_D = 0.7; the lift wake coefficient is c_{Ls} = 0.3; the reference cross size is b = 5 m. Given the polar symmetry, the vibration mode occur in pairs. The natural frequency of the structure is $n_D = n_L$ = 0.486 Hz; the parameter that defines the shape of the mode is ζ_D =

ζ_L = 2; the equivalent mass per unit length is m_e = 1600 kg/m; the structural damping is $\xi_{sD} = \xi_{sL}$ = 0.01. Moreover, the Strouhal number is St = 0.2.

The normalised limiting amplitude is assumed equal to a_L = 0.2; the aerodynamic damping parameter K_a varies on wind velocity, depending on turbulence intensity I_u and the Reynolds number Re according to Pagnini and Piccardo (2017) model.

The numerical simulation estimates some other critical parameters. The critical velocity is $\bar{u}_{cr}$ = 13.5 m/s; the Scruton number is Sc = 6.43 ; the peak deflection factor is g_s = 2.966.

The critical section which is subjected to fatigue verification is at height z = 34 m.

Structural characteristics	
Height	100 m
Fundamental frequency	0.486 Hz
Modal shape factor	2
Structural damping	0.01
Scruton number	6.43
Critical wind velocity	13.5 m/s
Equivalent mass	1600 kg/m
Height of critical section	34 m

Tab. 5.4: Structural characteristics of the steel chimney.

Table 5.4 summarizes the main dynamical properties of the structure.

The numerical simulation provides the crosswind structural response, in terms of displacements at the top of the structure or bending moment at z = 34 m, which can be translated into crosswind stress in the critical cross-section (Fig. 5.20).

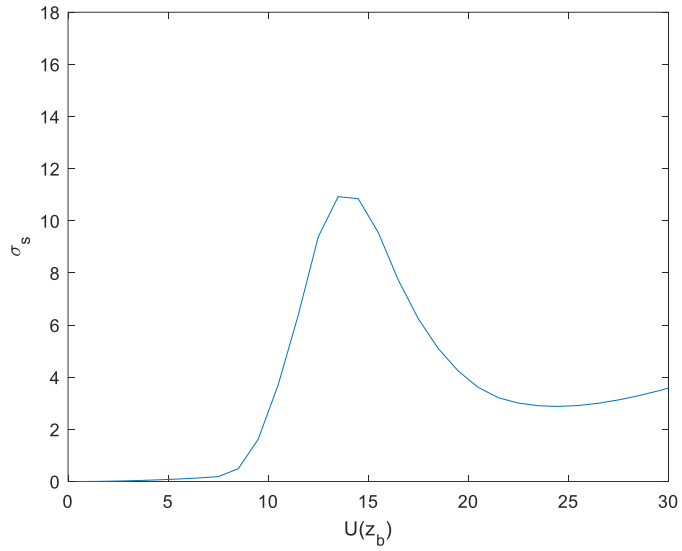

Fig. 5.20: Crosswind response in terms of normal stress at the height z = 34 m of the structure.

The standard deviation of the maximum displacement at the top of the structure is $\sigma_{d,max}$ = 0.155 m, the peak deflection value $\bar{y}_{d,max}$ = 0.460 m. The standard deviation of the normal stress at the height z = 34 m of the structure, in correspondence of $\bar{u}_{cr}$, is $\sigma_{s,max}$ = 10.93 N/mm^2 and the maximum stress is $\bar{y}_{s,max}$ = 32.4 N/mm^2, then the maximum stress cycles amplitude correspondent with $\bar{u}_{cr}$ is $\Delta_{s,max} = 2\,\bar{y}_{s,max}$ = 64.8 N/mm^2.

By applying the suitable counting methods described at the beginning of Section 5.3, the cycle histogram can be obtained (Fig. 5.21). This diagram shows numerous blocks at intermediate wind velocity due to vortex shedding and also many blocks at high wind velocity due to lateral turbulence. Vortex shedding effects on the response are evident in proximity of critical wind velocity, while lateral turbulence effects dominate at high wind velocity values.

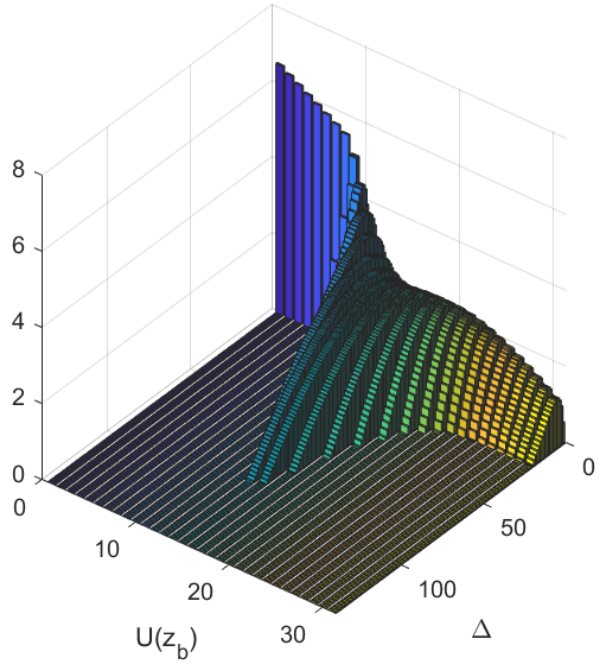

Fig. 5.21: Histogram of the stress cycles .

Fatigue damage is analysed in the critical structural section according to the Eurocode 3 (2005). The cross-section is classified as Category 50 and the number of cycles that causes the failure at different values of amplitude Δ_{sj} is provided by the concerning *S*-*N* fatigue curve. The damage histogram is obtained calculating the fractional damages d_{ij} (Fig. 5.22). The damage is concentrated in the intermediate range of the wind velocity, where great amplitude cycles due to vortex shedding arise. The fatigue phenomenon is dominated by the vortex shedding.

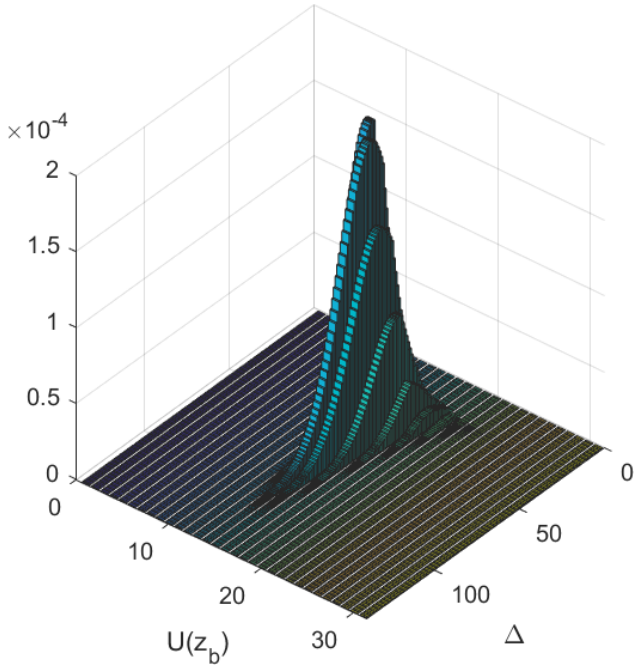

Fig. 5.22: Histogram of the fractions of damage.

These two histograms (Figures 5.21 and 5.22) refer to 1 year life-time of the structure. Then, making the sum of all fractional damages the annual total damage is calculated D = 0.0204 and then the predicted fatigue life T_F = 48.9 years.

The standard deviation of the fluctuating stress in the critical section on varying the reference mean velocity is shown in Fig. 5.20. It can be observed that the diagram is due to two different contributions: the one due to the lateral turbulence and the one due to the vortex shedding. The latter is dominant with respect to the former, although the lateral turbulence seems to be not negligible at high wind velocity values. The diagram shows a transition regime, in fact in correspondence of the critical wind velocity there is a quite wide range of wind velocity characterized by resonant crosswind response. This is confirmed by the quite low value of the Scruton number Sc = 6.43 and by the peak deflection factor is g_s = 2.966, which is in between of $\sqrt{2}$ and 4. Due to such phenomenon, vortex shedding effects in the low wind velocity range are larger than lateral turbulence effects at high wind velocity values. In addition to VIV crosswind structural response, there is also a high probability of occurrence of wind velocities that causes such response. For this reason, fatigue phenomenon is probably mainly due to vortex shedding effects. The value of T_F = 48.9 years is considered as an actual and reliable prediction.

The procedure is repeated neglecting the number of cycles associated with gust-excited vibrations, considering just the cycles associated with VIV. The estimated fatigue life is again T_F = 49.5 years. Negligible error is committed.

The procedure is repeated neglecting the number of cycles associated with VIV, considering just the cycles associated with gust-excited vibrations. The estimated fatigue life is T_F = 4242 years because gust-excited vibrations do not produce significant fatigue damage.

In this case it is possible to analyse separately lateral turbulence-induced fatigue and vortex shedding-induced fatigue, since only the second of these two contributions influences the fatigue life prediction. The committed error is considered as negligible.

At engineering level, two separated methods can be applied in crosswind fatigue: the crosswind turbulence-induced fatigue method proposed in the present thesis and, separately, the standard verification of VIV-induced fatigue (Eurocode 1, 2005; CNR 2008, 2018). Results of these two analytical methods are presented and discussed below.

- Applying the Eurocode 1, climatological parameters depend on the Italian zone 7 in which the chimney is located (see Section 4.3.2, Fig. 4.6, Tab. 4.3). Therefore, the reference mean wind velocity, in correspondence with a mean return period of 50 years, is $\bar{u}_{ref}$ = 28 m/s (with ΔT = 10 min). The parent population of the mean wind velocity is modelled by a Weibull distribution (Equation (2.32)) using the parameters F_0 = 0, k = 1.35, c = 4.20 m/s.

Following code provisions, the mean wind profile and the mean wind velocity pressure can be obtained in function of z; the aerodynamic coefficients and the reference size are defined, so the mean alongwind aerodynamic force per unit height is calculated. By applying this force along the structural axis in alongwind direction, the mean maximum bending moment at the height of the chimney z = 34 m can be estimated, being equal to 13189 kNm. It is calculated the mean value of the alongwind stress process $\bar{s}_{D,ref}$ = 45.186 N/mm^2. The permanent loadings-induced stress in the examined section is calculated as $\bar{s}_P$ = 4.972 N/mm^2.

The longitudinal turbulence intensity I_u and the longitudinal turbulence length scale L_u at the site are obtained in function of z. It is defined the reference height above ground, Z_{eq} = 60 m, at which $I_u(Z_{eq})$ = 0.1563 and $L_u(Z_{eq})$ = 154.72.

Therefore, the standard deviation of the alongwind nominal stress in the section of the considered structural detail, $\sigma_{D,ref}$, is evaluated by means of Equation (4.13), in which γ_F = 1.35, the quasi-static response factor B_D^2 = 0.5865 and the resonant response factor R_D^2 = 0.4402. $\sigma_{D,ref}$ = 19.327 N/mm^2 is obtained. The expected frequency value of the alongwind stress process in the critical section, evaluated at reference wind velocity $\bar{u}_{ref}$, is $\nu_{D,ref}$ = 0.318 Hz, calculated by Equation (4.14). The expected frequency

of the quasi-static part of the alongwind stress process in the critical section, evaluated at reference wind velocity $\bar{u}_{ref}$, is $\nu_{D,Q,ref}$ = 0.119 Hz, calculated by Equation (4.15) assuming τ = 1 s. The normalized variance of the resonant part of the alongwind stress process in the critical section, evaluated at reference wind velocity $\bar{u}_{ref}$, is $\lambda_{D,R,ref}$ = 0.429, calculated by Equation (4.16). The exponent of the power law $\alpha_{\sigma,D}$ = 2.260 is given by Equation (4.18) where R^2_{Dfat} = 0.129. The exponent of the power law $\alpha_{\lambda,D}$ = 1.249 is given by Equation (4.20).

On the other hand, the mean value of the crosswind stress process $\bar{s}_{L,ref}$ = 0 N/mm^2, according to Equation (4.21), in which μ_L = 0/0.7 = 0. The standard deviation of the crosswind nominal stress in the section of the considered structural detail, $\sigma_{L,ref}$, is evaluated by means of Equation (4.23), in which γ_F = 1.35, the quasi-static response factor B^2_L = 0.0859 and the resonant response factor R^2_L = 0.5157. $\sigma_{L,ref}$ = 14.794 N/mm^2 is obtained. The expected frequency value of the crosswind stress process in the critical section, evaluated at reference wind velocity $\bar{u}_{ref}$, is $\nu_{L,ref}$ = 0.450 Hz, calculated by Equation (4.24). The expected frequency of the quasi-static part of the crosswind stress process in the critical section, evaluated at reference wind velocity $\bar{u}_{ref}$, is $\nu_{L,Q,ref}$ = 0.160 Hz, calculated by Equation (4.28) assuming τ = 1 s. The normalized variance of the resonant part of the crosswind stress process in the critical section, evaluated at reference wind velocity $\bar{u}_{ref}$, is $\lambda_{L,R,ref}$ = 0.857, calculated by Equation (4.29). The exponent of the power law $\alpha_{\sigma,L}$ = 2.529 is given by Equation (4.31) where R^2_{Lfat} = 0.2030. The exponent of the power law $\alpha_{\lambda,L}$ = 0.287 is given by Equation (4.33).

Dealing with alongwind and crosswind detailed calculation, Equations (3.4), (3.5), (3.57)-(3.60) (see Tab. 3.2 in Sections 3.3 and 4.2) are applied obtaining values in Tab. 5.5. As concerns alongwind fatigue (first column of Tab. 5.5), the analytical procedure leads to a mean total damage in the unit time equal to $\bar{D}(1) = 8 \cdot 10^{-4}$ (Eq. (3.5)), therefore the fatigue life of the structure is predicted as 1282 years (Eq. (3.4)). On the other hand, dealing with crosswind fatigue analysis, values in the second column of Tab. 5.5 are obtained, leading to a mean total damage in the unit time equal to $\bar{D}(1) = 5 \cdot 10^{-4}$ (Eq. (3.5)), therefore the fatigue life of the structure is predicted as 2078 years (Eq. (3.4)).

	Alongwind buffeting-induced fatigue analysis	Crosswind buffeting-induced fatigue analysis
$\bar{D}_0(1)$	0.0028	0.0011
C_{BM}	0.5216	1.000
C_M	1.1187	1.0298
C_{SN}	0.4813	0.4269
$\bar{D}(1)$	$8 \cdot 10^{-4}$	$5 \cdot 10^{-4}$
T_F	1282 years	2078 years

Tab. 5.5: Calculation of the fatigue life induced by alongwind and crosswind turbulence.

The alongwind 0 level solution $\bar{D}_0(1)$ results twice as large as the value in crosswind direction, due to larger standard deviation of alongwind response. The bi-modal factor C_{BM} reduces the 0 level damage taking into account the quasi-static part of the response spectrum; in alongwind assessment the quasi-static part of the response has a high role, strongly reducing the total damage; on the contrary, in crosswind assessment the role of quasi-static part of the response is small, prevailing the resonant contribution, $\lambda_{L,R,ref} = 0.857$. In this case, the simplified formula to estimate the input parameters and the simplifying assumptions at the basis of the method cause a bi-modal factor slightly higher than the unit. By assuming $\tau = 1$ s in the expected frequency of the quasi-static part of the crosswind stress process calculation, $C_{BM} = 1.0477$, while by assuming $\tau = 3$ s $C_{BM} = 0.8534$. Consistently with the choice in alongwind fatigue analysis, it is taken $\tau = 1$ s, however considering $C_{BM} = 1$ as an upper limit of this corrective factor; thus it does not influence the total damage. The mean stress corrective factor C_M slightly increases the total damage in both analysis, meaning that the mean response to wind loading is not all that important. Finally, the fatigue curve factor C_{SN} strongly reduces the damage in both cases, taking into account the cut-off limit of fatigue resistance in steel details. All these considerations highlight that in both alongwind and crosswind analyses, turbulence-induced fatigue can be neglected. In general, the chimney under consideration does not suffer fatigue phenomenon due to atmospheric turbulence.

It is worth notice that the proposed analytical verification results on the safe side with respect to the numerical procedure which considers only gust-excited vibrations effects ($T_F = 4242$ years).

- In addition, the standard calculation of VIV-induced fatigue (Eurocode 1, 2005; CNR 2008, 2018) is applied, independently from the previous turbulence verification.

Following code provisions, the equivalent static force per unit length $F_{L,eq}(z)$, given by Eq. (5.15), is applied perpendicular to the mean wind direction and to the axis of the structure or structural element. The equivalent static action is associated with vortex shedding in resonance with the structure. It is therefore necessary to firstly determine the critical velocity, that is the mean wind velocity that cause resonance, and the relative Scruton number.

The critical wind velocity $\bar{u}_{cr}$ is given by Equation (5.2), where n_L = 0.486 Hz is the natural frequency in crosswind direction; b = 5 m is the characteristic size, namely the diameter at the tip of the chimney where the mode shape is maximum; *St* is the Strouhal number. The Strouhal number is a function of the Reynolds number and therefore of the critical wind velocity; in principle, the solution of Equation (5.2) thus requires an iterative calculation. It is possible to proceed as done for Chimney 1 (Section 5.3.1). The Strouhal number is *St* = 0.22 and $\bar{u}_{cr}$ = 11.05 m/s. According to provisions, the verification related to the critical wind velocity is required provided that $\bar{u}_{cr}$ is lower than the mean wind velocity at the tip of the structure, with return period R = 500 years (11.05 m/s < 46.70 m/s).

The Scruton number is given by the Equation (5.3), where m_e = 1640 kg/m is the equivalent mass per unit length and the damping factor is ξ_L = 0.01, non-including aerodynamic damping; then *Sc* = 6.59, a quite low value.

So far, the parameters values estimated analytically are very similar to the ones in the numerical simulation. Now, calculation of the static equivalent crosswind force per unit length $F_{L,eq}(z)$ caused by critical vortex shedding is carried out by using Eq. (5.15). The mass per unit length of the structure $m(z)$ and the crosswind normalized structural mode shape $\Phi_L(z) = (z/h)^{\zeta}$, h = 100 m and ζ_L = 2, are calculated in function of the coordinate along the structure axis *z*; the crosswind natural frequency of the structure is n_L = 0.486 Hz; the dimensionless parameter C_R, which depends on the critical velocity $\bar{u}_{cr}$ = 11.05 m/s, on the tip mean wind velocity $\bar{u}(R = 50 years)$ = 38.68 m/s and on the tip mean wind velocity $\bar{u}(R = 500 years)$ = 46.70 m/s, is estimated equal to 1 according to CNR provisions; then, it is required the calculation of the peak tip deflection $\bar{y}_{max}$, which is performed by using the spectral method.

The peak deflection value is given by Equation (5.11), multiplying the standard deviation of the deflection σ_s, here called $\sigma_{d,max}$, by the peak deflection factor g_s.

The parameter g_s (Eq. (5.16)) depends on the Scruton number *Sc* = 6.59 and on the aerodynamic damping parameter $K_a = K_{a,max} C_I$. Since *Re* = 3.68 10^6, $K_{a,max}$ = 1; moreover, since $\bar{u}_{cr}$ = 11.05 m/s, z_{cr} =

100 m and $I_u(z_{cr})$ = 0.1448, the turbulence factor C_I = 0.56; then K_a = 0.56. Therefore, by using Equation (5.16), g_s = 1.999 (CNR, 2018).

The parameter $\sigma_{d,max}$ is given by Equations (5.17)-(5.19) for a_L = 0.4, Sc = 6.59, K_a = 0.56, thus c_1 = 0.00535 (Eq. (5.18)); ρ = 1.25 kg/m^3, b = 5 m, h = 100 m, m_e = 1640 kg/m, K_a = 0.56, C_c = 0.01, St = 0.22, then c_2 = 1.1575 10^{-5} (Eq. (5.19)). Therefore, $\sigma_{d,max}/b$ = 0.108 (Eq. (5.17)), so $\sigma_{d,max}$ = 0.541 m.

Lastly, by applying the Equation (5.11), $\bar{y}_{max}$ = 1.999 · 0.541 = 1.081 m is obtained, a quite large value.

Therefore, the standard deviation of the maximum displacement at the top of the structure is $\sigma_{d,max}$ = 0.541 m, the peak deflection value $\bar{y}_{d,max}$ = 1.081 m. The large difference between these values and the ones obtained by the numerical simulation is mainly due to differences in input parameters, especially a_L, as well as in Chimney 1 (Section 5.3.1; Pagnini and Piccardo, 2017).

The static equivalent crosswind force $F_{L,eq}(z)$ (Eq. (5.15)) associated with resonant vortex shedding can be applied to the structure, expressing z in m, m in kg/m obtaining the force in N/m. The mean maximum bending moment obtained at the height of the chimney z = 34 m is estimated equal to 4.086 · 10^4 kNm. Then, it is calculated the mean maximum normal stress at this cross-section of the structure (z = 34 m), $\bar{y}_{s,max}$ = 139.98 N/mm^2, which is multiplied by the safety factor for fatigue analysis γ_F = 1.35, so $\bar{y}_{s,max}$ = 188.97 N/mm^2. The maximum stress cycles amplitude correspondent with $\bar{u}_{cr}$ is $\Delta_{s,max}$ = 2 $\bar{y}_{s,max}$ = 377.95 N/mm^2.

Fatigue analysis can be carried out. The number of load cycles which lead to collapse are given by $N_C = a_1/\Delta_{s,max}^{m_1}$ considering the first straight line of the *S-N* curve. The detail category is 50, m_1 = 3, $a_1 = 2 \cdot 10^6 \cdot 50^3 = 250000000000$. It is estimated N_C = 4630.7. Calculation of the number of load cycles caused by resonant vortex shedding during the nominal lifetime of the structure, 50 years, is performed by applying Equation (5.20), where V_N = 1576800000 s is the life-time; n_L = 0.486 Hz is the natural frequency of crosswind mode; ε_0 = 0.3 is the bandwidth factor describing the band of wind velocities with vortex-induced vibrations; $\bar{u}_{cr}$ = 11.05 m/s is the critical wind velocity of vortex shedding; $\bar{u}_0$ = 0.2 · 38.68 = 7.74 m/s is a reference value of the wind velocity. It is estimated N = 1.221 · 10^8, so it is verified $N \geq 10^4$.

The total damage in 50 years is given by the ratio $D = N/N_C$ = 2.64 · 10^4, which corresponds to a fatigue life $T_F = 50/D$ = 2 · 10^{-3} years.

The prediction of the fatigue life according to VIV-induced fatigue procedure proposed by code (Eurocode 1, 2005; CNR 2008, 2018) gives a very low value, much less than 1 year. The value of T_F = 48.9 years is considered as the reliable prediction, so this method is hugely on the safe side. Table 5.6 presents a comparison between results of simulation and CNR procedure. The latter is considered in three

different possibilities: with all input parameters given according to the code, with a_L value equal to the one used in the simulation, with the response from the simulation.

Response calculation method	Numerical model $a_L = 0.2$	Standard method (Eurocode/CNR) $a_L = 0.4$	Standard method (Eurocode/CNR) $a_L = 0.2$	Numerical model $a_L = 0.2$
$\sigma_{d,max}$	0.155 m	0.541 m	0.296 m	0.155 m
$\Delta_{s,max}$	64.8 N/mm^2	377.95 N/mm^2	206.8 N/mm^2	64.8 N/mm^2
Fatigue prediction approach	Histograms calculation	Standard method (Eurocode/CNR)	Standard method (Eurocode/CNR)	Standard method (Eurocode/CNR)
T_F	48.9 years	$2 \cdot 10^{-3}$ years	$1 \cdot 10^{-2}$ years	0.38 years

Tab. 5.6: Outcomes comparison.

It is possible to notice from Tab. 5.6 that input parameters uncertainties have an important role in response estimation. Moreover, errors exponentially propagate in fatigue analysis. Starting from the same response estimation, fatigue standard method is simplified in a manner that provides values further on the safe side. It considers all the load cycles in correspondence of the critical mean wind velocity (Fig. 5.12), taking into account a Weibull probability density function of mean wind velocity implicit in Equation (5.20) and taking into account a sinusoidal deterministic stress process with cycle amplitude equal to $\Delta_{s,max} = 2\ \bar{y}_{s,max}$ during the whole time in which $\bar{u} = \bar{u}_{cr}$.

In conclusion, VIV-induced fatigue standard procedure tends to hugely underestimate the fatigue life value.

5.3.3. Case study: Chimney 2b

This case study is called Chimney 2b because it differences from Chimney 2a only for the external diameter in the upper trunk. The structure is again a steel chimney, 100 m tall, tapered again in its first 34 m above the ground. Its main characteristics are shown in Fig. 5.18, where R is the radius and t is the thickness of the shell. The chimney is composed by two trunks connected at z = 34 m; in order to decrease its tendency to lock-in, an inner layer of 5 cm of gunite is realised, which furnishes an added mass and increases the structural damping. The structural steel is Fe510 so the yielding limit stress of the structural material is f_y = 355 Mpa. The external diameters at the base and at z = 34 m are respectively 7.00 m and 4.40 m. The thickness is, respectively in the three portions in Fig. 5.18, 18 mm, 15 mm and 12 mm. The mass per unit height, m, and the moment of inertia of the cross section J_f are calculated.

The construction is placed in Italy, Liguria, at sea level. The roughness class is C, the exposure category is III, so k_r = 0.20, z_0 = 0.10 m, z_{min} = 5 m; furthermore, admitting that terrain is flat, c_t = 1.

Climatological analyses provide, in correspondence with a mean return period of 50 years, $\bar{u}_{ref}$ = 29 m/s (with ΔT = 10 min). The dynamic response of the structure is determined for 46 loading conditions, assuming wind velocity intervals of 1 m/s. The occurrence probability of each loading condition is given by Equation (2.32) using the parameters F_0 = 0.1943, k = 1.549, c = 4.629 m/s (Fig. 5.23).

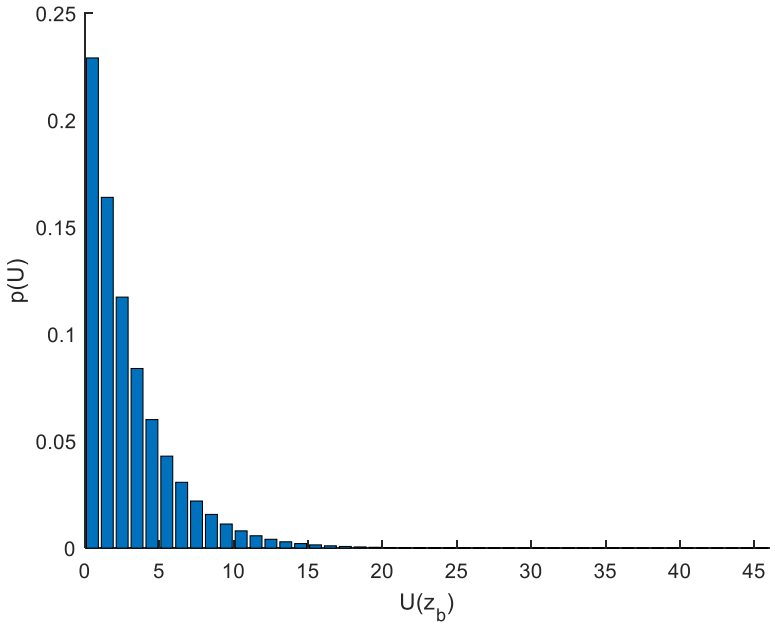

Fig. 5.23: Occurrence probability of the loading conditions.

Input parameters are defined. The drag coefficient is c_D = 0.7; the lift wake coefficient is c_{Ls} = 0.3; the reference cross size is b = 4.4 m. Given the polar symmetry, the vibration mode occur in pairs. The natural frequency of the structure is $n_D = n_L$ = 0.486 Hz; the parameter that defines the shape of the mode is $\zeta_D = \zeta_L$ = 2; the equivalent mass per unit length is m_e = 1440 kg/m; the structural damping is $\xi_{sD} = \xi_{sL}$ = 0.01. Moreover, the Strouhal number is St = 0.2.

The normalised limiting amplitude is assumed equal to a_L = 0.2; the aerodynamic damping parameter K_a varies on wind velocity, depending on turbulence intensity I_u and the Reynolds number Re according to Pagnini and Piccardo (2017) model.

The numerical simulation estimates some other critical parameters. The critical velocity is $\bar{u}_{cr}$ = 12.5 m/s; the Scruton number is Sc = 7.48; the peak deflection factor is g_s = 3.262.

The critical section which is subjected to fatigue verification is at height z = 34 m.

Structural characteristics	
Height	100 m
Fundamental frequency	0.486 Hz
Modal shape factor	2
Structural damping	0.01
Scruton number	7.48
Critical wind velocity	12.5 m/s
Equivalent mass	1440 kg/m
Height of critical section	34 m

Tab. 5.7: Structural characteristics of the steel chimney.

Table 5.7 summarizes the main dynamical properties of the structure.

The numerical simulation provides the crosswind structural response, in terms of displacements at the top of the structure or bending moment at z = 34 m, which can be translated into crosswind stress in the critical cross-section (Fig. 5.24).

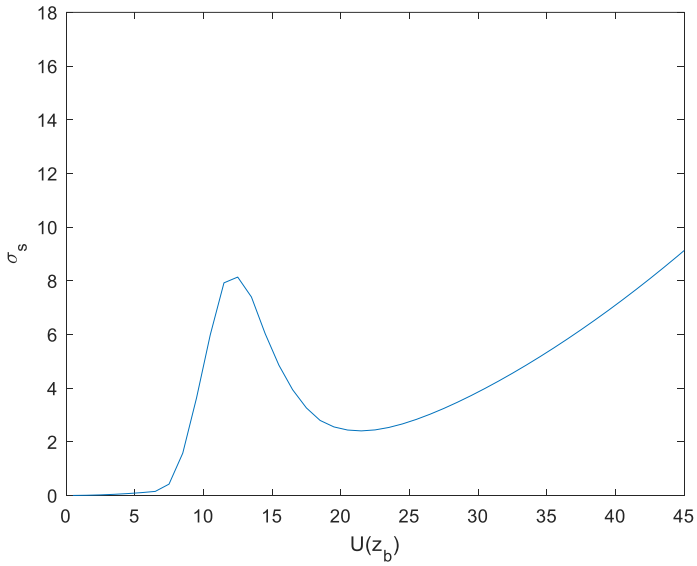

Fig. 5.24: Crosswind response in terms of normal stress at the height z = 34 m of the structure.

The standard deviation of the maximum displacement at the top of the structure is $\sigma_{d,max}$ = 0.099 m, the peak deflection value $\bar{y}_{d,max}$ = 0.324 m. The standard deviation of the normal stress at the height z = 34 m

of the structure in correspondence of $\bar{u}_{cr}$ is $\sigma_{s,max}$ = 8.14 N/mm^2 and the maximum stress is $\bar{y}_{s,max}$ = 26.54 N/mm^2, then the maximum stress cycles amplitude correspondent with $\bar{u}_{cr}$ is $\Delta_{s,max} = 2\,\bar{y}_{s,max}$ = 53.08 N/mm^2.

By applying the suitable counting methods described at the beginning of Section 5.3, the cycle histogram can be obtained (Fig. 5.25). This diagram shows numerous blocks at intermediate wind velocity due to vortex shedding and also many blocks at high wind velocity due to lateral turbulence. Vortex shedding effects on the response are evident in proximity of critical wind velocity, while lateral turbulence effects dominate at high wind velocity values.

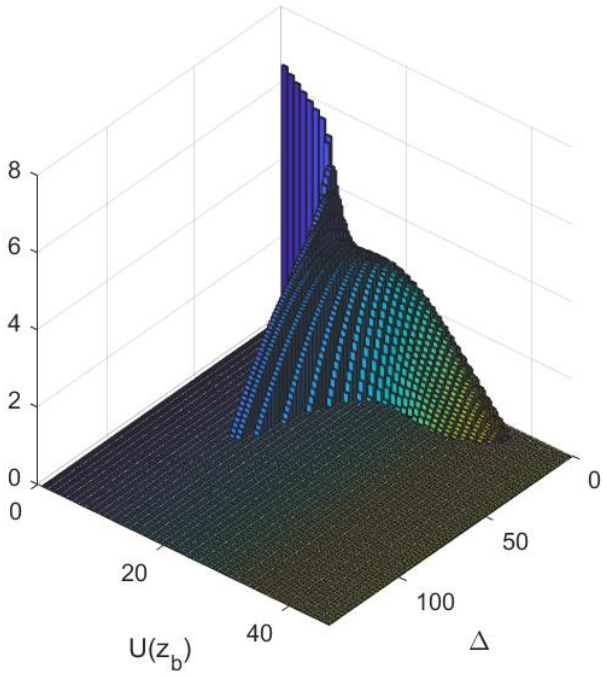

Fig. 5.25: Histogram of the stress cycles .

Fatigue damage is analysed in the critical structural section according to the Eurocode 3 (2005). The cross-section is classified as Category 50 and the number of cycles that causes the failure at different values of amplitude Δ_{sj} is provided by the concerning *S-N* fatigue curve. The damage histogram is obtained calculating the fractional damages d_{ij} (Fig. 5.26). The damage is concentrated in the intermediate range of the wind velocity, where large amplitude cycles due to vortex shedding arise. The fatigue phenomenon is dominated by the vortex shedding.

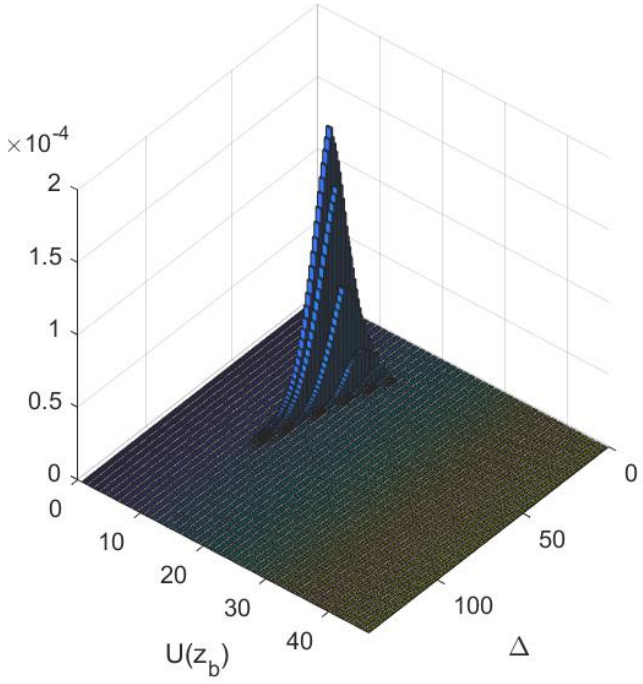

Fig. 5.26: Histogram of the fractions of damage.

These two histograms (Figures 5.25 and 5.26) refer to 1 year life-time of the structure. Then, making the sum of all fractional damages the annual total damage is calculated $D = 0.0102$ and then the predicted fatigue life $T_F = 98$ years.

The standard deviation of the fluctuating stress in the critical section on varying the reference mean velocity is shown in Fig. 5.24. It can be observed that the diagram is due to two different contributions: the one due to the lateral turbulence and the one due to the vortex shedding. In this case, the two contributions have an equivalent role in structural response, the latter is dominant at intermediate wind velocities, whereas the lateral turbulence is dominant at high wind velocity values. The diagram shows a transition regime, in fact in correspondence of the critical wind velocity there is a wide range of wind velocity characterized by resonant crosswind response. This is confirmed by the quite low value of the Scruton number $Sc = 7.48$ and by the peak deflection factor is $g_s = 3.262$, which is in between of $\sqrt{2}$ and 4. Vortex shedding effects in the low wind velocity range seem to be as large as lateral turbulence effects at high wind velocity values. As concerns fatigue, in addition to VIV crosswind structural response, there is a high probability of occurrence of wind velocities that causes such response. For this reason, fatigue phenomenon is probably mainly due to vortex shedding effects. The value of $T_F = 98$ years is considered as an actual and reliable prediction.

The procedure is repeated neglecting the number of cycles associated with gust-excited vibrations, considering just the cycles associated with VIV. The estimated fatigue life is again T_F = 99 years. Negligible error is committed.

The procedure is repeated neglecting the number of cycles associated with VIV, considering just the cycles associated with gust-excited vibrations. The estimated fatigue life is T_F = 9568 years because gust-excited vibrations do not produce significant fatigue damage.

In this case it is possible to analyse separately lateral turbulence-induced fatigue and vortex shedding-induced fatigue, since only the second of these two contributions influences the fatigue life prediction. The committed error is considered as negligible.

At engineering level, two separated methods can be applied in crosswind fatigue: the crosswind turbulence-induced fatigue method proposed in the present thesis and, separately, the standard verification of VIV-induced fatigue (Eurocode 1, 2005; CNR 2008, 2018). Results of these two analytical methods are presented and discussed below.

- Applying the Eurocode 1, climatological parameters depend on the Italian zone 7 in which the chimney is located (see Section 4.3.2, Fig. 4.6, Tab. 4.3). Therefore, the reference mean wind velocity, in correspondence with a mean return period of 50 years, is $\bar{u}_{ref}$ = 28 m/s (with ΔT = 10 min). The parent population of the mean wind velocity is modelled by a Weibull distribution (Equation (2.32)) using the parameters F_0 = 0, k = 1.35, c = 4.20 m/s.

Following code provisions, the mean wind profile and the mean wind velocity pressure can be obtained in function of z; the aerodynamic coefficients and the reference size are defined, so the mean alongwind aerodynamic force per unit height is calculated. By applying this force along the structural axis in alongwind direction, the mean maximum bending moment at the height of the chimney z = 34 m can be estimated, being equal to 11609 kNm. It is calculated the mean value of the alongwind stress process $\bar{s}_{D,ref}$ = 51.424 N/mm^2. The permanent loadings-induced stress in the examined section is calculated as $\bar{s}_P$ = 4.976 N/mm^2.

The longitudinal turbulence intensity I_u and the longitudinal turbulence length scale L_u at the site are obtained in function of z. It is defined the reference height above ground, Z_{eq} = 60 m, at which $I_u(Z_{eq})$ = 0.1563 and $L_u(Z_{eq})$ = 154.72.

Therefore, the standard deviation of the alongwind nominal stress in the section of the considered structural detail, $\sigma_{D,ref}$, is evaluated by means of Equation (4.13), in which γ_F = 1.35, the quasi-static response factor B_D^2 = 0.5874 and the resonant response factor R_D^2 = 0.4491. $\sigma_{D,ref}$ = 22.096 N/mm^2 is obtained. The expected frequency value of the alongwind stress process in the critical section, evaluated at reference wind velocity $\bar{u}_{ref}$, is $\nu_{D,ref}$ = 0.320 Hz, calculated by Equation (4.14). The expected frequency

of the quasi-static part of the alongwind stress process in the critical section, evaluated at reference wind velocity $\bar{u}_{ref}$, is $\nu_{D,Q,ref}$ = 0.119 Hz, calculated by Equation (4.15) assuming τ = 1 s. The normalized variance of the resonant part of the alongwind stress process in the critical section, evaluated at reference wind velocity $\bar{u}_{ref}$, is $\lambda_{D,R,ref}$ = 0.433, calculated by Equation (4.16). The exponent of the power law $\alpha_{\sigma,D}$ = 2.261 is given by Equation (4.18) where R^2_{Dfat} = 0.134. The exponent of the power law $\alpha_{\lambda,D}$ = 1.223 is given by Equation (4.20).

On the other hand, the mean value of the crosswind stress process $\bar{s}_{L,ref}$ = 0 N/mm^2, according to Equation (4.21), in which μ_L = 0/0.7 = 0. The standard deviation of the crosswind nominal stress in the section of the considered structural detail, $\sigma_{L,ref}$, is evaluated by means of Equation (4.23), in which γ_F = 1.35, the quasi-static response factor B^2_L = 0.0859 and the resonant response factor R^2_L = 0.5157. $\sigma_{L,ref}$ = 16.834 N/mm^2 is obtained. The expected frequency value of the crosswind stress process in the critical section, evaluated at reference wind velocity $\bar{u}_{ref}$, is $\nu_{L,ref}$ = 0.450 Hz, calculated by Equation (4.24). The expected frequency of the quasi-static part of the crosswind stress process in the critical section, evaluated at reference wind velocity $\bar{u}_{ref}$, is $\nu_{L,Q,ref}$ = 0.160 Hz, calculated by Equation (4.28) assuming τ = 1 s. The normalized variance of the resonant part of the crosswind stress process in the critical section, evaluated at reference wind velocity $\bar{u}_{ref}$, is $\lambda_{L,R,ref}$ = 0.857, calculated by Equation (4.29). The exponent of the power law $\alpha_{\sigma,L}$ = 2.529 is given by Equation (4.31) where R^2_{Lfat} = 0.2030. The exponent of the power law $\alpha_{\lambda,L}$ = 0.287 is given by Equation (4.33).

Dealing with alongwind and crosswind detailed calculation, Equations (3.4), (3.5), (3.57)-(3.60) (see Tab. 3.2 in Sections 3.3 and 4.2) are applied obtaining values in Tab. 5.8. As concerns alongwind fatigue (first column of Tab. 5.8), the analytical procedure leads to a mean total damage in the unit time equal to $\bar{D}(1)$ = 0.0013 (Eq. (3.5)), therefore the fatigue life of the structure is predicted as 753 years (Eq. (3.4)). On the other hand, dealing with crosswind fatigue analysis, values in the second column of Tab. 5.8 are obtained, leading to a mean total damage in the unit time equal to $\bar{D}(1) = 8 \cdot 10^{-4}$ (Eq. (3.5)), therefore the fatigue life of the structure is predicted as 1275 years (Eq. (3.4)).

	Alongwind buffeting-induced fatigue analysis	Crosswind buffeting-induced fatigue analysis
$\bar{D}_0(1)$	0.0042	0.0016
C_{BM}	0.5247	1.000
C_M	1.1311	1.0299
C_{SN}	0.5372	0.4722
$\bar{D}(1)$	0.0013	$8 \cdot 10^{-4}$
T_F	753 years	1275 years

Tab. 5.8: Calculation of the fatigue life induced by alongwind and crosswind turbulence.

The alongwind 0 level solution $\bar{D}_0(1)$ results almost three times as large as the value in crosswind direction, due to larger standard deviation of alongwind response. The bi-modal factor C_{BM} reduces the 0 level damage taking into account the quasi-static part of the response spectrum; in alongwind assessment the quasi-static part of the response has a high role, strongly reducing the total damage; on the contrary, in crosswind assessment the role of quasi-static part of the response is small, prevailing the resonant contribution, $\lambda_{L,R,ref} = 0.857$. In this case, the simplified formula to estimate the input parameters and the simplifying assumptions at the basis of the method cause a bi-modal factor slightly higher than the unit. By assuming $\tau = 1$ s in the expected frequency of the quasi-static part of the crosswind stress process calculation, $C_{BM} = 1.0477$, while by assuming $\tau = 3$ s $C_{BM} = 0.8534$. Consistently with the choice in alongwind fatigue analysis, it is taken $\tau = 1$ s, however considering $C_{BM} = 1$ as an upper limit of this corrective factor; thus it does not influence the total damage. The mean stress corrective factor C_M slightly increases the total damage in both analysis, especially in the alongwind calculation. Finally, the fatigue curve factor C_{SN} strongly reduces the damage in both cases, taking into account the cut-off limit of fatigue resistance in steel details. All these considerations highlight that in both alongwind and crosswind analyses, turbulence-induced fatigue can be neglected. In general, the chimney under consideration does not suffer fatigue phenomenon due to atmospheric turbulence.

It is worth notice that the proposed analytical verification results on the safe side with respect to the numerical procedure which considers only gust-excited vibrations effects ($T_F = 9568$ years). The great difference is due to the fact that in the analytical analysis the whole range of mean wind velocities is considered through the power law assumption, while the numerical procedure neglects the range

associated with the vortex shedding contribution, so the damage due to lateral turbulence reduces a lot. A more accurate prediction of the fatigue life resulted by gust-excited vibrations effects is an intermediate value between the two prediction.

- In addition, the standard calculation of VIV-induced fatigue (Eurocode 1, 2005; CNR 2008, 2018) is applied, independently from the previous turbulence verification.

Following code provisions, the equivalent static force per unit length $F_{L,eq}(z)$, given by Eq. (5.15), is applied perpendicular to the mean wind direction and to the axis of the structure or structural element. The equivalent static action is associated with vortex shedding in resonance with the structure. It is therefore necessary to firstly determine the critical velocity, that is the mean wind velocity that cause resonance, and the relative Scruton number.

The critical wind velocity $\bar{u}_{cr}$ is given by Equation (5.2), where n_L = 0.486 Hz is the natural frequency in crosswind direction; b = 4.4 m is the characteristic size, namely the diameter at the tip of the chimney where the mode shape is maximum; *St* is the Strouhal number. The Strouhal number is a function of the Reynolds number and therefore of the critical wind velocity; in principle, the solution of Equation (5.2) thus requires an iterative calculation. It is possible to proceed as done for Chimney 1 (Section 5.3.1) and Chimney 2 (Section 5.3.2). The Strouhal number is *St* = 0.22 and $\bar{u}_{cr}$ = 9.72 m/s. According to provisions, the verification related to the critical wind velocity is required provided that $\bar{u}_{cr}$ is lower than the mean wind velocity at the tip of the structure, with return period R = 500 years (9.72 m/s < 46.70 m/s).

The Scruton number is given by the Equation (5.3), where m_e = 1442 kg/m is the equivalent mass per unit length and the damping factor is ξ_L = 0.01, non-including aerodynamic damping; then *Sc* = 7.49, a quite low value.

So far, the parameters values estimated analytically are very similar to the ones in the numerical simulation. Now, calculation of the static equivalent crosswind force per unit length $F_{L,eq}(z)$ caused by critical vortex shedding is carried out by using Eq. (5.15). The mass per unit length of the structure $m(z)$ and the crosswind normalized structural mode shape $\Phi_L(z)=(z/h)^{\zeta}$, h = 100 m and ζ_L = 2, are calculated in function of the coordinate along the structure axis *z*; the crosswind natural frequency of the structure is n_L = 0.486 Hz; the dimensionless parameter C_R, which depends on the critical velocity $\bar{u}_{cr}$ = 9.72 m/s, on the tip mean wind velocity $\bar{u}(R=50\,years)$ = 38.68 m/s and on the tip mean wind velocity $\bar{u}(R=500\,years)$ = 46.70 m/s, is estimated equal to 1 according to CNR provisions; then, it is required the calculation of the peak tip deflection $\bar{y}_{max}$, which is performed by using the spectral method.

The peak deflection value is given by Equation (5.11), multiplying the standard deviation of the deflection σ_s, here called $\sigma_{d,max}$, by the peak deflection factor g_s.

The parameter g_s (Eq. (5.16)) depends on the Scruton number Sc = 7.49 and on the aerodynamic damping parameter $K_a = K_{a,max}\, C_I$. Since Re = 2.85 10^6, $K_{a,max}$ = 1; moreover, since $\bar{u}_{cr}$ = 9.72 m/s, z_{cr} = 100 m and $I_u(z_{cr})$ = 0.1448, the turbulence factor C_I = 0.66; then K_a = 0.66. Therefore, by using Equation (5.16), g_s = 1.950 (CNR, 2018).

The parameter $\sigma_{d,max}$ is given by Equations (5.17)-(5.19) for a_L = 0.4, Sc = 7.49, K_a = 0.66, thus c_1 = 0.00756 (Eq. (5.18)); ρ = 1.25 kg/m^3, b = 4.4 m, h = 100 m, m_e = 1442 kg/m, K_a = 0.66, C_c = 0.01, St = 0.22, then c_2 = 7.6597 10^{-6} (Eq. (5.19)). Therefore, $\sigma_{d,max}/b$ = 0.125 (Eq. (5.17)), so $\sigma_{d,max}$ = 0.550 m.

Lastly, by applying the Equation (5.11), $\bar{y}_{max}$ = 1.950 · 0.550 = 1.072 m is obtained, a quite large value.

Therefore, the standard deviation of the maximum displacement at the top of the structure is $\sigma_{d,max}$ = 0.550 m, the peak deflection value $\bar{y}_{d,max}$ = 1.072 m. The large difference between these values and the ones obtained by the numerical simulation is mainly due to differences in input parameters, especially a_L, as well as in Chimney 1 and Chimney 2a (Section 5.3.1; Section 5.3.2; Pagnini and Piccardo, 2017).

The static equivalent crosswind force $F_{L,eq}(z)$ (Eq. (5.15)) associated with resonant vortex shedding can be applied to the structure, expressing z in m, m in kg/m obtaining the force in N/m. The mean maximum bending moment obtained at the height of the chimney z = 34 m is estimated equal to 3.566 · 10^4 kNm. Then, it is calculated the mean maximum normal stress at this cross-section of the structure (z = 34 m), $\bar{y}_{s,max}$ = 157.96 N/mm^2, which is multiplied by the safety factor for fatigue analysis γ_F = 1.35, so $\bar{y}_{s,max}$ = 213.24 N/mm^2. The maximum stress cycles amplitude correspondent with $\bar{u}_{cr}$ is $\Delta_{s,max}$ = 2 $\bar{y}_{s,max}$ = 426.48 N/mm^2.

Fatigue analysis can be carried out. The number of load cycles which lead to collapse are given by $N_C = a_1 / \Delta_{s,max}^{m_1}$ considering the first straight line of the *S-N* curve. The detail category is 50, m_1 = 3, $a_1 = 2 \cdot 10^6 \cdot 50^3 = 250000000000$. It is estimated N_C = 3222.8. Calculation of the number of load cycles caused by resonant vortex shedding during the nominal lifetime of the structure, 50 years, is performed by applying Equation (5.20), where V_N = 1576800000 s is the life-time; n_L = 0.486 Hz is the natural frequency of crosswind mode; ε_0 = 0.3 is the bandwidth factor describing the band of wind velocities with vortex-induced vibrations; $\bar{u}_{cr}$ = 9.72 m/s is the critical wind velocity of vortex shedding; $\bar{u}_0$ = 0.2 · 38.68 = 7.74 m/s is a reference value of the wind velocity. It is estimated N = 1.497 · 10^8, so it is verified $N \geq 10^4$.

The total damage in 50 years is given by the ratio $D = N/N_C$ = 4.65 · 10^4, which corresponds to a fatigue life $T_F = 50/D$ = 1 · 10^{-3} years.

The prediction of the fatigue life according to VIV-induced fatigue procedure proposed by code (Eurocode 1, 2005; CNR 2008, 2018) gives a very low value, much less than 1 year. The value of T_F = 98 years is considered as the reliable prediction, so this method is hugely on the safe side. Table 5.9 presents a comparison between results of simulation and CNR procedure. The latter is considered in three different possibilities: with all input parameters given according to the code, with a_L value equal to the one used in the simulation, with the response from the simulation.

Response calculation method	Numerical model $a_L = 0.2$	Standard method (Eurocode/CNR) $a_L = 0.4$	Standard method (Eurocode/CNR) $a_L = 0.2$	Numerical model $a_L = 0.2$
$\sigma_{d,max}$	0.099 m	0.550 m	0.286 m	0.099 m
$\Delta_{s,max}$	53.08 N/mm^2	426.48 N/mm^2	222.06 N/mm^2	53.08 N/mm^2
Fatigue prediction approach	Histograms calculation	Standard method (Eurocode/CNR)	Standard method (Eurocode/CNR)	Standard method (Eurocode/CNR)
T_F	98 years	$1 \cdot 10^{-3}$ years	$8 \cdot 10^{-3}$ years	0.56 years

Tab. 5.9: Outcomes comparison.

It is possible to notice from Tab. 5.9 that input parameters uncertainties have an important role in response estimation. Moreover, errors exponentially propagate in fatigue analysis. Starting from the same response estimation, fatigue standard method is simplified in a manner that provides values further on the safe side. It considers all the load cycles in correspondence of the critical mean wind velocity (Fig. 5.12), taking into account a Weibull probability density function of mean wind velocity implicit in Equation (5.20) and taking into account a sinusoidal deterministic stress process with cycle amplitude equal to $\Delta_{s,max} = 2\ \bar{y}_{s,max}$ during the whole time in which $\bar{u} = \bar{u}_{cr}$.

In conclusion, VIV-induced fatigue standard procedure tends to hugely underestimate the fatigue life value.

5.3.4. Case study: Chimney 3

The structure in this Section is a steel chimney, which is 30 m high and has constant radius and variable thickness (Fig. 5.27). The external diameter is 1.00 m and the thickness is, respectively in the two structural portions in Fig. 5.27, 10 mm and 7 mm. The structural steel is Fe510 so the yielding limit stress of the structural material is f_y = 355 Mpa. The mass per unit height, m, and the moment of inertia of the cross section J_f are calculated.

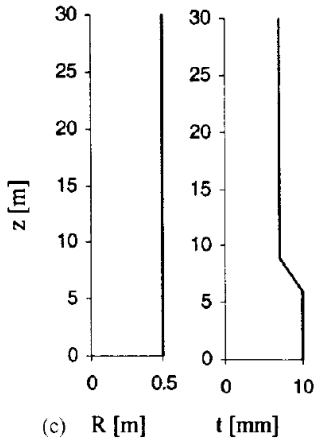

Fig. 5.27: Radius and thickness.

The construction is placed in Italy, Liguria, at sea level. The roughness class is C, the exposure category is III, so $k_r = 0.20$, $z_0 = 0.10$ m, $z_{min} = 5$ m; furthermore, admitting that terrain is flat, $c_t = 1$.

Climatological analyses provide, in correspondence with a mean return period of 50 years, $\bar{u}_{ref} = 29$ m/s (with $\Delta T = 10$ min). The dynamic response of the structure is determined for 46 loading conditions, assuming wind velocity intervals of 1 m/s. The occurrence probability of each loading condition is given by Equation (2.32) using the parameters $F_0 = 0.1943$, $k = 1.549$, $c = 4.629$ m/s (Fig. 5.23).

Input parameters are defined. The drag coefficient is $c_D = 0.7$; the lift wake coefficient is $c_{Ls} = 0.3$; the reference cross size is $b = 1$ m. Given the polar symmetry, the vibration mode occur in pairs. The natural frequency of the structure is $n_D = n_L = 1.27$ Hz; the parameter that defines the shape of the mode is $\zeta_D = \zeta_L = 1.7$; the equivalent mass per unit length is $m_e = 160$ kg/m; the structural damping is $\xi_{sD} = \xi_{sL} = 0.006$. Moreover, the Strouhal number is $St = 0.2$.

The normalised limiting amplitude is assumed equal to $a_L = 0.2$; the aerodynamic damping parameter K_a varies on wind velocity, depending on turbulence intensity I_u and the Reynolds number Re according to Pagnini and Piccardo (2017) model.

The numerical simulation estimates some other critical parameters. The critical velocity is $\bar{u}_{cr} = 7.5$ m/s; the Scruton number is $Sc = 9.65$; the peak deflection factor is $g_s = 3.528$.

The critical section which is subjected to fatigue verification is at the base of the structure.

Structural characteristics	
Height	30 m
Fundamental frequency	1.27 Hz
Modal shape factor	1.7
Structural damping	0.006
Scruton number	9.65
Critical wind velocity	7.5 m/s
Equivalent mass	160 kg/m
Height of critical section	0 m

Tab. 5.10: Structural characteristics of the steel chimney.

Table 5.10 summarizes the main dynamical properties of the structure.

The numerical simulation provides the crosswind structural response, in terms of displacements at the top of the structure or bending moment at the base, which can be translated into crosswind stress in the critical cross-section (Fig. 5.28).

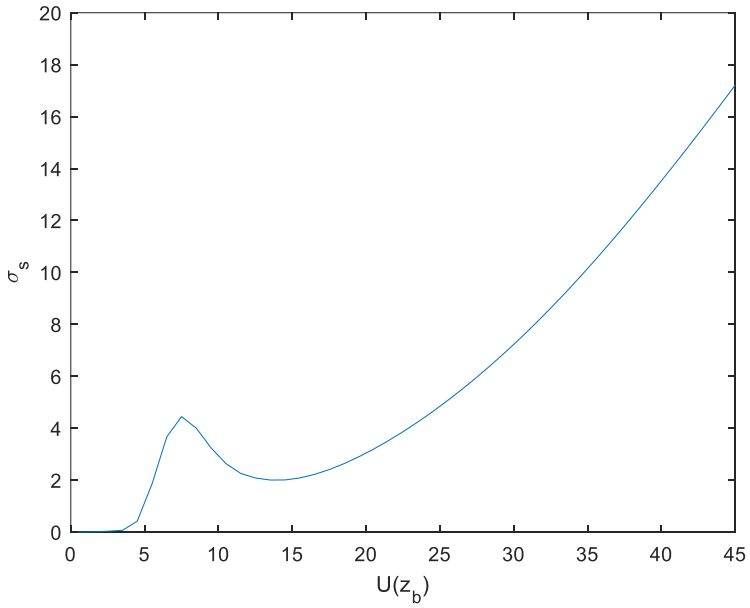

Fig. 5.28: Crosswind response in terms of normal stress at the base of the structure.

The standard deviation of the maximum displacement at the top of the structure in correspondence of $\bar{u}_{cr}$ is $\sigma_{d,max}$ = 0.010 m, the peak deflection value is $\bar{y}_{d,max}$ = 0.034 m. The standard deviation of the normal stress at the base of the structure, in correspondence of $\bar{u}_{cr}$, is $\sigma_{s,max}$ = 4.45 N/mm^2 and the maximum stress is $\bar{y}_{s,max}$ = 15.70 N/mm^2, then the maximum stress cycles amplitude correspondent with $\bar{u}_{cr}$ is $\Delta_{s,max}$ = 2 $\bar{y}_{s,max}$ = 31.40 N/mm^2.

By applying the suitable counting methods described at the beginning of Section 5.3, the cycle histogram can be obtained (Fig. 5.29). This diagram shows a number of blocks at intermediate wind velocity due to vortex shedding and also numerous blocks at high wind velocity due to lateral turbulence. Vortex shedding effects on the response are evident in proximity of critical wind velocity, while lateral turbulence effects dominate at high wind velocity values.

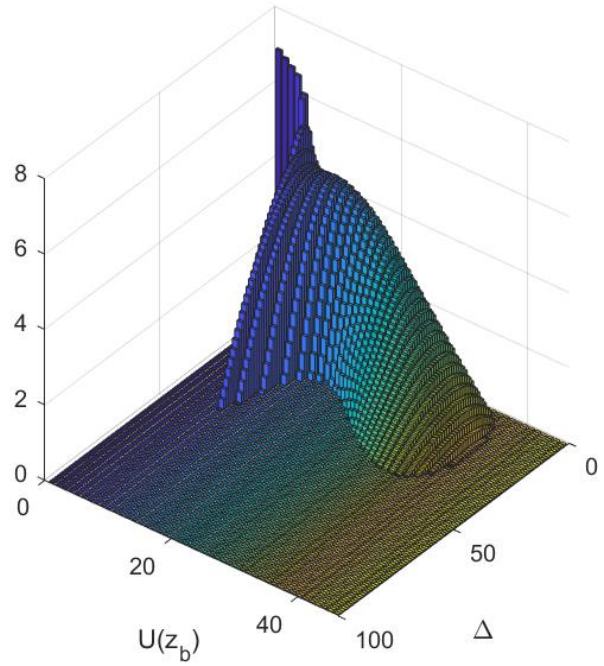

Fig. 5.29: Histogram of the stress cycles .

Fatigue damage is analysed in the critical structural section according to the Eurocode 3 (2005). The cross-section is classified as Category 50 and the number of cycles that causes the failure at different values of amplitude Δ_{sj} is provided by the concerning *S-N* fatigue curve. The damage histogram is obtained calculating the fractional damages d_{ij} (Fig. 5.30). The damage is concentrated in the intermediate range of the wind velocity, where large amplitude cycles due to vortex shedding arise. The fatigue phenomenon is dominated by the vortex shedding.

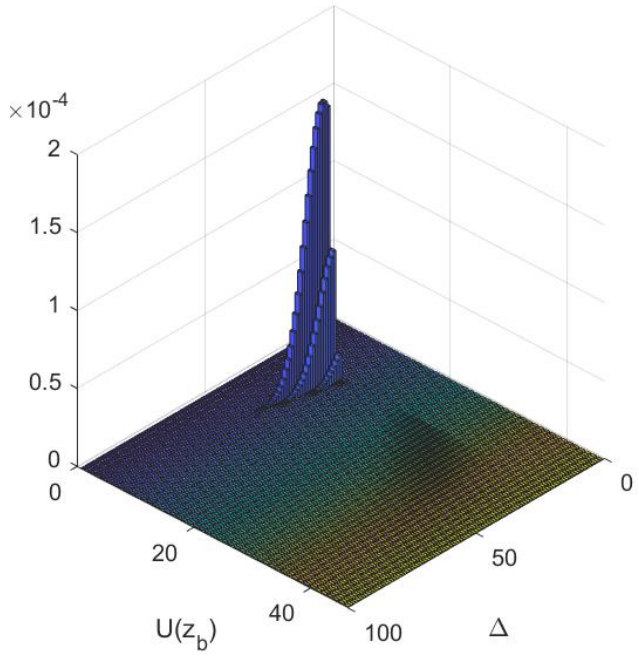

Fig. 5.30: Histogram of the fractions of damage.

These two histograms (Figures 5.29 and 5.30) refer to 1 year life-time of the structure. Then, making the sum of all fractional damages the annual total damage is calculated $D = 0.0031$ and then the predicted fatigue life $T_F = 321$ years.

The standard deviation of the fluctuating stress in the critical section on varying the reference mean velocity is shown in Fig. 5.28. It can be observed that the diagram is due to two different contributions: the one due to the lateral turbulence and the one due to the vortex shedding. In this case, vortex shedding effects in the low wind velocity range are quite limited, while lateral turbulence effects dominate at high wind velocity values. As concerns fatigue, there is a high probability of occurrence of wind velocities that causes VIV response. For this reason, fatigue phenomenon is however probably due to vortex shedding effects, as shown in Fig. 5.30. The value of $T_F = 321$ years is considered as an actual and reliable prediction.

The procedure is repeated neglecting the number of cycles associated with gust-excited vibrations, considering just the cycles associated with VIV. The estimated fatigue life is again $T_F = 334$ years. The committed error is considered as negligible.

The procedure is repeated neglecting the number of cycles associated with VIV, considering just the cycles associated with gust-excited vibrations. The estimated fatigue life is $T_F = 8531$ years because gust-excited vibrations do not produce significant fatigue damage.

In this case it is possible to analyse separately lateral turbulence-induced fatigue and vortex shedding-induced fatigue, since only the second of these two contributions influences the fatigue life prediction. The committed error is considered as negligible.

At engineering level, two separated methods can be applied in crosswind fatigue: the crosswind turbulence-induced fatigue method proposed in the present thesis and, separately, the standard verification of VIV-induced fatigue (Eurocode 1, 2005; CNR 2008, 2018). Results of these two analytical methods are presented and discussed below.

- Applying the Eurocode 1, climatological parameters depend on the Italian zone 7 in which the chimney is located (see Section 4.3.2, Fig. 4.6, Tab. 4.3). Therefore, the reference mean wind velocity, in correspondence with a mean return period of 50 years, is $\bar{u}_{ref}$ = 28 m/s (with ΔT = 10 min). The parent population of the mean wind velocity is modelled by a Weibull distribution (Equation (2.32)) using the parameters F_0 = 0, k = 1.35, c = 4.20 m/s.

Following code provisions, the mean wind profile and the mean wind velocity pressure can be obtained in function of z; the aerodynamic coefficients and the reference size are defined, so the mean alongwind aerodynamic force per unit height is calculated. By applying this force along the structural axis in alongwind direction, the mean maximum bending moment at base of the chimney can be estimated, being equal to 169.3 kNm. It is calculated the mean value of the alongwind stress process $\bar{s}_{D,ref}$ = 22.221 N/mm^2. The permanent loadings-induced stress in the examined section is calculated as $\bar{s}_P$ = 1.794 N/mm^2.

The longitudinal turbulence intensity I_u and the longitudinal turbulence length scale L_u at the site are obtained in function of z. It is defined the reference height above ground, Z_{eq} = 18 m, at which $I_u(Z_{eq})$ = 0.1926 and $L_u(Z_{eq})$ = 79.79.

Therefore, the standard deviation of the alongwind nominal stress in the section of the considered structural detail, $\sigma_{D,ref}$, is evaluated by means of Equation (4.13), in which γ_F = 1.35, the quasi-static response factor B_D^2 = 0.6684 and the resonant response factor R_D^2 = 0.4723. $\sigma_{D,ref}$ = 12.339 N/mm^2 is obtained. The expected frequency value of the alongwind stress process in the critical section, evaluated at reference wind velocity $\bar{u}_{ref}$, is $\nu_{D,ref}$ = 0.817 Hz, calculated by Equation (4.14). The expected frequency of the quasi-static part of the alongwind stress process in the critical section, evaluated at reference wind velocity $\bar{u}_{ref}$, is $\nu_{D,Q,ref}$ = 0.135 Hz, calculated by Equation (4.15) assuming τ = 1 s. The normalized variance of the resonant part of the alongwind stress process in the critical section, evaluated at reference wind velocity $\bar{u}_{ref}$, is $\lambda_{D,R,ref}$ = 0.414, calculated by Equation (4.16). The exponent of the power law $\alpha_{\sigma,D}$ =

2.245 is given by Equation (4.18) where R^2_{Dfat} = 0.144. The exponent of the power law $\alpha_{\lambda,D}$ = 1.224 is given by Equation (4.20).

On the other hand, the mean value of the crosswind stress process $\bar{s}_{L,ref}$ = 0 N/mm^2, according to Equation (4.21), in which μ_L = 0/0.7 = 0. The standard deviation of the crosswind nominal stress in the section of the considered structural detail, $\sigma_{L,ref}$, is evaluated by means of Equation (4.23), in which γ_F = 1.35, the quasi-static response factor B^2_L = 0.0957 and the resonant response factor R^2_L = 0.6529. $\sigma_{L,ref}$ = 9.996 N/mm^2 is obtained. The expected frequency value of the crosswind stress process in the critical section, evaluated at reference wind velocity $\bar{u}_{ref}$, is $\nu_{L,ref}$ = 1.186 Hz, calculated by Equation (4.24). The expected frequency of the quasi-static part of the crosswind stress process in the critical section, evaluated at reference wind velocity $\bar{u}_{ref}$, is $\nu_{L,Q,ref}$ = 0.182 Hz, calculated by Equation (4.28) assuming τ = 1 s. The normalized variance of the resonant part of the crosswind stress process in the critical section, evaluated at reference wind velocity $\bar{u}_{ref}$, is $\lambda_{L,R,ref}$ = 0.872, calculated by Equation (4.29). The exponent of the power law $\alpha_{\sigma,L}$ = 2.564 is given by Equation (4.31) where R^2_{Lfat} = 0.2466. The exponent of the power law $\alpha_{\lambda,L}$ = 0.276 is given by Equation (4.33).

Dealing with alongwind and crosswind detailed calculation, Equations (3.4), (3.5), (3.57)-(3.60) (see Tab. 3.2 in Sections 3.3 and 4.2) are applied obtaining values in Tab. 5.11. As concerns alongwind fatigue (first column of Tab. 5.11), the analytical procedure leads to a mean total damage in the unit time equal to $\bar{D}(1)$ = $1.97 \cdot 10^{-4}$ (Eq. (3.5)), therefore the fatigue life of the structure is predicted as 5071 years (Eq. (3.4)). On the other hand, dealing with crosswind fatigue analysis, values in the second column of Tab. 5.11 are obtained, leading to a mean total damage in the unit time equal to $\bar{D}(1)$ = $2.3 \cdot 10^{-4}$ (Eq. (3.5)), therefore the fatigue life of the structure is predicted as 4350 years (Eq. (3.4)).

	Alongwind buffeting-induced fatigue analysis	Crosswind buffeting-induced fatigue analysis
$\bar{D}_0(1)$	0.0019	$8.4 \cdot 10^{-4}$
C_{BM}	0.3101	0.8657
C_M	1.0529	1.0106
C_{SN}	0.3159	0.3128
$\bar{D}(1)$	$1.97 \cdot 10^{-4}$	$2.3 \cdot 10^{-4}$
T_F	5071 years	4350 years

Tab. 5.11: Calculation of the fatigue life induced by alongwind and crosswind turbulence.

The alongwind 0 level solution $\bar{D}_0(1)$ results twice as large as the value in crosswind direction, due to little larger standard deviation of alongwind response. The bi-modal factor C_{BM} reduces the 0 level damage taking into account the quasi-static part of the response spectrum; in alongwind assessment the quasi-static part of the response has a high role, strongly reducing the total damage; on the contrary, in crosswind assessment the role of quasi-static part of the response is small, prevailing the resonant contribution, $\lambda_{L,R,ref} = 0.872$. The mean stress corrective factor C_M slightly increases the total damage in both analysis. Finally, the fatigue curve factor C_{SN} strongly reduces the damage in both cases, taking into account the cut-off limit of fatigue resistance in steel details. Outcomes highlight that in both alongwind and crosswind analyses, turbulence-induced fatigue can be neglected. In general, the chimney under consideration does not suffer fatigue phenomenon due to atmospheric turbulence.

It is worth notice that the proposed analytical verification results on the safe side with respect to the numerical procedure which considers only crosswind gust-excited vibrations effects (T_F = 8531 years).

- In addition, the standard calculation of VIV-induced fatigue (Eurocode 1, 2005; CNR 2008, 2018) is applied, independently from the previous turbulence verification.

Following code provisions, the equivalent static force per unit length $F_{L,eq}(z)$, given by Eq. (5.15), is applied perpendicular to the mean wind direction and to the axis of the structure or structural element. The equivalent static action is associated with vortex shedding in resonance with the structure. It is therefore necessary to firstly determine the critical velocity, that is the mean wind velocity that cause resonance, and the relative Scruton number.

The critical wind velocity $\bar{u}_{cr}$ is given by Equation (5.2), where n_L = 1.27 Hz is the natural frequency in crosswind direction; b = 1 m is the characteristic size, namely the diameter at the tip of the chimney where the mode shape is maximum; St is the Strouhal number. The Strouhal number is a function of the Reynolds number and therefore of the critical wind velocity; in principle, the solution of Equation (5.2) thus requires an iterative calculation. It is possible to proceed as done for Chimney 1 (Section 5.3.1). The Strouhal number is St = 0.2 and $\bar{u}_{cr}$ = 6.35 m/s. According to provisions, the verification related to the critical wind velocity is required provided that $\bar{u}_{cr}$ is lower than the mean wind velocity at the tip of the structure, with return period R = 500 years (6.35 m/s < 38.56 m/s).

The Scruton number is given by the Equation (5.3), where m_e = 164 kg/m is the equivalent mass per unit length and the damping factor is ξ_L = 0.006, non-including aerodynamic damping; then Sc = 9.87.

So far, the parameters values estimated analytically are very similar to the ones in the numerical simulation. Now, calculation of the static equivalent crosswind force per unit length $F_{L,eq}(z)$ caused by critical vortex shedding is carried out by using Eq. (5.15). The mass per unit length of the structure $m(z)$ and the crosswind normalized structural mode shape $\Phi_L(z)=(z/h)^{\zeta}$, h = 30 m and ζ_L = 1.7, are calculated in function of the coordinate along the structure axis z; the crosswind natural frequency of the structure is n_L = 1.27 Hz; the dimensionless parameter C_R, which depends on the critical velocity $\bar{u}_{cr}$ = 6.35 m/s, on the tip mean wind velocity $\bar{u}(R=50 years)$ = 31.94 m/s and on the tip mean wind velocity $\bar{u}(R=500 years)$ = 38.56 m/s, is estimated equal to 1 according to CNR provisions; then, it is required the calculation of the peak tip deflection $\bar{y}_{max}$, which is performed by using the spectral method.

The peak deflection value is given by Equation (5.11), multiplying the standard deviation of the deflection σ_s, here called $\sigma_{d,max}$, by the peak deflection factor g_s.

The parameter g_s (Eq. (5.16)) depends on the Scruton number Sc = 9.87 and on the aerodynamic damping parameter $K_a = K_{a,max} C_I$. Since Re = 4.23 10^5, $K_{a,max}$ = 0.834; moreover, since $\bar{u}_{cr}$ = 6.35 m/s, z_{cr} = 30 m and $I_u(z_{cr})$ = 0.1753, the turbulence factor C_I = 0.88; then K_a = 0.74. Therefore, by using Equation (5.16), g_s = 2.255 (CNR, 2018).

The parameter $\sigma_{d,max}$ is given by Equations (5.17)-(5.19) for a_L = 0.4, Sc = 9.87, K_a = 0.74, thus c_1 = -0.00541 (Eq. (5.18)); ρ = 1.25 kg/m^3, b = 1 m, h = 30 m, m_e = 164 kg/m, K_a = 0.74, C_c = 0.014, St = 0.2, then c_2 = 7.834 10^{-6} (Eq. (5.19)). Therefore, $\sigma_{d,max}/b$ = 0.026 (Eq. (5.17)), so $\sigma_{d,max}$ = 0.026 m.

Lastly, by applying the Equation (5.11), $\bar{y}_{max}$ = 2.255 · 0.026 = 0.059 m is obtained.

Therefore, the standard deviation of the maximum displacement at the top of the structure in correspondence of $\bar{u}_{cr}$ is $\sigma_{d,max}$ = 0.026 m, the peak deflection value $\bar{y}_{d,max}$ = 0.059 m. The difference

between these values and the ones obtained by the numerical simulation is mainly due to differences in input parameters (Sections 5.3.1, 5.3.2, 5.3.3; Pagnini and Piccardo, 2017).

The static equivalent crosswind force $F_{L,eq}(z)$ (Eq. (5.15)) associated with resonant vortex shedding can be applied to the structure, expressing z in m, m in kg/m obtaining the force in N/m. The mean maximum bending moment obtained at the base of the chimney is estimated equal to 156.7 kNm. Then, it is calculated the mean maximum normal stress at this cross-section of the structure (z = 0 m), $\bar{y}_{s,max}$ = 20.57 N/mm^2, which is multiplied by the safety factor for fatigue analysis γ_F = 1.35, so $\bar{y}_{s,max}$ = 27.77 N/mm^2. The maximum stress cycles amplitude correspondent with $\bar{u}_{cr}$ is $\Delta_{s,max} = 2\ \bar{y}_{s,max}$ = 55.53 N/mm^2.

Fatigue analysis can be carried out. The number of load cycles which lead to collapse are given by $N_C = a_1 / \Delta_{s,max}^{m_1}$ considering the first straight line of the *S-N* curve. The detail category is 50, m_1 = 3, $a_1 = 2 \cdot 10^6 \cdot 50^3 = 250000000000$. It is estimated N_C = 1459902.2. Calculation of the number of load cycles caused by resonant vortex shedding during the nominal lifetime of the structure, 50 years, is performed by applying Equation (5.20), where V_N = 1576800000 s is the life-time; n_L = 1.27 Hz is the natural frequency of crosswind mode; ε_0 = 0.3 is the bandwidth factor describing the band of wind velocities with vortex-induced vibrations; $\bar{u}_{cr}$ = 6.35 m/s is the critical wind velocity of vortex shedding; $\bar{u}_0$ = $0.2 \cdot 31.94$ = 6.39 m/s is a reference value of the wind velocity. It is estimated $N = 4.420 \cdot 10^8$, so it is verified $N \geq 10^4$.

The total damage in 50 years is given by the ratio $D = N/N_C = 3.03 \cdot 10^2$, which corresponds to a fatigue life $T_F = 50/D$ = 0.17 years.

The prediction of the fatigue life according to VIV-induced fatigue procedure proposed by code (Eurocode 1, 2005; CNR 2008, 2018) gives a very low value, less than 1 year. The value of T_F = 321 years is considered as the reliable prediction, so this method is hugely on the safe side. Table 5.12 presents a comparison between results of simulation and CNR procedure. The latter is considered in three different possibilities: with all input parameters given according to the code, with a_L value equal to the one used in the simulation, with the response from the simulation.

Response calculation method	Numerical model a_L = 0.2	Standard method (Eurocode/CNR) a_L = 0.4	Standard method (Eurocode/CNR) a_L = 0.2	Numerical model a_L = 0.2
$\sigma_{d,max}$	0.010 m	0.026 m	0.024 m	0.010 m
$\Delta_{s,max}$	31.40 N/mm^2	55.53 N/mm^2	51.85 N/mm^2	31.40 N/mm^2
Fatigue prediction approach	Histograms calculation	Standard method (Eurocode/CNR)	Standard method (Eurocode/CNR)	Standard method (Eurocode/CNR)
T_F	321 years	0.17 years	0.20 years	1.26 years

Tab. 5.12: Outcomes comparison.

It is possible to notice from Tab. 5.12 that in this case a_L definition has a quite low role in response estimation, which is probably more influenced by other input parameters. Again, it can be observed that errors and uncertainties exponentially propagate in fatigue analysis. By starting from the same response estimation, fatigue standard method again does not provide a fatigue life value closer to the one obtained by the numerical analysis. Fatigue standard method is simplified in a manner that provides values further on the safe side. It considers all the load cycles in correspondence of the critical mean wind velocity (Fig. 5.12), taking into account a Weibull probability density function of mean wind velocity implicit in Equation (5.20) and taking into account a sinusoidal deterministic stress process with cycle amplitude equal to $\Delta_{s,max} = 2\ \bar{y}_{s,max}$ during the whole time in which $\bar{u} = \bar{u}_{cr}$.

In this case, the maximum amplitude stress cycle corresponds to the second broken line of the resistance *S-N* curve, the intermediate one (Eurocode 3, 2005). Even in cases with a really small response, it seems as, whenever the maximum amplitude stress cycle is above the cut-off limit of the fatigue *S-N* curve, the VIV-induced fatigue standard procedure tends to not verify any structure under consideration.

In conclusion, VIV-induced fatigue standard procedure tends to hugely underestimate the fatigue life value.

5.3.5. Case study: Pole

By way of example, a different structural typology is examined. Since chimneys are usually more sensitive to vortex induced vibrations, an example pole is chosen to investigate a structure which is characterized by a negligible VIV response. It is studied if separation of effects in fatigue analysis would be allowed at engineering level, also in such case. A summary Table is reported at the end of this Section, which confirm this idea.

The structure in this Section is a steel pole, which is 30 m high and has variable radius and variable thickness. The reference external diameter is equal to 0.35 m and additional masses of non-structural elements weight on the pole, so that the total weight is about 2750 kg. The structural steel is Fe510 so the yielding limit stress of the structural material is f_y = 355 Mpa.

The construction is placed in Italy, Zone 2 according to Italian code (see Section 4.3.2, Fig. 4.6, Tab. 4.3). The reference mean wind velocity, in correspondence with a mean return period of 50 years, is $\bar{u}_{ref}$ = 25 m/s (with ΔT = 10 min). The parent population of the mean wind velocity is modelled by a Weibull distribution (Equation (2.32)) using the parameters F_0 = 0, k = 1.15, c = 2.75 m/s. The roughness class is D, the exposure category is IV, so k_r = 0.22, z_0 = 0.30 m, z_{min} = 8 m; furthermore, admitting that terrain is flat, c_t = 1. The dynamic response of the structure is determined for 29 loading conditions, assuming wind velocity intervals of 1 m/s.

Input parameters are defined. The drag coefficient is c_D = 2.8; the lift coefficient is c_L = 1.0; the lift wake coefficient is c_{Ls} = 0.8; the reference cross size is b = 0.35 m. Given the polar symmetry, the vibration mode occur in pairs. The natural frequency of the structure is $n_D = n_L$ = 0.77 Hz; the parameter that defines the shape of the mode is $\zeta_D = \zeta_L$ = 2; the equivalent mass per unit length is m_e = 75 kg/m; the structural damping is $\xi_{sD} = \xi_{sL}$ = 0.005. Moreover, the Strouhal number is St = 0.16.

The normalised limiting amplitude is assumed equal to a_L = 0.2; the aerodynamic damping parameter K_a varies on wind velocity, depending on turbulence intensity I_u and the Reynolds number Re according to Pagnini and Piccardo (2017) model.

The numerical simulation estimates some other critical parameters. The critical velocity is $\bar{u}_{cr}$ = 2.5 m/s; the Scruton number is Sc = 30.77; the peak deflection factor is g_s = 4.146. These values predict that VIV would produce quite small oscillation amplitudes in resonant conditions.

The critical section which is subjected to fatigue verification is at the base of the structure.

The numerical simulation provides the crosswind structural response, in terms of displacements at the top of the structure or bending moment at the base, which can be translated into crosswind stress in the critical cross-section (Fig. 5.31).

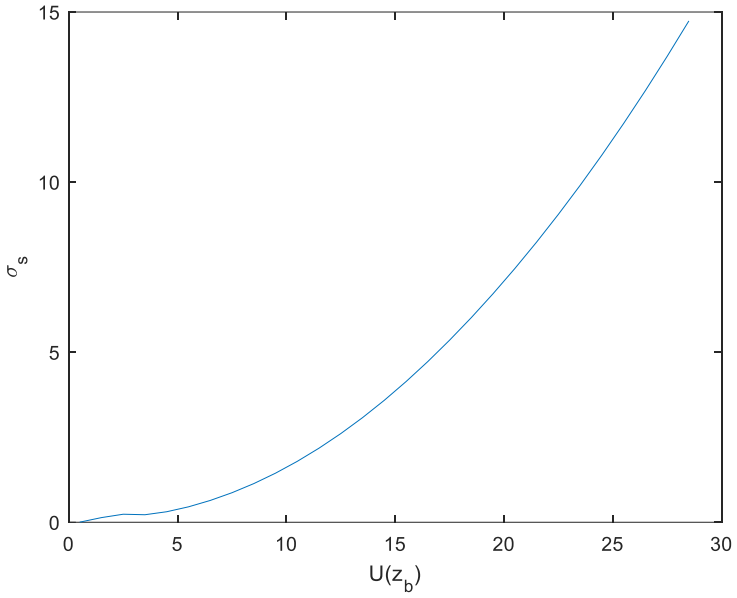

Fig. 5.31: Crosswind response in terms of normal stress at the base of the structure.

The standard deviation of the displacement at the top of the structure in correspondence of $\bar{u}_{cr}$ is $\sigma_{d,max}$ = 0.002 m, the peak deflection value is $\bar{y}_{d,max}$ = 0.009 m. The standard deviation of the normal stress at the base of the structure, in correspondence of $\bar{u}_{cr}$, is $\sigma_{s,max}$ = 0.24 N/mm^2 and the maximum stress is $\bar{y}_{s,max}$ = 0.99 N/mm^2, then the maximum stress cycles amplitude correspondent with $\bar{u}_{cr}$ is $\Delta_{s,max}$ = 2 $\bar{y}_{s,max}$ = 1.98 N/mm^2.

The standard deviation of the normal stress at the base of the structure in correspondence of $\bar{u}$ = 28.5 m/s is $\sigma_{s,max}$ = 14.74 N/mm^2 and the maximum stress is $\bar{y}_{s,max}$ = 69.84 , then the maximum stress cycles amplitude correspondent with $\bar{u}$ = 28.5 m/s is $\Delta_{s,max}$ = 2 $\bar{y}_{s,max}$ = 139.68 N/mm^2.

By applying the suitable counting methods described at the beginning of Section 5.3, the cycle histogram can be obtained (Fig. 5.32). This diagram shows the number of blocks increasing with the mean wind velocity and the stress amplitude.

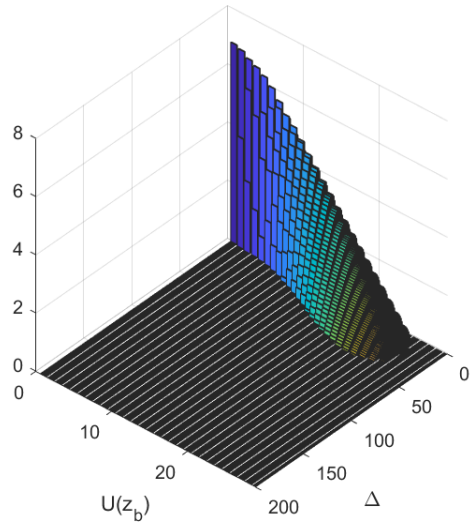

Fig. 5.32: Histogram of the stress cycles .

Fatigue damage is analysed in the critical structural section according to the Eurocode 3 (2005). The cross-section is classified as Category 36 and the number of cycles that causes the failure at different values of amplitude Δ_{sj} is provided by the concerning *S*-*N* fatigue curve. The damage histogram is obtained calculating the fractional damages d_{ij} (Fig. 5.33). The damage is spread at high range of the wind velocity, where larger amplitude cycles due to lateral turbulence arise. Vortex shedding effects are not evident neither on the response nor on the fatigue histograms.

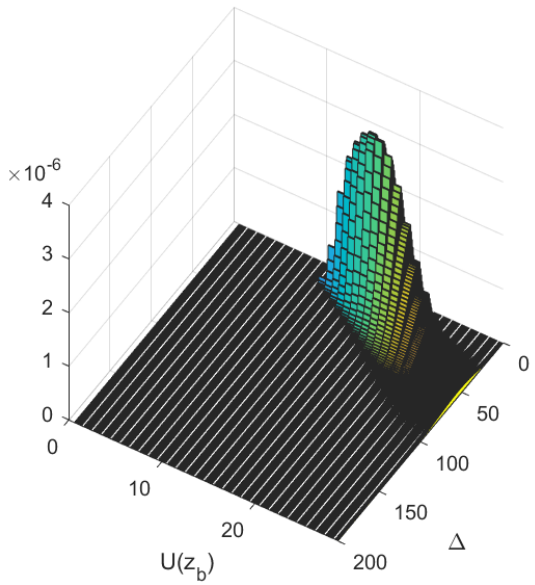

Fig. 5.33: Histogram of the fractions of damage.

These two histograms (Figures 5.32 and 5.33) refer to 1 year life-time of the structure. Then, making the sum of all fractional damages the annual total damage is calculated $D = 5 \cdot 10^{-4}$ and then the predicted fatigue life T_F = 1930 years.

The standard deviation of the fluctuating stress in the critical section on varying the reference mean velocity is shown in Fig. 5.31. It can be observed that vortex shedding effects in the low wind velocity range are negligible, while lateral turbulence effects dominate at high wind velocity values. As concerns fatigue, there is a high probability of occurrence of wind velocities that causes VIV response. Nevertheless, fatigue phenomenon is probably due only to lateral turbulence effects, as shown in Fig. 5.33. The value of T_F = 1930 years is considered as an actual and reliable prediction.

The procedure is repeated neglecting the number of cycles associated with gust-excited vibrations, considering just the cycles associated with VIV. The estimated fatigue life is T_F tending to ∞.

The procedure is repeated neglecting the number of cycles associated with VIV, considering just the cycles associated with gust-excited vibrations. The estimated fatigue life is T_F = 1930 years because gust-excited vibrations produce the whole fatigue damage. The committed error is considered as null.

Also in this case it is possible to analyse separately lateral turbulence-induced fatigue and vortex shedding-induced fatigue, since only the first of these two contributions influences the fatigue life prediction.

5.3.6. Summary and comparison of results

Table 5.13a summarizes the five case studies. At the end of this Section 5.3 it can be concluded that separation of effects in fatigue analysis might be allowed at engineering level, even if it is uncorrected in principle. This is due to the fact that VIV contribution on fatigue is always amplified by the high probability of occurrence of low and intermediate range of wind velocities (Fig. 5.34). Therefore, unless VIV response is totally negligible (pole case study), its contribution on fatigue analysis is always dominant.

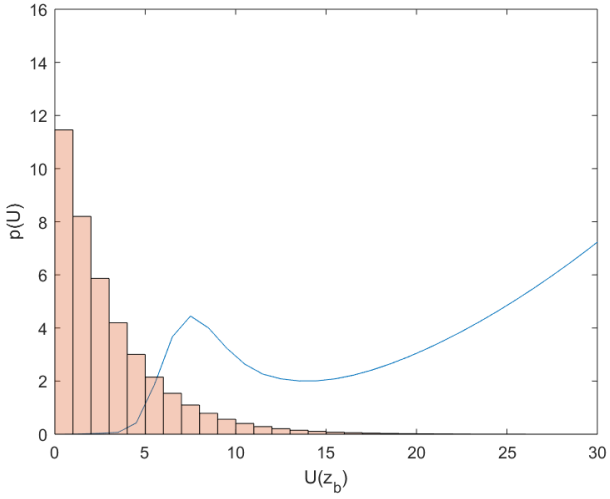

Fig. 5.34: Crosswind response and probability of occurrence of mean wind velocity.

Table 5.13b summarizes the different approaches used to analyse the example chimneys in this Section 5.3. The fatigue life has been calculated through numerical analyses (numerical simulation calculates crosswind response and then cycle and damage histograms are obtained) over the whole range of wind velocity, over the VIV range of wind velocity and over the gust range of wind velocity; the fatigue life has been calculated through theoretical analyses (VIV-induced fatigue standard method and gust-induced fatigue method, proposed in the current thesis).

	Damage histogram	Fatigue life
Chimney1 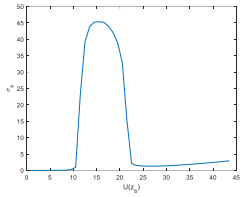	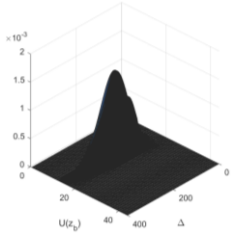	T_F = 1.46 years T_F = 1.46 years (only VIV) $T_F \rightarrow \infty$ (only crosswind gust buffeting)
Chimney 2a 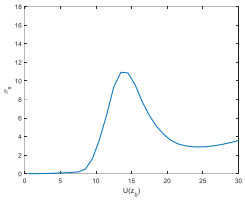	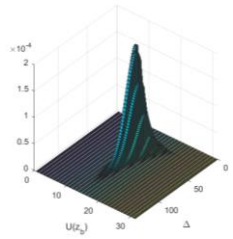	T_F = 48.9 years T_F = 49.5 years (only VIV) T_F = 4242 years (only crosswind gust buffeting)
Chimney 2b 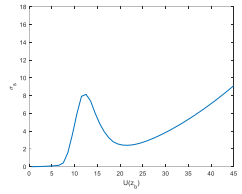	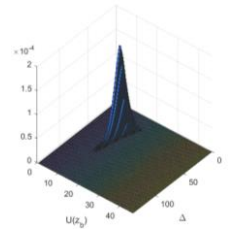	T_F = 98 years T_F = 99 years (only VIV) T_F = 9568 years (only crosswind gust buffeting)
Chimney 3 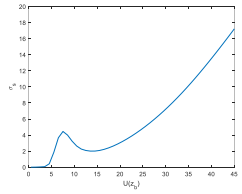	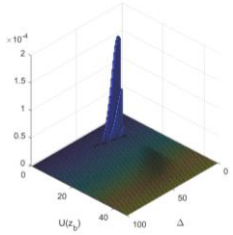	T_F = 321 years T_F = 334 years (only VIV) T_F = 8531 years (only crosswind gust buffeting)
Pole 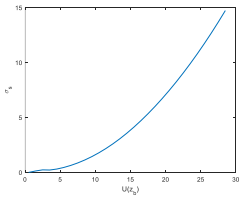	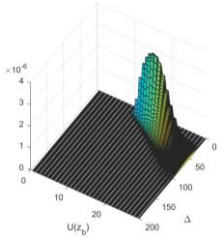	T_F = 1930 years $T_F \rightarrow \infty$ (only VIV) T_F = 1930 years (only crosswind gust buffeting)

Tab. 5.13a: Summary of the results.

	Numerical analysis	Analytical methods
Chimney1 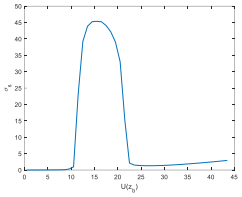	T_F = 1.46 years T_F = 1.46 years (only VIV) $T_F \rightarrow \infty$ (only crosswind gust buffeting)	T_F = 0.0055 years → VIV (standard method) $T_F = 2 \cdot 10^5$ years → crosswind gust (proposed method)
Chimney 2a 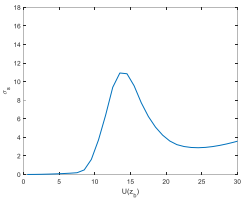	T_F = 48.9 years T_F = 49.5 years (only VIV) T_F = 4242 years (only crosswind gust buffeting)	T_F = 0.0019 years → VIV (standard method) T_F = 2078 years → crosswind gust (proposed method)
Chimney 2b 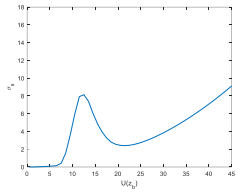	T_F = 98 years T_F = 99 years (only VIV) T_F = 9568 years (only crosswind gust buffeting)	T_F = 0.0011 years → VIV (standard method) T_F = 1275 years → crosswind gust (proposed method)
Chimney 3 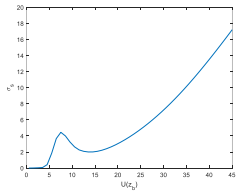	T_F = 321 years T_F = 334 years (only VIV) T_F = 8531 years (only crosswind gust buffeting)	T_F = 0.1652 years → VIV (standard method) T_F = 4350 years → crosswind gust (proposed method)

Tab. 5.13b: Summary of the results.

5.4. REVIEW OF THE VIV-INDUCED FATIGUE STANDARD METHOD

Once the possibility of separating crosswind effects in fatigue analysis is considered, two separated engineering methods can be applied in crosswind fatigue: the lateral turbulence-induced fatigue method proposed in the present thesis and, separately, the standard verification of VIV-induced fatigue (Eurocode 1, 2005; CNR 2008, 2018). According to the latter, the example chimneys analysed in Sections 5.3.1, 5.3.2, 5.3.3 and 5.3.4, result always strongly not verified. Hence, VIV-induced fatigue standard method requires a critical analysis, because it seems to provide too much preventive results compared with numerical simulations.

By applying this method, the total damage is simply given by the ratio $D = N/N_C$, in which the number of cycles due to VIV, N, is estimated by means of an approximated expression critically discussed in Sections 5.4.1 and 5.4.2 and the number of load cycles leading to collapse, N_C, depends on the VIV response prediction, which is strongly affected by uncertainties (Section 5.4.3).

This consolidated fatigue verification method, included in international codes, is discussed in the present Section 5.4 and a new preventive proposal is eventually introduced (Section 5.4.4).

5.4.1. Weibull model of the parent population of the mean wind velocity

The standard design procedure to evaluate VIV-induced fatigue is introduced and explained in Section 5.2.4, as concerns both response and fatigue calculations. Once the peak deflection of the structure, $\bar{y}_{max}$, is evaluated according to the spectral model, the equivalent static force per unit length, $F_{L,eq}(z)$, given by Equation (5.15), is applied perpendicularly to the mean wind direction and to the axis of the structure or structural element. It allows to calculate the bending moment and the normal stress in the critical cross-sections. Then, the maximum stress cycles amplitude correspondent with $\bar{u}_{cr}$ is $\Delta_{s,max}$, which corresponds to twice as the calculated stress. The number of load cycles with constant amplitude $\Delta_{s,max}$ which lead to collapse is N_C, that is given by the considered S-N curve. Calculation of the number of load cycles N caused by resonant vortex shedding during the nominal lifetime of the structure V_N, usually 50 years, is performed by applying Equation (5.20). The total damage in 50 years is given by the ratio $D = N/N_C$, the fatigue life is calculated as $T_F = V_N/D$.

Equation (5.20) estimates the number of cycles due to VIV, N, implicitly considering the local climatology through a Weibull distribution (Ruscheweyh, 1988). All the cycles are considered with the maximum amplitude in correspondence of the critical mean wind velocity (Fig. 5.12), taking into account the probability of occurrence of $\bar{u}_{cr}$. The expression derives from:

$$N = V_N n_L(\varepsilon_0 \bar{u}_{cr})\, p_{Weibull}(\bar{u}_{cr}) \tag{5.22}$$

where V_N is the life-time in seconds, namely the nominal life-time of the structure or structural element; n_L is the natural frequency of crosswind mode in Hz, equivalent of 1/s; the product $(\varepsilon_0 \bar{u}_{cr})$ is the band of wind velocities with vortex-induced vibrations, which is equal to $0.3\bar{u}_{cr}$ according to the code, an interval $\Delta\bar{u}$ which increases with the critical velocity value; $p_{Weibull}(\bar{u}_{cr})$ is the probability density function of the mean wind velocity evaluated in correspondence of the critical wind velocity of vortex shedding. By substituting the Weibull model expression, it is obtained:

$$N = V_N n_L (\varepsilon_0 \bar{u}_{cr}) \left\{ \frac{k}{c} \left(\frac{\bar{u}}{c} \right)^{k-1} \exp\left[-\left(\frac{\bar{u}}{c} \right)^{k} \right] \right\} \tag{5.23}$$

and by substituting $\bar{u} = \bar{u}_{cr}$, k=2 and c=$\bar{u}_0$:

$$N = V_N n_L (\varepsilon_0 \bar{u}_{cr}) \left\{ \frac{2}{\bar{u}_0} \left(\frac{\bar{u}_{cr}}{\bar{u}_0} \right) \exp\left[-\left(\frac{\bar{u}_{cr}}{\bar{u}_0} \right)^{2} \right] \right\} \tag{5.24}$$

which leads to Equation (5.20).

This means that the considered Weibull model has a fixed shape parameter k=2 and a scale parameter equal to $\bar{u}_0 = 0.2 \cdot \bar{u}(R = 50 years; z = z_{cr})$. The parent population distribution model of the mean wind velocity implicit in the formula differs from the one adopted in this thesis for Italian territory, which is the one proposed in CNR deriving from Pagnini and Solari (2009, 2016) (see Section 4.3.2, Fig. 4.6, Tab. 4.3). According to the latter, k is provided for different Italian zones and $c = (0.2k - 0.12)\bar{u}_{ref}$.

Naming Weibull-EC (Eurocode) the model in Equation (5.20) and Weibull-CNR the one used in the present thesis, a comparison of the two proposal is carried out.

Zones	u_{ref} (m/s)	k	c
1	25	1.00	2.00
2	25	1.15	2.75
3	27	1.20	3.24
4	28	1.35	4.20
5	28	1.50	5.04
6	28	1.35	4.20
7	28	1.35	4.20
8	30	1.50	5.40
9	31	1.15	3.41

Tab. 5.14: Italian zones and related $\bar{u}_{ref}$, k and c parameter values according to Weibull-CNR.

Table 5.14 shows that Weibull-CNR considers local climatology at the zone in which the territory is conventionally subdivided. Reference mean wind velocities and the shape parameters of the Weibull are given as constants, whereas the scale parameters depend on k and $\bar{u}_{ref}$ according to the expression $c = (0.2k - 0.12)\bar{u}_{ref}$. The use of this expression is straightforward: starting from the knowledge of k and $\bar{u}_{ref}$, it furnishes c. Assuming $F_0 = 0$, i.e., neglecting wind calms, as it seems to be the trend of the measurements carried out by modern sensors, Eq. (2.21) of the hybrid Weibull density function provides a sound approximation of the parent distribution. Therefore, according to Weibull-CNR model, all climatological parameters depend on the conventional zone.

This model (Pagnini and Solari, 2016) derived from a wide database of anemometric measurements. Several anemometric Italian recordings have been investigated under different circumstances. A number of data have been analysed specifically for the research of Pagnini and Solari. Another set of data has been derived from investigations concerning Italian key structures and infrastructures (Freda and Solari 2010), in the framework of the Liguria region meteorological assessment (Castino et al. 2003), and for the European project Wind and Ports (Solari et al. 2012). Data have been supplied by the Italian Air Force and include eight daily records of the mean wind velocity and direction, averaged over 10 min, taken every 3 h. Recordings include also daily maxima averaged over 1–5 s and other meteorological information, such as atmospheric pressure and temperature, which is very useful for data correction. The time length of the data logging is about 50 years for each station. In addition, data have been recovered from the definition of the Italian wind zone map (Ballio et al. 1999). The data come from older investigations carried out by ENEL, the Italian national agency for electricity. These records cover short periods, but include all measures on the next 10 min. Since they are not fully homogeneous with the former groups of data, just their inherent heterogeneity strengthens the robustness of the results illustrated by Pagnini and Solari. Fig. 5.35 shows the location of the anemometric stations used for their study.

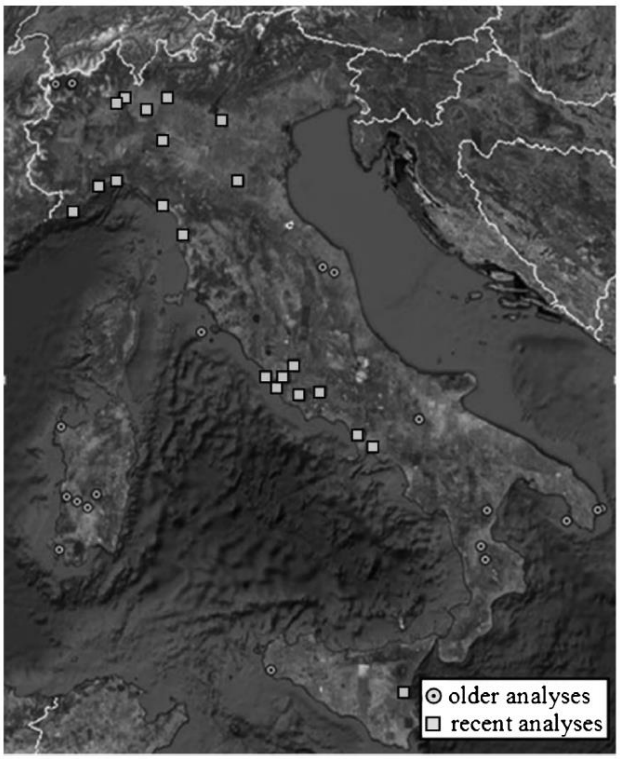

Fig. 5.35: Italian anemometric stations (Pagnini and Solari, 2016; map © Google Earth, data SIO, NOAA, U.S. Navy, NGA, GEBCO); older analyses until 1999 and recent analyses from 2003.

Wind speed measures have been submitted to a careful check and correction process concerning all the values exceeding a suitable threshold (Burlando et al. 2013). The evolution of the mean wind speed in proximity of questionable data has been compared with the evolution of the atmospheric pressure. The values that are clearly incoherent with synoptic conditions have been discarded, considering also that the available data do not allow to single out local and short duration wind events such as thunderstorms (De Gaetano et al. 2014). In this way, non-synoptic phenomena ruling extreme wind velocities have been excluded from the data set.

All the actual anemometric recordings have been transformed into reference values, i.e., velocity values ideally recorded at 10 m height over a flat homogeneous terrain with roughness length of $z_0 = 0.05$ m. When the surrounding terrain is flat or almost flat, a detailed roughness length map of the terrain surrounding the anemometer has been created, and the transformation has been carried out through the procedure recommended by ESDU (1993). In the case of complex orography, besides the roughness length map, a numerical model of the terrain topography has been implemented, and the analysis has been carried out by the mass consistent WINDS code (Burlando et al. 2007a, b, 2010). In the most complex cases, an advanced procedure that generalizes the ESDU model has been nested inside the WINDS code by means of a downscaling aimed at studying the local wind field of the meteorological stations at a smaller scale (Burlando et al. 2013).

Analysis of the distribution of the parent population wind velocities has been carried out by means of the Weibull model. Table 5.15 shows a general overview of the processed data, separating the stations according to the conventional Italian zones. For each station, it lists the location, the reference wind velocity and the model parameters of the parent wind velocity distribution.

The reference mean wind velocity is obtained by the parent population method (Gomes and Vickery, 1977; ESDU, 1990; Lagomarsino et al., 1992).

The Weibull model is fitted by adopting the resistant method (Hoaglin et al. 1983) over non-zero velocity values by giving prominence to high wind velocities.

This procedure investigates the data in a linear plot, sorting the values in increasing order and dividing data into three groups, left, middle, and right, as equal in size as it is possible. Within each of these thirds, the median abscissa (x-value) and the median ordinate (y-value) are found, separately, in order to obtain three summary points. In a Weibull probability paper, the fitting line is defined. By adopting this procedure, the group of high and extreme rare values is accounted for with the same weight of the group of the low frequent speeds. This means that intense wind speeds turn out to be privileged.

For fatigue analysis, it is difficult to establish, a priori, whether it is better a fitting procedure focused either on the lower and middle range wind velocities or on the higher values, which belong to the tail of the distribution, as damage is generally spread over a wide range of intermediate values. However, it has been noticed that the damage histogram is generally significant on the right tail of the mean wind velocity distribution.

Zones	Regions – Provinces	Stations	U(50years)	k	c
1	Lombardia – Bergamo	Bergamo	24.5	0.97	1.79
	Lombardia – Varese	Malpensa	27.5	0.95	1.98
	Piemonte – Novara	Novara	26.2	0.88	1.55
	Lombardia – Milano	Linate	26.2	0.93	1.77
	Veneto – Verona	Verona	27.8	1.02	2.33
	Valle d'Aosta – Aosta	Verrayes	24.1	1.53	4.35
	Valle d'Aosta – Aosta	Garin	26.5	1.39	4.14
	Valle d'Aosta – Aosta	Vetan	31.5	1.1	3.12
2	Emilia Romagna – Piacenza	Piacenza	21.5	1.15	2.38
	Emilia Romagna – Bologna	Bologna	21.25	1.23	2.62
3	Toscana – Pisa	Pisa	25.2	1.24	3.2
	Lazio – Roma	Guidonia	25.9	1.33	3.79
	Lazio – Roma	Fiumicino	23.7	1.42	3.88
	Lazio – Roma	Ciampino	29.8	1.24	3.82
	Lazio – Roma	Pratica M	22.3	1.52	4.04
	Lazio – Frosinone	Frosinone	27	1.15	2.85
	Lazio – Latina	Latina	25.9	1.24	3.25
	Campania – Caserta	Grazzanise	26.1	1.32	3.72
	Campania – Napoli	Capodichino	30.5	1.16	3.37
	Marche – Macerata	Cingoli	39.2	1.04	3.45
	Marche – Macerata	Macerata	27.7	1.09	2.51
	Puglia – Foggia	Faeto	37.7	1.47	6.54
	Puglia – Lecce	La Palascia	24.6	1.76	5.43
	Puglia – Otranto	Consalvi	26.1	1.51	4.7
	Calabria – Cosenza	Oriolo	33	1.25	4.12
	Calabria – Cosenza	San Demetrio	38.8	1.39	6.36
	Calabria – Cosenza	Camigliatello	33.4	1.24	4.08
4	Sicilia – Catania	Catania	27.7	1.23	3.4
5	Sardegna – Nuoro	Aritzo	33.2	1.51	5.95
	Sardegna – Sud Sardegna	Tuili	28.1	1.53	4.78
6	Sardegna – Sassari	Fiume Santo	26.2	1.41	4.19
	Sardegna – Oristano	Cirras	30.2	1.12	3.26
	Sardegna – Oristano	Monte Arci	33.3	1.45	5.8
	Sardegna – Sud Sardegna	S. Caterina	25.1	1.45	4.17
7	Liguria – Genova	Genova	28	1.48	4.92
	Liguria – Savona	Savona	27	1.48	4.74
	Liguria – Spezia	Spezia	25	1.12	2.6
	Liguria – Imperia	Imperia	25	1.06	2.24
9	Toscana – Grosseto	Le Porte	30.6	1.29	4.15

Tab. 5.15: Italian zones and related data set of Italian stations.

The Italian data set is enriched by anemometric recordings taken over stations located in other European countries. Such data have been downloaded from the web site of the National Climatic Data Center (2014). The examined data refer to anemometric stations at airports, and were not transformed into reference values because detailed models of those areas were not available. However, in indicative terms, it is assumed that airport sites do not differ so much from the reference terrain. The results of the statistical study of this data set are given in Table 5.16.

Moreover, Kemper and Feldmann (2011) report a summary table of some locations in Germany and considered climatological parameters according to European Wind Atlas (Troen and Petersen, 1989). In this document the Weibull parameters have been derived for 208 European sites based on daily measurements of three wind velocities at consistent times of day. The Table from Kemper and Feldmann (2011) includes 15 German locations and it complements Table 5.16 of European anemometric stations. Also in this case records are not homogeneous, they are considered just to possibly strengthen the robustness of the Weibull-CNR model.

Country	European Stations	*U*(50years)	*k*	*c*
Denmark	Koeben	24	1.85	5.86
Denmark	Snaeffel	35.9	1.81	8.78
Netherlands	Amsterdam	27.6	1.55	5.3
U.K.	London	20.4	1.53	3.78
France	Limonge	18	1.58	3.45
Croatia	Zagreb	31	0.89	1.65
Spain	Barcelona	23.9	1.41	3.93
Greece	Athens	22.5	1.64	4.65
Germany	Berlin	25	1.99	4.99
	Braunschweig	25	1.81	4.8
	Bremen	27.5	1.88	5.06
	D¨usseldorf	22.5	1.8	4.68
	Frankfurt a. Main	22.5	1.8	4.68
	Hamburg	25	1.92	5.17
	Hannover	25	1.8	4.97
	Helgoland	30	1.82	5.65
	Hof	22.5	1.72	4.71
	List/Sylt	30	1.83	6.03
	M¨unchen	25	1.22	3.81
	N¨urnberg	22.5	1.38	3.67
	Saarbr¨ucken	22.5	1.79	4.62
	Stuttgart	22.5	1.24	3.07
	Weissenburg	22.5	1.31	3.88

Tab. 5.16: Data set of European stations.

It is worth notice that the shape parameter k ranges between about 0.9 and 1.5 in Italian territory, whereas k is higher, getting closer to k=2, in the northern European countries.

According to Pagnini and Solari research, parameters c and k are somewhat correlated. The fitting of the population data shows a noteworthy relation between c, k and the 50 years reference wind velocity $\bar{u}_{ref}$, therefore they proposed the expression of c obtained by a linear regression. It is a simple and reliable expression, directly applicable in the engineering and codification sectors, which joints the parent population and extreme value distribution of the mean wind speed models. This expression fits the measured data very well; the data provided by the recent Italian analyses, the old Italian analyses, and the analyses carried out in other countries are quite equally distributed and homogeneously contribute to the soundness of the obtained analytical relationship between the Weibull parameters k and c and the reference wind velocity $\bar{u}_{ref}$. The expression of $c = (0.2k - 0.12)\bar{u}_{ref}$ provides good estimates in a simple format.

Comparing this Weibull-CNR model with the one included in Eurocode formula (Eq. (5.20)), the former is based on a data set of mean wind velocity at a fixed height z = 10 m, instead the Weibull-EC model is related to $z = z_{cr}$ of the structure, which is the height of the cross-section where the critical vortex shedding phenomenon occurs. Considering that the distribution of the parent population of the mean wind velocity does not vary significantly with the height z at which the mean wind speed is measured, in the following it is assumed for sake of simplicity that z_{cr} = 10 m to have comparable Weibull functions.

As concerns the Weibull-EC model, it has a fixed shape parameter k=2 and a scale parameter equal to $\bar{u}_0 = 0.2 \cdot \bar{u}(R = 50 years; z = z_{cr})$. Therefore, the scale parameter $\bar{u}_0$ is a function of the mean wind velocity at a fixed height, which is defined by the code on the basis of the reference wind velocity $\bar{u}_{ref}$ and the exposure category. Table 5.17 shows the Weibull parameters for different exposure categories considering z_{cr} = 10 m as a constant.

u_{ref} (m/s)	k	*Exposure Category*	$\bar{u}_0$
25	2	I	5.87
		II	5.03
		III	4.61
		IV	3.86
		V	3.06
27	2	I	6.34
		II	5.44
		III	4.97
		IV	4.17
		V	3.30
28	2	I	6.58
		II	5.64
		III	5.16
		IV	4.32
		V	3.43
30	2	I	7.05
		II	6.04
		III	5.53
		IV	4.63
		V	3.67
31	2	I	7.28
		II	6.24
		III	5.71
		IV	4.78
		V	3.79

Tab. 5.17: Mean wind velocity $\bar{u}_{ref}$ and density function parameters values according to Weibull-EC model.

Table 5.17 considers possible standard conditions in Italian territory and it shows that the scale parameter $\bar{u}_0$ is more sensitive to exposure category variation than to the mean wind velocity $\bar{u}_{ref}$ value.

Exposure categories take account of wind direction and of roughness and topography of the terrain surrounding the construction in a simplified manner: mean wind velocity, turbulence intensity and peak velocity pressure depend on three parameters: terrain factor k_r, roughness length z_0 and minimum height

z_{min}, given as a function of the exposure category of the construction site. This is assigned as a function of the site geographical location and of the terrain roughness class, evaluated in qualitative terms. By following standard approach, the scale parameter is equal to $\bar{u}_0 = 0.2 \cdot \bar{u}_{ref} k_r \ln\left(z_{cr}/z_0\right) c_t$, in which c_t is the topography coefficient, given as a function of site topographic features, usually assumed equal to 1.

Exposure Category	$E[\bar{u}_0]$
I	6.62
II	5.68
III	5.19
IV	4.35
V	3.45

Tab. 5.18: Mean scale parameter $\bar{u}_0$ on varying exposure category according to Weibull-EC model.

Table 5.18 gives an idea of the scale parameter variation on exposure category according to Weibull-EC model.

A first general comparison between the two Weibull models is represented in Figure 5.36.

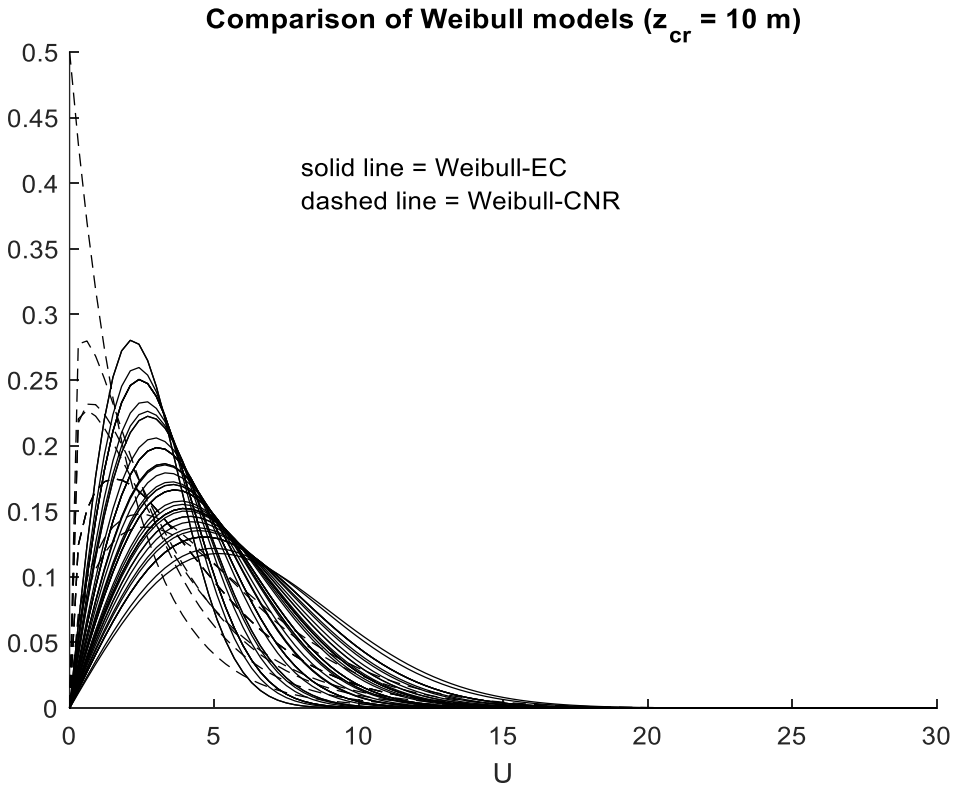

Fig. 5.36: Representation of all standard Weibull curves according to the two models.

At first glance it can be noted that Weibull-CNR curves tend to be flattened to the left of the diagram, due to the fact that this model considers different *k* values lower than 2 for different areas. Weibull-EC curves depend on a constant shape parameter *k*=2 so they are more "spread" in a wider range of mean wind velocity and they vary only on varying scale parameter $\bar{u}_0$. It is more difficult to identify how *c* or $\bar{u}_0$ influences the curves in the two models. It may be notice that *c* tends to be lower than $\bar{u}_0$ and for this reason Weibull-CNR curves tend to be higher for small values of mean wind velocity and lower for large values of mean wind velocity. Figure 5.37 shows the same comparison subdividing the curves for the Italian zones.

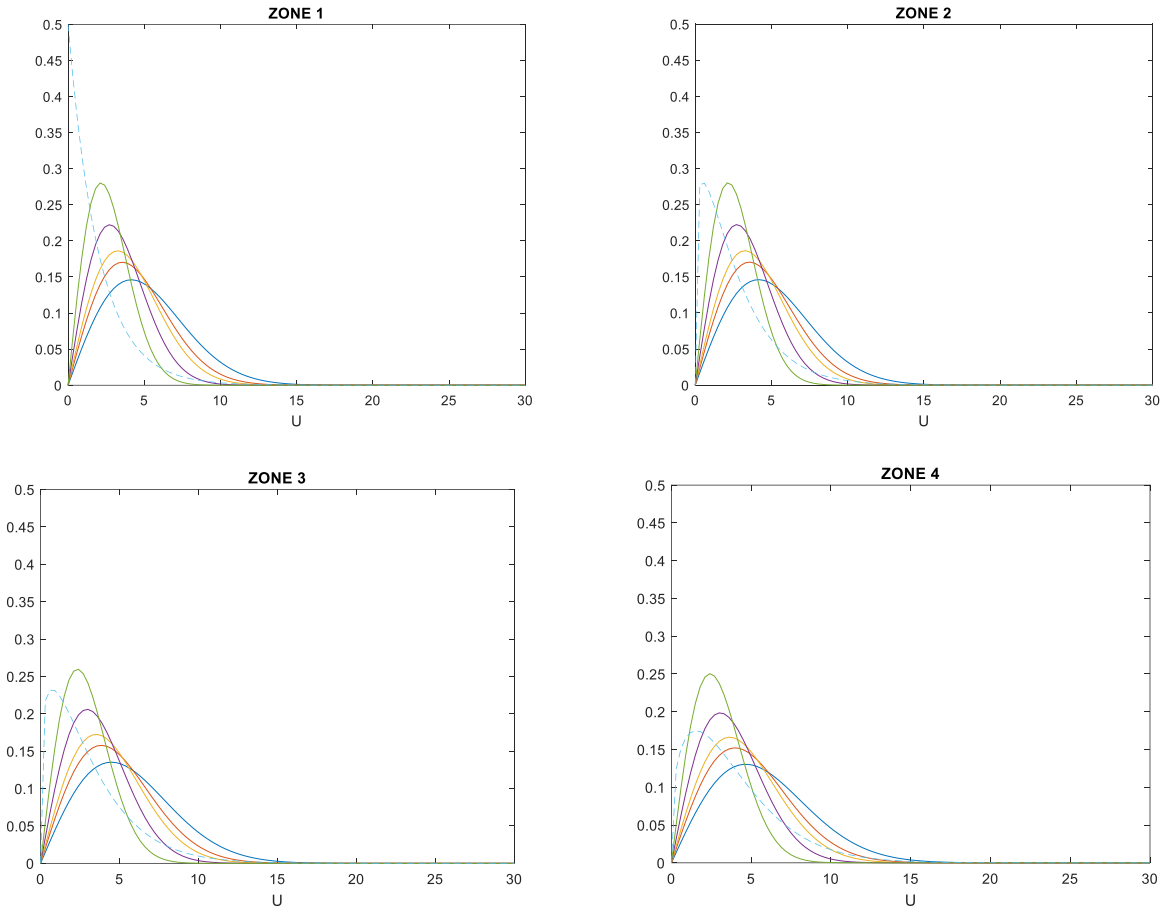

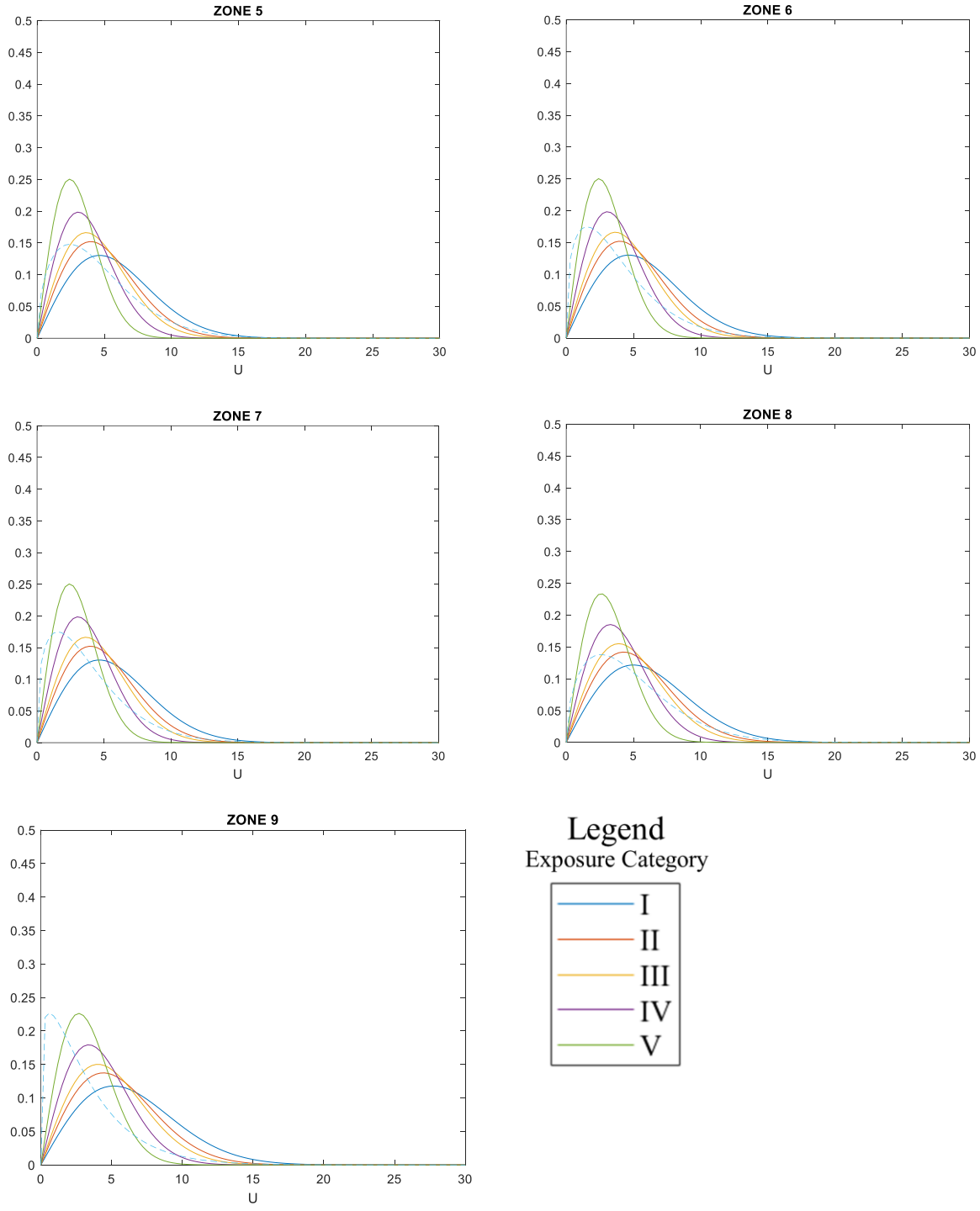

Fig. 5.37: Representation of Weibull curves according to the two models for different Italian zones (solid line = Weibull-EC; dashed line = Weibull-CNR).

It has been found that for higher structures with a z_{cr} > 10 m, only Weibull-EC curves change, flattening down (Fig. 5.38). As concerns fatigue analysis, this might significantly change fatigue damage prediction when z_{cr} is higher.

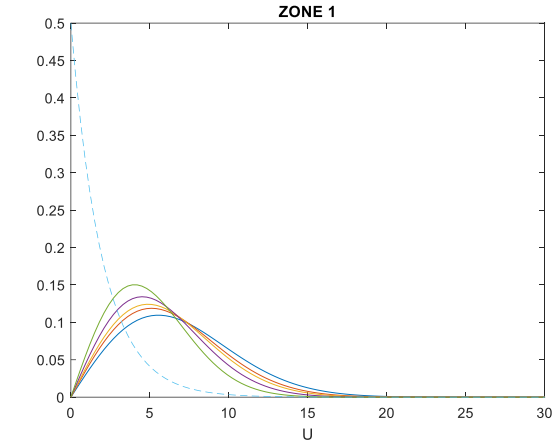
ZONE 1
0.5
0.45
0.4
0.35
0.3
0.25
0.2
0.15
0.1
0.05
0
0 5 10 15 20 25 30
U

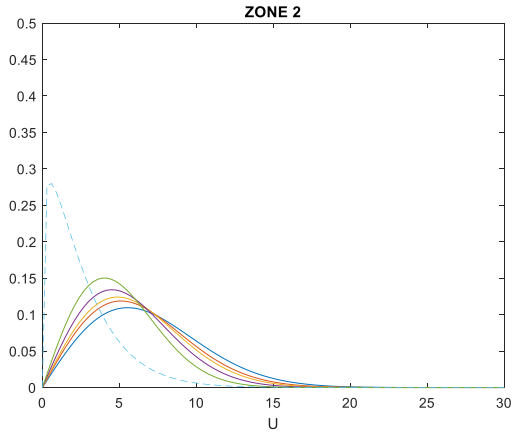
ZONE 2
0.5
0.45
0.4
0.35
0.3
0.25
0.2
0.15
0.1
0.05
0
0 5 10 15 20 25 30
U

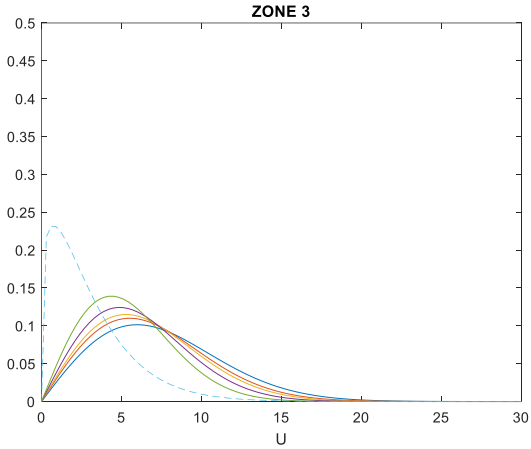
ZONE 3
0.5
0.45
0.4
0.35
0.3
0.25
0.2
0.15
0.1
0.05
0
0 5 10 15 20 25 30
U

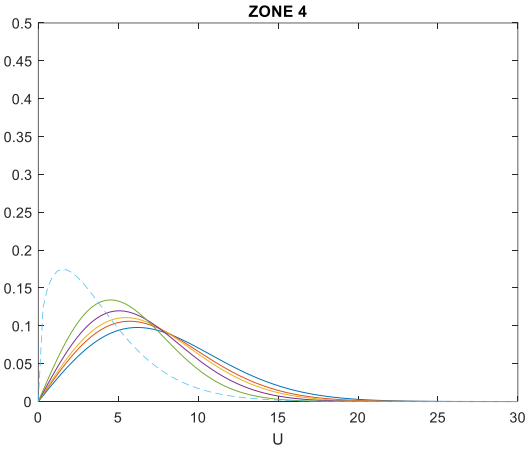
ZONE 4
0.5
0.45
0.4
0.35
0.3
0.25
0.2
0.15
0.1
0.05
0
0 5 10 15 20 25 30
U

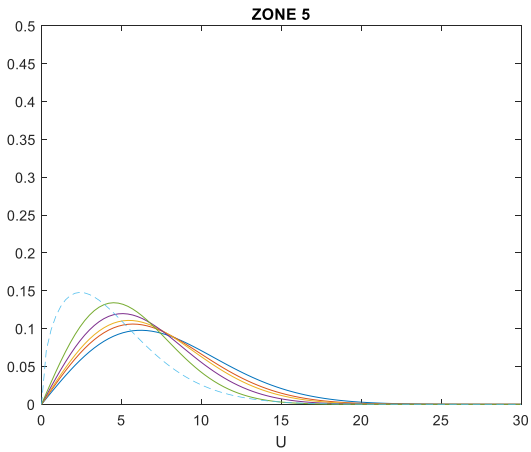
ZONE 5
0.5
0.45
0.4
0.35
0.3
0.25
0.2
0.15
0.1
0.05
0
0 5 10 15 20 25 30
U

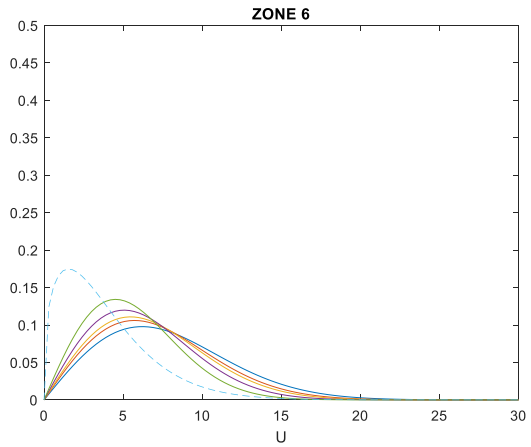
ZONE 6
0.5
0.45
0.4
0.35
0.3
0.25
0.2
0.15
0.1
0.05
0
0 5 10 15 20 25 30
U

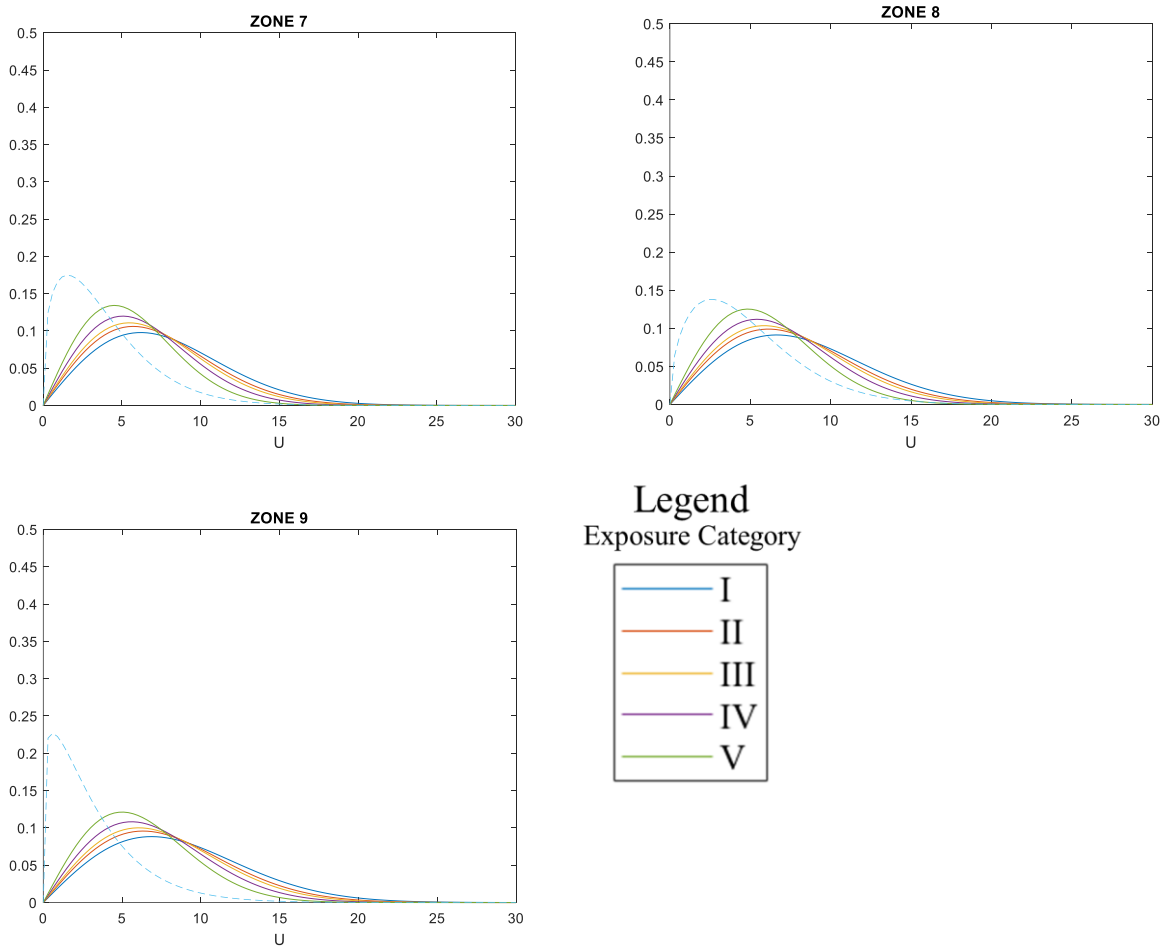

Fig. 5.38: Representation of Weibull curves according to the two models for different Italian zones (solid line = Weibull-EC; dashed line = Weibull-CNR); z_{cr} = 100 m.

In order to compare the scale parameters according to the two different Weibull model, Figure 5.39 shows c and $\bar{u}_0$ for different exposure categories. When exposure category tends to 1 (flatter terrains) the two Weibull models provide really different values for the scale parameter, when exposure category tends to 5 the two Weibull models provide values in the same range.

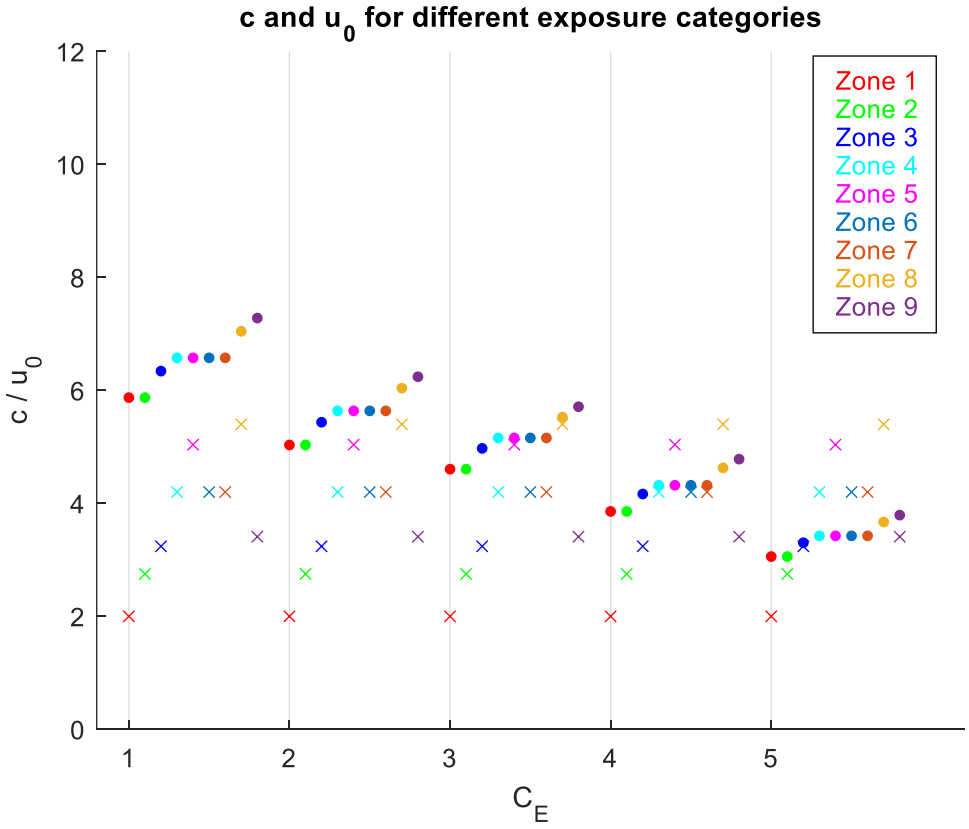

Fig. 5.39: Scale parameters according to Weibull-EC model ($\bar{u}_0$, points) and to Weibull-CNR model (c, crosses) for different exposure categories C_E.

Following all these considerations concerning the differences of the two Weibull models, it comes an attempt to establish the more suitable one with reference to the data set of Italian and foreign anemometric measures used for Weibull-CNR calibration (see Figure 5.35; Tables 5.15 and 5.16).

Firstly, Fig. 5.40 shows the Weibull curves of Italian stations (Tab. 5.15) subdivided with regard to Italian zones. It is also reported the standard Weibull-CNR curve associated with each zone. Then, Fig. 5.41 provides the Weibull curves of Italian stations (Tab. 5.15) subdivided with regard to exposure categories. It is also reported the standard Weibull-EC curve associated with each exposure category, considering an average value of k = 1.28 and values of $\bar{u}_0$ provided by Table 5.18.

In both Figures 5.40 and 5.41, solid lines represent Weibull curves of single Italian stations and dashed lines represent curves of Weibull-CNR (Fig. 5.40) or Weibull-EC (Fig. 5.41).

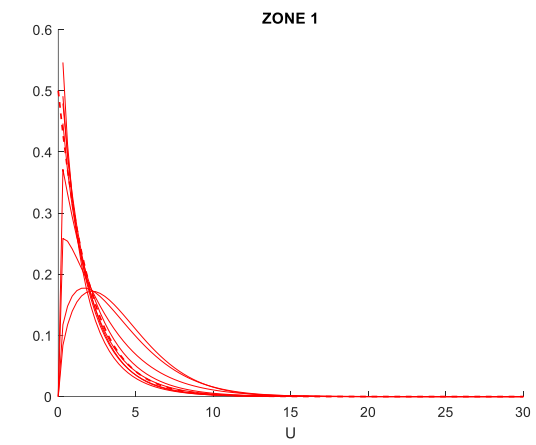
ZONE 1
0.6
0.5
0.4
0.3
0.2
0.1
0
0 5 10 15 20 25 30
U

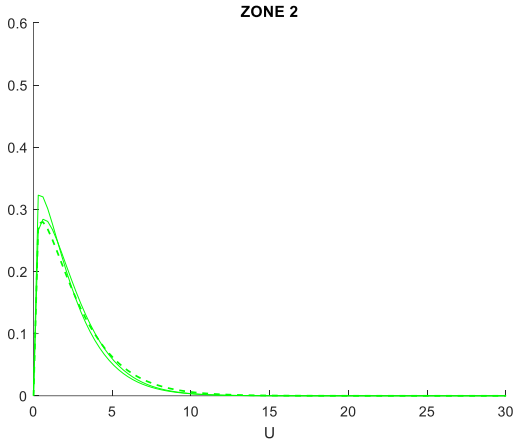
ZONE 2
0.6
0.5
0.4
0.3
0.2
0.1
0
0 5 10 15 20 25 30
U

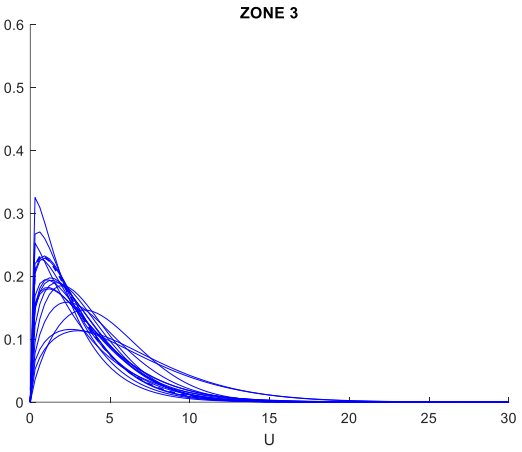
ZONE 3
0.6
0.5
0.4
0.3
0.2
0.1
0
0 5 10 15 20 25 30
U

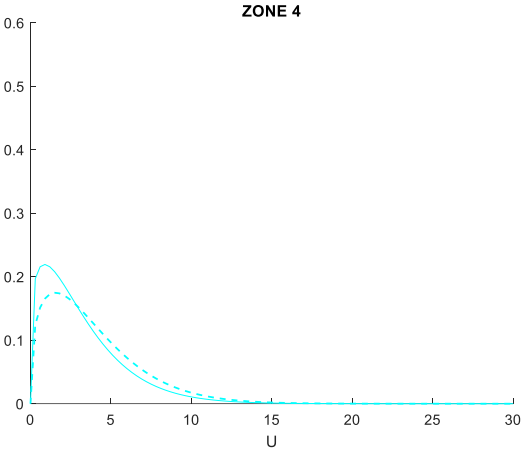
ZONE 4
0.6
0.5
0.4
0.3
0.2
0.1
0
0 5 10 15 20 25 30
U

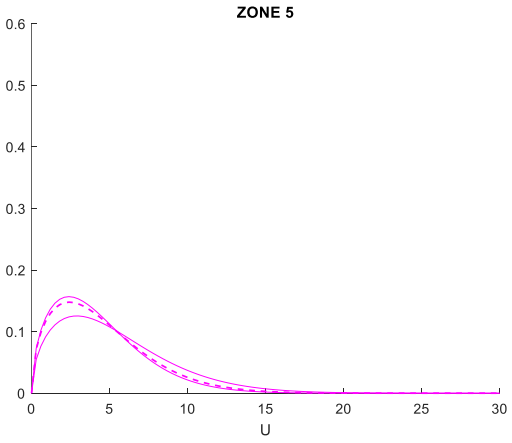
ZONE 5
0.6
0.5
0.4
0.3
0.2
0.1
0
0 5 10 15 20 25 30
U

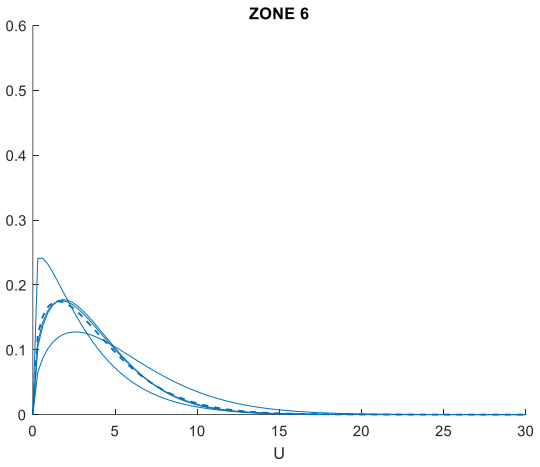
ZONE 6
0.6
0.5
0.4
0.3
0.2
0.1
0
0 5 10 15 20 25 30
U

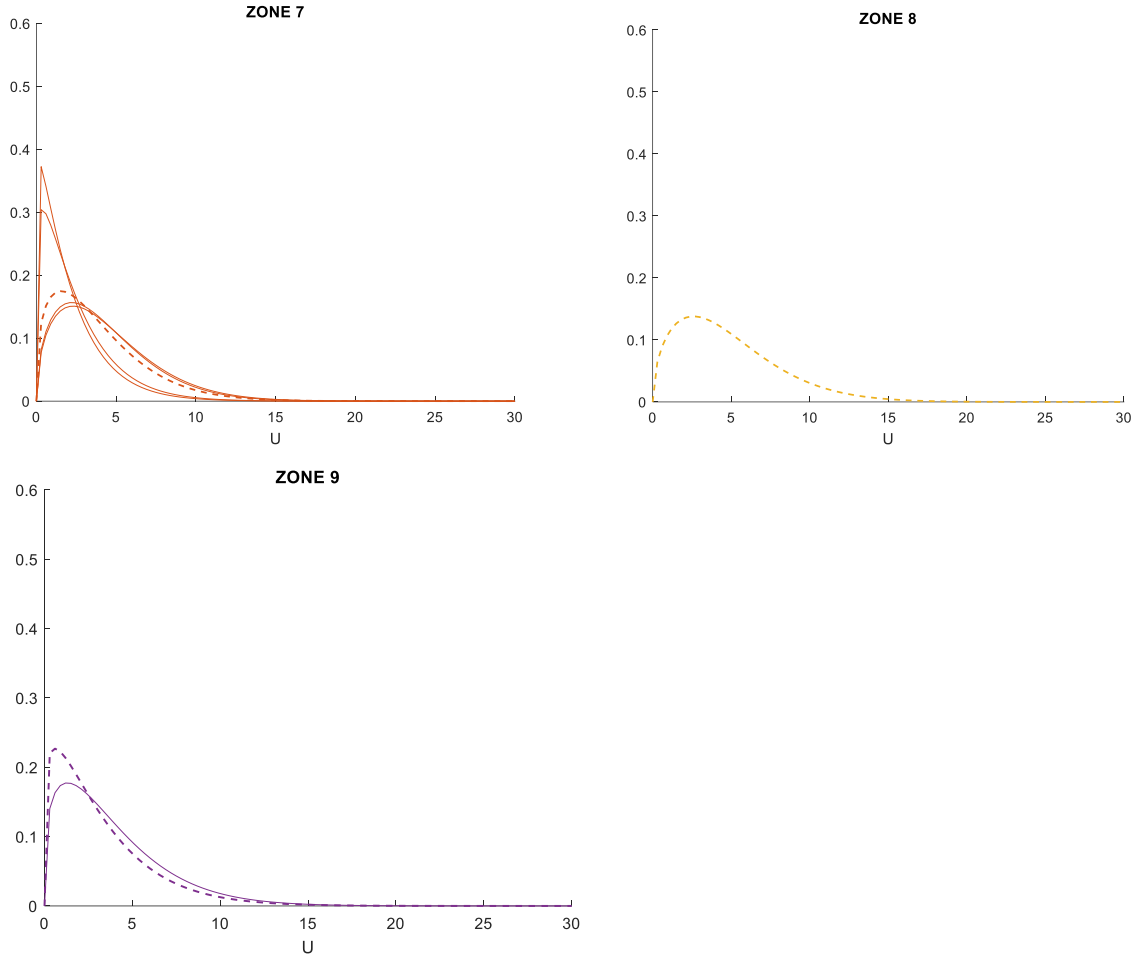

Fig. 5.40: Weibull functions of Italian stations grouped for Italian zones (solid lines) and related standard Weibull-CNR curve (dashed lines).

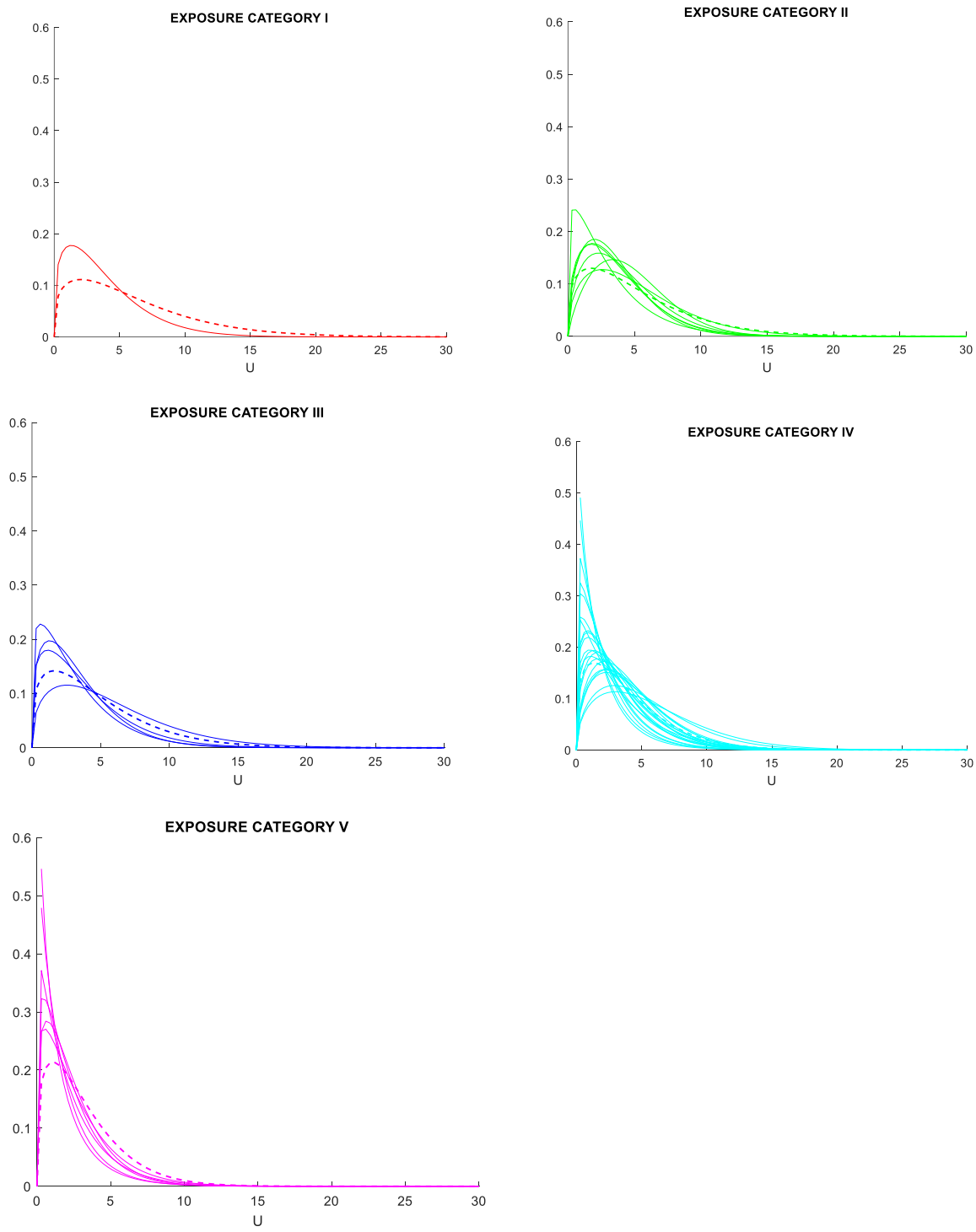

Fig. 5.41: Weibull functions of Italian stations grouped for exposure categories (solid lines) and related standard Weibull-EC curve (dashed lines).

In both models Weibull-CNR and Weibull-EC, stations are grouped unequally (for example, Zone 3 is densely populated, whereas other zones included only few stations). Moreover, it can not be easily derived from these diagrams if standard curves are on the safe side with respect to the stations samples,

because when a standard curve is higher in a range of small mean wind velocity it is lower in a range of large mean wind velocity, and vice versa. In fatigue analysis it is impossible to establish a priori which velocity range has a more relevant impact on damage accumulation.

In particular the two different approaches to define the Weibull scale parameter in CNR and EC methods make the comparison and the identification of the more suitable model more difficult. Figure 5.42 furnishes the scale parameters associated with Italian stations (points) in function of the zone (different colours) and in function of the exposure category (abscissa); in this diagram solid lines represents the scale parameter $\bar{u}_0$ definition according to Weibull-EC model and dashed lines represents the scale parameter *c* definition according to Weibull-CNR model. Parameter $\bar{u}_0$ varies slightly on the zone and largely on the exposure category, whereas parameter *c* varies only on the zone.

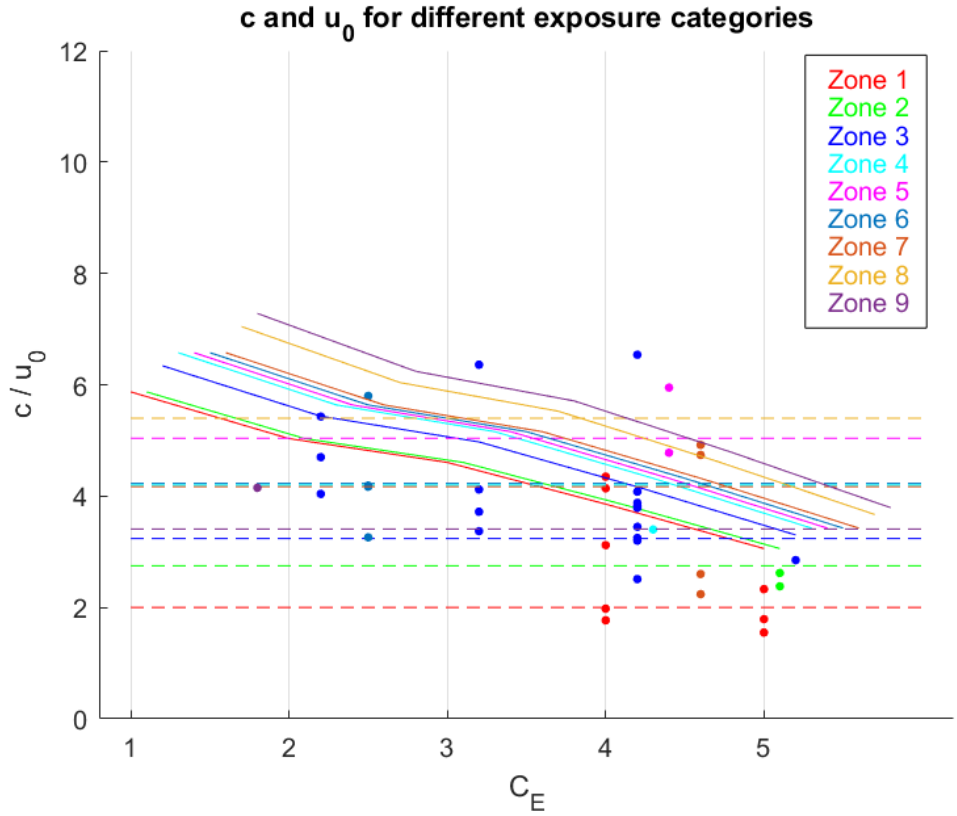

Fig. 5.42: Scale parameters according to Weibull-EC model ($\bar{u}_0$, solid lines) and to Weibull-CNR model (*c*, dashed lines) for different exposure categories C_E and different Italian zones; scale parameters values associated with each Italian station (points).

Since the point cloud representing the data set is widespread in the diagram, neither of Weibull models is a meaningful fitting according to this representation. Therefore, the choice is to take into consideration the correlation between the climatological parameters, as Pagnini and Solari studied, including this time predictions according to both Weibull models EC and CNR (Fig. 5.43, Fig. 5.44).

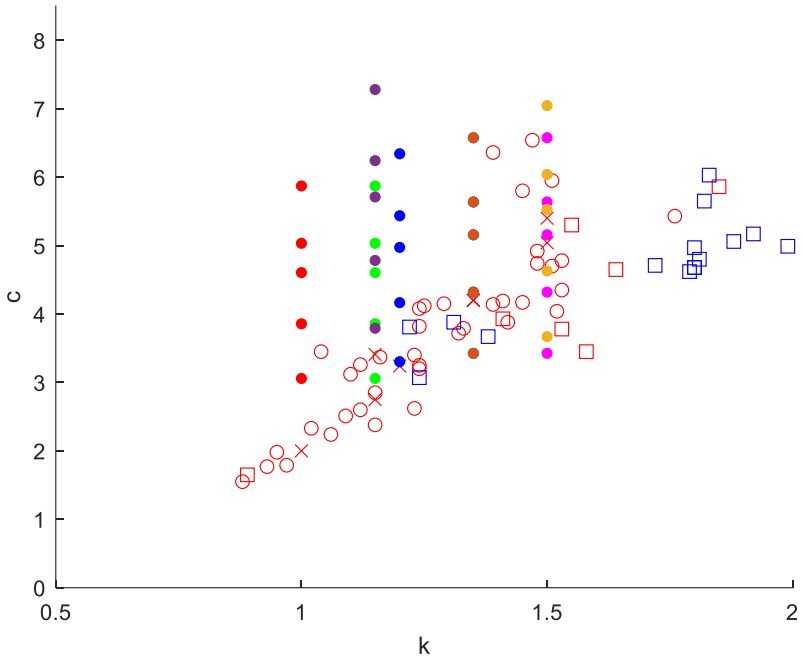

Fig. 5.43: Relationship between the Weibull parameters: red circles = Italian stations database (old and recent analyses); squares = European station database (red Pagnini and Solari 2016; blue Kemper and Feldmann, 2011); red crosses = Weibull-CNR; coloured points = Weibull-EC.

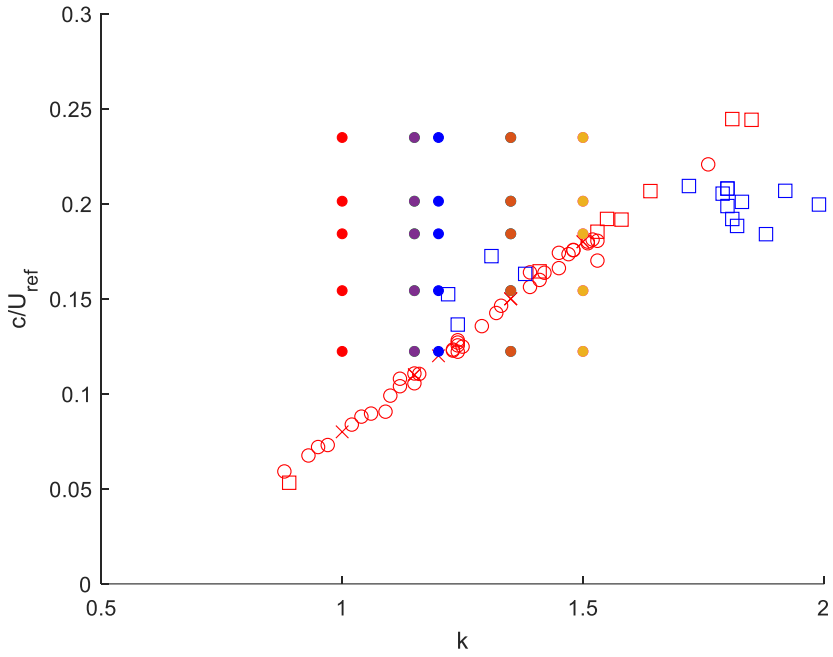

Fig. 5.44: Relationship between the Weibull parameters and the reference wind velocity: red circles = Italian stations database (old and recent analyses); squares = European station database (red Pagnini and Solari 2016; blue Kemper and Feldmann, 2011); red crosses = Weibull-CNR; coloured points = Weibull-EC.

In order to better visualize the points representing the relationship between the Weibull parameters and the reference wind velocity according to Weibull-EC model, an alteration is made in Fig. 5.43 and 5.44. Weibull-EC model considers k=2 as a constant, then all concerning points would be flattened to the right of the diagrams on a vertical line with abscissa equal to 2. That would make complicated a comparison between the scale parameter according the two approaches EC and CNR. For this reason in both CNR crosses and EC points the shape parameter k is given according to Table 5.14, in function of Italian zones (points with different colours). This allows to compare the two models with regard to the definition of the scale parameter c or $\bar{u}_0$.

It can be noted that the fitting of the population data shows a noteworthy relation between parameters c and k and the reference wind velocity $\bar{u}_{ref}$, this being evident for both Italian and European stations, although German stations (blue squares) show a slightly different behaviour. Since the difference becomes apparent going from Fig. 5.43 to Fig. 5.44, this is probably due to reference wind velocity $\bar{u}_{ref}$. Such reference parameter was likely evaluated with a different approach by European Wind Atlas (1989). Furthermore, wind speed measurements are strongly not homogeneous with the rest of the database. In conclusion, the linear approximation provided by Pagnini and Solari expression $c = (0.2k - 0.12)\bar{u}_{ref}$ (2016) is considered to fit the measured data very well.

It is evident, through red crosses positions in Fig. 5.44, that Weibull-CNR model is exactly consistent with sample data, since it is based on the linear approximation, while Weibull-EC model provides really scattered points. The latter does not express well the relationship between the Weibull parameters and the reference wind velocity, appearing less suitable to model the parent population of mean wind velocity on the base of the database taken into account.

It may be concluded that Weibull-EC model does not suit well Italian mean wind probabilistic conditions, as regards both shape and scale parameters. A clear consequence is that Equation (5.20) to calculate the number of cycles associated with VIV, N, is not sufficiently reliable at least in Italian territory. More accurate analyses are required for other countries.

To confirm this consideration, the most data populated Italian zone is considered. It deals with Zone 3, as Tab. 5.15, Fig. 5.40 and Fig. 5.42 show. The lowest and the highest Weibull curves provided by the stations measurements are considered as actual boundaries in this zone and they are called Weibull-min (Faeto station) and Weibull-max (Macerata station). These two stations are both considered in exposure category IV. Figure 5.45 represents these two curves and Weibull-CNR and Weibull-EC for zone 3 and C_E = IV.

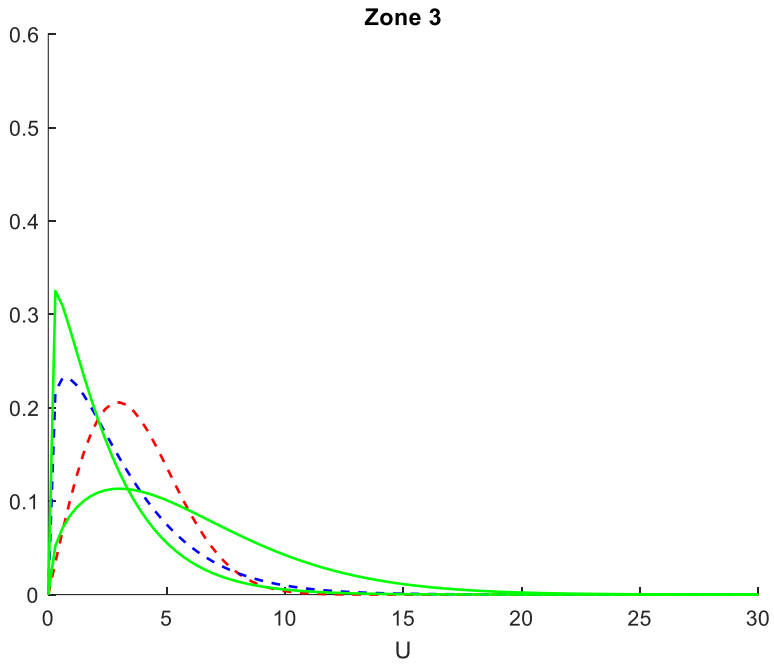

Fig. 5.45: Weibull-min and Weibull-max (green); Weibull-CNR (blue); Weibull-EC (red).

Solid lines are referred to actual curves obtained from statistical analysis of data measured by stations. Dashed lines are referred to standard curves obtained from the two different models, CNR and EC for the zone of the considered stations. The estimated errors of the standard curves is shown in Table 5.19.

Standard Weibull curve	*Actual Weibull curve*	*Error (difference between areas)*
Weibull-CNR	Weibull-min	Er(CNR) = 0.658
Weibull-CNR	Weibull-max	Er(CNR) = 0.205
Weibull-EC	Weibull-min	Er(EC) = 0.593
Weibull-EC	Weibull-max	Er(EC) = 0.645

Tab. 5.19: Errors of the two Weibull models in Zone 3 with respect to Weibull-min and Weibull-max.

Errors in Table 5.19 are estimated as the non-overlapping areas under the curves. They are quite similar, except the one referred to Weibull-CNR and Weibull-max curves, which is much lower, as expected from Figure 5.45. Although the errors are quite small concerning the areas under the curves, in fatigue analysis the error might be extremely greater because of the non-linearity of the phenomenon. Furthermore, different ranges of mean wind velocity have different weights on final damage estimation, but it is not possible to define a priori which wind velocity intervals are more important.

These statements can be confirmed by analysing fatigue of any example structure, which is located in Zone 3 in Italy, and by comparing results obtained by using different Weibull curves. It can be used the

Weibull-CNR model corresponding to Zone 3, the Weibull-EC model for Zone 3 and exposure category III, and the Weibull curves from the database (Tab. 5.15) associated with stations in Zone 3 with exposure category III.

The alongwind-induced fatigue verification method proposed in this thesis is applied to an antenna supporting metal pole, as an example. The structure is located in Zone 3, with exposure category III, and by adopting the Weibull-CNR model ($\bar{u}_{ref}$ = 27 m/s; k = 1.2; c = 3.24) the predicted fatigue life is equal to 271 years (detailed calculation). This calculated time would significantly change if a different Weibull function is taken into account. In the considered database (Tab. 5.15) there are four stations in Zone 3 associated with exposure category III: Grazzanise ($\bar{u}_{ref}$ = 26.1 m/s; k = 1.32; c = 3.72), Capodichino ($\bar{u}_{ref}$ = 30.5 m/s; k = 1.16; c = 3.37), Oriolo ($\bar{u}_{ref}$ = 33 m/s; k = 1.25; c = 4.12) and San Demetrio ($\bar{u}_{ref}$ = 38.8 m/s; k = 1.39; c = 6.36). Under the hypothesis that the considered structure is placed in these four locations, four different predictions of the fatigue life are obtained, shown in Table 5.20. Moreover, the Weibull-EC model for Zone 3 and exposure category III is considered and also in this case the fatigue life is calculated.

Weibull	$\bar{u}_{ref}$	k	c	σ_{ref}	T_F	*Er(CNR)*	*Er(EC)*
CNR	27 m/s	1.2	3.24	19.58 N/mm^2	271 years	-	-
EC	27 m/s	2	4.97	19.58 N/mm^2	4947 years	-	-
Grazzanise	26.1 m/s	1.32	3.72	17.97 N/mm^2	331 years	-18 %	$1.4 \cdot 10^3$ %
Capodichino	30.5 m/s	1.16	3.37	26.52 N/mm^2	106 years	156 %	$4.6 \cdot 10^3$ %
Oriolo	33 m/s	1.25	4.12	32.34 N/mm^2	54 years	405 %	$9.1 \cdot 10^3$ %
San Demetrio	38.8 m/s	1.39	6.36	48.69 N/mm^2	4.5 years	5957 %	$1.1 \cdot 10^5$ %

Tab. 5.20: Alongwind fatigue analysis of an antenna pole on varying mean wind velocity distribution models.

It seems that Weibull-CNR model is more advisable than Weibull-EC one, nevertheless the error is huge in most of the cases. This depends mainly on the differences in the standard deviation value of the alongwind stress in the critical section σ_{ref}, evaluated at reference wind velocity $\bar{u}_{ref}$. The differences in the mean wind velocity with a 50-year return period, at 10 m height on a flat homogeneous terrain with roughness length 0.05 m are not aim of this study, so it is considered also the case in which σ_{ref} does not vary, and different $\bar{u}_{ref}$, k and c only influence the Weibull functions of the parent population of the mean wind velocity (Tab. 5.21).

Weibull	$\bar{u}_{ref}$	*k*	*c*	σ_{ref}	T_F	*Er(CNR)*	*Er(EC)*
CNR	27 m/s	1.2	3.24	19.58 N/mm^2	271 years	-	-
EC	27 m/s	2	4.97	19.58 N/mm^2	4947 years	-	-
Grazzanise	26.1 m/s	1.32	3.72	19.58 N/mm^2	256 years	6 %	$1.8 \cdot 10^3$ %
Capodichino	30.5 m/s	1.16	3.37	19.58 N/mm^2	248 years	9 %	$1.9 \cdot 10^3$ %
Oriolo	33 m/s	1.25	4.12	19.58 N/mm^2	221 years	23 %	$2.1 \cdot 10^3$ %
San Demetrio	38.8 m/s	1.39	6.36	19.58 N/mm^2	53 years	412 %	$9.2 \cdot 10^3$ %

Tab. 5.21: Alongwind fatigue analysis of the antenna pole on varying parent population distribution models of the mean wind velocity.

It can be concluded that in the analysed case study, Weibull-CNR model suits well most of the specific locations cases, this not being true for Weibull-EC model. However, more accurate analysis on the extreme value distributions of the mean wind velocity are required in order to obtain a reliable stress value in the critical section. This is extremely more important in fatigue analysis since response parameters uncertainties increase exponentially calculating fatigue damage and fatigue life. Additionally, since the sensitivity of the final result, in terms of fatigue life, to the mean wind climate model is so high, its refinement is proved to be the crucial aspect of the fatigue model; any other refinement elsewhere would be useless if the mean wind climate model is uncertain. A first initial step in this direction is proposed below.

By establishing that Weibull-CNR model may probably be more reliable, at least in Italian territory, than Weibull-EC model, Equation (5.20), which estimates the number of cycles due to VIV, *N*, implicitly considering the local climatology through a Weibull distribution, may be hence modified:

$$N = 2V_N n_L \varepsilon_0 \left(\frac{\bar{u}_{cr}}{c}\right)^k \exp\left[-\left(\frac{\bar{u}_{cr}}{c}\right)^k\right] \tag{5.25}$$

where *k* is provided for different Italian zones by Tab. 5.14 or Tab. 4.3 (Section 4.3.2) and $c = (0.2k - 0.12)\bar{u}_{ref}$; V_N is the life-time in seconds, namely the nominal life-time of the structure or structural element; n_L is the natural frequency of crosswind mode; ε_0 is the bandwidth factor describing the band of wind velocities with vortex-induced vibrations, which is in the range 0.1 – 0.3 (0.3 is the value recommended by the code); $\bar{u}_{cr}$ is the critical wind velocity of vortex shedding (see Eq. (5.2)).

5.4.2. Band of wind velocities with vortex-induced vibrations

The equation which estimates the number of cycles due to VIV, *N*, (Eq. (5.20)) may be improved as concerns the implicit Weibull distribution of the parent population of the mean wind velocity (Section

5.4.1, Eq. (5.25)) but also as concerns the band of wind velocities associated with resonant vortex-induced vibrations. This second issue concerns the fact that the maximum response evaluation is estimated by the code procedure only in correspondence of one specific wind velocity, the critical one, and then the peak of the crosswind structural response is considered over a range of wind velocity (Fig. 5.46). This range depends on the bandwidth factor ε_0, whose value is recommended by the code equal to $\varepsilon_0 = 0.3$.

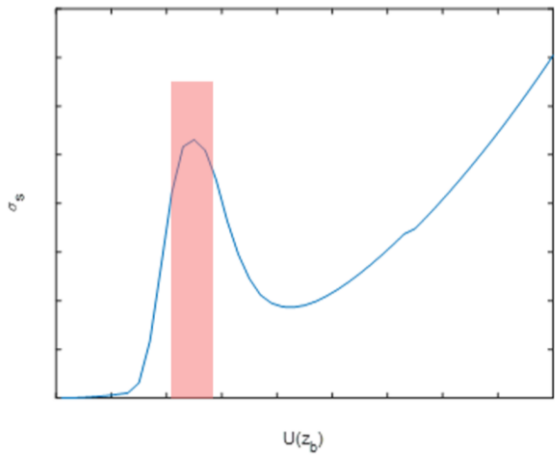

Fig. 5.46: Qualitative representation of the considered crosswind response (red) to estimate fatigue due to VIV effects according to Eurocode approach.

In Figure 5.46 it is shown that the standard approach considers the response as null on the whole range of mean wind velocity, except for the band of wind velocities associated with vortex-induced vibrations, given by the product ($\varepsilon_0 \bar{u}_{cr}$), which is an interval $\Delta\bar{u}$ which increases with the critical velocity value. With this range of wind speeds is associated a constant maximum response, which is the one calculated through the static equivalent crosswind force $F_{L,eq}(z)$ (Eq. (5.15)) associated with resonant vortex shedding. This approach tends to provide values of response on the safe side.

The present Section 5.4.3 deals with the bandwidth factor ε_0 estimation. Since it has been found that VIV-induced fatigue standard verification method results overmuch safe in most cases, it is likely that $\varepsilon_0 = 0.3$ is a value on the safe side, that in some cases should be reduced.

Section 5.2 introduces and describes the vortex shedding phenomenon, its effects and the related mathematical models. In particular, the “lock-in” aeroelastic phenomenon is characterized by critically large oscillations of the structure and aeroelastic instability in correspondence of a certain range of wind speeds. Over this range of mean wind velocity, the vortex shedding frequency n_s, proportional to $\bar{u}$, synchronizes with the natural frequency of the structure n_L (constant), therefore the proportionality between n_s and $\bar{u}$ is lost over an interval $\Delta\bar{u}$.

As wind speed increases, the vortex shedding frequency n_s at a section increases according to the Strouhal relationship (Eq. (5.1)). When is less than, but close to, the natural frequency (n_L) of the structure, and if the local motion amplitude is sufficiently large, the shedding frequency locks into the natural frequency. As wind speed increases further, the condition $n_s = n_L$ remains fixed until, at some upper limit of the lock-in range, the shedding frequency suddenly jumps to the value given by the natural Strouhal number.

The lock-in range increases with increasing local amplitude and it is this that determines the lower and upper values of n_s/n_L at which lock-in is initiated and terminated. This means that the wind velocity interval increases with low Scruton number *Sc*, since in this condition, vibrations induced by vortex shedding may be very large and dangerous. Therefore, lock-in high probability of occurrence depends on small *Sc* and low structural damping ξ_s.

Goswami et al. (1993a) studied experimentally vortex-induced vibration of circular cylinders, presenting a huge data set in detail. This work was aimed to re-evaluate and corroborate the data of Feng (1968), and to generate detailed experimental data necessary for the development of the current analytical model. Vortex-induced response of a spring-mounted circular cylinder was observed in a low-speed wind tunnel. Lift displacement of the cylinder and velocity fluctuations in the wake region were recorded. The experiments were designed to provide insight into the effects of various control variables upon the evolution of vortex shedding and vortex-induced vibration. The phenomenon of the fluid-body system synchronization was observed and recorded.

Figures 5.47 and 5.48 show response amplitudes as a function of reduced velocity for various levels of mechanical damping. The two figures correspond to two different sets of experiments carried out under identical conditions (Goswami et al. 1993a).

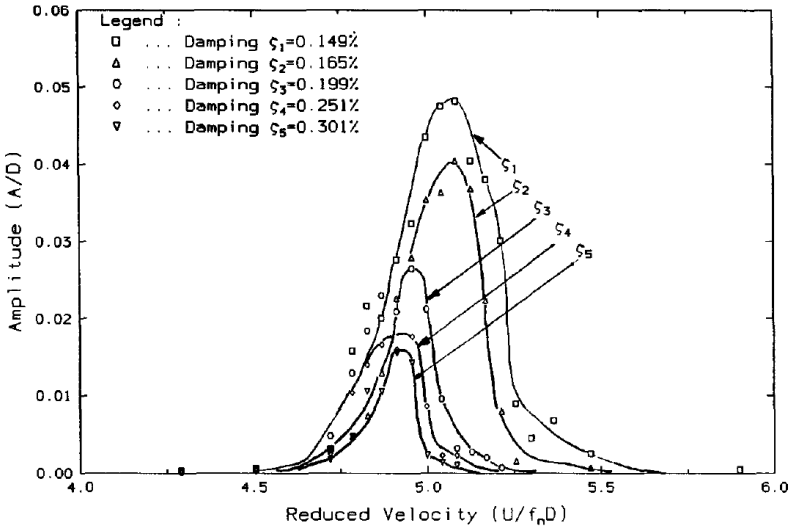

Fig. 5.47: Amplitude versus wind velocity for different mechanical damping values (run 1, © Goswami et al. 1993a).

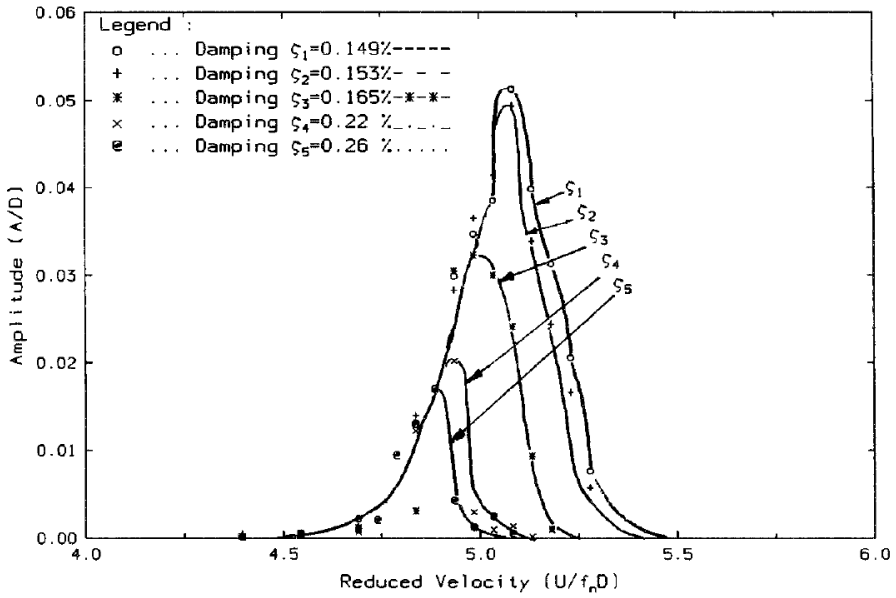

Fig. 5.48: Amplitude versus wind velocity for different mechanical damping values (run 2, © Goswami et al. 1993a).

It can be observed how the lock-in wind range increases with decreasing structural damping ξ_s.

The Scruton number (Eq. (5.3)) is a key parameter reflecting the combined effect of fluid-structure mass ratio and the level of mechanical damping ξ_s in the system. The experiments carried out by Goswami and co-workers provide the variation of maximum amplitude with Scruton number; by comparing their results to earlier empirical curve suggested by Griffin et al. (1975) the experimental investigations were validated (Fig. 5.49).

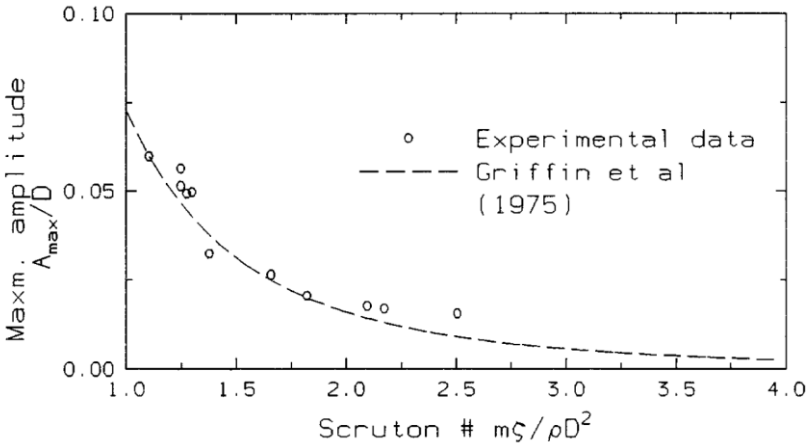

Fig. 5.49: Maximum amplitude versus Scruton number (© Goswami et al. 1993a).

In Fig. 5.50, the range of reduced velocities over which the wake was synchronized by the tested cylinder is plotted versus Scruton number. It may be seen that the lower limit of the lock-in band remains virtually un-affected by variations in mass ratio and mechanical damping. However, the upper limit of synchronization, i.e. the velocity at which lock-in ceases to occur, is reduced with increasing Scruton number thus causing the lock-in range to shrink. This feature is also evident from Figs. 5.47 and 5.48.

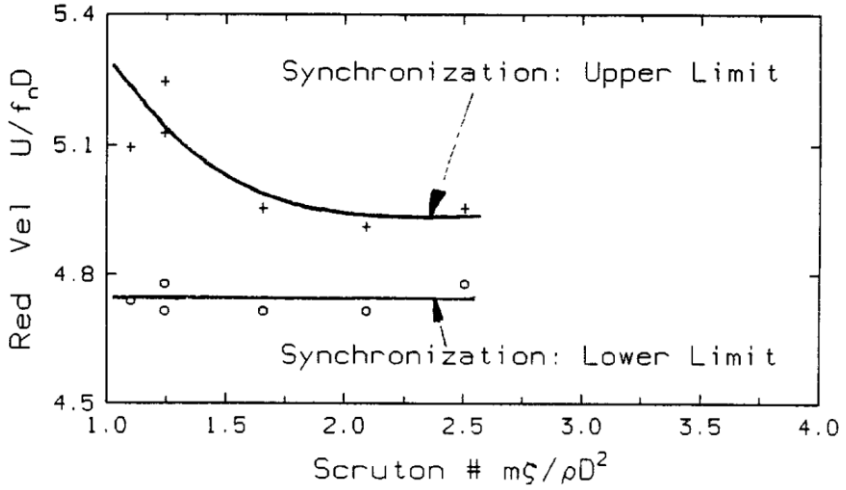

Fig. 5.50: Range of synchronization versus Scruton number (© Goswami et al. 1993a).

Based on the data of (Goswami et al., 1993a), ESDU 96030 (1998) proposes the following empirical criteria, one for two-dimensional flow and one for three-dimensional flow. The lower and upper velocity limits at which lock-in is initiated and terminated are defined in function of local motion amplitude. The influence of Scruton number *Sc* is empirically implicit.

For two-dimensional flow:

$$\bar{u}_{lower} = \left\{ 0.95 + 0.03\exp\left[-330 \left(\frac{\sigma_{d,max}}{b} \right)^{1.7} \right] \right\} \frac{n_L b}{St} \tag{5.26}$$

$$\bar{u}_{upper} = \left\{ 1.1 - 0.08\exp\left[-10^4 \left(\frac{\sigma_{d,max}}{b} \right)^{1.9} \right] \right\} \frac{n_L b}{St} \tag{5.27}$$

where $\sigma_{d,max}$ is the maximum deflection amplitude and b is the related local diameter (characteristic size at z_{cr}).

For three-dimensional flow there are no systematic data giving lock-in criteria. However, ESDU document provide a criteria based on a numerical analysis of the response data of Wootton (Wootton, 1968) for a number of models that exhibit lock-in behaviour. By iterative calculation, lock-in criteria for the tip region and for the main span region have been deduced. For the main span region the criteria are

approximated by Equations (5.26) and (5.27) for two-dimensional flow. For the tip region different criteria emerge which are approximated:

$$\bar{u}_{lower} = \left\{0.88 + 0.03\exp\left[-1.3\cdot10^{4}\left(\frac{\sigma_{d,max}}{b}\right)^{2.4}\right]\right\}\frac{n_L b}{St} \tag{5.28}$$

$$\bar{u}_{upper} = \left\{1.2 - 0.18\exp\left[-1.8\cdot10^{5}\left(\frac{\sigma_{d,max}}{b}\right)^{3.5}\right]\right\}\frac{n_L b}{St} \tag{5.29}$$

These criteria apply for increasing wind speed.

Since the present thesis focuses on cases of cantilever slender structures in a three-dimensional flow, Equations (5.28) and (5.29) are taken under consideration, in which $\sigma_{d,max}$ is the maximum deflection amplitude and b is the characteristic size at $z_{cr} = h_{tot}$.

The bandwidth factor ε_0 expression is here derived according to this approach and it is described below:

$$\varepsilon_0 = \frac{\bar{u}_{upper} - \bar{u}_{lower}}{\bar{u}_{cr}} = \left\{1.2 - 0.18\exp\left[-1.8\cdot10^{5}\left(\frac{\sigma_{d,max}}{b}\right)^{3.5}\right]\right\} - \left\{0.88 + 0.03\exp\left[-1.3\cdot10^{4}\left(\frac{\sigma_{d,max}}{b}\right)^{2.4}\right]\right\} \tag{5.30}$$

$$\varepsilon_0 = 0.32 - 0.18\exp\left[-1.8\cdot10^{5}\left(\frac{\sigma_{d,max}}{b}\right)^{3.5}\right] - 0.03\exp\left[-1.3\cdot10^{4}\left(\frac{\sigma_{d,max}}{b}\right)^{2.4}\right] \tag{5.31}$$

Equation (5.31) express the bandwidth factor ε_0 in function of the maximum normalized motion amplitude associated with VIV. The trend of ε_0 according to Eq. (5.31) is represented in Figure 5.51.

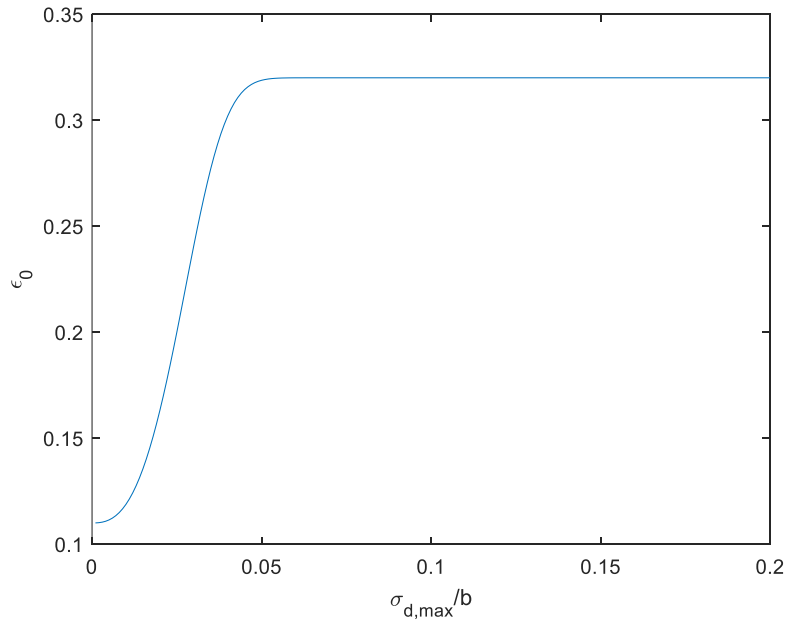

Fig. 5.51: Bandwidth factor ε_0 versus the maximum normalized motion amplitude associated with VIV.

The diagram shows that ε_0 varies in the range 0.1 – 0.3, approximately, which is consistent with code indications. The recommended value of 0.3 is taken by Eurocode on the safe side.

In order to prevent the underestimation of fatigue life, standard Equation (5.20) of the number of cycles due to VIV may be corrected. The first issue concerns the assumption of the Weibull-CNR model, then Equation (5.20) is modified in Equation (5.25) (Section 5.4.1), the second issue concerns the bandwidth factor ε_0, which may be expressed in function of the maximum normalized motion amplitude associated with VIV (Eq. (5.31)). The new proposal is summarized in Table 5.22.

Standard expression of N	
$N = 2V_N n_L \varepsilon_0 \left(\frac{\bar{u}_{cr}}{\bar{u}_0}\right)^2 \exp\left[-\left(\frac{\bar{u}_{cr}}{\bar{u}_0}\right)^2\right]$	(5.20)
$\bar{u}_0 = 0.2 \cdot \bar{u}_{ref} k_r \ln\left(z_{cr}/z_0\right) c_t$	
$\varepsilon_0 = 0.3$	
Proposed novel expression of N	
$N = 2V_N n_L \varepsilon_0 \left(\frac{\bar{u}_{cr}}{c}\right)^k \exp\left[-\left(\frac{\bar{u}_{cr}}{c}\right)^k\right]$	(5.25)
k	(Tab. 4.3); (Tab. 5.14)
$c = \left(0.2k - 0.12\right)\bar{u}_{ref}$	(Tab. 5.14)
$\varepsilon_0 = 0.32 - 0.18\exp\left[-1.8 \cdot 10^5 \left(\frac{\sigma_{d,max}}{b}\right)^{3.5}\right] - 0.03\exp\left[-1.3 \cdot 10^4 \left(\frac{\sigma_{d,max}}{b}\right)^{2.4}\right]$	(5.31)

Tab. 5.22: Standard expression and new proposal to calculate the number of cycles due to VIV, *N*.

A comparison between the two approaches is carried out in Section 5.4.4.

5.4.3. VIV response uncertainties propagation

The standard design procedure to evaluate VIV-induced fatigue, introduced Section 5.2.4, often results to underestimate the fatigue life prediction (Section 5.3), being too much on the safe side. The total damage is given by the ratio $D = N/N_C$, in which the number of cycles due to VIV, N, is usually overestimated by means of Equation (5.20) (Sections 5.4.1 and 5.4.2) and the number of load cycles leading to collapse, N_C, is usually underestimated.

N_C depends on the VIV response prediction and on the considered fatigue resistance *S-N* curve (Section 2.2; Eurocode 3, 2005; Eurocode 9, 1998; IIW Recommendations, 2016; Aluminum Design Manual,

2015). The number of load cycles leading to collapse is provided by $N_C = a_k \big/ \left(\Delta_{s,\max}^{m_k}\right)$ in which index *k* represents the considered *k*-th broken line of the *S*-*N* curve; $\Delta_{s,max} = 2\,\bar{y}_{s,max}$ is the maximum stress cycles amplitude correspondent with $\bar{u}_{cr}$ equal to twice as the mean maximum normal stress at the critical cross-section of the structure, calculated by the application of the static equivalent crosswind force $F_{L,eq}(z)$ (Eq. (5.15)). Whenever the response to VIV excitation is overestimated, which is usual applying approximated standard recommendations, N_C is hugely underestimated.

The propagation of uncertainties is a very critical issue in this procedure. The current Section 5.4.3 focuses on VIV predicted response, which is strongly affected by uncertainties. The standard spectral method (Section 5.2) evaluates the input parameters in a really approximated manner indeed. The role of input parameters uncertainties is analysed below, showing that errors in parameter estimates give rise to very large scatter in the response assessment, pointing out a set of quantities whose role is crucial.

It was estimated that the more sophisticated approach according to ESDU 96030 (1998) is subjected to a quite large uncertainty of calculated responses. It is not possible to provide simple quantitative guidance concerning this issue. If the response is of the random amplitude type the comparison with those full-scale measurements considered to be the most reliable and other wind-tunnel data suggests that the uncertainty in the peak standard deviation amplitude will be about 15% to 20%. If the response prediction shows that multiple solutions of the narrow-band type exist then the structure is more unstable and the uncertainty in the calculated values is likely to be greater (on average, about ± 30%).

The standard spectral method proposed by Eurocode 1 (2005) and CNR (2008, 2018) is expected to be subjected to much higher uncertainties. Daly (1986) showed 64 chimneys which have been experimentally or full-scale investigated, comparing the observed response with the predicted one according to spectral method (Fig. 5.52). It can be observed that in many cases Vickery and Basu model hugely overestimates the response to VIV, being much on the safe side and losing its reliability.

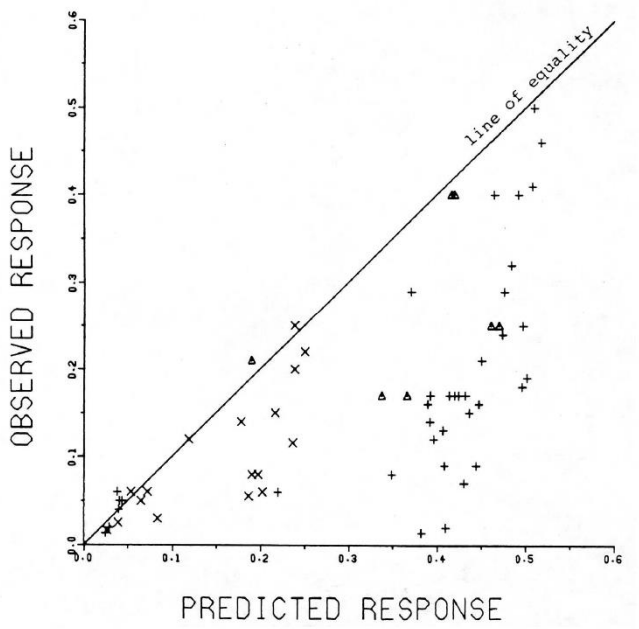

Fig. 5.52: Observed response versus predicted response of different chimneys (© Daly, 1986).

It is worth notice that the uncertainties analysis carried out in the present Section 5.4.3 deals with a comparison between the analytical predicted responses and numerical estimations of example chimneys (Section 5.3) instead of more reliable full-scale measurements or wind-tunnel data. Also the numerical model is based on spectral model according to Pagnini and Piccardo (2017) generalized gust factor technique. The analysis considers inherent randomness and epistemic uncertainties and disregards errors due to the calculation model.

Let $\tilde{R}$ be a quantity representative of the response of a structural system. It can be expressed as the sum of the estimated response in the parameters, R, and of the error committed by the calculation model. In the range of interest of this study, the information about the error committed by the calculation model is scanty. By considering as adequate the model of the structural behaviour which estimates the response R, this estimation is a function of a set of parameters listed by a vector $\boldsymbol{x} = \{x_1, x_2, .. x_i ..\}^T$. As the evaluation of these quantities is affected by uncertainties, the errors inherent their estimate propagate over R. A number of procedures exist which allow to propagate the uncertainties; some of them are particularly advantageous when the relationship which links R to $\boldsymbol{x}$ is analytical. Referring to Kareem (1987), Solari (1996) and Pagnini and Repetto (2012) for a brief overview of the different procedures in the field of wind engineering, the present work recalls the mean value Taylor series expansions (referred to as TSE).

TSE expands the original function around the mean value of $\boldsymbol{x}$, i.e. $\boldsymbol{x}_0 = \{x_{01}, x_{02}, .. x_{0i} ..\}^T$:

$$R(\boldsymbol{x}) \cong R\Big|^{\boldsymbol{x}_0} + \sum_i (x_i - x_{i0}) \frac{\partial R}{\partial x_i}\Big|^{\boldsymbol{x}_0} + \frac{1}{2}\sum_{ij}(x_i - x_{i0})(x_j - x_{j0}) \frac{\partial^2 R}{\partial x_i \partial x_j}\Big|^{\boldsymbol{x}_0} + \ldots \tag{5.32}$$

where the superscript $\Big|^{\boldsymbol{x}_0}$ denotes quantities evaluated in $\boldsymbol{x}_0$. Applying statistical operators to Eq. (5.32), the statistical moments of R are obtained as a function of the statistical moments of $\boldsymbol{x}$.

The approximation of Eq. (5.32) is usually taken at the first order. The use of derivative terms of order higher than the first increases the precision in a neighbourhood of the expansion point, but is endowed by three main drawbacks: (1) it is a time consuming task for a large vector $\boldsymbol{x}$; (2) statistical moments of order higher than two are usually unavailable; (3) when the uncertainties are large, the precision might decrease when the actual value of $\boldsymbol{x}$ is far from the expansion point. However, the error of the linear approximation can be bounded by using the second order terms to derive the mean value of R, while the variance is calculated retaining up to the first order terms, but using such mean value (Solari, 1997):

$$E[R] \cong R\Big|^{\boldsymbol{x}_0} + \vartheta \cdot \frac{1}{2}\sum_{ij} \frac{\partial^2 R}{\partial x_i \partial x_j}\Big|^{\boldsymbol{x}_0} Cov[x_i, x_j] \tag{5.33}$$

$$V[R] \cong \sum_{ij} \frac{\partial R}{\partial x_i}\Big|^{\boldsymbol{x}_0} \frac{\partial R}{\partial x_j}\Big|^{\boldsymbol{x}_0} Cov[x_i, x_j] + \vartheta \cdot \frac{1}{4}\sum_{ijhk} \frac{\partial^2 R}{\partial x_i \partial x_j}\Big|^{\boldsymbol{x}_0} \frac{\partial^2 R}{\partial x_h \partial x_k}\Big|^{\boldsymbol{x}_0} Cov[x_i, x_j] Cov[x_h, x_k] \tag{5.34}$$

where $E[.]$, $V[.]$ and $Cov[.]$ are the mean, the variance and the covariance operators; $\vartheta = 0$ approximates Eq. (5.32) at the first order (in the following related to as FOSM method); $\vartheta = 1$ considers the second order terms for the calculation of the mean.

Let $R_1(\boldsymbol{x})$ and $R_2(\boldsymbol{x})$ be two different quantities of the structural response. In general, they are correlated. Expanding R_1 and R_2 in Taylor series as in Eq. (5.32), their mean values and variances can be obtained by Eqs. (5.33) and (5.34); the covariance is expressed by:

$$Cov[R_1, R_2] \cong \sum_{ij} \frac{\partial R_1}{\partial x_i}\Big|^{\boldsymbol{x}_0} \frac{\partial R_2}{\partial x_j}\Big|^{\boldsymbol{x}_0} Cov[x_i, x_j] + \vartheta \cdot \frac{1}{4}\sum_{ijhk} \frac{\partial^2 R_1}{\partial x_i \partial x_j}\Big|^{\boldsymbol{x}_0} \frac{\partial^2 R_2}{\partial x_h \partial x_k}\Big|^{\boldsymbol{x}_0} Cov[x_i, x_j] Cov[x_h, x_k] \tag{5.35}$$

TSE is particularly suitable when $R(\boldsymbol{x})$ is described by analytical models. In this case, the procedure can be implemented through symbolic calculation tools. Moreover, facing with few parameters, TSE can be developed by closed form solutions, giving a direct functional relationship which links R to each uncertain quantity. However, when $R(\boldsymbol{x})$ is a non-linear function and the uncertainties are very large, TSE evaluation loses precision.

The most uncertain parameters directly involved in standard spectral method are the equivalent mass per unit length, m_e, the Scruton number, Sc, the aerodynamic damping parameter, K_a, and the normalized limiting amplitude a_L. In fact, by considering Eq. (5.11), K_a and Sc influence the peak deflection factor g_s and all four parameters influence the standard deviation of the deflection σ_s, also called $\sigma_{d,max}$ in the

present thesis. The formulation taken into account includes Equations (5.11), (5.15), (5.16), (5.17), (5.18) and (5.19), then with the influence function technique the bending moment is determined considering the structure as a cantilever, therefore the normal maximum stress at the critical section $\overline{y}_{s,max}$ can be estimated by the Navier equation according to Saint Venant model.

Therefore, quantities K_a, Sc, m_e and a_L can be grouped in the vector $\boldsymbol{x}$. In this study, they are considered uncorrelated.

Appling FOSM TSE (Eqs. (5.33) and (5.34) with ϑ=0) to the considered formulation to estimate VIV response, and considering the effect related to a given uncertain parameter x_i, the mean value and the coefficient of variation of the normal maximum stress at the critical section can be expressed by:

$$E\left[\overline{y}_{s,max}\right] \cong \overline{y}_{s,max}\Big|^{\mathbf{x}_0} \tag{5.36}$$

$$\rho_i\left[\overline{y}_{s,max}\right] \cong \Pi_{x_i}\left[\overline{y}_{s,max}\right]\rho_i\left[x_i\right] = \left(\frac{\partial \overline{y}_{s,max}}{\partial x_i}\Big|^{\mathbf{x}_0} \frac{x_{0i}}{\overline{y}_{s,max}\Big|^{\mathbf{x}_0}}\right)\rho_i\left[x_i\right] \tag{5.37}$$

where $\rho_i\left[x_i\right]$ is the coefficient of variation of the parameter x_i and $\Pi_{x_i}\left[\overline{y}_{s,max}\right]$ is the propagation factor.

Taking the input parameters vector $\boldsymbol{x}$ under investigation, the analytical development of $\Pi_{x_i}\left[\overline{y}_{s,max}\right]$ is simple and expressive and supplies some general, even approximated, information about the role of uncertainties over the overall response.

Among the four considered parameters, the most relevant role is played by K_a and Sc, in a quite similar and opposing relevance. Their uncertainties propagates through both the peak deflection factor g_s and the standard deviation of the deflection $\sigma_{d,max}$, mainly through the latter. Each of them, K_a or Sc, contrasts its own effect on $\sigma_{d,max}$ and g_s. Although each of these two parameters slightly balances its propagation effect in $\overline{y}_{s,max}$, they remain the two most influencing parameters, because they influence much more $\sigma_{d,max}$ than g_s. The role of m_e and a_L is less important, equal in $\sigma_{d,max}$ and in $\overline{y}_{s,max}$ because they do not influence the peak deflection factor g_s.

In order to complete the above considerations as concerns fatigue, the same kind of analysis is carried out considering the total damage $D = N/N_C$. In this case, the input parameters vector is $\boldsymbol{x} = \{V_N, n_L, \varepsilon_0, \overline{u}_{cr}, \overline{u}_0, m(z), \overline{y}_{max}, h, \Delta_C, m_k, \gamma_F, (b/2)\}^T$ and also Equation (5.20) is taken into account. Δ_C is the detail category corresponding to $N_C = 2 \times 10^6$, used together with m_k to evaluate N_C associated with $\Delta_{s,max}$. Again, input parameters are considered uncorrelated for sake of simplicity, even if they are not actually.

Among the concerning input parameters, only V_N, n_L, ε_0, $\overline{u}_{cr}$, $\overline{u}_0$ influence the estimation of N, almost in equal amount. The first three parameters are linear with N, the last two are opposed to each other and

influences the number of load cycle estimation quite linearly too. On the other hand, the quantities n_L, $m(z)$, $\bar{y}_{max}$, h, Δ_C, m_k, γ_F, $(b/2)$ influence very much N_C. It is worth notice that if the correlation between parameters was taken into account, also $\bar{u}_{cr}$ would influence N_C. Uncertainties of m_k propagate more than the others because it is an exponent, but the uncertainty inherent the fatigue curve parameters for steel details are mainly quantified as the distance between two consecutive curves on the grid, therefore as the uncertainties of Δ_C, rather than the slopes of the curves. Multiple fatigue tests are carried out at a given stress level, in strictly controlled conditions, in order to define reliable *S-N* curves. Uncertainties are due to experimental tests, sensitive to a variety of uncertain factors, and they are also due to the method adopted to derive the standard curves and to the non-coincidence between the reference details and the joint under analysis. Uncertainties could be even larger for other materials, such as aluminium alloys and composites materials (Muc, 2002, Jha et al., 2005).

Leaving out the m_k uncertainties propagation role and leaving out also the safety factor and the geometrical parameters, all other quantities uncertainties, n_L, $m(z)$, $\bar{y}_{max}$, Δ_C, exponentially propagate through the term N_C and, consequently, D.

Focusing on uncertainties propagation analysis in the response prediction, the procedure summarized in the present Section is applied to two case studies. These are the example chimneys analysed in Sections 5.3.3 and 5.3.4, Chimney 2b and Chimney 3, respectively. Tables 5.23 and 5.24 shows the obtained results.

	a_L	K_a	Sc	m_e
$\Pi_{x_i}\left[\sigma_{d,max}\right]$	0.97	4.50	-4.51	-0.02
$\Pi_{x_i}\left[g_s\right]$	0	-0.81	0.81	0
$\Pi_{x_i}\left[\bar{y}_{s,max}\right]$	0.97	3.69	-3.70	-0.02
$E[x_i]$	0.4	0.658	7.49	1442
$\rho_i\left[x_i\right]\%$	30	30	30	30
$E\left[\bar{y}_{s,max}\right]$	69.15	69.15	69.15	69.15
$\rho_i\left[\bar{y}_{s,max}\right]$ %	29.08	110.68	-111.14	-0.46
$\rho_i\left[x_i\right]\%$	50	30	30	15
$\rho_i\left[\bar{y}_{s,max}\right]\%$	48.47	110.68	-111.14	-0.23

Tab. 5.23: Statistical moments of $\boldsymbol{x}=\{K_a, Sc, m_e, a_L\}^T$ and TSE uncertainty propagation (Chimney 2b).

	a_L	K_a	Sc	m_e
$\Pi_{x_i}\left[\sigma_{d,max}\right]$	0.05	6.66	-7.13	-0.48
$\Pi_{x_i}\left[g_s\right]$	0	-0.93	0,93	0
$\Pi_{x_i}\left[\bar{y}_{s,max}\right]$	0.05	5.73	-6.21	-0.48
$E[x_i]$	0.4	0.74	9.87	164
$\rho_i\left[x_i\right]\%$	30	30	30	30
$E\left[\bar{y}_{s,max}\right]$	34.67	34.67	34.67	34.67
$\rho_i\left[\bar{y}_{s,max}\right]$ %	1.43	171.90	-186.19	-14.28
$\rho_i\left[x_i\right]\%$	50	30	30	15
$\rho_i\left[\bar{y}_{s,max}\right]\%$	2.39	171.90	-186.19	-7.14

Tab. 5.24: Statistical moments of $\boldsymbol{x}=\{K_a, Sc, m_e, a_L\}^T$ and TSE uncertainty propagation (Chimney 3).

By applying FOSM TSE (Eqs. (5.36) and (5.37)) on these two case studies, the uncertainties propagation of $\boldsymbol{x}=\{K_a, Sc, m_e, a_L\}^T$ through VIV response, evaluated by means of standard spectral method, is investigated.

Information given by the propagation factors are included in the first three rows of each Table. Quantities K_a and Sc are the most relevant and they slightly influence the peak deflection factor g_s, they mainly influence the standard deviation of the deflection $\sigma_{d,max}$ and therefore the normal maximum stress at the critical section $\bar{y}_{s,max}$. Their role results quite similar and opposed. The role of m_e and a_L is less important, equal in $\sigma_{d,max}$ and in $\bar{y}_{s,max}$ because they do not influence the peak deflection factor g_s.

The mean value and the coefficient of variation of the input parameters are reported in the fourth and the fifth rows. At first stage it is considered that all x_i quantities are subjected to the same level of uncertainty, i.e. $\rho_i\left[x_i\right]$=30%. Then, the mean value and the coefficient of variation of the normal maximum stress at the critical section are shown. Chimney 2b is characterized by a crosswind maximum stress, evaluated in the mean values of the parameters, equal to $E\left[\bar{y}_{s,max}\right]$ = 69.15 N/mm^2. Chimney 3 is characterized by $E\left[\bar{y}_{s,max}\right]$ = 34.67 N/mm^2. The coefficients of variation with respect to K_a and Sc are the

largest, especially in Chimney 3. They reach the value $\rho_{Sc}\left[\overline{y}_{s,max}\right]$ = 186.19% (Chimney 3), which is extremely critical.

Then, it is considered that x_i quantities are subjected to different levels of uncertainty. It is chosen $\rho_{a_L}\left[a_L\right]$=50%, $\rho_{K_a}\left[K_a\right]$=30%, $\rho_{Sc}\left[Sc\right]$=30%, $\rho_{m_e}\left[m_e\right]$=15%, according to qualitative considerations on the way in which input parameters are provided by the code (Section 5.2.4) and according to considerations on damping by Pagnini and Repetto (2012). The related coefficient of variation of the normal maximum stress at the critical section is shown in the last row of the two Tables. Obviously, only $\rho_{a_L}\left[\overline{y}_{s,max}\right]$ and $\rho_{m_e}\left[\overline{y}_{s,max}\right]$ changes with respect to the previous analysis with all $\rho_i\left[x_i\right]$=30%.

The critical issue is that the greatly uncertain input parameters representative of damping, are also the most relevant in the propagation of uncertainties through VIV response prediction. Chimney 3 is the more sensitive as concerns the propagation of uncertainties inherent three of the four considered parameters (K_a, Sc and m_e), including the most critical ones (K_a and Sc). This example structure is smaller, more lightweight and more rigid of Chimney 2b, and it is characterized by a slightly larger Sc.

In conclusion of the present Section 5.4.3, since the propagation of errors is exponentially significant in VIV response and fatigue estimations, an extremely accuracy in input parameters definition is required, paying main attention on K_a and Sc quantities. The use of integrating provisions and recommendations, as well as available experimental or numerical data, is strongly recommended.

5.4.4. Comparison between standard method and the proposed formulation

As standard method to evaluate VIV-induced fatigue (Eurocode 1, 2005; CNR 2008, 2018), introduced in Section 5.2.4, tends to hugely underestimate the fatigue life prediction (Section 5.3), a new proposal to evaluate the number of cycles due to VIV, N, is introduced in Sections 5.4.1 and 5.4.2. Equation (5.20) is reformulated by means of Equations (5.25) and (5.31) (see Table 5.22).

A comparison between standard method and the proposed formulation is carried out, concerning the four example chimneys introduced and analysed in Sections 5.3.1, 5.3.2, 5.3.3 and 5.3.4. Table 5.25 reports, as concerns these four case studies, the fatigue life predictions obtained from the numerical analysis and the results obtained from VIV-induced fatigue standard method (calculations in Sections 5.3.1, 5.3.2, 5.3.3 and 5.3.4).

	Numerical analysis	Standard method
Chimney1 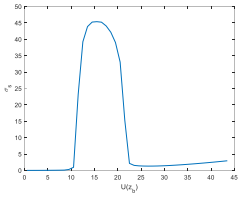	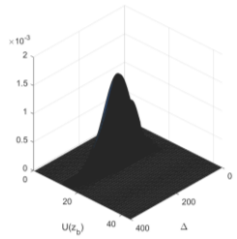 T_F = 1.46 years T_F = 1.46 years (only VIV)	T_F = 0.0055 years
Chimney 2a 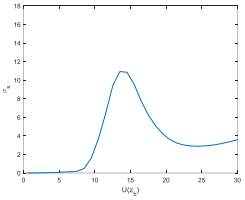	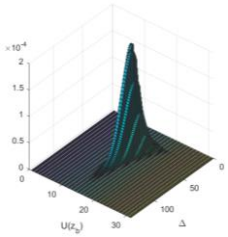 T_F = 48.9 years T_F = 49.5 years (only VIV)	T_F = 0.0019 years
Chimney 2b 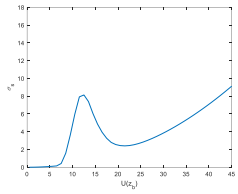	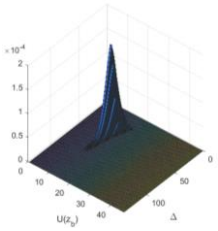 T_F = 98 years T_F = 99 years (only VIV)	T_F = 0.0011 years
Chimney 3 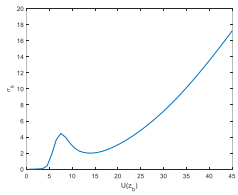	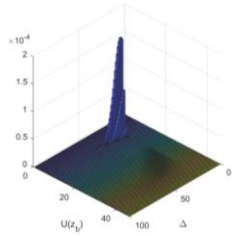 T_F = 321 years T_F = 334 years (only VIV)	T_F = 0.1652 years

Tab. 5.25: Summary of the results from the numerical analysis and from VIV-induced fatigue standard method.

By taking into account that $T_F > V_N$ verifies the structure and $T_F < V_N$ do not verify the structure, with the nominal lifetime of the structure equal to 50 years, it is possible to observe from the numerical analysis that:

- Chimney 1, with a dominant VIV effect on crosswind response, is really critical concerning VIV fatigue phenomenon (not verified);
- Chimney 2a, with a quite dominant VIV effect on crosswind response, is quite critical concerning VIV fatigue phenomenon (not verified);
- Chimney 2b, with a quite apparent VIV effect on crosswind response, is not critical concerning VIV fatigue phenomenon (verified);
- Chimney 3, with an unimportant VIV effect on crosswind response, is totally not critical concerning VIV fatigue phenomenon (verified).

By considering these outcomes as reliable, it is evident that VIV-induced fatigue standard method is too preventive, giving too safe and unreliable results, with $T_F < 1$ year for each of these case studies. All structures are extremely not verified (see also Tables 5.3, 5.6, 5.9 and 5.12).

Table 5.26 summarizes a comparison between standard approach and the new preliminary proposal of a novel calculation of the number of cycles due to VIV, *N*, (Tab. 5.22). As concerns response, both cases with the maximum stress amplitude $\Delta_{s,max}$, correspondent with the critical wind velocity, evaluated by means of numerical simulation and by means of Eurocode procedure are considered.

	N counting approach	VIV response $\Delta_{s,max}$	T_F
Chimney 1	Eurocode 1 and CNR Eq.(5.20)	Standard method (408.4 N/mm^2)	0.0055 years
	New proposal Eqs.(5.25),(5.31)	Standard method (408.4 N/mm^2)	0.0288 years
	Eurocode 1 and CNR Eq.(5.20)	Simulation (129.02 N/mm^2)	0.1728 years
	New proposal Eqs.(5.25),(5.31)	Simulation (129.02 N/mm^2)	0.9120 years
	Numerical analysis		1.46 years
Chimney 2a	Eurocode 1 and CNR Eq.(5.20)	Standard method (377.95 N/mm^2)	0.0019 years
	New proposal Eqs.(5.25),(5.31)	Standard method (377.95 N/mm^2)	0.0052 years
	Eurocode 1 and CNR Eq.(5.20)	Simulation (64.8 N/mm^2)	0.3790 years
	New proposal Eqs.(5.25),(5.31)	Simulation (64.8 N/mm^2)	1.3167 years
	Numerical analysis		48.9 years
Chimney 2b	Eurocode 1 and CNR Eq.(5.20)	Standard method (426.48 N/mm^2)	0.0011 years
	New proposal Eqs.(5.25),(5.31)	Standard method (426.48 N/mm^2)	0.0024 years
	Eurocode 1 and CNR Eq.(5.20)	Simulation (53.08 N/mm^2)	0.5623 years
	New proposal Eqs.(5.25),(5.31)	Simulation (53.08 N/mm^2)	1.2327 years
	Numerical analysis		98 years
Chimney 3	Eurocode 1 and CNR Eq.(5.20)	Standard method (55.53 N/mm^2)	0.1652 years
	New proposal Eqs.(5.25),(5.31)	Standard method (55.53 N/mm^2)	0.2888 years
	Eurocode 1 and CNR Eq.(5.20)	Simulation (31.40 N/mm^2)	1.2575 years
	New proposal Eqs.(5.25),(5.31)	Simulation (31.40 N/mm^2)	2.2109 years
	Numerical analysis		321 years

Tab. 5.26: Comparison between standard approach and the new preliminary proposal to calculate the number of cycles due to VIV, N; two different levels of estimation of VIV-induced maximum response are considered.

It is worth notice that by passing from the standard calculation to the novel proposed calculation of N, the fatigue life increases in all the cases. More influential is to pass from the standard method to the simulation to estimate the maximum VIV-induced response in correspondence of the critical velocity.

This is expectable since the uncertainties propagation analysis carried out in Section 5.4.3 demonstrates that errors propagates more through N_C than N.

However, rather than using standard method, it can be observed that by adopting simulation response outcomes and the new formulation to determine N, the resulting fatigue life values are larger, as expected, but still far from the numerical analysis results. In Chimney 1 a relative error of 37.5% is committed, in Chimney 2a a relative error of 97% is committed, in Chimney 2b a relative error of 99% is committed and in Chimney 3 a relative error of 99% is committed. This proves the statement that a great role is played by the adopted standard model, which assumes that all the load cycles are counted in correspondence of the critical mean wind velocity, therefore N is equal to the number of times in which $\bar{u} = \bar{u}_{cr}$ during the nominal life-time of the structure, and to this number of cycles is associated the maximum stress cycle amplitude $\Delta_{s,max} = 2\,\bar{y}_{s,max}$ in the considered critical cross-section (Fig. 5.53).

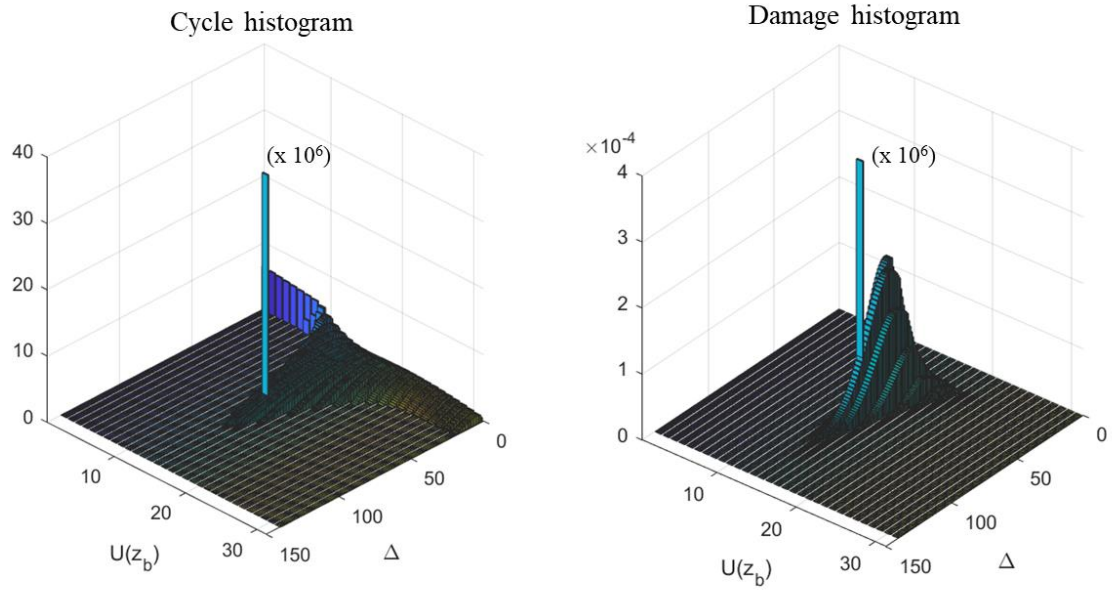

Fig. 5.53: Representation of the fatigue standard approach approximation, compared to cycle and damage histograms.

The response model provides too preventive results because of two main reasons: (1) input parameters uncertainties and (2) equivalent static force model uncertainties.

The fatigue model provides too preventive results because of two additional main reasons: (1) $\Delta_{s,max}$ is not characterized by a constant probability of occurrence equal to 1 for a fixed mean wind velocity value, but it follows a Rayleigh distribution; (2) by concentrating all cycles in around the critical velocity and considering only $\Delta_{s,max}$, the number of cycles associated to small amplitudes, which should correspond to the second broken line of the *S-N* curve or to the cut-off limit, counts more than it should in damage

calculation. In fact, the damage obtained calculating the fractional damages d_{ij} associates different values of amplitude Δ_{sj} with the related number of cycles that causes failure $N_{C,j}$ which is provided by the concerning *S-N* fatigue curve.

In conclusion of the present Chapter 5 it can be assert that in crosswind fatigue analysis separation of effects is a reasonable approximation, even if it is not a rigorous approach. Two independent assessments can be carried out, one for lateral turbulence-induced fatigue analysis and one for VIV-induced fatigue analysis. On the other hand, the standard approximation which considers all the load cycles counted in correspondence of the critical mean wind velocity, associated with the maximum stress cycle amplitude $\Delta_{s,max}$, is too preventive, distancing from reliable values of damage and fatigue life.

Further research in this field is therefore necessary. A very first initial step is carried out in the present thesis: the most evident criticisms of the VIV-induced fatigue standard method are outlined in detail; a preliminary new proposal about the equation to estimate the number of cycles that stresses the critical structural detail is made; input parameters that mostly affect response and fatigue predictions are identified.

CHAPTER 6 – EXAMPLES OF FATIGUE CALCULATIONS FOR BUFFETING

6.1. INTRODUCTION

The present thesis deals with a general method of wind-induced fatigue analysis of slender structures. The analytical model introduced, discussed and generalized in Chapters 2, 3 and 4, which concerns alongwind and crosswind buffeting-induced fatigue assessment, is finally applied to some case studies. In Chapter 5 the separation of effects approximation in crosswind fatigue analysis is discussed and approved, with regard to engineering standard level of verifications. Therefore, by assuming that two independent assessments can be carried out, one for lateral turbulence-induced fatigue analysis and one for VIV-induced fatigue analysis, the previous Chapter shows some example applications. In order to complete the whole research work, also some applications of the generalized buffeting-induced fatigue method are reported below.

The present Chapter 6 includes six example slender structures, analysed according to the buffeting-induced fatigue method proposed in the present thesis. In this instance, the focus is mainly on alongwind assessment; the sixth example is analysed as concerns both alongwind and crosswind buffeting-induced fatigue. To simplify the analyses, all the structures are assumed to be of standard types, with a nominal lifetime V_N = 50 years. Since the procedure is described in detail in the first four Chapters and since Section 5.3 shows how to apply the method to some case studies (Sections 5.3.1, 5.3.2, 5.3.3 and 5.3.4), in the following part only input parameters values and results are presented, omitting the procedure steps description.

Each case study is critically discussed, concerning different issues. Steel and aluminium structures are dealt with, therefore different resistance fatigue curve types require to be taken into account. A structure sensitive to both longitudinal and lateral turbulence effects is analysed. The two levels of calculation, simplified and detailed, are applied. The reliability of the proposed solutions compared with the inspections or with the numerical solutions is illustrated. The most noteworthy engineering considerations, from both a qualitative and a quantitative viewpoint, are pointed out.

It is worth notice that the method is effective only for slender structures or structural elements with a comparable quasi-static and resonant contributions on dynamic response. It means that the method is reliable if applied on sufficiently flexible structures, rather than stiffer ones. This is evident from Figures 4.8 and 4.9 (Section 4.3.4), which represent the bi-modal corrective factor C_{BM} on varying stiffness (different colours). This factor is used to correct the 0 level solution of damage taking into account the bi-modal bandwidth characterizing the stress process. It can be observed that more rigid elements

correspond to lower values of C_{BM}, while more flexible ones correspond to higher values of this factor. The fundamental frequency range considered in these figures is from 0.36 Hz (high C_{BM}) to 1.69 Hz (low C_{BM}). The cases in which the natural frequency of a structural element is far higher, for example when it reaches few units, C_{BM} tends to 0. The consequence is that the estimated fatigue damage would be null and fatigue life would be predicted as infinite. Unfortunately, some particular cases of rigid structures sensitive to turbulence induced fatigue do exist. In such cases the proposed model is unreliable and more research in this field is required. A first attempt to analysed the problem has been made very recently (Lanza, 2020).

The Chapter is subdivided as follows.

Three steel poles are analysed as concerns alongwind-induced fatigue. Section 6.2 shows the application of simplified and detailed calculation, showing that the former performs a preliminary preventive screening and the latter provides the actual prediction. This double check is done also for other following examples. Section 6.3 shows a comparison between the analytical method and a numerical analysis. Section 6.4 highlights the importance of identifying non-standard conditions, which can divert the outcomes.

Two structures are analysed referring to *S-N* fatigue curves which are different from the one associated with normal stresses in steel structural details. Section 6.5 deals with a fatigue resistance curve associated with shear stresses in steel elements, Section 6.6 deals with an aluminium structure.

Finally, Section 6.7 presents the study of a mast structure sensitive to both longitudinal an lateral turbulence.

6.2. ANTENNA SUPPORTING POLE

The structure examined in this Section is a metal pole whence an antenna support covered by a fiberglass cylinder stands out (Fig. 6.1). This case study is referred to the antenna supporting metal pole examined in CNR document (2018) as one of the example applications.

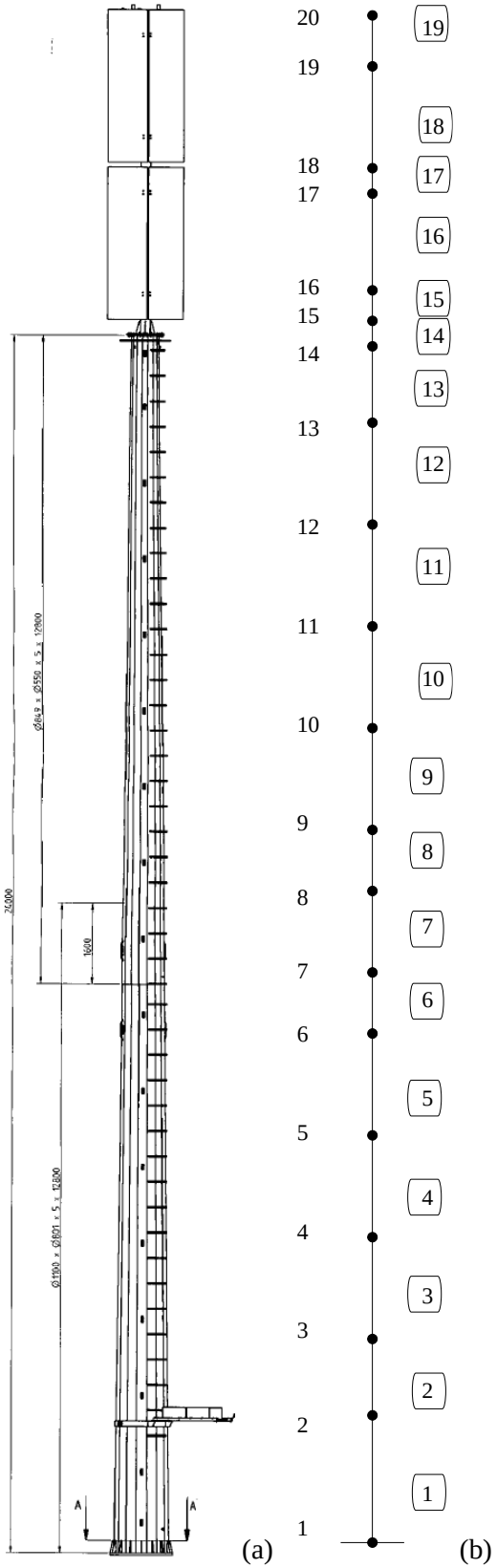

Fig. 6.1: Antenna support pole (a) and finite elements model (b) (Figure © CNR, 2018).

The whole structure is 30 m tall and it is composed of a 24 m long galvanized steel shaft and a 6 m long antenna steel support. The shaft is made of two truncated cones of sixteen-sided polygon cross-sections coupled with a 1600 mm overlap. The antenna support is made of a tubular section. The pole supports 4 antenna dishes at a height of 23.5 m, 6 antennas at a height of 29 m, a rack along the shaft, a welded flanged joint at the top of the shaft and a ring at a height of 2.5 m. The fiberglass cylinder has a 1500 mm diameter and it is 6 m long (as the antenna support). Table 6.1 provides a synthetic description of the structure. It is schematized as a beam cantilevered at the base.

Detail	Weight (N)	Height
Galvanized truncated cone (1100-801) x 5 x 12800	15600	0-12.8m
Galvanized truncated cone (849-550) x 5 x 12800	11450	11.2-24.0m
Rack	1200	0-24.0m
Rack ring	430	2.5m
4 antenna dishes	1600	23.5m
Welded flanged joint	1780	24m
Antenna support 193.7 x 7.1 x 6000	1970	24.0-30.0m
6 antennas	2700	29m
Fiberglass cylinder 1500 x 6000	2160	24.0-30.0m

Tab. 6.1: Description of the structure.

Referring to a finite elements model schematization, made of 20 nodes and 19 elements (Figure 6.1b), Table 6.2 further provides the height z_k and the concentrated mass M_k related to each node k. Table 6.3 provides the diameter d_j, the thickness t_j and the distributed mass m_j related to each element j.

k	z_k (m)	M_k (kg)
1	0.0	20
2	2.5	63
3	4.0	20
4	6.0	20
5	8.0	20
6	10.0	20
7	11.2	20
8	12.8	20
9	14.0	20
10	16.0	20
11	18.0	20
12	20.0	20
13	22.0	20
14	23.5	180
15	24.0	232
16	24.6	-
17	26.5	-
18	27.0	108
19	29.0	270
20	30.0	54

Tab. 6.2: Concentrated masses.

J	b_j (m)	s_j (m)	m_j (kg/m)
1	1.071	0.005	131
2	1.024	0.005	126
3	0.983	0.005	121
4	0.936	0.005	115
5	0.890	0.005	109
6	0.852	0.005	104
7	0.830	0.01	202
8	0.798	0.005	98
9	0.760	0.005	93
10	0.714	0.005	87
11	0.667	0.005	82
12	0.620	0.005	76
13	0.573	0.005	70
14	0.573	0.005	70
15	0.1937	0.0071	33
16	0.1937	0.0071	33
17	0.1937	0.0071	33
18	0.1937	0.0071	33
19	0.1937	0.0071	33

Tab. 6.3: Distributed masses.

The construction is located in central Italy at sea level. Applying the rules given by codes, this corresponds to Zone 3. It is also assumed the exposure category III.

Alongwind analysis is performed according to both simplified and detailed calculations and the outcomes are shown in Table 6.4. The method is applied by following standard provisions (Eurocode/CNR) and the procedure described in the present thesis.

	Simplified calculation	Detailed calculation
s_u	510 N/mm^2	510 N/mm^2
m_1	3	3
Δ_C	36 N/mm^2	36 N/mm^2
N_L	10^7	10^7
Cut-off	Yes	Yes
n_D	0.92 Hz	0.92 Hz
h_{tot}	30 m	30 m
b_{ref}	0.69 m	0.69 m
Z_{eq}	18 m	18 m
$\bar{u}_{ref}$	27 m/s	27 m/s
k		1.20
C_E	III	III
$\bar{s}_P$	2.261 N/mm^2	2.261 N/mm^2
$\bar{s}_{D,ref}$	27.31 N/mm^2	27.31 N/mm^2
$\sigma_{D,ref}$	19.58 N/mm^2	19.58 N/mm^2
$\nu_{D,ref}$	0.740 Hz	0.740 Hz
$\nu_{D,Q,ref}$	0.134 Hz	0.134 Hz
$\lambda_{D,R,ref}$	0.648	0.648
$\alpha_{\sigma,D}$		2.411
$\alpha_{\lambda,D}$		0.782
$\bar{D}_0(1)$	0.1596	0.0092
C_{BM}	0.7633	0.5426
C_M	1.0897	1.0741
C_{SN}	0.7411	0.6837
$\bar{D}(1)$	0.0984	0.0037
T_F	10.2 years	271 years

Tab. 6.4: Outcomes from analytical procedure (alongwind analysis).

The mean yearly damage $\bar{D}(1)$ = 0.0984 and the fatigue life T_F = 10.2 years are obtained by applying the simplified calculation. Since the nominal life value is larger than the fatigue life simplified estimation, this antenna supporting pole requires detailed analysis for alongwind induced fatigue.

The mean fatigue wind velocity is given by $\bar{u}_{fat}\left(Z_{eq}\right) = 0.5 \cdot \bar{u}_{ref}\left(Z_{eq}\right)$. In order to calculate parameters $\alpha_{\sigma,D}$ e $\alpha_{\lambda,D}$ response factors are used. In the lack of anemometric databases measured in situ, the shape factor of the Weibull probability distribution of the mean wind velocity at the site is given according to the Italian zone in which the structure is located. By applying the detailed method to calculate the parameters A_0, A_{BM}, A_M, A_{SN}, B_{SN} (see Tab. 4.1 in Section 4.2), the basic mean yearly damage, the bi-modal factor, the mean stress factor, the fatigue curve factor, the mean yearly damage and the related fatigue life are obtained.

The corrective factors strongly reduce the 0 level solution of damage, taking into account the bi-modal nature of the stress process and the non-linearity of the considered *S-N* curve. It is calculated that, for this steel structure, T_F = 271 years. Since this time $T_F > V_N$, the structure is verified for alongwind induced fatigue.

6.3. URBAN LIGHT POLE

The alongwind-induced fatigue procedure is applied to a slender urban light pole of steel material, already analysed in (Repetto and Solari, 2006, 2009, 2012) and mentioned in Section 2.3.2. The structure exhibited fatigue damage, the fatigue life obtained by Monte Carlo simulation was 40 years and their bi-modal solution was 35 years of predicted fatigue life. The agreement was considered as very good. The main characteristics of the structure are shown in Fig. 6.2, where R is the radius, m is the mass per unit length, and Φ is the first modal shape.

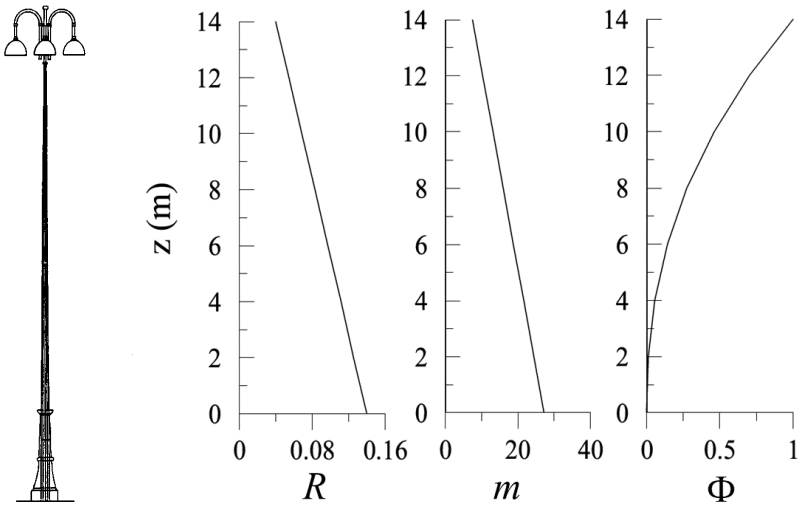

Fig. 6.2: Scheme, radius, mass per unit length and first modal shape of the pole.

The structure is 14 m high; its shaft consists of two parts connected at z = 2.2 m, both tapered with octagonal section, in steel of constant thickness t = 4 mm. The lighting device at the top is schematized as a concentrated mass M = 145 kg, whose centre of gravity is z = 14.9 m high. The area of the lighting surface exposed to wind is 1.85 m x 1.80 m = 3.33 m^2. The fundamental frequency is n_D = 0.549 Hz. The pole is in Italy, at sea level, on a flat terrain with roughness length z_0 = 0.1 m.

6.3.1. Numerical analysis

The damping ratio is ξ = 0.005. The drag coefficient of the shaft and of the light device is 1.2 and 0.3, respectively. The reference wind velocity with a 50 year return period is $\bar{u}_{ref}$ = 28 m/s, with a time interval ΔT = 600 s. The probability density function of the mean wind velocity is given by the Weibull model (Equation (2.21), Section 2.3.1) with k = 1.500, c = 5.0400 m/s and F_0 = 0 (Fig. 6.3a). The turbulence properties are schematized by the model described by Solari and Piccardo (2001).

The alongwind-induced response and the stress at the base of the pole are evaluated by the method proposed in (Piccardo and Solari, 2002) and the approximation provided by the power law approximation (see Equation (2.38) in Section 2.3.3). Figure 6.3b shows the standard deviation of the stress; $\sigma_{D,ref}$ = 27 N/mm^2. Repetto and Solari (2009) demonstrated that Eqs. (2.38) and (2.39) furnish a precise estimate of σ_D (i.e. the fundamental parameter of the analysis) in the whole range of the mean velocity; moreover, it furnishes a good approximation of ν_D and $\lambda_{D,R}$ in the range of the moderate and high mean velocities, where the main fatigue damage is expected; outside, the approximations are always on the safe side.

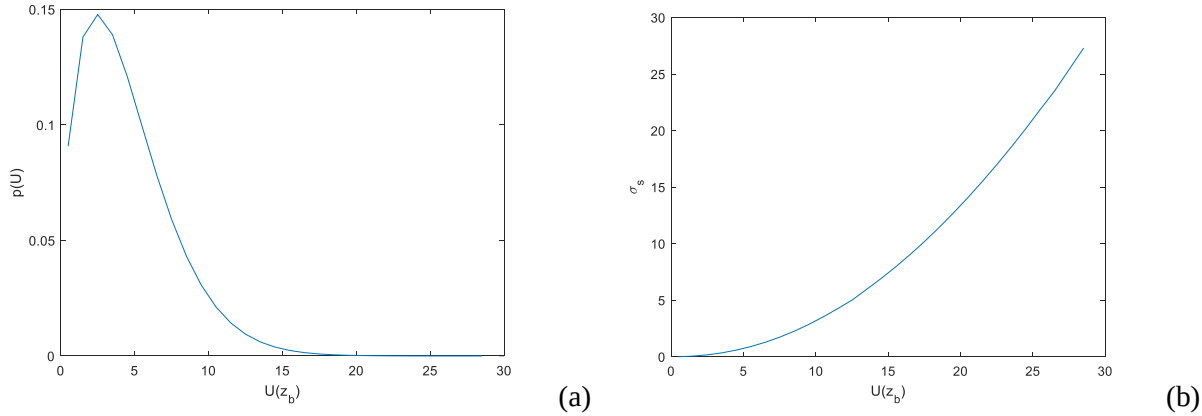

Fig. 6.3: Probability density function of the parent population of the mean wind velocity (a); alongwind stress standard deviation on varying mean wind velocity (b).

The fatigue damage is analysed in the critical cross-section at the base of the structure. According to Eurocode 3 (2005) it is classified as Category 36 and described by a trilinear curve (see Figure 2.5 and Equation (2.8) in Section 2.2.2).

By applying the bi-modal counting method, the cycle histogram is obtained (Fig. 6.4) and by means of the linear Miner rule the damage histogram is obtained too (Fig. 6.5). These diagrams are referred to one year. The resulting fatigue life is T_F = 36.5 years. This result is in accordance with (Repetto and Solari, 2006).

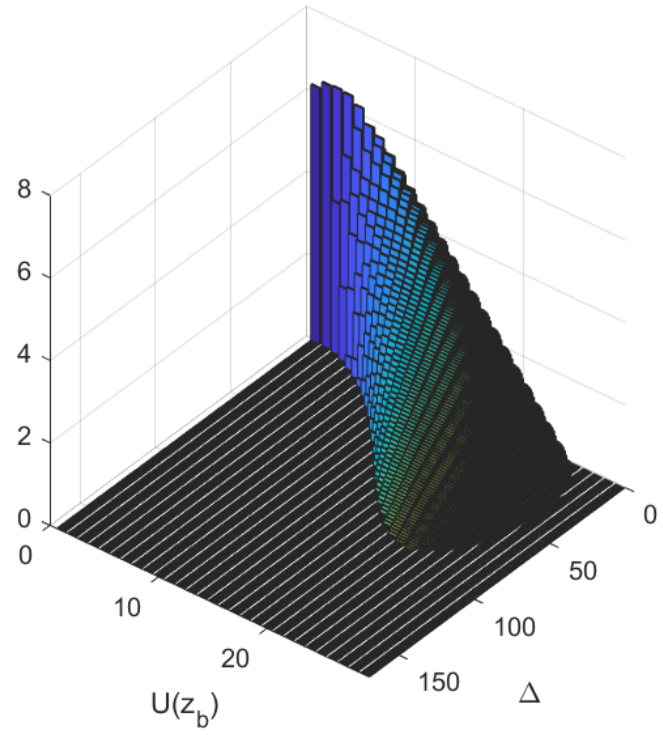

Fig. 6.4: Cycle histogram.

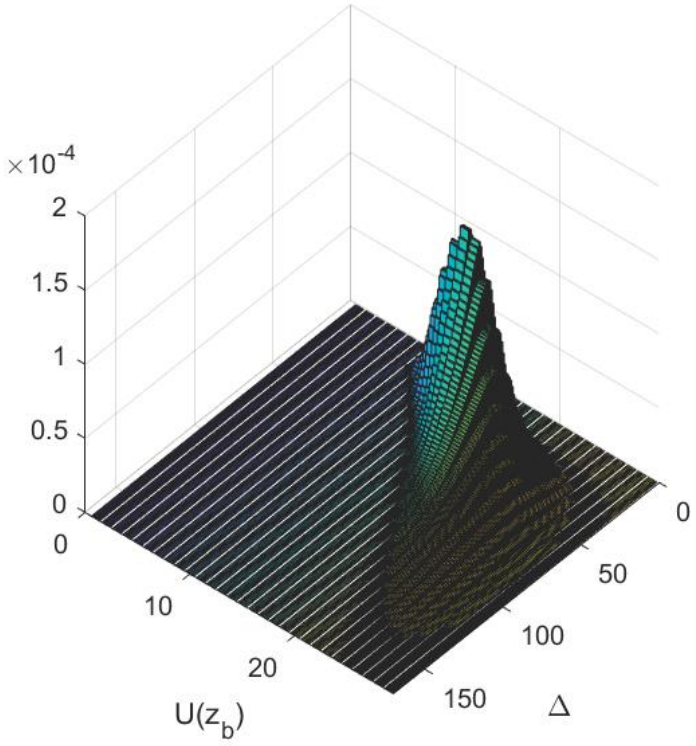

Fig. 6.5: Damage histogram.

6.3.2. Analytical analysis

At a first stage the method is applied by using some input data from the numerical analysis, such as the damping ratio is $\xi = 0.005$, the same climatological parameters, the alongwind response represented by the reference standard deviation of the stress $\sigma_{D,ref} = \gamma_F \cdot 27$ N/mm^2. The analysis is carried out by using both simplified and detailed calculation (Table 6.5).

	Simplified calculation	Detailed calculation
s_u	510 N/mm^2	510 N/mm^2
m_1	3	3
Δ_C	36 N/mm^2	36 N/mm^2
N_L	10^7	10^7
Cut-off	Yes	Yes
n_D	0.549 Hz	0.549 Hz
h_{tot}	14.9 m	14.9 m
b_{ref}	0.151 m	0.151 m
Z_{eq}	8.94 m	8.94 m
$\bar{u}_{ref}$	28 m/s	28 m/s
k		1.5
C_E	III	III
$\bar{s}_P$	1.072 N/mm^2	1.072 N/mm^2
$\bar{s}_{D,ref}$	19.98 N/mm^2	19.98 N/mm^2
$\sigma_{D,ref}$	36.45 N/mm^2	36.45 N/mm^2
$\nu_{D,ref}$	0.527 Hz	0.527 Hz
$\nu_{D,Q,ref}$	0.144 Hz	0.144 Hz
$\lambda_{D,R,ref}$	0.923	0.923
$\alpha_{\sigma,D}$		2.555
$\alpha_{\lambda,D}$		0.148
$\bar{D}_0(1)$	0.7337	0.0727
C_{BM}	1.0000	1.0000
C_M	1.0616	1.0492
C_{SN}	0.8916	0.8680
$\bar{D}(1)$	0.6945	0.0662
T_F	1.4 years	15.1 years

Tab. 6.5: Outcomes from analytical procedure (alongwind analysis), with some input parameters given by numerical analysis.

Then the method is merely applied by following standard provisions (Eurocode/CNR) and the procedure described in the present thesis (Table 6.6).

	Simplified calculation	Detailed calculation
s_u	510 N/mm^2	510 N/mm^2
m_1	3	3
Δ_C	36 N/mm^2	36 N/mm^2
N_L	10^7	10^7
Cut-off	Yes	Yes
n_D	0.549 Hz	0.549 Hz
h_{tot}	14.9 m	14.9 m
b_{ref}	0.151 m	0.151 m
Z_{eq}	8.94 m	8.94 m
$\bar{u}_{ref}$	28 m/s	28 m/s
k		1.35
C_E	III	III
$\bar{s}_P$	1.072 N/mm^2	1.072 N/mm^2
$\bar{s}_{D,ref}$	72.91 N/mm^2	72.91 N/mm^2
$\sigma_{D,ref}$	54.51 N/mm^2	54.51 N/mm^2
$\nu_{D,ref}$	0.403 Hz	0.403 Hz
$\nu_{D,Q,ref}$	0.144 Hz	0.144 Hz
$\lambda_{D,R,ref}$	0.539	0.539
$\alpha_{\sigma,D}$		2.271
$\alpha_{\lambda,D}$		0.715
$\bar{D}_0(1)$	1.8748	0.2071
C_{BM}	0.8430	0.6523
C_M	1.2082	1.1463
C_{SN}	0.9534	0.9646
$\bar{D}(1)$	1.8205	0.1494
T_F	0.5 years	6.7 years

Tab. 6.6: Outcomes from analytical procedure (alongwind analysis).

The difference between results of Tables 6.5 and 6.6 is due to: the damping ratio, which is estimated as $\xi = \xi_s + \xi_a = 0.002 + 0.049 = 0.051$ according to code provisions; climatological parameter k (Italian zone 7); the alongwind response represented by the reference standard deviation of the stress, calculated by following codes and formula in Chapter 4, on the safe side, $\sigma_{D,ref} = \gamma_F \cdot 40.37$ N/mm^2. The former Table deals with a really flexible structure (low damped), then the response is dominated by the resonant part; the latter Table concerns a less flexible metallic pole (more damped), then the response is more clearly bi-modal. This consideration explains why in the first case the standard deviation of the alongwind response is larger than the mean value, differently from the second case.

By comparing the fatigue life $T_F = 36.5$ years, resulting from the numerical analysis, with the fatigue life values calculated analytically in the present Section, it can be seen that the second ones are on the safe side, as it is presumed by a verification method at standard level, becoming safer even when the structure is considered as stiffer according to standard provisions. Simplified calculation results as a warning in both Tables, leading to very conservative results. The structure is critical as regard alongwind-induced fatigue even though the detailed calculation is carried out.

In Table 6.6 the most relevant corrective factor is the bi-modal one, as expected, due to the relevant contribution of the quasi-static part of the response, reducing the 0 level damage. The mean stress factor, higher than 1, and the fatigue curve factor, less than 1, slightly influence the 0 level solution. In the previous Table 6.5 corrective factors are less relevant, quite balancing each other; in this case the response is considered as totally resonant, therefore C_{BM} is taken equal to 1 (upper limit).

6.4. ANEMOMETRIC POLE

The structure examined in this Section is an anemometric pole, 10 m high, composed of a steel shaft with an octagonal section, whose diameter varies linearly from 220 mm at bottom to 78 mm at top. The pole bears an anemometer at the top, a photovoltaic panel at $z = 9$ m and a metallic box at $z = 2$ m, represented as concentrated masses of 8 kg, 16 kg and 58 kg, respectively. This simple structure exhibited a premature collapse one year after its installation, caused by a fatigue crack in the base welding joint (Repetto and Solari, 2010; Section 2.3.2).

During its short life, the anemometer continuously registered the ten-minute mean wind velocity. Therefore, in the abovementioned work, it was possible to adopt the bi-modal counting method in order to examine the stress state and the fatigue damage associated with the wind loading conditions. The probability of occurrence of the loading conditions was associated only with the mean wind velocity variation, assuming neutral atmospheric conditions, as no information about the directional distribution and the atmospheric stratification were measured at the site. The histogram of mean wind velocity was

obtained from the measured wind velocity time history. The maximum mean wind velocity measured at the top of the pole, $\bar{u}(z=10\text{m})$ = 32.5 m/s, is higher than the mean wind velocity with 50 years of return period, evaluated at the design stage according to the national standard code (CNR, 2008, 2018), $\bar{u}_{ref}$ = 28 m/s; it is also worth noting that this value was exceeded 3 times in one year during independent events.

The statistical analysis of the measured mean wind velocity, even if based on a poor database, showed some critical aspects. The Weibull probability distribution of the data population is characterized by a probability of zero values F_0 = 0.0115, and parameters k = 1.202 and c = 5.439 m/s. Adopting the relationship proposed by Pagnini and Solari (2016) between the Weibull parameters and the maximum wind velocity with 50 years of return period, this latter results $\bar{u}_{ref}$ = 45 m/s.

Independently of the accuracy of the above estimates, the site is an exposed ridge characterized by local windy conditions well above those prescribed by the Italian code. The topography is considered by means of a topography coefficient c_t equal to 1.2 (CNR, 2008, 2018). The exposure category is III.

The structure is schematized as a vertical cantilever beam. The fundamental frequency is n_D = 2.04 Hz. The damping is assumed as ξ = 0.005. The drag coefficient of the shaft at the reference height z = 0.6 h is c_D = 1.2 for a mean wind velocity from 0 to 27 m/s, c_D = 1.1 for a mean wind velocity from 27 to 35 m/s.

In (Repetto and Solari, 2010), the alongwind and crosswind responses at the base of the structure, on varying the top mean wind velocity from 0 to 35 m/s with a velocity step of 1 m/s, were determined. Alongwind and crosswind responses were both mainly due to turbulence and grow with the mean wind velocity. The maximum stress at the maximum registered wind velocity, $\bar{u}(z=10\text{m})$ = 32.5 m/s, resulted $s_{D,\max}$ = 170 N/mm^2. It was well below the yield limit of the material f_y = 355 MPa. The wind-induced fatigue damage was evaluated expressing the cycle histogram by means of the bi-modal counting method. The fatigue resistance was described by the *S-N* curve of the critical section. The choice of the most suitable *S-N* curve was a crucial point in the procedure, as no standard detail matched the actual geometry of the welded joint, realized with fillet welds between the base plate and the shaft. The quality of the joint was observed and considered as not good, with several macroscopic defects. Thus, a hot spot analysis (IIW, 2016) was carried out in order to determine the *S-N* curve for the actual geometry, starting from the FEM models of the actual joint and of the reference joint reported in Standards and classifies as category 40 (Eurocode 3, 2005) (Fig. 6.6). The final choice associated the fatigue resistance with the detail category 36. The alongwind damage histogram, consisting of the mean fractions of damage on varying the measured mean wind velocity value, was determined. The fatigue damage concentrated in the range of high wind velocities, between 20 and 30 m/s. This result was quite anomalous in comparison with other experiences with similar structures, where the wind-induced fatigue damage usually concentrated in the range of moderate wind velocities, between 10 and 20 m/s. This situation was a consequence of the

special windy condition of the site; in particular, it was due to a parent distribution of the wind velocity at the site shifted towards high wind velocities.

71	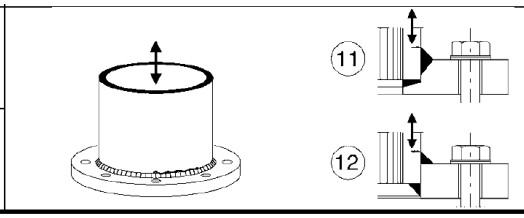	11) Tube socket joint with 80% full penetration butt welds.	11) Weld toe ground. $\Delta\sigma$ computed in tube.
40		12) Tube socket joint with fillet welds.	12) $\Delta\sigma$ computed in tube.

Fig. 6.6: Eurocode 3 reference structural detail category 40.

The fatigue life was predicted equal to 2 years. This outcomes is really critical, in accordance with the observed failure of the structure.

In the following the structure is analysed as concerns alongwind-induced fatigue, by applying the method dealt with in the present thesis (Tab. 6.7). It is worth notice that, by considering the maximum wind velocity with 50 years of return period previously estimated, $\bar{u}_{ref}$ = 45 m/s, the fatigue wind velocity value for the Italian territory results equal to 22.5 m/s, just in the range of the exhibited fatigue damage.

	Detailed calculation
s_u	510 N/mm^2
m_1	3
Δ_C	36 N/mm^2
N_L	10^7
Cut-off	Yes
n_D	2.04 Hz
h_{tot}	10 m
b_{ref}	0.1348 m
Z_{eq}	6 m
$\bar{u}_{ref}$	45 m/s
k	1.202
C_E	III
$\bar{s}_P$	0.846 N/mm^2
$\bar{s}_{D,ref}$	69.23 N/mm^2
$\sigma_{D,ref}$	91.37 N/mm^2
$\nu_{D,ref}$	1.905 Hz
$\nu_{D,Q,ref}$	0.180 Hz
$\lambda_{D,R,ref}$	0.872
$\alpha_{\sigma,D}$	2.563
$\alpha_{\lambda,D}$	0.274
$\bar{D}_0(1)$	1.9083
C_{BM}	0.8186
C_M	1.1710
C_{SN}	0.9936
$\bar{D}(1)$	1.8176
T_F	0.6 years

Tab. 6.7: Outcomes from analytical procedure (alongwind analysis).

If the climatological parameters were estimated according to code, for example, by considering the structure in Zone 7, it would be $\bar{u}_{ref}$ = 28 m/s and k = 1.35.

In this case, if the alongwind response was derived from the measured value of the maximum stress at the maximum registered wind velocity, $s_{D,\max}$ = 170 N/mm^2, therefore it would be calculated $\bar{s}_{D,ref}$ = 47.04 N/mm^2 and $\sigma_{D,ref}$ = 47.43 N/mm^2. The fatigue life would be predicted equal to 3.9 years.

If only code provisions were be taken into account, then it would be $\bar{u}_{ref}$ = 28 m/s and k = 1.35, $\bar{s}_{D,ref}$ = 18.61 N/mm^2 and $\sigma_{D,ref}$ = 18.76 N/mm^2; the fatigue life would be predicted equal to 97.9 years.

It can be concluded that collapse is mainly linked with the particular windy condition of the site. The safety factor adopted in structural design may cover this anomalous situation from the ultimate limit state point of view, while it is completely inadequate from the fatigue point of view.

6.5. TRAFFIC SIGNAL SUPPORT STRUCTURE

Traffic-signal-support structures with cantilevered mast arms are known to exhibit large-amplitude vibrations under wind actions. Many damages have been reported in literature and many studies have been addressed to such kind of structures (e.g. Wieghaus et al. 2017). Based on full-scale measurement of a traffic-signal-support structure, Zuo and Letchford (2010) demonstrated that two types of excitation mechanisms, vortex-shedding and buffeting actions, lead to main vibration effects.

A wide inspection campaigns on sign support steel structures have been recently carried out by IIS (Italian Institute of Welding), monitoring the presence and the characteristics of damage. On the whole, 67 structures have been inspected, with different structural schemes, ages and locations. Despite all the structures have been verified at ULS, inspections indicated presence of fatigue damage in many welded or bolted joints; the risk has been classified as low for 0% of structures, intermediate for 48%, high for 28% and very high for 24%. Many of them have been repaired, some have been definitely removed.

One of the “flag-frame” structures has been evaluated by adopting the procedure presented in this thesis. The cantilever structure is composed by a vertical element linked to a horizontal “arm” at 7.49 m height. Structural elements are made of steel Fe510 with square cross-section; the section dimension is variable with the height in the vertical structural component and it is constant in the horizontal one. The connection of the post to the ground is typically end plate jointed; the connection of the post to the horizontal “arm” is a welded joint; the horizontal “arm” is composed by three trunks, connected by end plate joints. The structure supports two traffic signals; the central one is 2 m high and 5 m wide and the extreme one is 1.8 m high and 3 m wide. The installation of this structure is quite recent, since it was less than 10 years ago. Figure 6.7 reports a schematic representation of the structure, putting in evidence four joints.

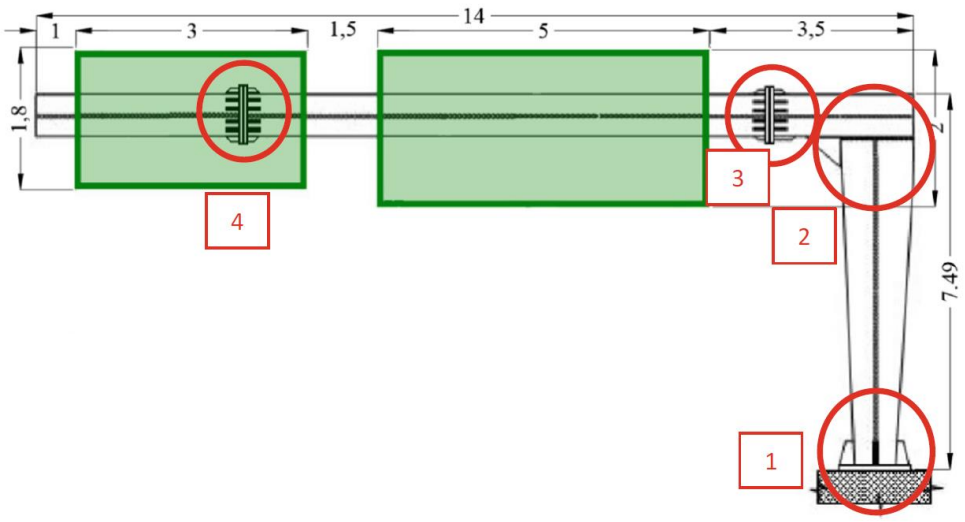

Fig. 6.7: Schematic representation of the considered “flag-frame” sign support structure.

Despite ULS verifications were met, inspections have found out critical damage in some joints, actually. In particular, the most critical detail is Joints 2. The stress state and the fatigue damage associated with the wind loading conditions is examined in this critical joint.

A modal analysis of the structure has been carried out and Table 6.8 shows the characteristics of the first five vibration modes.

Modes	Period [s]	*n* [s]	Description
First	0.571	1.752	Longitudinal (horizontal element)
Second	0.531	1.869	Transversal (vertical and horizontal element)
Third	0.170	5.889	Transversal (vertical and horizontal element)
Fourth	0.115	8.681	Longitudinal (horizontal element)
Fifth	0.059	16.979	Transversal (horizontal element)

Tab. 6.8: First five vibration modes, periods, natural frequencies and brief description.

The probability of occurrence of the loading conditions is associated only with the mean wind velocity with 50 years of return period, $\bar{u}_{ref}$. The site is located in the conventional Italian Zone 3 (CNR, 2008, 2018), therefore $\bar{u}_{ref}$ = 27 m/s; k = 1.20; the fatigue velocity, $\bar{u}_{fat}$, is equal to 13.5 m/s.

6.5.1. Analytical analysis with equivalent ideal stresses

Wind loading and alongwind dynamic response evaluations are based on the standard prescriptions, obtaining the nominal stresses in the critical section. The structure is verified according to ULS, vortex

shedding and galloping verifications. Stress status in Joint 2 is characterized by shear stress, due to the wind-induced torsional effect on the structure ($\bar{\tau}_{D,ref}$ = 25.76 N/mm^2). Due to the limited information about fatigue resistance for shear stress in this kind of joints, it is firstly considered the ideal normal stress in the joint (reported in Table 6.9).

For this critical joint, the category detail is again selected according to Eurocode 3 (2005). The choice of the most suitable *S-N* curve is a crucial point in the procedure. The geometric detail of the actual joint is not provided in Eurocode classification, therefore detail category 36 is assumed on the safe side.

The simplified calculation of the proposed procedure has been applied to Joint 2, showing a resulting preliminary fatigue life value lower than 1 year. Thus, the detailed calculation has been applied (Table 6.9).

	Simplified calculation	Detailed calculation
s_u	510 N/mm^2	510 N/mm^2
m_1	3	3
Δ_C	36 N/mm^2	36 N/mm^2
N_L	10^7	10^7
Cut-off	Yes	Yes
n_D	1.752 Hz	1.752 Hz
h_{tot}	7.49 m	7.49 m
b_{ref}	0.685 m	0.685 m
Z_{eq}	4.347 m	4.347 m
$\bar{u}_{ref}$	27 m/s	27 m/s
k		1.20
C_E	III	III
$\bar{s}_P$	33.27 N/mm^2	33.27 N/mm^2
$\bar{s}_{D,ref}$	44.62 N/mm^2	44.62 N/mm^2
$\sigma_{D,ref}$	43.10 N/mm^2	43.10 N/mm^2
$\nu_{D,ref}$	1.377 Hz	1.377 Hz
$\nu_{D,Q,ref}$	0.150 Hz	0.150 Hz
$\lambda_{D,R,ref}$	0.617	0.617
$\alpha_{\sigma,D}$		2.395
$\alpha_{\lambda,D}$		0.868
$\bar{D}_0(1)$	3.1667	0.1886
C_{BM}	0.6648	0.4310
C_M	1.3848	1.3507
C_{SN}	0.9212	0.9202
$\bar{D}(1)$	2.6853	0.1010
T_F	0.4 years	9.9 years

Tab. 6.9: Outcomes from analytical procedure (alongwind analysis) taking into account the ideal normal stress in Joint 2.

The fatigue life of Joints 2 obtained with simplified calculation is hugely not verified, therefore detailed calculation is required. A reliable fatigue life of about 10 years is obtained, a value that is still lower than design life, showing that the structure is not verified according to the proposed procedure, as expected.

The 0 level solution of damage is strongly sensitive to stress value. Bi-modal factor reduces hugely this damage estimation; mean stress factor ups this value by around 30%; fatigue curve factor reduces slightly damage estimate because stress ranges are high enough to be far from the cut-off limit in the considered *S-N* curve. Due to the strong non-linearity of the fatigue damage accumulation, the propagation of uncertainties is significant. Despite this, the result obtained with the proposed procedure is well in line with the inspection, which had pointed out large damages in this joint.

This is not equally true for the method proposed in actual European standard codes. Applying the Eurocode 1 (part 1–4) calculation for alongwind-induced fatigue evaluation it is possible to figure out cycle counting N_g to reach or exceed an effect value ΔS due to wind loading in 50 years of return period. ΔS is expressed as a rate of S_k, which is assumed equal to the maximum normal stress range in the considered structural section. Figure 6.8 shows $\Delta S/S_k$ respect to N_g in percentage terms for Joint 2.

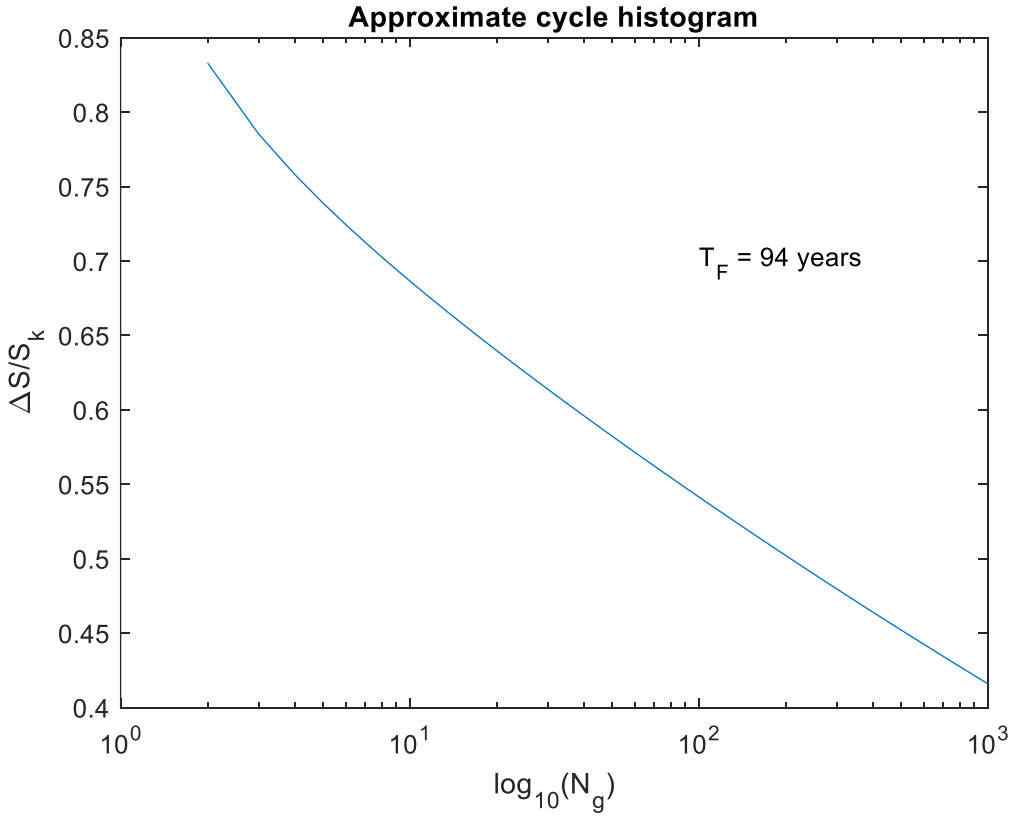

Fig. 6.8: Alongwind-induced fatigue life evaluated by Eurocode 1 (2005) procedure for Joint 2.

The equation provided by Eurocode allows to obtain N_g respect to ΔS variation. Knowing the detail category and its fatigue resistance *S-N* curve, it is also possible to know *N* respect to ΔS variation, which is the number of cycles that leads the structure to collapse. Total damage in 50 years is the summation, or the integral, of damage fractions $N_g(\Delta S)/N(\Delta S)$. Applying the standard procedure for the case in analysis, a fatigue life of T_F = 94 years is obtained. It is therefore clear that this counting cycle equation isn't reliable in the present case, since the obtained outcome is completely not coherent with inspection report and it is critically not on the safe side.

Finally, a comparison of the results obtained with different local climate conditions has been carried out, pretending to locate the sign support structure in every Italian zone defined in CNR code. As expected, fatigue life is heavily dependent on reference wind velocity and Weibull shape parameter *k*, varying from about 32 years to about 2 years of residual life (Fig. 6.9). Since this type of structure is widespread in the territory, considering a fatigue verification procedure is so much important, for design of new structures and for planning inspections campaign.

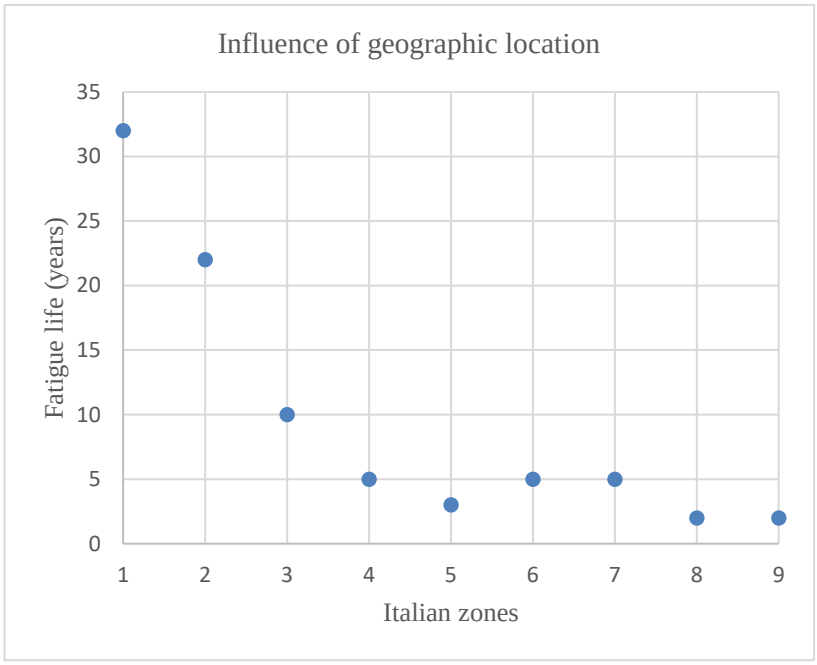

Fig. 6.9: Fatigue life values of the structure obtained referred to different Italian geographical zones.

In conclusion, traffic-sign support structures have been proved to be turbulence-sensitive structural types. The comparison between the inspection and the outcome of the proposed method shows a very good agreement, while the European standard assessment provides unreliable and unsafe results in this case. A strong dependency on climatological input parameters has been again pointed out, showing the importance of an accurate definition of Weibull parameter *k* in different areas.

The choice of the *S-N* curve greatly affects the results and constitute a crucial point in the analysis of such a simple structural type, thus extensive fatigue tests should be carried out in order to create a catalogue of *S-N* curves ad hoc for the details usually adopted by this structural typology. This is particularly critical for shear stress induced fatigue, for which the standard fatigue resistance curves are only related to circular section and furnish unrealistic resistance values in civil structural details.

6.5.2. Analytical analysis with shear stresses

In the current Section 6.5.2 it is presented the attempt to analyse the structure as concerns alongwind-induced fatigue taking into account the actual shear stresses that characterized the considered joint. There are really limited information about fatigue resistance for shear stress in this kind of joints, this being a shortcoming in structural engineering.

Eurocode 3 (2005) and IIW (2016) provide only two bilinear fatigue strength curves for shear stress ranges, one is referred to as Category 80 and one as Category 100. They present a cut-off limit in correspondence of $N_L = 10^8$. The slope of the first broken line is $m_1 = 5$ (see Figure 4.3 in Section 4.2). For this critical joint, the category detail can not be selected on the basis of these documents, because the geometric detail of the actual joint is not provided in their catalogue, not even close.

The choice is to apply the *hot spot* method included in (IIW, 2016), by referring to the *S-N* curve for assessing the fatigue resistance of a detail on the basis of structural hot spot stress (see Section 2.2.2), given by the recommendations for the material and for the welded conditions. It is chosen Category 80.

Therefore, the value of the structural hot spot stress range is determined by means of a finite element model of the structural detail (Fig. 6.10), so that stress raising effects due to the geometry are included, excluding that due to the local weld profile itself.

Fig. 6.10: Finite element model (red corresponds to high stress values).

Simplified and detailed calculations of the proposed generalized procedure has been applied to Joint 2 (Table 6.10).

	Simplified calculation	Detailed calculation
s_u	510 N/mm^2	510 N/mm^2
m_1	5	5
Δ_C	80 N/mm^2	80 N/mm^2
N_L	10^8	10^8
Cut-off	Yes	Yes
n_D	1.752 Hz	1.752 Hz
h_{tot}	7.49 m	7.49 m
b_{ref}	0.685 m	0.685 m
Z_{eq}	4.347 m	4.347 m
$\bar{u}_{ref}$	27 m/s	27 m/s
k		1.20
C_E	III	III
$\bar{s}_P$	0 N/mm^2	0 N/mm^2
$\bar{s}_{D,ref}$	72.64 N/mm^2	72.64 N/mm^2
$\sigma_{D,ref}$	70.17 N/mm^2	70.17 N/mm^2
$\nu_{D,ref}$	1.377 Hz	1.377 Hz
$\nu_{D,Q,ref}$	0.150 Hz	0.150 Hz
$\lambda_{D,R,ref}$	0.617	0.617
$\alpha_{\sigma,D}$		2.395
$\alpha_{\lambda,D}$		0.868
$\bar{D}_0(1)$	2.3670	0.2186
C_{BM}	0.6046	0.4006
C_M	1.8261	1.5562
C_{SN}	1.0000	1.0000
$\bar{D}(1)$	2.6133	0.1363
T_F	0.4 years	7.3 years

Tab. 6.10: Outcomes from analytical procedure (alongwind analysis) taking into account the hot spot shear stress in Joint 2.

The analytical analysis with shear stresses leads to consistent outcomes, as well. This case study constitutes a first validation of the wind-induced fatigue generalized method, valid for different kinds of *S-N* fatigue resistance curves.

6.6. ALUMINIUM POLE

With increased use of welded aluminium light poles along highways and in industrial service applications such as parking lots, harbours, stadiums, etc., it is important that they are sustainable and resist fluctuating wind induced stresses or fatigue loading.

Forty-one welded aluminium shoe base light poles were fatigue tested in the structures laboratory of the University of Akron (Daneshkhah and Menzemer, 2017). A design *S-N* curve for the specific shoe base details used on the light poles was developed by using the fatigue life of the test specimens. The proposed *S-N* curve, which was derived from the test results, includes the endurance limit in high cycle regime. Among forty-one aluminium shoe base light poles, twenty-six specimens failed (63.4%) and the remaining survived (run-outs).

The researchers compared their proposal, corresponding to the extracted lower bound which provides approximately 97.5 percent probability of survival, to the Aluminum Design Manual's (2015) category F1. The *S-N* curve is useful for investigating the fatigue behaviour of the light poles during analysis for wind induced loadings.

In this Section 6.6 an example aluminium pole, 15 m tall, is used to apply the turbulence-induced fatigue generalized method. Only alongwind analysis is carried out. The aim is to make a comparison of the results obtained by considering three different fatigue resistance limits. The *S-N* curves provided by the mentioned paper (the experimental one and the one provided by the Aluminum Design Manual's, 2015, category F1) and the curve provided by IIW document (IIW, 2016), Category 12, are taken under consideration.

The structure is considered in Zone 7, exposure category III, a concentrated mass of 1 kN is located at the top of the pole, a simple finite elements model provide the value of the natural frequency. The assessments are described by Table 6.11.

	IIW resistance curve	ADM resistance curve	Experimental curve
s_u	310 N/mm^2	310 N/mm^2	310 N/mm^2
m_1	3	7.31	10.2
Δ_C	12 N/mm^2	27.40 N/mm^2	39.4 N/mm^2
N_L	10^7	10^7	10^7
Cut-off	No	Yes	Yes
m_2	22	-	-
n_D	0.63 Hz	0.63 Hz	0.63 Hz
h_{tot}	15 m	15 m	15 m
b_{ref}	0.254 m	0.254 m	0.254 m
Z_{eq}	9 m	9 m	9 m
$\bar{u}_{ref}$	28 m/s	28 m/s	28 m/s
k	1.35	1.35	1.35
C_E	III	III	III
$\bar{s}_P$	0.601 N/mm^2	0.601 N/mm^2	0.601 N/mm^2
$\bar{s}_{D,ref}$	30.89 N/mm^2	30.89 N/mm^2	30.89 N/mm^2
$\sigma_{D,ref}$	33.57 N/mm^2	33.57 N/mm^2	33.57 N/mm^2
$\nu_{D,ref}$	0.557 Hz	0.557 Hz	0.557 Hz
$\nu_{D,Q,ref}$	0.144 Hz	0.144 Hz	0.144 Hz
$\lambda_{D,R,ref}$	0.783	0.783	0.783
$\alpha_{\sigma,D}$	2.457	2.457	2.457
$\alpha_{\lambda,D}$	0.407	0.407	0.407
$\bar{D}_0(1)$	1.2931	24.4644	739.0281
C_{BM}	0.8302	0.7740	0.8702
C_M	1.1134	1.8723	2.9346
C_{SN}	0.9997	1.0000	1.0000
$\bar{D}(1)$	1.1949	35.453	1887.2435
T_F	0.8 years	0.03 years	$5 \cdot 10^{-4}$ years

Tab. 6.11: Outcomes from analytical procedure (alongwind analysis) taking into account three different *S-N* curves as fatigue resistance of the base aluminium detail.

The obtained results are really critical. It may be expected that the structure would be strongly not verified, due to the fact that it is really flexible, the response is large in the critical section, the aluminium material is definitely more sensitive to fatigue phenomenon than steel material (*S-N* curves are much lower, indeed). The unexpected consideration is that the most critical result is obtained from the case in which experimental curve is used. This means that, at least for aluminium, codes and recommendations are not on the safe side in some cases.

This issue certainly requires more research work. Although in the three columns of Tab. 6.11 it can be observed that the detail category becomes higher, so the fatigue life would increase, also the slope of the first line of the *S-N* curves becomes higher, this would decrease the fatigue life. When the stress range is quite large, this second parameter, m_1, has an exponentially more relevant role in the fatigue life estimation rather than Δ_C. This is the reason why both $\bar{D}_0(1)$ and C_M raise their values.

6.7. ANTENNA MAST

Antenna mast structures are built in such a large and growing number. They are characterized by increasing height, lightness, slenderness and complicated shape that make them extremely sensitive to complex aeroelastic phenomena and wind-excited vibrations, such as to require refined analyses in order to capture their physical behaviour. An impressive number of damage and collapses that increasingly involved these structures, often due to wind-excited fatigue, but in many cases not so well understood, emphasizes their susceptibility to wind actions and their potentially dangerous role in the anthropogenic territory.

A case study concerning a real antenna mast, taken from existing literature (Nguyen et al., 2015), is analysed. This structure is a telecommunication antenna mast composed by two steel shafts with tubular circular section, whose total height is h_{tot} = 30 m (Fig. 6.11). The first shaft is 24 m long; the outer diameter of its section, whose thickness is constant and equal to 5 mm, varies from 950 mm at the bottom to 350 mm at the top; the cables attached along this shaft have a distributed mass per unit length 5 kg/m. The second shaft, put above the first one, is 6 m long and carries 6 antennas. Its section has constant outer diameter 193.7 mm and constant thickness 7.1 mm; the total mass of the shaft is 540 kg. A stair is placed along the whole structure and has a mass per unit length 7 kg/m. The additional components, namely the stair, the cables and the antennas, give rise to a distributed mass eccentricity; however, they are assumed to be ineffective with regard to the structural stiffness.

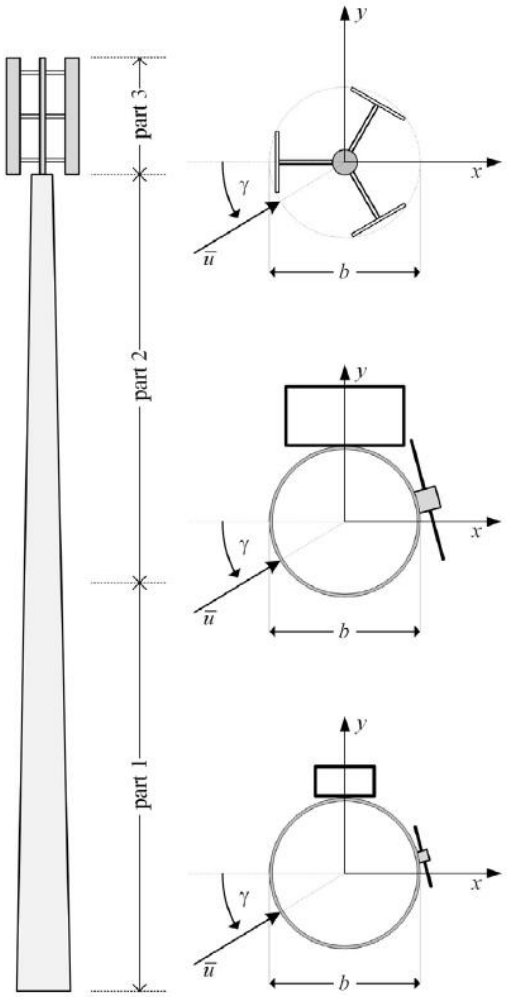

Fig. 6.11: Schematic representations of the antenna mast and of cross-sections at different heights (Figure © Nguyen et al., 2015).

The pole is located in a terrain characterized by a roughness length z_0 = 0.3 m and a basic reference wind velocity $\bar{u}_{ref}$ = 25 m/s; the mean wind velocity profile is logarithmic. Assuming that the reference height is Z_{eq} = 24 m, i.e. the top of the main shaft, the design mean wind velocity at such a height is equal to 23.6 m/s. The aerodynamic characteristics of the structure have been determined by static wind tunnel experiments (Nguyen et al., 2015). The first natural (flexural) frequency in both alongwind and crosswind directions is $n_{\omega 1}$ = 0.77 Hz. The test-case clearly points out the importance of mechanical and aerodynamic eccentricities; in fact, the presence of external devices such as cables and stairs substantially changes the drag coefficient, which results deeply dependent on the direction of the oncoming flow; in addition, large lift forces arise that rapidly change on varying the wind direction.

The proposed procedure to evaluate alongwind and crosswind-induced fatigue results easy to apply from an engineering point of view (Tab. 6.12). The considered *S-N* fatigue curve corresponds to steel

detail category 36 provided by IIW (2016), so that $m_1 = 3$, $\Delta_C = 36$ and $N_L = 10^7$; $a^{I} = 7.44$ and $a^{II} = -3.81$. The shape parameter of the Weibull probability distribution of wind velocities k is taken equal to 1.15. The steel failure characteristic stress is considered as $s_u = 510$ N/mm^2.

	Alongwind buffeting-induced fatigue analysis	Crosswind buffeting-induced fatigue analysis
s_u	510 N/mm^2	510 N/mm^2
m_1	3	3
Δ_C	36 N/mm^2	36 N/mm^2
N_L	10^7	10^7
Cut-off	Yes	Yes
$n_{\omega 1}$	0.77 Hz	0.77 Hz
h_{tot}	30 m	30 m
b_{ref}	0.35 m	0.35 m
Z_{eq}	24 m	24 m
$\bar{u}_{ref}$	25 m/s	25 m/s
k	1.15	1.15
C_E	IV	IV
$\bar{s}_P$	1.818 N/mm^2	1.818 N/mm^2
$\bar{s}_{\omega,ref}$	39.07 N/mm^2	10.16 N/mm^2
$\sigma_{\omega,ref}$	29.26 N/mm^2	32.35 N/mm^2
$\nu_{\omega,ref}$	0.567 Hz	0.727 Hz
$\nu_{\omega,Q,ref}$	0.127 Hz	0.171 Hz
$\lambda_{\omega,R,ref}$	0.543	0.892
$\alpha_{\sigma,\omega}$	2.321	2.558
$\alpha_{\lambda,\omega}$	0.920	0.221
$\bar{D}_0(1)$	0.0241	0.0286
C_{BM}	0.4928	1.0000
C_M	1.0951	1.0456
C_{SN}	0.8247	0.8566
$\bar{D}(1)$	0.0107	0.0256
T_F	93.2 years	39.0 years

Tab. 6.12: Calculation of the fatigue life induced by alongwind and crosswind turbulence.

In both alongwind and crosswind analyses, the 0 level solutions results comparable, with a slightly larger value in crosswind direction, due to larger standard deviation of crosswind response. The bi-modal factor C_{BM} reduces the 0 level damage taking into account the quasi-static part of the response spectrum; in alongwind assessment the quasi-static part of the response has a high role, strongly reducing the total damage; on the contrary, in crosswind assessment the role of quasi-static part of the response is reduced, prevailing the resonant contribution, thus also the reduction of the total damage is lower. This is due to shift of the spectral content of the lateral turbulence towards higher frequency values, which causes a greater contribution of the resonant part of the response of the steel mast. The mean stress corrective factor C_M slightly increases the total damage in both analysis, meaning that the mean response to wind loading is not all that important. Finally, the fatigue curve factor C_{SN} reduces the damage in both cases to the almost same extent, taking into account the cut-off limit of fatigue resistance in steel details. All these considerations highlight that, due to the difference between alongwind and crosswind response spectral characteristics, crosswind turbulence-induced fatigue is widely more critical than alongwind-induced fatigue. In general, the procedure outlines outcomes in accordance with (Nguyen et al., 2015) about the critical issue of exceptional large lift forces on this structure due to mechanical and aerodynamic eccentricities, showing that this also propagates fatigue damage.

In conclusion, crosswind turbulence-induced response and fatigue is actually disregarded in antenna mast structural typology and engineering calculations idealize antenna masts as polar symmetric structures, even if this is usually not correct. Nevertheless, these structures are complex both in mechanical and aerodynamic terms. Such an aspect greatly contributes to make antenna masts sensitive to potential instabilities caused by aeroelastic phenomena and exposed to intense and non-conventional wind-excited vibrations. The proposed method allows to catch the main feature of the fatigue damage phenomenon also in non-conventional situations with quite simple calculation procedure.

CHAPTER 7 – CONCLUSIONS

This thesis develops a general model of the wind-induced fatigue analysis of slender structures, at standard level. It derives from the closed form solution proposed by Repetto and Solari (2012) and it is generalized in order to be suitable for engineering calculations and code provisions. The work contains critical discussions and original contributions on a wide range of different matters, comprehending the fatigue analysis and the wind-induced response.

Chapter 2 revises the current state of the art as regard wind-induced fatigue on slender structures. The first part of the Chapter is devoted to illustrate most common fatigue analysis approaches for structures. Fatigue phenomenon and resistance concepts are introduced, then cycles counting methods and fatigue damage evaluation starting from the spectral properties of the loading process are dealt with. Cycles counting methods proposed in literature for stationary Gaussian narrow-band and broad-band processes are discussed, focusing on the bi-modal cycles counting method by Repetto and Solari (2006) which can be effectively applied to bi-modal processes, which are typical of wind-induced response. The second part of the Chapter concerns the fundamentals of alongwind-induced fatigue methods. It firstly provides a general framework of the wind field, loading and response of slender structures and an overview of concerning mathematical models, commonly adopted by literature and standards. Focusing on alongwind vibrations due to turbulence, fatigue damage may occur in slender flexible structures and some verification methods have been developed in engineering research field. The basic aspects of alongwind-induced fatigue method by Repetto and Solari (2012) are underlined.

Chapter 3 proposes a new generalization of the closed form solution of fatigue damage due to alongwind structural vibrations. The whole formulation is derived analytically in accordance with the old derivation, but in this case a wide range of resistance fatigue curve types, suitable for different materials and different cyclic loading conditions, are covered. The novelty concerns in particular the definition of a generalized fatigue curve factor, whose aim is to correct the damage estimation by taking into account the bi-linear curve trend given by recent international recommendations. The final simplified analytical formulation results in complete accordance with Eurocode format for wind induced Ultimate Limit State analysis.

Since Chapter 3 contains analytical derivations of equations, Appendix A summarizes mathematics not explicitly included in the main Chapter, which are however useful for a full understanding of the final results.

Chapter 4 begins to deal with crosswind-induced fatigue analysis. At this stage, vortex induced vibrations effects are totally neglected and only gust buffeting is taken under consideration. The analytical model presented in previous Chapter 3 can be suitable for both alongwind and crosswind buffeting-induced fatigue analyses. Initially, Chapter 4 summarizes the whole generalized formulation, then two levels of calculations are introduced and derived for particular common cases. The *detailed calculation* may be reasonably adopted in engineering applications to evaluate reliable values of fatigue life of wind-induced fatigue sensitive structures, whereas the *simplified calculation* may provide easy results on the safe side. The application of the latter level of calculation allows to exclude preventively slender structures which are completely not sensitive to wind-induced fatigue from a more detailed and burdensome analysis. This is useful from the perspective of being included among standard verifications. The set of required input parameters is discussed, in particular simple expressions coherent with standard format are defined for both alongwind and crosswind fatigue analysis.

Chapter 5 reports a more comprehensive discussion about crosswind-induced fatigue analysis, taking into account the joint effect of vortex shedding and lateral turbulence. In the first part of the Chapter the vortex shedding phenomenon and its effects on slender structures are described and the most common concerning mathematical models are introduced. A focus is placed on code design procedures to calculated response and fatigue. Although engineering procedures reasonably use to estimate separately crosswind maximum response to gust buffeting and to critical vortex shedding conditions, there's no guarantee such assumption would provide reliable fatigue predictions. This is due to the strong non-linearity of fatigue phenomenon, so that superposition principle is not valid. Therefore, the possibility of separating the effects of the vortex shedding in fatigue analysis is investigated. The significance of different contributions to crosswind-induced fatigue is examined numerically for different case studies (4 example metallic chimneys and 1 pole). Once the possibility of separating the effects in crosswind fatigue analysis is confirmed, at least at standard verification level, the final part of the Chapter deals with VIV-induced fatigue standard method, currently used, and its criticisms. Remarks are focused on two issues: (a) the equation provided by codes to calculate the cycle number due to VIV is too approximated, it is critically discussed and compared to a new preliminary proposal; (b) the role of parameters uncertainties in response and in fatigue evaluations is investigated. It is found out that, by considering as a reasonable approximation the separation of effects in crosswind fatigue analysis, two independent assessments can be carried out for lateral turbulence and for VIV-induced fatigue, but the standard method to predict VIV-induced fatigue life results as too approximated and not reliable compared with numerical simulations. As regards the calculation of the cycle number N due to VIV, a new expression is therefore proposed; on the other hand, the cycle number leading to collapse N_C is affected by huge uncertainties and its estimation would require further research.

Finally, Chapter 6 shows the application of the buffeting-induced fatigue method on some different real case studies. The proposed model is discussed and validated by comparisons with numerical analyses and real inspections. The generalized formulation results useful and to study different situations, such as structural details subjected to shear stresses conditions, slender structures of different materials or slender structures strongly sensitive to lateral turbulence vibrations.

The present work can be further developed in different directions.

As regards the proposed general procedure to assess alongwind and crosswind buffeting-induced fatigue of slender structures, three observations are made. The proposed method does not consider a directional analysis, considering only the most critical direction, as constant, on the safe side (Repetto and Solari, 2004). As first future perspective, the model may be generalized including a directional analysis; however, it would require additional analysis on directional local climatology, not easily suitable at standard level. Secondly, the joint effect of other variable loadings on the structure is not considered; numerical analysis constitutes the only possible approach so far. Third, the model may be extended considering also wind-induced fatigue due to non-synoptic events, starting from the existing literature research of non-stationary processes, coming to fatigue phenomenon considerations in this field.

As regards the standard method to predict VIV-induced fatigue life, following remarks in Chapter 5, further research in this field seems to be necessary. Standard approximation considers all the load cycles counted in correspondence of the critical mean wind velocity; these are all associated with the maximum stress cycle amplitude. Such simplification turns out to be too preventive, distancing from reliable values of damage and fatigue life. Following the preliminary proposed expression to calculate the cycle number N due to VIV, a novel approach at standard level should be required in future.

APPENDIX A

Starting from equations in Tab. 3.1, it is possible to obtain simplified equations in Tab. 3.2 following steps below.

A.1 – 0 level solution of damage

Eq. (3.15) is rewritten considering the relationship $a_1 = N_C \cdot \Delta_C^{m_1}$ with $N_C = 2 \times 10^6$:

$$\bar{D}_0(1) = \frac{\left(2\sqrt{2}\right)^{m_1}}{2 \cdot 10^6 \Delta_C^{m_1}} \left(\frac{\sigma_{ref}}{\bar{u}_{ref}^{\alpha_\sigma}}\right)^{m_1} \frac{\nu_{ref}}{\bar{u}_{ref}^{\alpha_\nu}} (1 - F_0) c^{(\alpha_\nu + m_1 \alpha_\sigma)} \Gamma\left(\frac{m_1}{2} + 1\right) \Gamma\left(\frac{\alpha_\nu + m_1 \alpha_\sigma + k}{k}\right) \tag{A.1}$$

where $\alpha_\nu = 0$ and $F_0 = 0$ may be assumed:

$$\bar{D}_0(1) = \frac{\left(2\sqrt{2}\right)^{m_1}}{2 \cdot 10^6 \Delta_C^{m_1}} \left(\frac{\sigma_{ref}}{\bar{u}_{ref}^{\alpha_\sigma}}\right)^{m_1} \nu_{ref}\, c^{m_1 \alpha_\sigma} \Gamma\left(\frac{m_1}{2} + 1\right) \Gamma\left(\frac{m_1 \alpha_\sigma + k}{k}\right) \tag{A.2}$$

In Italian territory the Weibull parameters k and c may be linked with the reference velocity by the relationship $c = (0.2k - 0.12)\bar{u}_{ref}$:

$$\bar{D}_0(1) = \frac{\left(2\sqrt{2}\right)^{m_1}}{2 \cdot 10^6 \Delta_C^{m_1}} \sigma_{ref}{}^{m_1} \nu_{ref} (0.2k - 0.12)^{m_1 \alpha_\sigma} \Gamma\left(\frac{m_1}{2} + 1\right) \Gamma\left(\frac{m_1 \alpha_\sigma + k}{k}\right) \tag{A.3}$$

The last gamma Function may be solved according to Eq. (3.55):

$$\Gamma\left(\frac{m_1 \alpha_\sigma + k}{k}\right) = \left(\frac{\frac{m_1 \alpha_\sigma + k}{k}}{\mathrm{e}}\right)^{\left(\frac{m_1 \alpha_\sigma + k}{k}\right)} \sqrt{\frac{2\pi}{\frac{m_1 \alpha_\sigma + k}{k}}} = \left(\frac{m_1 \alpha_\sigma}{k} + 1\right)^{\left(\frac{m_1 \alpha_\sigma}{k} + 0.5\right)} \exp\left[-\left(\frac{m_1 \alpha_\sigma}{k} + 1\right)\right] \sqrt{2\pi} \tag{A.4}$$

Eq. (3.57) of simplified 0 level solution of damage in 1 year may be obtained by substituting Eq. (A.4) in Eq. (A.3) and multiplying by the constant 31536000 s (seconds in 1 year).

It is worth notice that one gamma Function remains also in the simplified equation (3.57). It can be easily solved knowing the parameter m_1 of the concerned *S-N* fatigue curve.

$$\Gamma\left(\frac{m_1}{2} + 1\right)$$
$$\left\{\Gamma(\mathrm{x}+1) = \mathrm{x}\,\Gamma(\mathrm{x}); \quad \Gamma(1) = 1; \quad \Gamma\left(\frac{1}{2}\right) = \sqrt{\pi}\right\} \tag{A.5}$$

Therefore, when m_1 = 3 then $\Gamma\left(m_1/2+1\right)=3/4\sqrt{\pi}$; when m_1 = 4 then $\Gamma\left(m_1/2+1\right)=2$; when m_1 = 5, $\Gamma\left(m_1/2+1\right)=15/8\sqrt{\pi}$; etc.

A.2 – Bi-modal factor

Eq. (3.25) is rewritten assuming $\alpha_v=0$ and $c=\left(0.2k-0.12\right)\bar{u}_{ref}$:

$$C_{BM}=\frac{v_{Q,ref}}{v_{ref}}+\frac{n_1}{v_{ref}}\lambda_{R,ref}^{\left(\frac{m_1}{2}\right)}\left(0.2k-0.12\right)^{\left(\frac{m_1}{2}\alpha_\lambda\right)}\frac{\Gamma\left(\dfrac{\dfrac{m_1}{2}\alpha_\lambda+m_1\alpha_\sigma+k}{k}\right)}{\Gamma\left(\dfrac{m_1\alpha_\sigma+k}{k}\right)} \tag{A.6}$$

where gamma Functions may be solved according to Eq. (3.56):

$$\frac{\Gamma\left(\dfrac{m_1\alpha_\lambda}{2k}+\dfrac{m_1\alpha_\sigma+k}{k}\right)}{\Gamma\left(\dfrac{m_1\alpha_\sigma+k}{k}\right)}=\frac{\sqrt{2\pi}\mathrm{e}^{-\frac{m_1\alpha_\sigma+k}{k}}\left(\dfrac{m_1\alpha_\sigma+k}{k}\right)^{\frac{m_1\alpha_\sigma+k}{k}+\frac{m_1\alpha_\lambda}{2k}-\frac{1}{2}}}{\sqrt{2\pi}\mathrm{e}^{-\frac{m_1\alpha_\sigma+k}{k}}\left(\dfrac{m_1\alpha_\sigma+k}{k}\right)^{\frac{m_1\alpha_\sigma+k}{k}-\frac{1}{2}}}=\left(\frac{m_1\alpha_\sigma+k}{k}\right)^{\frac{m_1\alpha_\lambda}{2k}} \tag{A.7}$$

Eq. (3.58) of simplified bi-modal factor can be obtained by substituting Eq. (A.7) in Eq. (A.6).

A.3 – Mean stress factor

Eq. (3.37) is rewritten assuming $\alpha_v=0$ and $c=\left(0.2k-0.12\right)\bar{u}_{ref}$:

$$C_M=\left(\frac{s_u}{s_u-\bar{s}_p}\right)^{m_1}\left[1+\frac{m_1\bar{s}_{ref}}{\left(s_u-\bar{s}_p\right)}\left(0.2k-0.12\right)^2\frac{\Gamma\left(\dfrac{m_1\alpha_\sigma+k+2}{k}\right)}{\Gamma\left(\dfrac{m_1\alpha_\sigma+k}{k}\right)}\right] \tag{A.8}$$

where gamma Functions may be solved according to Eq. (3.56):

$$\frac{\Gamma\left(\dfrac{2}{k}+\dfrac{m_1\alpha_\sigma+k}{k}\right)}{\Gamma\left(\dfrac{m_1\alpha_\sigma+k}{k}\right)}=\frac{\sqrt{2\pi}\mathrm{e}^{-\frac{m_1\alpha_\sigma+k}{k}}\left(\dfrac{m_1\alpha_\sigma+k}{k}\right)^{\frac{m_1\alpha_\sigma+k}{k}+\frac{2}{k}-\frac{1}{2}}}{\sqrt{2\pi}\mathrm{e}^{-\frac{m_1\alpha_\sigma+k}{k}}\left(\dfrac{m_1\alpha_\sigma+k}{k}\right)^{\frac{m_1\alpha_\sigma+k}{k}-\frac{1}{2}}}=\left(\frac{m_1\alpha_\sigma+k}{k}\right)^{\frac{2}{k}} \tag{A.9}$$

Eq. (3.59) of simplified mean stress factor can be obtained by substituting Eq. (A.9) in Eq. (A.8).

A.4 – Generalized fatigue curve factor

The actual novelty of this step of the research regards the fatigue curve factor formulation, that in Repetto and Solari procedure (2012) corrects the 0 level solution taking into account the specific trilinear

S-N fatigue curve trend of steel structural details subjected to normal stresses, furnished by Eurocode. Here this hypothesis of fixed *S-N* curve in a bi-logarithmic diagram is overcome, generalizing the formulation of the C_{SN} factor covering different possible fatigue curve types presented in standards and recommendation.

Rewriting the expression (3.53) of the fatigue curve factor, Eqs. (A.10) and (A.11) are obtained:

$$C_{SN}=\frac{1}{\tilde{D}-\tilde{L}}\left\{r\frac{\Gamma\left(\frac{\alpha_v+(m_1+1)\alpha_\sigma+k}{k}\right)}{\Gamma\left(\frac{\alpha_v+m_1\alpha_\sigma+k}{k}\right)}\left[\Gamma_{inc}\left(t_D,\frac{\alpha_v+(m_1+1)\alpha_\sigma+k}{k}\right)-\Gamma_{inc}\left(t_L,\frac{\alpha_v+(m_1+1)\alpha_\sigma+k}{k}\right)\right]\right.$$
$$\left.+\tilde{D}\left[1-\Gamma_{inc}\left(t_D,\frac{\alpha_v+m_1\alpha_\sigma+k}{k}\right)\right]-\tilde{L}\left[1-\Gamma_{inc}\left(t_L,\frac{\alpha_v+m_1\alpha_\sigma+k}{k}\right)\right]\right\} \tag{A.10}$$

$$r=\frac{\sigma_{ref}c^{\alpha_\sigma}}{\Delta_C\bar{u}_{ref}^{\alpha_\sigma}};\quad t_D=\left(\frac{\tilde{D}}{r}\right)^{k/\alpha_\sigma};\quad t_L=\left(\frac{\tilde{L}}{r}\right)^{k/\alpha_\sigma} \tag{A.11}$$

where $\tilde{D}$ and $\tilde{L}$ = non dimensional parameters depending on curve *S-N* different trends, whose value are obtained analyzing empirically the Chi factor χ_{SN} (Eqs. (3.43), (3.44) and (3.45)). Different *S-N* bilinear curves are considered, associating each trend with a different couple of values of $\tilde{D}$ and $\tilde{L}$.

Considering the simplification $\alpha_v=0$:

$$C_{SN}=\frac{1}{\tilde{D}-\tilde{L}}\left\{r\frac{\Gamma\left(\frac{(m_1+1)\alpha_\sigma+k}{k}\right)}{\Gamma\left(\frac{m_1\alpha_\sigma+k}{k}\right)}\left[\Gamma_{inc}\left(t_D,\frac{(m_1+1)\alpha_\sigma+k}{k}\right)-\Gamma_{inc}\left(t_L,\frac{(m_1+1)\alpha_\sigma+k}{k}\right)\right]\right.$$
$$\left.+\tilde{D}\left[1-\Gamma_{inc}\left(t_D,\frac{m_1\alpha_\sigma+k}{k}\right)\right]-\tilde{L}\left[1-\Gamma_{inc}\left(t_L,\frac{m_1\alpha_\sigma+k}{k}\right)\right]\right\} \tag{A.12}$$

C_{SN} depends on the stress level, on the *S-N* curve and on the wind parameters, in accordance with the non-dimensional ratio r^{k/α_σ} (Eq. (A.11)). Three distinct ranges of C_{SN} occur depending on r^{k/α_σ} (Fig. 3.4). In the first range, for small r^{k/α_σ} values, C_{SN} tends to 0 due to the effect of the eventual cut-off limit or high m_2 slope value of the *S-N* curve; so, C_{SN} drastically reduces the first level total damage. In the second range, for intermediate r^{k/α_σ} values, C_{SN} varies from 0 to 1 due to the moderate level of stress amplitude cycles which may correspond to the first or the second broken line of the effective *S-N* curve; so, C_{SN} reduces the first level total damage (less than in the first range). In the third range, for high r^{k/α_σ} values, C_{SN} = 1 due to the coincidence between the slope of the effective *S-N* curve and that adopted in the 0 level solution.

As already mentioned, numerical constant values of $\tilde{D}$ and $\tilde{L}$ are assumed for every combination of m_1, m_2 and N_L, leading to formation of groups of curves, some represented as examples in Fig. A.1.

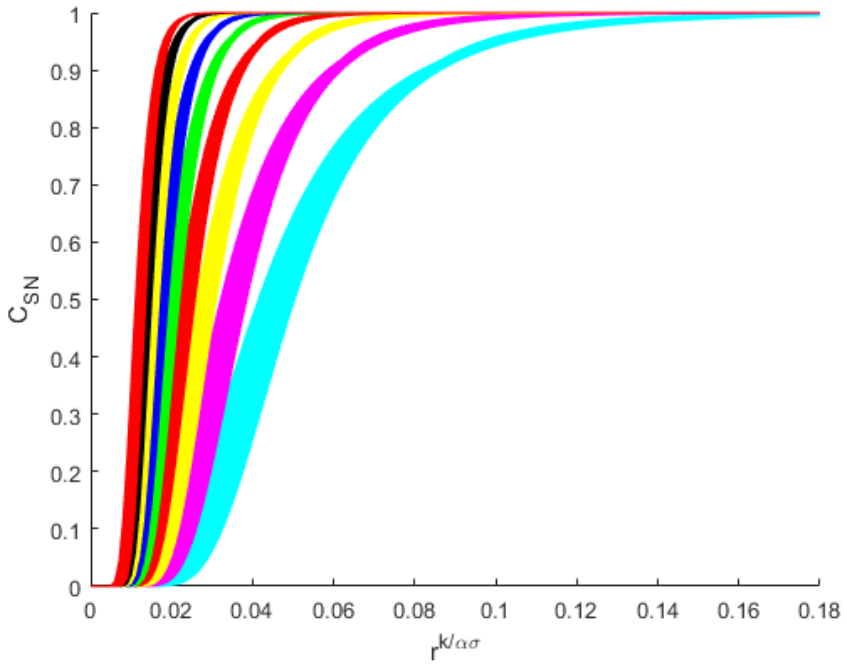

Fig. A.1: C_{SN} fatigue curve factor families of curves, concerning *S-N* fatigue curves with m_1 = 3-11 and $N_L = 10^7$.

Eq. (A.12) remains quite complex because of the presence of the Incomplete gamma Function, for which no suitable approximations have been proposed in the literature. To overcome this problem, it is worth noting that the groups of curves in function of r^{k/α_σ} (Fig. A.1) show a compact tendency that can be summarized in accordance with this equation:

$$C_{SN} = 1 - \exp\left\{-\left(A \cdot r^{\frac{k}{\alpha_\sigma}}\right)^B\right\} \tag{A.13}$$

where A and B have different values again depending on m_1, m_2 and N_L. Fig. A.2 shows one of the approximated fatigue curve factor C_{SN} (Eq. A.13, thick solid line), which summarizes the group of C_{SN} obtained with the closed form solution (Eq. A.12, dotted lines) as an example.

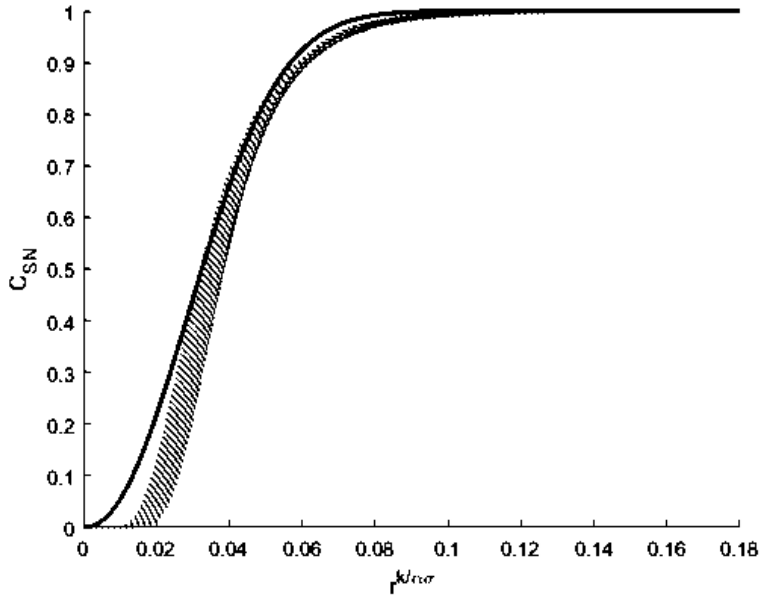

Fig. A.2: C_{SN} fatigue curve factor concerning *S-N* fatigue curves with $m_1 = 4$ and cut-off on $N_L = 10^7$: empirical approximation.

A and *B* in Eq. (A.13) are estimated empirically for every combination of m_1, m_2 and N_L and given in function of these three parameters. Equations proposed for *A* and *B* provide a simplified formulation of C_{SN}, given by Eq. (3.60) where $a^I = +7.44$ and $a^{II} = -3.81$ in the case of bilinear trend with slope m_1 and cut-off limits on N_L; $a^I = +6.33$ and $a^{II} = +2$ in the case of bilinear trend with two different slopes m_1 and m_2, separated on N_L knee.

REFERENCES

- AASHTO, American Association of State Highway and Transportation Officials, *Standard Specifications for Structural Supports for Highway Signs, Luminaires, and Traffic Signals*, 2018 edition.
- Acebedo R., Kim S.W., Hwang Y.C., Kim H.K., "Effect of turbulence length scale on vortex induced vibration of twin deck bridge section", in *Proc. Advances in Civil, Environmental and Materials Research, ACEM16*, Korea, 2016.
- Alexander L.A., Wood J., "A study of low-cycle fatigue failure of a galvanized steel lighting column", in *Eng Failure Anal*, 16, 2009, pp. 2153–2162.
- Aluminum Association, *Specification for Aluminum Structures: Aluminum Design Manual 2015*, Washington, DC, 2015.
- Anderson T.L., "Fracture mechanics: fundamentals and applications", CRC Press, Boca Raton, Florida, 1991.
- Atzori B., Meneghetti G., Rossi B., "Resistenza a fatica di strutture in leghe di alluminio: normative a confronto e verifica sperimentale", in *Frattura ed Integrità Strutturale*, 3(9), July 2009.
- Ballio G., Calado L., Castiglioni C.A., "Low cycle fatigue behaviour of structural steel members and connections", in *Fat. Fract. of Engng. Mat. & Struct.*, 20, 1997, pp. 1129-1146.
- Ballio G., Castiglioni C.A., "Approach to the seismic design of steel structures based on cumulative damage criteria", in *Earthquake Engng. & Struct. Dyn.*, 23, 1994, pp. 969-986.
- Ballio G., Lagomarsino S., Piccardo G., Solari G., "Probabilistic analysis of Italian extreme winds: Reference velocity and return criterion", in *Wind Struct.*, 2(1), 1999, pp. 51–68.
- Barsom J.M., "Fatigue crack propagation", Trans., ASME, Ser.B, 4, 1971.
- Basu R.I., Vickery B.J., "Across-wind vibrations of structure of circular cross-section. Part II. Development of a mathematical model for full-scale application", in *J. Wind Eng. Ind. Aerodyn.*, 12 (1), 1983, pp. 75–97.
- Bathias C., "Fatigue of composite materials", ISTE, London and John Wiley & Sons (Ed.), Fatigue of Materials and Structures: Application to Damage and Design, New York, 2011, pp. 179-204.
- Benedetti M., Fontanari V., Battisti L., "Structural Health Monitoring of Wind Towers: Residual Life Estimation", in *Smart Materials and Structures*, 22, 2013, pp. 1-13.
- Blevins R.D., "Flow-induced Vibration", second ed. *Krieger Publ Company*, Malabar FL, 2001.
- Brown B.F., "Stress corrosion cracking control measures", Nat. Bur. Stds., Monograph 156, 1977.
- Burlando M., Carassale L., Georgieva E., Ratto C.F., Solari G., "A simple and efficient procedure for the numerical simulation of wind fields in complex terrain", in *Boundary Layer Meteorol.*, 125(3), 2007a, pp. 417–439.
- Burlando M., De Gaetano P., Pizzo M., Repetto M.P., Solari G., Tizzi M., "Wind climate analysis in complex terrain", in *J. Wind Eng. Ind. Aerodyn.*, 123, 2013, pp. 349–362.
- Burlando M., Freda A., Ratto C.F., Solari G., "A pilot study of the wind speed along the Rome-Naples HS/HC railway line. Part 1—Numerical modelling and wind simulations", in *J. Wind Eng. Ind. Aerodyn.*, 98(8–9), 2010, pp. 392–403.
- Burlando M., Georgieva E., Ratto C.F., "Parameterization of the planetary boundary layer for diagnostic wind models", in *Boundary Layer Meteorol.*, 125(2), 2007b, pp. 389–397.

- Caracoglia L., Jones N.P., “Wind-induced failures of highway light poles during winter storms”, in *Proceedings of the ASME pressure vessels and piping division conference*, 2006, pp. 23–27.
- Castino F., Rusca L., Solari G., “Wind climate micro-zoning: A pilot application to Liguria region (north western Italy)”, in *J. Wind Eng. Ind. Aerodyn.*, 91(11), 2003, pp. 1353–1375.
- Cazaud R., “La fatigue des metaux”, (V Ed.), Pomey, Rabbe and Janssen Eds, Dunod, Paris, 1969.
- Chen X., “Extreme value distribution and peak factor of crosswind response of flexible structures with nonlinear aeroelastic effect”, in *J. Struct. Eng.*, 2014a.
- CICIND, International Committee on Industrial Chimneys, *Model Code for Steel Chimneys*, Revision 1, Amendment A, December 1999.
- Clobes M., Willecke A., "Life Cycle Analysis of a Guyed Mast Considering Gust and Vortex Excitation", in *Journal of the International Association for Shell and Spatial Structures: J. IASS*, 2014, pp. 131-141.
- CNR_DT_207, *Istruzioni per la valutazione delle azioni e degli effetti del vento sulle costruzioni*, Roma, 2008 (Review 2018).
- Cook N.J., Harris R.I., “Exact and general FT1 penultimate distributions of extreme wind speeds drawn from tail-equivalent Weibull parents”, in *Struct. Saf.*, 26(4), 2004, pp. 391–420.
- Daly A.F., “Evaluation of methods of predicting the across-wind response of chimneys”, *CICIND report*, Vol. 2, 1986.
- Daneshkhah A.R., Menzemer C.C., “Long-Term Fatigue Behavior of Aluminum Shoe-base Details Top Mounted Luminaries”, ASCE library, Structures Congress, 2017, pp. 375-385.
- Daniels S.J., Castro I.P., Xie Z.T., “Numerical analysis of freestream turbulence effects on the vortex-induced vibrations of a rectangular cylinder”, in *J. Wind Eng. Ind. Aerodyn.*, 153, 2016, pp. 13–25.
- Das G., Chakrabarty S., Dutta A.K., Das S.K., Gupta K.K., Ghosh R.N., “Failure analysis of a high mast lamp post”, in *Eng Failure Anal*, 13, 2006, pp. 1153–1158.
- Davenport A.G., “The application of statistical concepts to the wind loading of structures”, in *Proc. Inst. Civ. Eng*., 19(4), 1961, pp. 449–472.
- Davenport A.G., “The estimation of load repetitions on structures with application to wind induced fatigue and overload”, in *RILEM international symposium on the effects of repeated loading of materials and structures*, 1966, p. 118.
- Davis PJ., “Gamma function and related functions”, In *Abramowitz M, Stengun IA, editors*. Handbook of mathematical function. New York: Dover Publication; 1965, p. 25393 [Chapter 6].
- De Gaetano P., Repetto M.P., Repetto T., Solari G., “Separation and classification of extreme wind events from anemometric records”, in *J. Wind Eng. Ind. Aerodyn.*, 126, 2014, pp. 132–143.
- Deoliya R., Datta T.K., “Fatigue reliability analysis of microwave antenna towers due to wind”, in *Journal of Structural Engineering*, ASCE, 127(10), 2002, pp. 1221-1230.
- Dionne M., Davenport A.G., “A simple relationship between the gust response factor and fatigue damage”, in *J. Wind. Eng. Ind. Aerodyn.*, 30, 1988, pp. 45–54.
- Dirlik T., “Application of computers to fatigue analysis”, Ph.D. thesis, Warwick University, Warwick, 1985.
- Dowling N.E., “Fatigue Failure Prediction for Complicated Stress-Strain Histories”, in *Journal of Materials*, JMLSA, 7(1), 1972, pp. 71-87.
- Endo T., Mitsunaga K., Nakagawa H., "Fatigue of Metals Subjected to Varying Stress — Prediction of Fatigue Lives," in *Preliminary Proceedings of The Chugoku-Shikoku District Meeting*, The Japan Society of Mechanical Engineers, November, 1967, pp.41-44.

- Endo T., Mitsunaga K., Nakagawa H., Ikeda K., "Fatigue of Metals Subjected to Varying Stress — Low Cycle, Middle Cycle Fatigue," in *Preliminary Proceedings of The Chugoku-Shikoku District Meeting*, The Japan Society of Mechanical Engineers, November, 1967, pp. 45-48.
- Endo T. et al., "Rain flow method—the proposal and the applications". Memoir Kyushu Institute of Technical Engineering. Standard Practice for Cycle Counting in Fatigue Analysis. ASTM E 1049-85, 1974.
- ESDU (Engineering Sciences Data Unit), "The response of flexible structures to atmospheric turbulence", Item 76001, London, 1976.
- ESDU (Engineering Sciences Data Unit), "World-wide extreme wind speeds. Part 1: Origins and methods of analysis", Item 87034, London, 1990.
- ESDU (Engineering Sciences Data Unit), "Lift-curve slope for structural response calculations", Item 93013, London, 1993.
- ESDU (Engineering Sciences Data Unit), "Computer program for wind speeds and turbulence properties: Flat or hill sites in terrain with roughness changes", Item 92032, London, 1993.
- ESDU (Engineering Sciences Data Unit), "Response of Structures to Vortex Shedding. Structures of Circular or Polygonal Cross Section", Item 96030, London, 1998.
- European Committee for Standardization (CEN) (2005, corrigendum 2010). *EN 1991-1-4 – Eurocode 1 – Actions on structures – Part 1-4: General actions – Wind actions*.
- European Committee for Standardization (CEN) (2005). *EN 1993-1-9 – Eurocode 3 – Design of steel structures – Part 1-9: Fatigue*.
- European Committee for Standardization (CEN) (1998). *ENV 1999-2 – Eurocode 9 – Design of aluminium structures – Part 2: Structures susceptible to fatigue*.
- Facchinetti M.L., de Langre E., Biolley F., "Coupling of structure and wake oscillators in vortex-induced vibrations", in *J. Fluids Struct.*, 19, 2004, pp. 123–140.
- Farshidianfar A., Zanganeh H., "A modified wake oscillator model for vortex-induced vibration of circular cylinder for a wide range of mass-damping ratio", in *J. Fluids Struct.*, 26, 2010, pp. 430–441.
- Feng C.C., "The measurement of vortex-induced effects in a flow past stationary and oscillating circular and D-section cylinders", Master's thesis, Univ. of British Columbia, Vancouver, British Columbia, Canada, 1968.
- Freda A., Solari G., "A pilot study of the wind speed along the Rome-Naples HS/HC railway line. Part 2—Probabilistic analyses and methodology assessment", in *J. Wind Eng. Ind. Aerodyn.*, 98(8–9), 2010, pp. 404–416.
- Fricke W., "Fatigue analysis of welded joints: State of development", in *Marine Structures*, 16, 2003, pp.185-200.
- Fricke W., "Guideline for the fatigue assessment by notch stress analysis for welded structures", IIW document XIII-2240-08/XV-1289-08, 2008.
- Fricke W., "Recent developments and future challenges in fatigue strength assessment of welded joints", in *Proceedings of the Institution of Mechanical Engineers, Part C: Journal of Mechanical Engineering Science*, 2014, published 2015.
- Gilani A., Whittaker A., "Fatigue life of steel post structures", in *J Struct Eng*, ASCE, 126(3), 2000, pp. 322–340.
- Gomes L., Vickery B.J., "On the prediction of extreme wind speeds from the parent distribution", in *Journal of Wind Engineering and Industrial Aerodynamics*, 2, 1, 1977, pp. 21-36.
- Goodman, J., "Mechanics applied to engineering", Longmans Green, London, U.K., 1930.
- Goswami I., Scanlan R.H., Jones N.P., "Vortex-induced vibration of circular cylinders. I: experimental data", in *J. Engng Mech.*, Vol. 119, No. 11, 1993a.

- Goswami I., Scanlan R.H., Jones N.P., “Vortex-induced vibration of circular cylinders. II: new model”, in *J. Eng. Mech.*, ASCE, 119 (11), 1993, pp. 2288–2302.
- Griffin O.M., Skop R.A., Ramberg S.E., "The resonant vortex-excited vibrations of structures and cable systems", *Offshore Tech. Conf., Paper OTC-2319*, Houston, Texas, 1975.
- Gumbel E.J., “Statistics of extreme”, Columbia University, New York, 1958.
- Hamilton H.R., Riggs G.S., Puckett J.A., “Increasing damping in cantilevered traffic signal structures”, in *J Struct Eng*, ASCE, 126(4), 2000, pp. 530–537.
- Hansen S.O., “Vortex induced vibrations of line-like structures”, *CICIND Rep.* 15 (1), 1999.
- Hansen S.O., “Vortex-induced vibrations of structures”, in *Structural Engineers World Congress*, Bangalore, 2007.
- Hansen S.O., “Vortex-induced vibrations – the Scruton number revisited”, in *Proc. Inst. Civ. Eng. Struct. Build.* 166 (SB10), 2013, pp. 560–571.
- Harris R.I., “XIMIS, a penultimate extreme value method suitable for all types of wind climate”, in *J Wind Eng Ind Aerodyn*, 97, 2009, pp. 271–286.
- Hartlen R.T., Currie I.G., “Lift-oscillator model of vortex-induced vibration”, in *J. Eng. Mech. Div.*, ASCE, 96, 1970, pp. 577–591.
- Hoaglin D.C., Mosteller F., Tukey J.W., “Understanding robust and exploratory data analysis”, Wiley, New York, 1983.
- Holmes J.D., “Along-wind response of lattice towers. I: Derivation of expressions for gust response factors”, in *Eng. Struct.*, 16(4), 1994, pp. 287–292.
- Holmes J.D., “Fatigue life estimates under along-wind loading - closed-form solutions”, in *Engineering Structures* 24, 2002, pp. 109-114.
- Holmes J.D., “Response of cylindrical structures to vortex shedding in the natural wind”, in *Thompson, M.C., Hourigan, K. (Eds.), Proc. 13th Australasian Fluid Mechanics Conf.*, Melbourne, 1998, pp. 401–404.
- Holmes J. D., Moriarty W.W., “Application of the generalized Pareto distribution to extreme value analysis in wind engineering”, in *J. Wind Eng. Ind. Aerodyn.*, 83(1–3), 1999, pp. 1–10.
- Holmes J.D., Rofail A.W., “Recent developments in predictions of wind-induced fatigue life”, in *Proceedings WES08*, England, Guildford, 2008.
- IEA, International Energy Agency, *Recommended practices for wind turbine testing and evaluation – Part 3 – FATIGUE*, 1990.
- IIW, International Institute of Welding, *Recommendations for fatigue design of welding joints and components*, document XIII / XV revision, 2016 edition.
- Jenkinson A.F., “The frequency distribution of the annual maximum (or minimum) values of meteorological elements”, in *Q. R. Meteorolog. Soc.*, 81(348), 1955, pp. 158–171.
- Jha S.K., Larsen J.M., Rosenberger A.H., “The role of competing mechanisms in the fatigue life variability of a nearly fully-lamellar c-TiAl based alloy”, in *Acta Materialia* 53, 2005, pp. 1293–1304.
- Jia J., "Wind and structural modeling for an accurate fatigue life assessment of tubular structures", in *Engineering Structures*, 33, 2011, pp. 477-491.
- Jiao G., Moan T., “Probabilistic Analysis of Fatigue due to Gaussian Load Processes”, in *Prob Engng Mech*, 5, 1992, pp. 76–83.
- Kanninen M.F., Popelar C.H., “Advanced fracture mechanics”, Oxford University Press, New York, 1985, p. 22.
- Kareem A., “Wind effects on structures: a probabilistic viewpoint”, in *Probabilistic Engineering Mechanics* 25, 1987, pp. 166–200.

- Kawecki J., Zuranski J.A., “Cross-wind vibrations of steel chimneys – a new case history”, in *J. Wind Eng. Ind. Aerodyn.*, 95, 2007, pp. 1166–1175.
- Kemper, F.H., Feldmann, M., “Fatigue life prognosis for structural elements under stochastic wind loading based on spectral methods, Part I: Linear structures”, *Proceedings of the 8th International Conference on Structural Dynamics, EURODYN 2011,* July 4-6, Leuven, Belgium, 2011.
- Kemper F.H., “Damage Equivalence Concept for the Fatigue Design due to Gust Response”, in *Proceedings of the 15th International Conference on Wind Engineering*, Beijing, China, 2019.
- Klinger C., Hortmanns M., Ruscheweyh H., Wohler H., “Crane failures due to wind induced vibrations”, in *Stahlbau*, 65(10), 1996, pp. 377–391.
- Klinger C., Michael T., Bettge D., "Fatigue cracks in railway bridge hangers due to wind induced vibration - Failure analysis, measures and remaining service life estimation", in *Engineering Failure Analysis*, 43, 2014, pp. 232-252.
- Krenk S., Nielsen S.R.K., “Energy balanced double oscillator model for vortex-induced vibrations”, in *Journal of Engineering Mechanics*, Vol. 125, 1999, pp. 263-271.
- Lagomarsino S., Piccardo G., Solari G., “Statistical analysis of high return period wind speeds”, in *J. Wind Eng. Ind. Aerodyn.*, 41(1–3), 1992, pp. 485–496.
- Lanza Y., “Aerodinamica degli edifici a torre e danno per fatica indotto dalla turbolenza atmosferica sui sistemi di supporto alla facciata”, Master's thesis, Univ. of Genoa, Italy, 2020.
- Lutes L.D., Corazao M., Hu S.J., Zimmerman J., “Stochastic Fatigue Damage Accumulation”, in *J. Struct. Eng.*, 110(11), 1984, pp. 2585-2601.
- Marris A.W., “A review of vortex streets, periodic wakes and induced vibration phenomena”, in *J. Basic Eng., Trans. Am. Soc. Mech. Eng.*, 86, 1964, pp. 185-193.
- Mikitarenko M.A., Perelmuter A.V., “Safe fatigue life of steel towers under the action of wind vibrations”, in *J. Wind. Eng. Ind. Aerodyn.*, 74–76, 1998, pp. 1091–1100.
- Miner M., “Cumulative Damage in Fatigue”, Trans. A.S.M.E., 67, A159, 1945.
- Monin A.S., Obukhov A.M., “Basic laws of turbulent mixing in the ground layer of the atmosphere”, in *Trans. Geophys. Inst. Akad. Nauk. USSR*, 151, 1954, pp. 163–187.
- Muc A., “A fuzzy set approach to interlaminar cracks simulation problems”, in *International Journal of Fatigue* 24, 2002, pp. 419–427.
- National Climatic Data Center, U.S. Department of Commerce, “NNDC climate data online”, ncdc.noaa, 2014.
- Nguyen C.H., Freda A., Solari G., Tubino F., “Aeroelastic instability and wind-excited response of complex lighting poles and antenna masts”, in *Engineering Structures* 85, 2015, pp. 264–276.
- Niemi E., Fricke W., Maddox S.J., “Fatigue analysis of welded components—designer’s guide to structural hot-spot stress approach”, IIW doc. XIII-1819-00/XV-1090-01, update June 2003. Woodhead Publishing, Cambridge, UK, 2006.
- Pagnini L.C., Piccardo G., “A generalized gust factor technique for evaluating the wind–induced response of aeroelastic structures sensitive to vortex induced vibrations”, in *J. Fluids Struct.*, 70, 2017, pp. 181–200.
- Pagnini L.C., Piccardo G., Solari G., “VIV regimes and simplified solutions by the spectral model description”, in *Journal of Wind Engineering & Industrial Aerodynamics*, 198, 2020.
- Pagnini L.C., Repetto M.P., “The role of parameter uncertainties in the damage prediction of the alongwind-induced fatigue”, in *Journal of Wind Engineering and Industrial Aerodynamics*, 104-106, 2012, pp. 227-238.

- Pagnini L.C., Solari G., “Preliminary elements for an innovative wind map of Italy”, in *Proceedings of the EACWE5*, Florence, 2009.
- Pagnini L.C., Solari G., "Joint Modeling of the Parent Population and Extreme Value Distributions of the Mean Wind Velocity", in *Journal of Structural Engineering (ASCE)*, 142(2), 2016, pp. 1-10.
- Païdouissis M.P., Price S.J., de Langre E., “Fluid-structure Interactions – Cross-Flow Induced Instabilities”, *Cambridge Univ Press*, New York, 2011.
- Panofsky H.A., Dutton, J.A., “Atmospheric Turbulence: Models and Methods for Engineering Applications”, Wiley, New York, 1984.
- Paris P., Erdogan F., “A critical analysis of crack propagation laws”, in *J. Basic Eng.*, R. Trans. ASME 85, 1963, pp.528-534.
- Paris P.C., “The fracture mechanics approach to fatigue”, in *Fatigue – An Interdisciplinary Approach*, New York, 1964.
- Patel K., Freathy P., “A simplified method for assessing wind-induced fatigue damage”, in *Engineering Structures*, 6(4), 1984, pp. 268–273.
- Peil U., Behrens M., “Fatigue of tubular steel lighting columns under wind load”, in *Wind Struct*, 5, 2002, pp. 463–478.
- Peil U., Nolle H., “On fatigue of guyed masts due to wind load”, in *Proc., ICOSSAR '93*, Structural safety and reliability, Rotterdam, Balkema, 1994, pp. 1719-1722.
- Peterson R.E., “Interpretation of service fractures”, in Handbook of experimental stress analysis, *Ed. Hetenyi, John Wiley & Sons*, New York, 1960.
- Petrov A.A., “Dynamic response and life prediction of the steel structures under wind loading”, in *J. Wind. Eng. Ind. Aerodyn.*, 74–76, 1998, pp. 1057–1065.
- Piccardo G., Solari G., “3-D wind-excited response of slender structures: Closed form solution”, in *Journal of Structural Engineering*, 126(8), 2000, pp. 936–943.
- Piccardo G., Solari G., “Probabilistic 3-D turbulence modeling for gust buffeting of structures”, in *Prob Engng Mech*, 16, 2001, pp. 73-86.
- Piccardo G., Solari G., “3-D gust effect factor for slender vertical structures”, in *Probabilistic Engineering Mechanics*, 17(2), 2002, pp. 143–155.
- Pickands J., “ Statistical interference using order statistics”, in *Annals of Mathematical Statistics*, 3, 1975, pp. 119-131.
- Pritchard B.N., “Steel chimney oscillations: a comparative study of their reported performance versus predictions using existing design techniques”, in *Eng Struct*, 6, 1984, pp. 315–323.
- Repetto M.P., “Wind-induced response and fatigue of slender vertical structures”, PhD Thesis, University of Genoa, Italy, 2003.
- Repetto, M.P., “Cycles counting methods for bi-modal stationary Gaussian processes”, in *Probabilistic Engineering Mechanics*, 20(3), 2005, pp. 229–238.
- Repetto M.P., Solari G., “Dynamic alongwind fatigue of slender structures”, in *Engineering Structures*, 23(12), 2001, pp. 1622–1633.
- Repetto M.P., Solari G., “Dynamic crosswind fatigue of slender structures”, in *Wind and Structures*, 5(6), 2002, pp. 527–542.
- Repetto M.P., Solari G., “Directional wind-induced fatigue of slender vertical structures”, in *Journal of Structural Engineering*, 130(7), 2004, pp. 1032–1040.
- Repetto M.P., Solari G., "Bimodal alongwind fatigue of structures", in *Journal of Structural Engineering*, 132(6), 2006, pp. 899–908.
- Repetto, M.P., Solari, G. “Wind-induced fatigue of structures under neutral and non-neutral

atmospheric conditions", in *J. Wind Eng. Ind. Aerod.*, 95, 2007, pp. 1364-1383.

- Repetto, M.P., Solari, G., "Alongwind-induced fatigue of structures: closed form solution and engineering approximations", In *CD Proc. of the 11 ACWE*. Puerto Rico, 2008.
- Repetto M.P., Solari G., "Closed form solution of the alongwind-induced fatigue damage to structures", in *Engineering Structures*, 31(10), 2009, pp. 2414–2425.
- Repetto M.P., Solari G., "Wind-induced fatigue collapse of real slender structures", in *Engineering Structures*, 32, 2010, pp. 3888-3898.
- Repetto M.P., Solari G., "Closed-Form Prediction of the Alongwind-Induced Fatigue of Structures", in *Journal of Structural Engineering*, ASCE, 138, 2012, pp. 1149-1160.
- Rice S.O., "Mathematical Analysis of Random Noise", in *Bell System Technical Journal*, 1944.
- Robertson A.P., Hoxey R.P., Short J.L., Burges L.R., Smith B.W., Ko R.H.Y., "Wind-induced fatigue loading of tubular steel lighting columns", in *Wind and Structures*, 4, 2001, pp. 163-176.
- Robertson A.P., Holmes J.D., Smith B.W., "Verification of closed-form solutions of fatigue life under along-wind loading", in *Engineering Structures*, 26, 2004, pp. 1381-1387.
- Ruscheweyh H., "Vortex excited vibrations", in *Wind-excited vibrations of structures*, Sockel H. ed., Springer-Verlag, Wien, 1994, pp. 51-84.
- Ruscheweyh H., Sedlaceck G., "Crosswind vibrations of steel stacks – critical comparison between some recently proposed codes", in *J. Wind Eng. Ind. Aerodyn.*, 30, 1988, pp. 173–183.
- Rychlik I., "A new definition of the rainflow cycle counting method", in *International Journal of Fatigue*, 9, 1987, pp. 119-121.
- Rychlik I., "On the 'narrow-band' approximation for expected damage", in *Prob. Engng. Mech.*, 8, 1992, pp. 1-4.
- Rychlik I., "Characterization of random fatigue loads", in *Stochastic Approach to Fatigue*, CISM Course and Lectures n. 334, Ed. K. Sobczyk, Springer-Verlag, Wienn-New York, 1993.
- Schijve J., "Fatigue of structures and materials in the 20th century and the state of the art", in *International Journal of Fatigue*, 25, 2003, pp. 679–702.
- Scruton C., Flint A.R., "Wind-excited oscillations of structures", in *Proc. Inst. Civ. Eng.* 27 (4), 1964, pp. 673–702.
- Sharba M., Leman Z., Sultan M., Ishak M., Hanim M., "Glass-kenaf composites", in *BioResources*, 11(1), 2016, pp. 2665-2683.
- Shinozuka M., Jan C.M., "Digital simulation of random processes and its applications", in *J Sound Vibr*, 25, 1972, pp. 111-128.
- Skop R.A., Griffin O.M., "A model for the vortex-excited resonant response of bluff cylinders", in *J. Sound Vib.*, 27, 1973, pp. 225–233.
- Simiu E., Heckert N.A., "Extreme wind distribution tails: A 'peak over threshold' approach", in *J. Struct. Eng.*, ASCE, 122(5), 1996, pp. 539–547.
- Solari, G., "Wind speed statistics", In Lalas, D.P., Ratto, C.F. (Eds.). Modeling of the atmospheric flow fields. World Scientific Publishing, Singapore, 1996a.
- Solari G., "Evaluation and role of damping and period for the calculation of structural response under wind loads", in *Journal of Wind Engineering and Industrial Aerodynamics* 59, 1996, pp. 191–210.
- Solari G., "Wind-excited response of structures with uncertain parameters", in *Probabilistic Engineering Mechanics* 12 (2), 1997, pp. 75–87.

- Solari G., “Gust Buffeting of Slender Structures and Structural Elements: Simplified Formulas for Design Calculations and Code Provisions”, in *Journal of Structural Engineering*, (ASCE) 144(2), 2018.
- Solari G. et al., “The wind forecast for safety management of port areas”, in *J. Wind Eng. Ind. Aerodyn.*, 104–106, 2012, pp. 266–277.
- Spencer B.F., “Stochastic Diffusion Models for Fatigue Crack Growth and Reliability Estimation”, in *Stochastic Approach to Fatigue*, 1993, pp. 185-241.
- Takle E.S., Brown J.M., “Note on the use of Weibull statistics to characterize wind speed data”, in *Journal of Applied Meteorology*, 17, 1978, pp. 556-559.
- Tamura Y., Matsui G., “Wake-oscillator model of vortex-induced oscillation of circular cylinder”, in *Cermak, J.E. (Ed.), Proc. 5th Int Conf Wind Eng, Pergamon Press*, New York, 1979, pp. 1085-1094.
- Toro G.R., Cornell C.A., “Extremes of Gaussian processes with bimodal spectra” in *J Eng Mech*, 112(5), 1986, pp. 465–84.
- Troen I., Petersen E.L., “European wind atlas”, Risø National Laboratory, Roskilde, 1989.
- Van der Hoven I., “Power spectrum of horizontal wind speed in the frequency range from 0.0007 to 900 cycles per hour”, in *Journal of Meteorology*, 14, 1957, pp. 160-164.
- Vanmarke E.D., “Properties of spectral moments with application to random vibration”, in *J. Mech. Div.*, ASCE, 98, 1972.
- van Staalduinen P.C., “Wind loading and fatigue of steel framed masts”, in *EURODYN ’93 Proceedings*, Moan et al. Eds, Balkema, Rotterdam, 1993, pp. 1107-1113.
- Verboom G.K., van Koten H., “Vortex excitation: three design rules tested on 13 industrial chimneys”, in *J. Wind Eng. Ind. Aerodyn.*, 98, 2010, pp. 145–154.
- Verwiebe C., Glockner A., “Failure of steel chimneys due to vortex excited vibrations in the second mode”, in Proceedings of the XI ICWE, Texas Tech University, Lubbock, 2003.
- Vickery B.J., “ The response of chimneys and tower-like structures to wind loading. A State of the Art in ASCE Wind Engineering”, in *Proceedings of the Ninth International Conference on Wind Engineering, Davenport Sixtieth Birth Anniversary Volume*, New Delhi, Wiley Eastern Ltd., 1995, pp. 205–233.
- Vickery B.J., “Wind loads & design criteria for chimneys”, *CICIND report*, Vol. 14, No. 2, 1998.
- Vickery B.J., Basu R.I., “Across-wind vibrations of structures of circular cross-section. Part I: development of a mathematical model for two-dimensional conditions”, in *J. Wind Eng. Ind. Aerodyn.*, 12 (1), 1983a, pp. 49–74.
- Vickery B.J., Clark A.W., “Lift or across-wind response of tapered stacks”, in *J. Struct. Div.*, ASCE 98 (ST1), 1972, pp. 1–20.
- Violette R., de Langre E., Szydlowski J., “A linear stability approach to vortex-induced vibrations and waves”, in *J. Fluids Struct.*, 26, 2010, pp. 442–466.
- Wang J., Fu S., Baarholm R., Wu J., Larsen C.M., "Fatigue damage induced by vortex induced vibrations in oscillatory flow", in *Marine Structures*, 40, 2015, pp. 73-91.
- Weibull W., “A statistical distribution function of wide applicability”, in *J. Appl. Mech.*, 18, 1951, pp. 293-297.
- Wieghaus K.T., Mander J.B., Hurlebaus S., “Damage avoidance solution to mitigate wind-induced fatigue in steel traffic support structures”, in *Journal of Constructional Steel Research* 138, 2017, pp. 298–307.
- Wirsching P.H., Light M.C., “Fatigue under wide band random stresses”, in *Journal of the*

Structural Division, ASCE, 106 (7), 1980, pp. 1593-1607.

- Wohler A., "Zietschrift fur Bauwesen", 8, 10, 13, 16, 20, 1860-70.
- Wootton L.R., "The oscillations of model circular stacks due to vortex shedding at Reynolds numbers from 10^5 to $3x10^6$", NPL Aero Rep. 1267, National Physical Lab., Teddington, England, 1968.
- Wootton L.R., "The oscillations of large circular stacks in wind", in *Proc. Inst. Civ. Eng. Lond.* 43, 1969, pp. 573-598.
- Wyatt T.A., "An assessment of the sensitivity of lattice towers to fatigue induced by wind gusts", in *Eng. Struct.,* 6(4), 1984, pp. 256–261.
- Wyatt T.A., "Determination of gust action stress cycle counts for fatigue checking line-like steel structures", in *J Wind Eng Ind Aerodyn,* 92(5), 2004, pp. 359-374.
- Zuo D., Letchford C.W., "Wind-induced vibration of a traffic-signal-support structure with cantilevered tapered circular mast arm", in *Engineering Structures* 32, 2010, pp. 3171-3179.

SYMBOLS

- a_k = constant depending on the k-th broken line in a S-N fatigue resistance curve (Chapt. 2 – p. 10)
- a_L = normalized dimensionless limiting amplitude of VIV displacements (Chapt. 5 – p. 113)
- a^I ; a^{II} = constants for cases of bilinear S-N curves with or without the cut-off limit (Chapt. 3 – p. 76)
- A_0; A_{BM}; A_M; A_{SN} = non dimensional quantities given in function of the three parameters, k, $\alpha_{\sigma,\omega}$ and $\alpha_{\lambda,\omega}$, or as constants, depending on the calculation level of the buffeting-induced fatigue method (Chapt. 4 – p. 81)
- b = reference size of a slender structure (or structural element) cross section (Chapt. 2 – p. 35)
- B_{SN} = non dimensional quantity given in function of the three parameters, k, $\alpha_{\sigma,\omega}$ and $\alpha_{\lambda,\omega}$, or as constants, depending on the calculation level of the buffeting-induced fatigue method (Chapt. 4 – p. 81)
- B_ω = quasi-static response factor (Chapt. 4 – p. 93)
- c = Weibull distribution scale parameter (Chapt. 2 – p. 33)
- c_{Ls} = lift (vortex shedding) coefficient (Chapt. 5 – p. 110)
- c_t = topography coefficient (Chapt. 5 – p. 126)
- c_ω = drag/lift aerodynamic coefficient (Chapt. 4 – p. 92)
- C_{BM} = the corrective bi-modal factor (Chapt. 3 – p. 59)
- C_c = dimensionless parameter, function of the shape of the cross-section and possibly of the Reynolds number (Chapt. 5 – p. 120)
- C_E = exposure category (Chapt. 5 – p. 188)
- C_I = turbulence factor (Chapt. 5 – p. 121)
- C_M = the corrective mean stress factor (Chapt. 3 – p. 59)
- C_R = dimensionless parameter associated with the critical values of the mean wind velocity for long return periods R (Chapt. 5 – p. 119)
- C_{SN} = the corrective fatigue curve factor (Chapt. 3 – p. 59)
- $C_{z\varepsilon}$ = exponential decay coefficient of the ε turbulence component along z (Chapt. 4 – p. 100)

- $\mathrm{Coh}_{\varepsilon\eta}(M,M';n)$ = coherence function of ε(*M*;*t*) and η(*M'*;*t*) (Chapt. 2 – p. 34)
- *Cov*[.] = covariance operator (Chapt. 5 – p. 206)
- *d* = fraction of damage (Chapt. 2 – p. 11)
- d_j = fraction of damage induced by the *j*-th block of cycles of amplitude Δ_j (Chapt. 2 – p. 11)
- d_ε = constant in power spectral density function of the ε turbulence component (Chapt. 2 – p. 35)
- $\bar{d}(1,\bar{u})$ = mean fraction of damage because of $\bar{u}$ in the unit time (Chapt. 3 – p. 58)
- *D* = total cumulative damage (Chapt. 2 – p. 11)
- $\bar{D}$ = mean damage intensity (Chapt. 2 – p. 22)
- $\bar{D}(1)$ = the mean total damage in the unit time (Chapt. 3 – p. 58)
- $\bar{D}_0(1)$ = approximated *0 level solution* of the mean damage (Chapt. 3 – p. 59)
- $\tilde{D}$ = constant values selected for different bilinear S-N curves (Chapt. 3 – p. 71)
- e_i = wind loading effect associated to the *i*-th loading condition $\bar{u}=\bar{u}_{ref,i}$ (Chapt. 2 – p. 40)
- $\bar{e}_i$ = mean loading effect associated to the *i*-th loading condition $\bar{u}=\bar{u}_{ref,i}$ (Chapt. 2 – p. 40)
- e'_i = nil mean fluctuating loading effect associated to the *i*-th loading condition $\bar{u}=\bar{u}_{ref,i}$ (Chapt. 2 – p. 40)
- *E*[.] = mean operator (Chapt. 5 – p. 206)
- f_a = aerodynamic lift force due to motion-induced forces (Chapt. 5 – p. 110)
- f_{Ls} = vortex-induced force along the structure length (Chapt. 5 – p. 109)
- f_s = external fluctuating lift force due to vortex shedding (Chapt. 5 – p. 110)
- f_y = yield strength of a material (Chapt. 2 – p. 14)
- $\bar{f}_\omega$ = static aerodynamic force induced by reference mean velocity along the structure length (Chapt. 4 – p. 92)
- $F_{L,eq}(z)$ = equivalent static force per unit length due to vortex shedding (Chapt. 5 – p. 119)
- $F_\omega = F_x, F_y, F_\theta$ = alongwind force, crosswind force and torsional moment around *z* per unit length (Chapt. 2 – p. 35)
- $\bar{F}_\omega$ = mean value of F_ω (Chapt. 2 – p. 35)

- F'_{ω} = nil mean fluctuation of F_{ω} around $\bar{F}_{\omega}$ (Chapt. 2 – p. 35)
- F_0 = probability that wind velocity value is zero (Chapt. 2 – p. 33)
- g_s = peak deflection factor (Chapt. 5 – p. 117)
- h = height above the ground (Chapt. 2 – p. 35)
- h_a = coefficient for the in-phase component of the aerodynamic force due to vortex shedding (Chapt. 5 – p. 110)
- H = transfer function, namely mechanical admittance (Chapt. 2 – p. 28)
- $H(\bullet)$ = Heavyside's function (Chapt. 2 – p. 25)
- I_u = longitudinal turbulence intensity (Chapt. 4 – p. 93)
- J_f = moment of inertia of the cross section (Chapt. 5 – p. 125)
- k = Weibull distribution shape parameter (Chapt. 2 – p. 33)
- k_a = coefficient for the out-of-phase component of the aerodynamic force due to vortex shedding (Chapt. 5 – p. 110)
- $k^e_{\omega\varepsilon}$ = equivalent correlation factor for the effect e (Chapt. 4 – p. 100)
- $\tilde{k}$ = Von Karman constant (Chapt. 2 – p. 33)
- K_a = aerodynamic damping parameter (Chapt. 5 – p. 110)
- $K_{a,max}$ = maximum value of the aerodynamic damping parameter (Chapt. 5 – p. 121)
- l = length of a slender structure (or structural element) (Chapt. 2 – p. 35)
- L = Obukhov length (Chapt. 2 – p. 32)
- L_{ε} = integral length scale of ε turbulence component in the x direction (Chapt. 2 – p. 35)
- $\tilde{L}$ = constant values selected for different bilinear S-N curves (Chapt. 3 – p. 71)
- $m(z)$ = mass per unit length of the structure (Chapt. 5 – p. 119)
- m_e = equivalent mass per unit length (Chapt. 5 – p. 108)
- m_k = slope value of the k-th broken line in a S-N fatigue resistance curve (Chapt. 2 – p. 10)
- $\tilde{m}_0$, $\tilde{m}_1$, $\tilde{m}_2$, $\tilde{m}_4$ = spectral moments of a random process (Chapt. 2 – p. 23)
- M = point of coordinates x,y,z (Chapt. 2 – p. 34)
- M' = point of coordinates x',y',z' (Chapt. 2 – p. 34)
- n = the process frequency (Chapt. 2 - p. 22)

- n_j = the number of the cycles with constant amplitude Δ_j (Chapt. 2 - p. 11)
- $n_{NB,ij}$ = number of cycles of the narrow-band process associated with the *i*-th wind velocity interval $\Delta\bar{u}_i$ and with the *j*-th stress cycles amplitude Δ_j (Chapt. 5 – p. 124)
- $n_P\left(\Delta_j^*\right)$ = mean number of cycles with normalised amplitude Δ_j^* due to the process *P* (Chapt. 2 – p. 25)
- n_s = vortex shedding frequency or vortex shedding loading frequency (Chapt. 5 – p. 107)
- $n_{\omega,1}$ (or n_1) = first mode of vibration in ω-th direction, namely natural of fundamental frequency (Chapt. 2 – p. 38)
- $\bar{n}_{ij}$ = mean number of cycles with amplitude Δ_j around the mean stress $\bar{s}_i$ (Chapt. 2 - p. 40)
- $\hat{n}\left(\Delta_j^*\right)$ = number of the large cycles of a bi-modal process *X** (Chapt. 2 – p. 25);
- $\hat{n}_{ij}(T)$ = *j*-th large amplitude cycles induced by the *i*-th stress process during the time interval *T* (Chapt. 2 - p. 41)
- $\breve{n}\left(\Delta_j^*\right)$ = number of the small cycles of a bi-modal process *X** (Chapt. 2 – p. 25);
- $\breve{n}_{ij}(T)$ = *j*-th small amplitude cycles induced by the *i*-th stress process during the time interval *T* (Chapt. 2 - p. 41)
- *N* = the number of the cycles with constant amplitude Δ that produces fatigue failure (Chapt. 2 - p. 8) and the number of cycles caused by vortex excited oscillation (Chapt. 5 – p. 122)
- N_C = 2 million cycles (Chapt. 2 – p. 14)
- N_D = number of cycles corresponding to first knee of a trilinear *S-N* curve (Chapt. 2 – p. 15)
- N_L = number of cycles corresponding to the knee of a bilinear *S-N* curve or to the cut-off limit of a trilinear *S-N* curve (Chapt. 2 – p. 15)
- *p* = pressure (Chapt. 2 – p. 31)
- $\mathrm{p}_{\mathrm{U}}(\bar{u})$ = density function of the mean wind velocity population (Chapt. 2 – p. 33)
- $p_\Delta(\Delta)$ = probability density function of amplitudes of the random process (Chapt. 2 – p. 21)
- $p(\Delta|\bar{u})$ = probability density function of Δ, conditional to the occurrence of $\bar{u}$ (Chapt. 3 – p. 58)
- *P* = pseudo-envelope of a normalized bi-modal process *X** (Chapt. 2 – p. 24)
- P_h = directional probability, namely the probability that the wind blows from the *h*-th sector with nonzero velocity (Chapt. 2 – p. 50)
- P_i = probability that $\bar{u}_{ref,i}$ belongs to the *i*-th velocity interval (Chapt. 2 – p. 40)
- P_{ih} = joint probability that the mean wind velocity belongs to the *i*-th velocity interval and the wind blows from the *h*-th sector (Chapt. 2 – p. 49)
- P_{ihl} = joint probability that the mean wind velocity belongs to the *i*-th velocity interval, that the wind blows from the *h*-th directional sector, and that (1/L = Obukhov length) belongs to the *l*-th interval (Chapt. 2 – p. 51)

- P_{si} = pseudo-envelope of the stress process associated with the *i*-th wind loading condition (Chapt. 2 – p. 40)
- $P_U(\bar{u})$ = distribution function of the mean wind velocity population (Chapt. 2 – p. 33)
- q_{Rxi} = spectral bandwidth of the resonant part of the stress process in *x* direction induced by the *i*-th loading condition (Chapt. 2 – p. 41)
- *r* = wind-induced resultant forces acting on the structure (Chapt. 2 – p. 28)
- *r* = variable defined in generalized fatigue curve factor derivation (Appendix A – p. 252)
- *R* = return period (Chapt. 5 – p. 119)
- R_{HF} = envelope of the high frequency component X^*_{HF} of a normalized bi-modal process *X** (Chapt. 2 – p. 24)
- R_{Ri} = envelope of the resonant part of the stress process associated with the *i*-th wind loading condition (Chapt. 2 – p. 41)
- R_{ω} = resonant response factor evaluated with respect to the reference velocity (Chapt. 4 – p. 93)
- $R_{\omega fat}$ = resonant response factor evaluated with respect to the fatigue velocity (Chapt. 4 – p. 97)
- *Re* = Reynolds number (Chapt. 5 – p 105)
- *Ri* = Richardson number (Chapt. 2 – p. 32)
- *s* = wind-induced nominal stress (Chapt. 2 – p. 18)
- s_u = ultimate strength of a material (Chapt. 2 – p. 8)
- $\hat{s}$ = peak of the stress time history (Chapt. 3 – p. 60)
- $\bar{s}$ = mean static stress because of the mean wind velocity $\bar{u}$ (Chapt. 2 – p. 8)
- $\bar{s}_p$ = mean static stress because of the permanent and variable static loads (Chapt. 3 – p. 58)
- $\bar{s}_t$ = mean total static stress (Chapt. 3 – p. 58)
- *s*'= fluctuating stress (Chapt. 2 – p. 38)
- s'_{Qxi} = quasi-static part of fluctuating stress process in *x* direction induced by the *i*-th loading condition (Chapt. 2 – p. 41)
- s'_{Rxi} = resonant part of fluctuating stress process in *x* direction induced by the *i*-th loading condition (Chapt. 2 – p. 41)
- s'_{xi} = wind fluctuating stress in *x* direction induced by the *i*-th loading condition (Chapt. 2 – p. 40)
- $s'_{\omega,Q}$ = low frequency quasi-static part of s'_{ω} (Chapt. 2 – p. 38)
- $s'_{\omega,R}$ = high frequency resonant part of s'_{ω} (Chapt. 2 – p. 38)
- *S*-*N* = (*S* = stress; *N* = number of cycles) fatigue resistance curves for different material or structural component (Chapt. 2 – p. 5)
- $S_x(n)$ = one-sided power spectral density function of the stationary random process $X(t)$, expressed in

the domain of frequency *n* (Chapt. 2 – p. 22)

- $S_{\varepsilon}(z;n)$ = power spectral density function of ε(*M*;*t*) (Chapt. 2 – p. 34)
- $S_{\varepsilon\eta}(M,M';n)$ = cross-power spectral density function of ε(*M*;*t*) and η(*M'*;*t*) (Chapt. 2 – p. 34)
- *Sc* = Scruton number (Chapt. 5 – p 105)
- *St* = Strouhal number (Chapt. 5 – p 105)
- *t* = time (Chapt. 2 – p. 18) and structural element thickness (Chapt. 5 – p. 125)
- t_D ; t_L = variables defined in generalized fatigue curve factor derivation (Chapt. 3 – p. 72)
- *T* = period of time (Chapt. 2 – p. 18)
- T_i = duration time in which the structure undergoes the *i*-th loading condition (Chapt. 2 – p. 40)
- T_{ihl} = duration time in which the structure undergoes the *ihl*-th loading condition (Chapt. 2 – p. 51)
- T_F = the fatigue life of a structure or structural element (Chapt. 3 – p. 59)
- *T*° = temperature (Chapt. 2 – p. 31)
- *u* (or *U*) = wind velocity (Chapt.2 – p. 28)
- u_D ; u_L = variables defined in generalized fatigue curve factor derivation (Chapt. 3 – p. 71)
- u_g = gradient or geostrophic velocity (Chapt. 2 – p. 29)
- u_* = frictional velocity (Chapt. 2 – p. 33)
- $\bar{u}$ = mean wind velocity (Chapt. 2 – p. 31)
- $\bar{u}_{cr}$ = critical wind velocity to vortex shedding (Chapt. 5 – p. 107)
- $\bar{u}_{fat}$ = fatigue velocity, representative of the maximum fatigue condition (Chapt. 2 – p. 53)
- $\bar{u}_{ref}$ = reference mean wind velocity, e.g. the mean wind velocity with a 50-year return period, at 10 m height on a flat homogeneous terrain with roughness length 0.05 m (Chapt. 2 – p. 33)
- $\bar{u}_0$ = reference value of the wind velocity, and scale parameter of the Weibull model of the parent population of mean wind velocity given by Eurocode (Chapt. 5 – p. 122)
- *u*' = longitudinal turbulence component (Chapt. 2 – p. 31)
- *v*' = lateral turbulence component (Chapt. 2 – p. 31)
- *V*[.] = variance operator (Chapt. 5 – p. 206)
- V_N = nominal life-time of the structure or structural element (Chapt. 5 – p. 122)
- *w*' = vertical turbulence component (Chapt. 2 – p. 31)
- *x* = general time history (Chapt. 2 – p. 18) in this thesis used to represent structural response, namely the stress time history induced by wind in alongwind direction (Chapt. 2 – p. 28)

- X = stationary random process (Chapt. 2 – p. 22)
- X_{HF} = high frequency component of a bi-modal process X (Chapt. 2 – p. 23)
- X_{LF} = low frequency component of a bi-modal process X (Chapt. 2 – p. 23)
- X^* = normalized random process with respect to its standard deviation value (Chapt. 2 – p. 24)
- X^*_{HF} = high frequency component of a normalized process X^* (Chapt. 2 – p. 24)
- X^*_{LF} = low frequency component of a normalized process X^* (Chapt. 2 – p. 24)
- y = crosswind structural displacement (Chapt. 5 – p. 110)
- $\dot{y}$ = crosswind structural velocity (Chapt. 5 – p. 110)
- $\bar{y}_{max}$ = maximum crosswind response, or peak deflection value (Chapt. 5 – p. 117)
- $\bar{y}_{s,max}$ = maximum crosswind stress due to VIV (Chapt. 5 – p. 122)
- z = height (Chapt. 2 – p. 32) or axial coordinate (Chapt. 2 – p. 35)
- z_{cr} = critical height where resonant VIV occur (Chapt. 5 – p. 133)
- z_{eq} = reference local coordinate, also called equivalent coordinate (Chapt. 4 – p. 91)
- z_g = gradient or geostrophic height of the atmospheric boundary layer (Chapt. 2 – p. 29)
- z_{ref} = reference height to evaluate reference mean wind velocity $\bar{u}_{ref}$ (Chapt. 2 – p. 33)
- z_0 = roughness length of the terrain (or roughness parameter) (Chapt. 2 – p. 29)
- $z_{0,ref}$ = roughness length which characterizes a reference terrain (Chapt. 2 – p. 33)
- Z_{eq} = fixed reference height for evaluating external wind action on a structure in the wind flow, called reference height above ground (Chapt. 4 – p. 91)

- α_κ = exponent of the power law (Chapt. 2 – p. 52)
- γ_F = safety factor for fatigue analysis (Chapt. 4 – p. 93)
- $\Gamma(\bullet)$ = gamma Function (Chapt. 3 – p. 60)
- $\Gamma_{inc}(\bullet)$ = Incomplete gamma Function (Chapt. 3 – p. 69) (by naming variables L, t, n)
- $\delta(\bullet)$ = Dirac operator (Chapt. 2 – p. 33)
- Δ = stress cycles amplitude (Chapt. 2 – p. 8) = σ_{max} - σ_{min}
- Δ_C = the fatigue class (Chapt. 2 – p. 14)
- Δ_D = stress cycles amplitude corresponding to N_D (Chapt. 2 – p. 15)
- Δ_e = equivalent zero-mean amplitude (Chapt. 2 – p. 8)
- Δ^*_j = j-th normalised amplitude associated with the bi-modal process X^* (Chapt. 2 – p. 25)

- Δ_L = stress cycles amplitude corresponding to N_L, therefore corresponding to the "last knee" of a *S*-*N* curve (Chapt. 2 – p. 10)
- $\Delta_{s,max} = 2\,\bar{y}_{s,max}$ maximum stress cycle amplitude in the considered critical cross-section (Chapt. 5 – p. 122)
- ΔT = time conventional interval of 10 minutes (Chapt. 2 – p. 31)
- Δu_i = *i*-th velocity interval (Chapt. 2 – p. 34)
- ε_0 = bandwidth factor describing the band of wind velocities with vortex-induced vibrations (Chapt. 5 – p. 122)
- ζ_ω = parameter that defines the shape of the mode (Chapt. 5 – p. 127)
- θ = potential temperature (Chapt. 2 – p. 32)
- κ = generic stress parameter ($\kappa = \bar{s}$, σ, v, v_Q, λ_R) (Chapt. 2 – p. 52)
- κ_{fat} = κ evaluated in correspondence of $\bar{u}_{fat}$ (Chapt. 2 – p. 53)
- κ_{ref} = κ evaluated in correspondence of $\bar{u}_{ref}$ (Chapt. 2 – p. 52)
- λ = damage correction factor according to Wirsching and Light (1980) et seq. (Chapt. 2 – p. 23)
- λ_R (or $\lambda_{\omega,R}$) = normalized variance of the resonant part of the stress (Chapt. 2 – p. 38 and p. 52)
- $\lambda_{\omega,Q}$ = normalized variance of the quasi-static part of the stress $s'_{\omega,Q}$ (Chapt. 2 – p. 38)
- λ^*_{Qxi} = normalized variance of the quasi-static part of the stress process in *x* direction induced by the *i*-th loading condition (Chapt. 2 – p. 41)
- λ^*_{Rxi} = normalized variance of the resonant part of the stress process in *x* direction induced by the *i*-th loading condition (Chapt. 2 – p. 41)
- μ_L = crosswind static response factor (Chapt. 4 – p. 99)
- $v_P(x)$ = mean up-crossing rate of the pseudo-envelope *P* (Chapt. 2 – p. 25)
- v_Δ = expected frequency of amplitude (Chapt. 2 – p. 21)
- v_0 = mean rate of zero up-crossing of a process (Chapt. 2 – p. 22)
- v_ω = expected frequency of the wind-induced stress *s* (Chapt. 2 – p. 38)
- $\nu_{\omega,Q}$ = expected frequency of quasi static part of the fluctuating stress $s'_{\omega,Q}$ (Chapt. 2 – p. 38)
- $v_{0,Qxi}$ = expected frequency of the quasi-static part of the stress process in *x* direction induced by the *i*-th loading condition (Chapt. 2 – p. 41)
- ξ = damping ratio (Chapt. 2 – p. 52)
- ξ_a = aerodynamic damping (Chapt. 5 – p. 110)
- ξ_{eq} = equivalent damping (Chapt. 5 – p. 110)
- ξ_s = structural damping (Chapt. 5 – p. 108)

- $\Pi_{x_i}[\bullet]$ = propagation factor of the parameter x_i (Chapt. 5 – p. 207)
- ρ = air density, usually assumed as 1.25 kg/m^3 (Chapt. 4 – p. 92)
- $\rho_i[x_i]$ = coefficient of variation of the parameter x_i (Chapt. 5 – p. 207)
- σ (or σ_s) = standard deviation of the stress process (Chapt. 2 – p. 38)
- σ_{hs} = structural or geometric stress (Chapt. 2 – p. 12)
- $\sigma_{Lim} = a_L \cdot b$ standard deviation of the limiting amplitude of VIV displacements (Chapt. 5 – p. 112)
- σ_{max} = maximum value of the stress cycle (Chapt. 2 – p. 11)
- σ_{min} = minimum value of the stress cycle (Chapt. 2 – p. 11)
- σ_{nl} = non-linear peak stress caused by the local notch (Chapt. 2 – p. 12)
- σ_s = standard deviation of the crosswind deflection/stress due to VIV (Chapt. 5 – p. 117)
- σ_x = standard deviation of the general process X (Chapt. 2 – p. 22)
- σ_{xi} = standard deviation of the wind-induced stress in x direction in the i-th loading condition (Chapt. 2 – p. 42)
- σ_Δ = standard deviation of the stress range Δ (Chapt. 3 – p. 60)
- σ_ε = standard deviation of the turbulence component ε (Chapt. 2 – p. 35)
- σ_ω^2 = variance of the wind-induced stress s (Chapt. 2 – p. 38)
- $\sigma_{\omega,Q}$ = standard deviation of $s'_{\omega,Q}$ (Chapt. 2 – p. 38)
- $\sigma_{\omega,R}$ = standard deviation of $s'_{\omega,R}$ (Chapt. 2 – p. 38)
- τ = averaging time for the peak wind velocity (Chapt. 4 – p. 93)
- $\bar{\tau}_{D,ref}$ = mean shear stress due to the alongwind-induced effect of $\bar{u}_{ref}$ on the structure (Chapt. 6 – p. 235)
- υ = kinematic viscosity of the air (Chapt. 5 – p. 132)
- Φ_L = normalized crosswind structural mode shape (Chapt. 5 – p. 119)
- χ = transfer function, namely aerodynamic admittance (Chapt. 2 – p. 28)
- χ_{SN} = the *Chi factor* (Chapt. 3 – p. 69)

INDICES and SUBSCRIPTS

h = directional sectors index (Chapt. 2 – p. 34)

i = velocity intervals index (Chapt. 2 – p. 34), corresponding to wind loading conditions (Chapt. 2 – p. 40)

j = stress amplitude cycles index (Chapt. 2 – p. 11)

k = segment of *S-N* curve index (Chapt. 2 – p. 10)

l = Obukhov length conditions index (Chapt. 2 – p. 51)

d = displacement (Chapt. 5 – p. 127)

s = stress (Chapt. 2 – p. 18) or s = wake excitation (Chapt. 4 – p. 100)

Q, R = quasi-static, resonant part, respectively (Chapt. 2 – p. 38)

ref/fat = associated with reference/fatigue wind velocity (Chapt. 2 – p. 33 and p. 53)

$\varepsilon, \eta = u', v', w'$; ε turbulence component (Chapt. 2 – p. 34), η turbulence component in another position (Chapt. 2 – p. 34)

κ = stress parameters index ($\kappa = \bar{s}$, σ, ν, ν_Q, λ_R) (Chapt. 2 – p. 52)

ω = wind loading and response components index (ω-th component $\omega = x, y, \theta$) (Chapt. 2 – p. 35) (or $\omega = D, L$) (Chapt. 4 – p. 81)

REFERENCE SYSTEMS

x, y, and z = local Cartesian reference system with origin at o (Chapt. 2 – p. 30 and p. 35)

X, Y, and Z = global Cartesian reference system with origin at O (Chapt. 2 – p. 35)

SUMMARY OF INPUT PARAMETERS FOR BUFFETING INDUCED FATIGUE ANALYSIS: ALL DEFINITIONS IN CHAPTER 4

m_1; Δ_C; N_L = parameters of the considered *S-N* fatigue curve (Section 4.3.1);

a^I ; a^{II} = constant values depending on the shape of the considered *S-N* fatigue curve (Section 4.3.1);

k = shape parameter of the Weibull probability distribution of the current values of the wind velocity in situ (Section 4.3.2);

$n_{\omega 1}$ = first mode of vibration frequency in the ω-th direction (Section 4.3.1);

s_u = material failure characteristic stress (Section 4.3.1);

$\bar{s}_P$ = permanent loadings-induced stress in the examined section (calculated at serviceability) (Section 4.3.3);

$\bar{s}_{\omega,ref}$ = mean value of the stress process in the critical section, in ω-direction, evaluated at reference wind velocity (Sections 4.3.3, 4.3.4, 4.3.5);

$\sigma_{\omega,ref}$, = standard deviation of the stress process in the critical section, in ω-direction, evaluated at reference wind velocity (Sections 4.3.3, 4.3.4, 4.3.5);

$\nu_{\omega,ref}$, = expected frequency of the stress process in the critical section, in ω-direction, evaluated at reference wind velocity (Sections 4.3.3, 4.3.4, 4.3.5);

$\nu_{\omega,Q,ref}$, = expected frequency of the quasi-static part of the stress process in the critical section, in ω-direction, evaluated at reference wind velocity (Sections 4.3.3, 4.3.4, 4.3.5);

$\lambda_{\omega,R,ref}$, = normalized variance of the resonant part of the stress process in the critical section, in ω-direction, evaluated at reference wind velocity (Sections 4.3.3, 4.3.4, 4.3.5);

$\alpha_{\sigma,\omega}$ = exponent of the power law expressing the standard deviation of the fluctuating stress, σ_{ω}, on varying wind velocity (Sections 4.3.3, 4.3.4, 4.3.5);

$\alpha_{\lambda,\omega}$ = exponent of the power law expressing the normalized variance of the stress resonant part, $\lambda_{\omega,R}$, on varying wind velocity (Sections 4.3.3, 4.3.4, 4.3.5).